Andrei A. Snarskii · Igor V. Bezsudnov
Vladimir A. Sevryukov · Alexander Morozovskiy
Joseph Malinsky

Transport Processes in Macroscopically Disordered Media

From Mean Field Theory to Percolation

Springer

Transport Processes in Macroscopically Disordered Media

Andrei A. Snarskii · Igor V. Bezsudnov
Vladimir A. Sevryukov · Alexander Morozovskiy
Joseph Malinsky

Transport Processes in Macroscopically Disordered Media

From Mean Field Theory to Percolation

Springer

Andrei A. Snarskii
Department of General and Theoretical Physics
National Technical University of Ukraine "KPI"
Kiev
Ukraine

Igor V. Bezsudnov
Research and Development
ZAO "NPP Nauka-Service"
Moscow
Russia

Vladimir A. Sevryukov
ZAO "NPP Nauka-Service"
Moscow
Russia

Alexander Morozovskiy
Citibank
Staten Island, NY
USA

Joseph Malinsky
BCC
CUNY Graduate Center, Physics Program
Livingston, NJ
USA

ISBN 978-1-4419-8290-2 ISBN 978-1-4419-8291-9 (eBook)
DOI 10.1007/978-1-4419-8291-9

Library of Congress Control Number: 2016945936

Printed on acid-free paper

This Springer imprint is published by Springer Nature
The registered company is Springer Science+Business Media LLC New York

Dedicated to the memory of A.M. Dykhne

Preface

The basic problem described in this book is how one can find effective characteristics such as conductivity, dielectric permittivity, magnetic permeability, etc., knowing the distribution of different components constituting inhomogeneous medium.

We consider here a wide range of recent studies dedicated to the elucidation of the physical properties of macroscopically disordered systems. They are galvano-electric, thermoelectric, and elastic properties as well as behavior of 1/*f*-noise, current moments, and higher harmonic generation in composites at the threshold of percolation. Our goal in writing this book is to reflect on recent advances in our understanding of percolation systems and to present in coherent fashion a very wide range of transport phenomena in inhomogeneous disordered systems. We also tried to use, as much as possible, unifying treatment that would allow interdisciplinary view of apparently diverse physical properties to be treated at equal footing. We also regret in retrospect that many important areas of recent activities in field have not been included such as thermoelectric properties of composites.

The unity of treatments, by authors deep conviction, is main thrust here: connects phenomena that seem to be very different and yet so close under closer investigation. Their appearance seems to be strange under one book. For instance, one would not expect to see 1/f noise in percolation systems together with pinning and Abrikosov vortexes. Authors were trying to present material in a way to make it readily available to a typical reader who is familiar with undergraduate physics courses and is trying to familiarize himself with active research avenues in the advanced fields of condensed matter sciences, materials, etc. It is our hope that that present book would enable serious advance student to obtain most of described results with minimum time and paper. We use hierarchical model and believe that it is the most straightforward way to arrive at basic physical properties of complicated systems along with corresponding qualitative characteristics and functional dependencies.

We did not try to write a classic exhausting monograph, but rather straightforward set of useful tools and even recipes, so that reader could almost immediately "see" and "try" and even "feel" by his own hands or with simplest MathCad what and how composites behave.

Material of this book is presented in three parts. In the first one we describe two classes of the methods of studying macroscopically disordered media. In this first class we include mainly mean field techniques, which typically give reliable results in the cases when density number of one of phases is much smaller compared with another. Sometimes they work even for large density.

The second class of methods is usually intended to describe processes in vicinity of the threshold of percolation when small changes in number densities may cause big changes. One of the models is the so-called hierarchical model. In the second part of this book we consider the application of different techniques to a broad spectrum of physical properties of composites roughly one per chapter. The reader has to realize that it is next to impossible to study but all phenomena of transport in composites. Most obvious omissions are mechanical and electrical disruption of materials such as composites, processes of fluid dynamics in porous media, thermogalvanomagnetic phenomena, conductivity of many component media, quantum Hall effect, etc. Decisive role in our interest to what is described in this book was initiated by A.M. Dykhne. We dedicate this book to him.

We want to express our gratitude to many of our friends and coworkers. Many topics that have been exposed here benefited heavily on them. We thank I. Adrianov, B. Aranson, V. Archincheev, E. Baskin, E. Belozky, D. Bergman, J.L. Birman, A. Dzedzits, I. Kaganova, V. Kholod, A. Kolek, S. Kucherov, A. Lagarkov, B. Lev, B. Linchersky, S. Lukyanets, A. Palti, E. Pashitsky, A. Sarychev, A. Satanin, M. Shamonin, L. Shepp, A. Shik, B. Shklovskii, K. Slipchenko, Y. Strelniker, P. Tomchuk, K. Usenko, A. Vinogradov, and M. Zhenirovsky. We also thank CUNY for assistance.

Kiev, Ukraine — Andrei A. Snarskii
Moscow, Russia — Igor V. Bezsudnov
Staten Island, NY, USA — Vladimir A. Sevryukov
Livingston, NJ, USA — Alexander Morozovskiy
Joseph Malinsky

References

1. Antonov AC et al. (ed. Lagar'kov AN) (1990) Electrophysical properties of percolation systems. Moscow, IBTAN, 120 pp (in Russian)
2. Beran AM (1974) Application of statistical theories for the determination of thermal, electrical, and magnetic properties of heterogeneous materials. In: Sendeckyj GP (ed) Mechanics of composite materials, vol 2. Academic Press, San Diego, CA, p. 209–249
3. Berdichevsky V (2009) Variational principles of continuous mechanics I. Fundamentals. Springer, 529 pp

4. Berdichevsky V (2009) Variational principles of continuous mechanics II. Applications. Springer, 430pp
5. Bergman DJ, Stroud D (1992) Physical properties of macroscopically inhomogeneous media. Solid State Phys 46, 147–269
6. Clerc JP, Giraud G, Laugier JM and et al. (1990) The electrical conductivity of binary disordered systems, percolation clusters, fractals and related models. Adv Phys 39, 191–309
7. Cohen R, Havlin S (2010) Complex networks structure, robustness and function, 248pp
8. Ewing R, Hunt A (2009) Percolation theory for flow in porous media. In: Lecture notes in physics, 771pp
9. Hunt A, Ewing R, Ghanbarian B (2014) Percolation theory for flow in porous media 3rd ed., Springer, 446pp
10. Isichenko MB (1992) Percolation, statistical topography, and transport in random media. Rev Mod Phys 64, 961–1043
11. Kirpatrick S (1973) Percolation and conduction. Rev Mod Phys 45, 574–588
12. Nakayama T, Yakubo K, Orbach RL (1994) Dynamical properties of fractal networks: scaling, numerical simulation, and physical realization. Rev Mod Phys 66, 381–443
13. Pobedrja BE (1984) Mechanics of composite materials. Moscow University, 336pp (in Russian)
14. Sahimi M (1993) Flow phenomena in rocks: from continuum models to fractals, percolation, cellular automata, and simulated annealing. Rev Mod Phys 65, 1393–1534
15. Sahimi M (1994) Applications of percolation theory. Taylor&Francis, 258pp
16. Sahimi M (1998) Non-linear and non-local transport processes in heterogeneous media: from long-range correlated percolation to fracture and materials breakdown. Phys Rep 306, 213–395
17. Shvidler M (1985) Statistical hydromechanics of porous media. Nedra, Moscow, 288pp (in Russian)
18. Stauffer D, Aharony A (1992) Introduction to percolation theory, 2nd edn. Taylor&Francis, 181pp
19. Tarasevich Y (2002) Percolation: theory, applications and algorithms URSS. Moscow, 112pp. (in Russian)
20. Torquato S (2002) Random heterogeneous materials: microstructure and macroscopic properties, Springer-Verlag New York, 703pp
21. Vinogradov AP (2001) Electrodynamics of composite materials URSS. Moscow, 208pp. (in Russian)
22. Ziman JM (1979) Models of disorder: the theoretical physics of homogeneously disordered systems. Cambridge University Press, London, 538pp

Contents

Part I
Methods

Chapter 1
Introduction

1.1 Types of Macroscopically Disordered Media

When we consider macroscopically inhomogeneous media we usually understand that the characteristic sizes of inhomogeneity is much greater compared with any characteristic macroscopic lengths. For instance, if we consider DC conduction of the electric current, and we usually assume that we have a situation where the size of inhomogeneity is much larger than mean free path of the current density. In particular, this fact signifies that local Ohm's law is satisfied; connecting the current density $\mathbf{j}(\mathbf{r})$ to the electric field $\mathbf{E}(\mathbf{r})$ at arbitrary point of the medium $\mathbf{j}(\mathbf{r}) = \sigma(\mathbf{r})\mathbf{E}(\mathbf{r})$, and the nonuniformity of the medium is signaled by the special local conductivity $\sigma(\mathbf{r})$.

The macroscopic inhomogeneity may be continuous as well as discrete, depending on whether local conductivity $\sigma(\mathbf{r})$ is continuous or not. In the latter case we usually imply that we deal with two, three, and greater number of phases of media, where under word phase we understand set of regions with the common partial conductivities—$\sigma_1, \sigma_2, \ldots$.

There exist a huge number of different models of two-phased systems. For example, in some models it is assumed that there is set of spherical inclusions in host matrix. In more sophisticated models spherical shape is replaced by others shapes, ellipsoidal, for instance. In these cases one may introduce the distribution of the axial sizes of these ellipsoids, different characteristics of sizes of inclusions, different conductivities, etc. (see Fig. 1.1).

Effective kinetic coefficients correspond to the basic properties of transport processes in macroscopically disordered systems. They provide a global characterization of the inhomogeneous medium and describe basic physics due to typical sizes much larger compared to sizes of inhomogeneity of macroscopic deviations. In fact there are two fundamentally different treatments: in the former we assume the knowledge of local kinetic coefficients and we call it deterministic, in the latter

A.A. Snarskii et al., *Transport Processes in Macroscopically Disordered Media*, DOI 10.1007/978-1-4419-8291-9_1

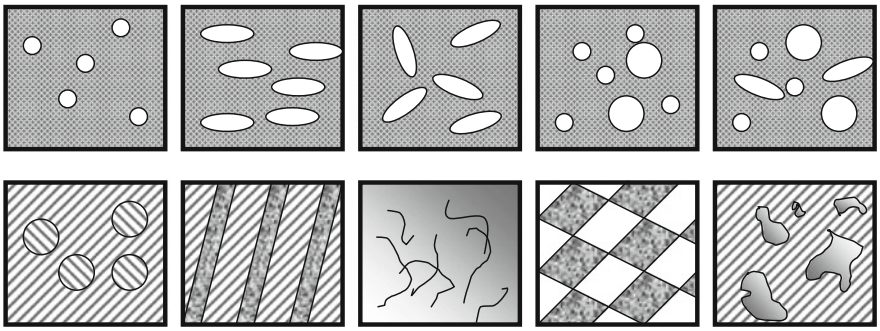

Fig. 1.1 Schematic representation of different disordered media: *Upper row*–one phase inclusions (*white area*) into the matrix; *lower row*—three pictures on the *left* show possible anisotropic inclusions

we know only them as random fields and we call it statistical one. Each of these treatments possesses their advantages and disadvantages. The deterministic treatment is usually applied for media with relatively simple structure; in the case of stochastic one we may experience definite difficulties with correlation between statistical description and physical observation of randomized disordered behavior of the kinetic coefficients. When one is trying to rigorously apply stochastic description he has to split original problem into two; first, estimation of kinetic coefficients at fixed dependence of local kinetic coefficients and only later should average over different realizations (ensembles). Effective kinetic coefficients, estimated at the first stage, always depend on concrete realization of local kinetic coefficients, though "… we always expect in correctly formulated theory the appearance of some kind of self-averaging, but, on the other hand, the theory as well as experiment deal with a sample of a certain realization" [3].

In what follows, we will always consider the self-averaging effective kinetic coefficients such as functionals of local kinetic coefficients, so that when sending the value of the volume of averaging to positive infinity, they approach the non-random limiting values. The process of self-averaging quantities has been extensively investigated in the quantum theory of random systems (see Chap. 2). There exists a very deep analogy between self-averaging in the quantum theory of random systems and the problems of foundations of classical statistical mechanics [2]. In fact one can see a very illuminating table in [1], where this analogy is traced rather directly. Following this example, we can supplement this idea with yet another Table (1.1) with data of local transport coefficients. Averages over volume of the field and the self-averaged currents do coincide with subsequent averages over all the realizations of random fields of local kinetic coefficients. Proceeding this way, one eventually needs only one concrete realization to determine effective unique set of kinetic coefficients.

Table 1.1 Correspondence between physical theories

Statistical mechanics	Theory of random systems	Macroscopically disordered medium
Phase space—space of points $\{p, q\}$, where p и q—sets of moments and coordinates	Space of functions $U(\mathbf{r})$, where $U(\mathbf{r})$—random potential, where carriers move	Space of functions like local kinetic coefficients, for instance local kinetic coefficients, such as local conductivity $\sigma(\mathbf{r})$
Any non-averaged physical function $f(p, q)$	Any non-averaged physical functional $A = A[U(\mathbf{r})]$	Fluxes and fields, for example $\mathbf{j} = \mathbf{j}[\sigma(\mathbf{r})]$ и $\mathbf{E} = \mathbf{E}[\sigma(\mathbf{r})]$
Time average corresponds to physical characteristics	Volume average corresponds to physical characteristics	Volume average corresponds to physical characteristics
Ergodic hypothesis: time average coincides with ensemble average	Ergodic hypothesis: average over volume coincides with mean over all random field realizations	Averaged fluxes and fields coincide with mean realizations of random fields of local kinetics

1.2 Classification of Physical Properties. Physical Analogies

Seemingly, a great number of different geometries signify the main difficulty in our ability of evaluation of the effective kinetic coefficients as functions of concentrations and their distribution. One unifying picture has never emerged. Situation is rather delicate and even there is not a simple answer to whether effective properties have to be anisotropic or not. We have to mention that no one ever suggested exhaustive complete classification of possible geometric phases. However, for each individual case such a description does exist; for example, two-phase systems with spherically shaped inclusions with known distribution function of different diameters. Of course, there exist much more sophisticated models of more complicated structures, for instance, those ones which include the information about macro- and micro-imperfections while their characteristic sizes could be bigger, equal, or smaller than mean free path and even more complicated ones.

Up to this point, we have mainly mentioned as an example of effective kinetic coefficients only effective electric conductivity, i.e., only for electric conduction in random media. However, many other kinetic processes, such as heat conduction, for instance, up to notational difference are very similar in their nature and could be treated accordingly (Table 1.2). Of course, we can mention problems of very different physical phenomena such as evaluation of elastic properties of random media, where a very different treatment is required.

Table 1.2 Different physical phenomena

Physical phenomena	Thermodynamic flux and equation, which describes it in stationary	Thermodynamic force and equation which describes it in stationary case	Law of physics
Electrical conductivity	$\mathbf{j}$, $\operatorname{div}\mathbf{j}=0$	$\mathbf{E}$, $\operatorname{curl}\mathbf{E}=0$	Ohm's law $\mathbf{j}=\sigma\mathbf{E}$
Thermal conductivity	$\mathbf{q}$, $\operatorname{div}\mathbf{q}=0$	$\mathbf{g}=-\nabla T$, $\operatorname{curl}\mathbf{g}=0$	Fourier's law $\mathbf{q}=\kappa\mathbf{g}$
Diffusion	$\mathbf{p}$, $\operatorname{div}\mathbf{p}=0$	$\mathbf{s}=-\nabla T$, $\operatorname{curl}\mathbf{s}=0$	Fick's law $\mathbf{p}=\kappa\mathbf{s}$

$\mathbf{j}$—electric current density, $\mathbf{E}$—electric field, $\mathbf{q}$—density of heat flow, $\mathbf{g}=-\nabla T$—temperature gradient, $\mathbf{p}$—density of flux of particles, $\mathbf{s}=-\nabla n$—gradient of number density

It is a rather surprising fact that there exists a whole family of problems of finding effective properties of the media with the macroscopic disorder which can be effectively reduced to above-mentioned technique. For Instance, the problem of high-temperature hopping conductivity in doped semiconductor is such a problem (Chap. 8).

References

1. Bonch-Bruevich V, Zvagin I, Kiper R et al (1981) Electronic theory of inhomogeneous semiconductors. Nauka, p 384 (in Russian)
2. Lifshits IM, Gredeskul SA, Pastur LA (1988) Introduction to the theory of disordered systems. Wiley, New York, p 462
3. Volovik GE, Dzyaloshinskiĭ IE (1978) Additional localized degrees of freedom in spin glasses. Sov Phys JETP 48:555–559

Chapter 2
The Methods of Description of Random Media

2.1 Effective Kinetic Coefficients, or What Do We Measure

In order to make an illustration of the description of a macroscopically random medium let us consider a sample, consistent mainly of some homogeneous material, which includes also one or two inclusions of another material and having simple geometric shape. One can solve the problem of spatial distribution, for example, of electric field in this sample exactly. If we consider sufficiently large number of inclusions and/or if they are randomly distributed, then we find that problem usually cannot be solved analytically and even numerically. Though, in many cases we do not even need to look for exact solution. In fact, we often are not even interested in detailed solution simply because typically in experiment we can measure only some averaged characteristics, such number densities of inclusions, their shapes, geometries, and sizes.

There exist media, for which, in many practical cases, one can obtain sufficient description. They are so-called uniform in mean. If one looks at sufficiently large samples of this medium, he finds their properties to be close to each other (Fig. 2.1).

Let us clarify the meaning of uniform in mean medium by the example of electrical conductivity in inhomogeneous electric conducting media. Suppose a local Ohm's law is valid, and thus $\mathbf{E}(\mathbf{r}) = \rho(\mathbf{r}) \cdot \mathbf{j}(\mathbf{r})$, where $\mathbf{E}(\mathbf{r})$—electric field, $\mathbf{j}(\mathbf{r})$—current density, and $\rho(\mathbf{r})$—local resistivity. Resistances of above mentioned pieces will be same even though their special orientations in each sample will be different. Figure 2.2 depicts measurement of resistance in such sample.

This resistance is a functional on $\mathbf{j}(\mathbf{r})$ and $\mathbf{E}(\mathbf{r})$:

$$R = R[\mathbf{j}(\mathbf{r}), \mathbf{E}(\mathbf{r})]. \tag{2.1.1}$$

Let us pick an electric resistivity which we will call as ρ_e, such that the total resistance of the same shape and size of homogeneous conductor R_e would be equal R, Fig. 2.3. This medium might be called medium of comparison.

A.A. Snarskii et al., *Transport Processes in Macroscopically Disordered Media*, DOI 10.1007/978-1-4419-8291-9_2

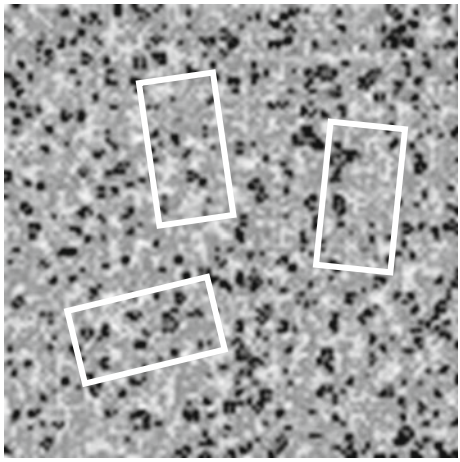

Fig. 2.1 Microscopically inhomogeneous medium. Shown are microscopically different samples of medium, with the same characteristics

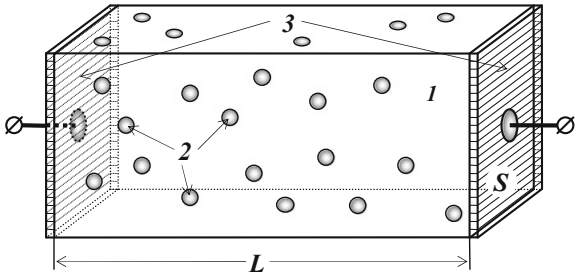

Fig. 2.2 Measuring resistance of the sample of the uniform in mean. *1*, *2*—phases making up the medium, *3*—pieces of contact ($\rho_3 \ll \rho_{1,2}$)

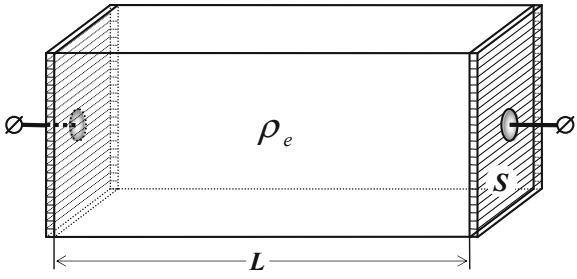

Fig. 2.3 A sample of the medium of comparison, which coincides with the similar sample of the chosen inhomogeneous media

Simple analysis shows, that ρ_e—coefficient of proportionality between $\langle \mathbf{E} \rangle$ and average current density

$$\langle \mathbf{E} \rangle = \rho_e \langle \mathbf{j} \rangle, \tag{2.1.2}$$

Indeed, for the sample of the length L and cross-sectional area S while $\langle \mathbf{E} \rangle \parallel \langle \mathbf{j} \rangle$ one can write (we skip here obvious vector notation)

$$\langle E\rangle L = \rho_e L(\langle j\rangle S/S),$$

Thus voltage $U = \langle E\rangle L$ and current $I = \langle j\rangle S$ are related through following formula

$$U = (\rho_e L/S)I,$$

In the other words, we obtain the well-known relationship for a resistance of a sample, measured in typical experiment

$$R_e = \rho_e L/S, \tag{2.1.3}$$

We give here the definition of macroscopically inhomogeneous medium. It is a medium where the characteristic size of inhomogeneity a_0 is much larger than any typical physical characteristics ℓ, for instance, mean-free-path of electric charge. We express this fact by writing the following inequalities

$$\sqrt[3]{V} \gg a_o \gg \ell, \tag{2.1.4}$$

where $\sqrt[3]{V}$—characteristic size of the sample. One can introduce for macroscopically inhomogeneous medium the function $\rho(\mathbf{r})$—local conductivity, thus fulfilling relation

$$\mathbf{E}(\mathbf{r}) = \rho(\mathbf{r})\mathbf{j}(\mathbf{r}),$$

Introduced earlier in (2.1.2) effective kinetic coefficient ρ_e is called by "effective resistivity of the composite medium". Generally speaking, ρ_e and $\langle\rho\rangle$ do not coincide. They are same in the obvious case of flat-layered medium. One can instead of using ρ_e—resistivity, utilize σ_e—effective conductivity, which effectively connects averaged over volume values of fields and currents

$$\langle\mathbf{j}\rangle = \sigma_e\langle\mathbf{E}\rangle, \quad \sigma_e = 1/\rho_e. \tag{2.1.5}$$

In complete analogy one can speak of the other effective kinetic coefficients (EKC) such as: thermal conductivity, thermo-EMF, Young modulus, etc.

$$\langle\mathbf{q}\rangle = -\kappa_e\langle\nabla T\rangle, \tag{2.1.6}$$

$$\langle\mathbf{j}\rangle = -\sigma_e\langle\nabla\xi\rangle - \sigma_e\alpha_e\langle\nabla T\rangle, \tag{2.1.7}$$

where κ_e—EKC of thermal conductivity, σ_e and α_e—EKC of conductivity and thermo-EMF.

It is worthy mentioning EKC, which is different from their specific characteristics of subsequent homogeneous ones. In Fig. 2.4 we show the medium with elongated longitudinally inclusions. Even though locally medium is isotropic effective resistivity is a second rank tensor.

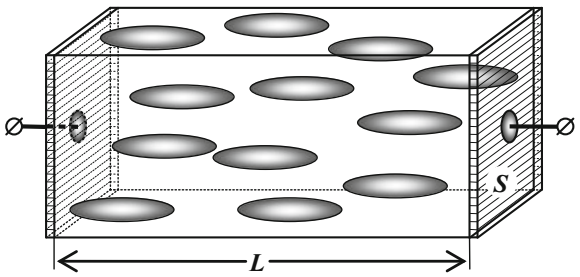

Fig. 2.4 Inhomogeneous medium with elongated longitudinal inclusions

$$\rho = \rho(\mathbf{r}) = \begin{cases} \rho_1, \mathbf{r} \in O_1, \\ \rho_2, \mathbf{r} \in O_2, \end{cases} \tag{2.1.8}$$

Introduction of EKC is connected to the idea that as long as we are able to find them, we are in position to calculate many integral properties of the concrete samples of the medium, for instance, resistance of a sample with arbitrary geometry and connect it to an experimental value.

In some cases EKC could be defined slightly differently, for instance, for $\hat{\sigma}_e$ we can define

$$\hat{\sigma}_e = \frac{\langle \sigma(\mathbf{r})\mathbf{E}^2(\mathbf{r}) \rangle}{\langle \mathbf{E}(\mathbf{r}) \rangle^2}, \tag{2.1.9}$$

This expression immediately follows from (for example [3])

$$\langle \mathbf{E}\mathbf{j} \rangle = \langle \mathbf{E} \rangle \langle \mathbf{j} \rangle, \tag{2.1.10}$$

which is correct provided that we completely neglect boundary effects. Indeed, substituting in left hand side of formula (2.1.10) expression for current density $\mathbf{j} = \sigma\mathbf{E}$, and using in right hand side the fact, that (2.1.5) $\langle \mathbf{j} \rangle = \sigma_e \langle \mathbf{E} \rangle$ we obtain (2.1.9), arriving at a reasonable result that the effective conductivity could be understood as a normalized averaged Joule heat production.

The validity of (2.1.10) (detailed discussion and generalization of (2.1.10) see in [1] could be understood in the following simplified way. Writing the expression for an effective electric field in the following form

$$\mathbf{E}(\mathbf{r}) = \langle \mathbf{E} \rangle - \nabla\varphi(\mathbf{r}), \tag{2.1.11}$$

where potential $\varphi(\mathbf{r})$ corresponds to the field, scattered by inhomogeneities

$$\langle \nabla\varphi(\mathbf{r}) \rangle = 0.$$

The difference between left and right hand sides in (2.1.11) could be transformed into surface integration

$$\langle \mathbf{Ej} \rangle - \langle \mathbf{E} \rangle \langle \mathbf{j} \rangle = \frac{1}{V} \int \mathbf{Ej} \, \mathrm{d}V - \langle \mathbf{E} \rangle \langle \mathbf{j} \rangle = \frac{1}{V} \int \langle \mathbf{E} \rangle \mathbf{j} \, \mathrm{d}V - \langle \mathbf{E} \rangle \langle \mathbf{j} \rangle - \frac{1}{V} \int \nabla \varphi \mathbf{j} \, \mathrm{d}V.$$

First two terms cancel, and the third one yields with the help of $\mathrm{div}\mathbf{j} = 0$ following result:

$$\frac{1}{V} \int \nabla \varphi \mathbf{j} \, \mathrm{d}V = \frac{1}{V} \int \nabla (\varphi \mathbf{j}) \, \mathrm{d}V = \frac{1}{V} \int \varphi \mathbf{j} \, \mathrm{d}\mathbf{S}, \tag{2.1.12}$$

which vanishes in the limit $V \to \infty$.

Vanishing of the surface integral in (2.1.12) can be achieved in samples of finite sizes by appropriate boundary conditions and distribution of phases

2.2 Correlation Length and Self-averaging

So far we always assumed that EKC's could be uniquely introduced, if the characteristic length of the sample is large enough. Now we will suggest more rigorous definition of "large enough characteristic size". For this purpose we will introduce correlation length ξ, or correlation radius.

Let $\varphi(\mathbf{r})$—some random physical field, and $\rho(\varphi, \mathbf{r})\mathrm{d}\varphi$ is a probability to find values of φ in interval $(\varphi; \varphi + \Delta\varphi)$ around $\mathbf{r}$. Ergodic hypothesis is the statement that expectation value of a random process can be done as an ensemble integration

$$\langle \varphi \rangle = \frac{1}{V} \int \varphi(\mathbf{r}) \, \mathrm{d}\mathbf{r} = \int \varphi \rho(\varphi) \, \mathrm{d}\varphi. \tag{2.2.1}$$

We use S-point moment, and S-point function, or distribution $P_s(\varphi_1, \mathbf{r}_1; \varphi_2, \mathbf{r}_2; \ldots; \varphi_s, \mathbf{r}_s)$. If $S = 2$, and using assumption that random field is homogeneous and isotropic we have

$$P_2(\varphi_1, \mathbf{r}_1; \varphi_2, \mathbf{r}_2) \equiv P_2(\varphi_1, \varphi_2; r), \tag{2.2.2}$$

where $r = |\mathbf{r}_2 - \mathbf{r}_1|$. This function posses following limited boundary properties:

$$P_2(\varphi_1, \varphi_2; r) \to \begin{cases} \delta(\varphi_1 - \varphi_2)\rho(\varphi_1, \varphi_2), & r \to 0, \\ \rho(\varphi_1) \cdot \rho(\varphi_2), & r \to \infty. \end{cases}$$

Introducing autocorrelation function

$$\Gamma(r) = \frac{\langle \varphi(0)\varphi(\mathbf{r})\rangle}{\langle \varphi^2\rangle} \equiv \frac{\int \varphi_1\varphi_2 P_2(\varphi_1,\varphi_2,r)\ \mathrm{d}\varphi_1\mathrm{d}\varphi_2}{\int |\varphi^2|\rho(\varphi)\ \mathrm{d}\varphi}, \tag{2.2.3}$$

then

$$\Gamma(r) \to \begin{cases} 1, & r \to 0, \\ 0, & r \to \infty. \end{cases}$$

According to [5] one may define the correlation length and similar different areas of continuous random field $\varphi(\mathbf{r})$, as its characteristic topological signature, or the typical spacial size

$$\xi^2 = \frac{\int r^2\Gamma(r)\ \mathrm{d}^3 r}{\int \Gamma(r)\ \mathrm{d}^3 r}., \tag{2.2.4}$$

Relatively uniform medium, therefore, in addition to the sizes of different inclusions and distances among them ("microscopic" sizes), possesses yet another characteristic length ξ. Effective properties of the parts of media with sizes $L \gg \xi$ will be the same.

As it is well known, for the Gaussian random field [4, 5]

$$\Gamma(r) \sim \mathrm{e}^{-r/\xi}, \tag{2.2.5}$$

As the appropriate example we will again consider a conducting medium. Uniqueness of σ_e requires, that the average values $\langle \mathbf{j}\rangle$ and $\langle \mathbf{E}\rangle$ in the relationship $\langle \mathbf{j}\rangle = \sigma_\mathrm{e}\langle \mathbf{E}\rangle$ would not depend on the location, where we choose a sample or on random realization of different conducting phases. Condition (2.2.1) signifies the fact that the correlation among their distribution is rather weak. This example will also serve as an indicator of the property which we call self-averaging [2]. We define it in the following way. For arbitrary realization ω of the random $\sigma(r)$ there exists a unique value of σ_e, such that $\langle \mathbf{j}\rangle_\omega = \sigma_\mathrm{e}\langle \mathbf{E}\rangle_\omega$. In other words, σ_e does not depend on ω, and averaging over volume coincides with averaging over ensemble of different realizations (ergodic hypothesis)

References

1. Balagurov BY (1987) Galvanomagnetic properties of inhomogeneous media in a weak magnetic field Sov. Phys JETP 66:1079–1087
2. Bonch-Bruevich V, Zvagin I, Kiper R (1981) Electronic theory of inhomogeneous semiconductors Nauka, M, 384 p (in Russian)
3. Dykhne AM (1970) Contluctivity of a two-dimensional two-phase system Sov. Phys JETP 32:63–64

4. Monin AC, Yaglom AM (1965) Statistical hydromechanics, v.1 Nauka, Moscow 640 p (in Russian)
5. Ziman JM (1979) Models of disorder: the theoretical physics of homogeneously disordered systems. Cambridge University Press, London, 538 p

Chapter 3
Effective Conductivity of Macroscopically Disordered Media

3.1 Double-Sided Estimates of the Effective Kinetic Coefficients

Let us ask a question: what can be learned of the effective kinetic coefficient, if very little is known about the medium characteristics. After all, even for an approximate determination of the effective kinetic coefficient one should have some information on the medium, the concentration of inclusions, their shape, mutual arrangement, etc. It appears that there exists a certain minimum of information that allows obtaining double-sided estimates of the effective kinetic coefficient value which are often referred to as "bounds." Using additional information on the characteristics of medium, the "bounds" can be narrowed, specifying possible bounds of the effective kinetic coefficient, i.e., the larger information is taken into account, the narrower are the "bounds."

Consider double-sided restrictions on the effective kinetic coefficients by an example of the effective conductivity σ_e of a double-phase medium with conductivities of its component phases σ_1 and σ_2. For certainty, we will assume $\sigma_1 > \sigma_2$. Evidently, the simplest and at the same time the widest bounds of σ_e will be governed by inequalities

$$\sigma_2 \leq \sigma_e \leq \sigma_1, \tag{3.1.1}$$

which means that σ_e cannot be larger than maximum conductivity of medium $\sigma_{max} = \sigma_1$ and smaller than minimum $\sigma_{min} = \sigma_2$. The second in complexity and, naturally, a narrower "bound" can be obtained using additional information on the medium, for instance, phase concentration.

Consider a case in Fig. 3.1a with alternation of parallel layers of different phases. We will average the expression $j_x = \sigma(y)E_x$ (direction of axes is evident from Fig. 3.1)

A.A. Snarskii et al., *Transport Processes in Macroscopically Disordered Media*, DOI 10.1007/978-1-4419-8291-9_3

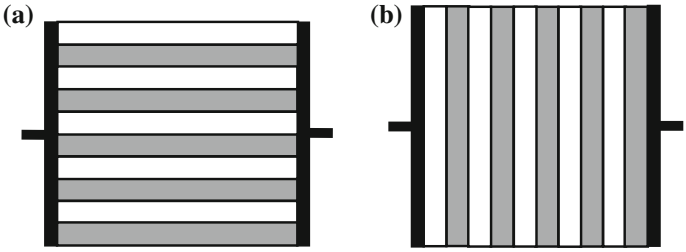

Fig. 3.1 Examples of phase arrangements whereby sample conductivity: **a** is maximum $\sigma_{\max} = \sigma_{[|}$; **b** is minimum $\sigma_{\min} = \sigma_{\perp}$

$$\left\langle \frac{1}{\sigma(y)} j_{\mathrm{x}} \right\rangle = \left\langle \frac{1}{\sigma} \right\rangle j_x = \langle E_x \rangle, \quad \text{whence} \langle j_{\mathrm{x}} \rangle = \left\langle \frac{1}{\sigma} \right\rangle^{-1} \langle E_x \rangle.$$

Besides, $\langle j_x \rangle = \sigma_{\perp}^{\mathrm{e}} \langle E_x \rangle$. Comparing these values, we find $\sigma_{\perp} = \langle 1/\sigma \rangle^{-1}$. In a similar way one can find $\sigma_{||} = \langle \sigma \rangle$, here $\sigma_{\perp}$ and $\sigma_{||}$ are components of the effective conductivity tensor along and across the layers

$$\hat{\sigma}_{\mathrm{e}} = \begin{pmatrix} \sigma_{||} & 0 \\ 0 & \sigma_{\perp} \end{pmatrix}. \tag{3.1.2}$$

In this case $\langle \sigma \rangle = p\sigma_1 + (1-p)\sigma_2$, and $\langle \sigma^{-1} \rangle = p/\sigma_1 + (1-p)/\sigma_2$, where p is phase concentration σ_1. Whence

$$\langle \sigma^{-1} \rangle^{-1} = \frac{\sigma_1 \sigma_2}{p\sigma_2 + (1-p)\sigma_1} \leq \sigma_{\mathrm{e}} \leq p\sigma_1 + (1-p)\sigma_2 = \langle \sigma \rangle \tag{3.1.3}$$

Inequalities (3.1.3) were first established by Wiener. The left boundary value was found by Voigt, the right—by Reis. Note that for the average isotropic medium the achievement of bounds (3.1.3) is impossible.

The general concept of derivation of double-sided estimates is based on the existence of principle of functional minimum equal in the case of conducting medium to energy dissipation (the Joule heat release):

$$\Phi = \int_V (\mathbf{Ej}) \mathrm{d}V. \tag{3.1.4}$$

In the stationary case $E = -\nabla\varphi$ and, as can be easily shown, from functional minimum (3.1.4) there follows $\operatorname{div} \mathbf{j} = 0$. Indeed, writing down (3.1.4) as

$$\Phi[\sigma, \nabla\varphi] = \int F(\sigma, \nabla\varphi) \mathrm{d}V, F = \sigma(\nabla\varphi)^2, \tag{3.1.5}$$

from the Euler's equation for F

$$\sum_k \frac{\partial}{\partial x_k} \frac{\partial F}{\partial \left(\frac{\partial \varphi}{\partial x_k}\right)} - \frac{\partial F}{\partial \varphi} = 0, \tag{3.1.6}$$

we obtain at once $\operatorname{div} \mathbf{j} = 0$, i.e., those distributions of fields $\mathbf{E}(\mathbf{r})$ and currents $\mathbf{j}(\mathbf{r})$ which satisfy Maxwell's equations and assign minimum to functional Φ (3.1.4). Hence follows a general concept of constructing two-sided estimates—selection from different physical considerations of functions $\mathbf{j}(\mathbf{r})$ and $\mathbf{E}(\mathbf{r})$ (they are called "trial"), so that $\Phi[\sigma, \nabla\varphi]$ (3.1.4) be as low as possible. The application of a variational principle to construction of double-sided estimates (in particular, generalization for the anisotropic case) is given in [6], see also [3], Chap. 6.

Now we derive the relation (3.1.3) in a more general form. For this purpose we will use the previously obtained relation $\langle \mathbf{E} \cdot \mathbf{j} \rangle = \langle \mathbf{E} \rangle \cdot \langle \mathbf{j} \rangle$ (see paragraph 2.1). Taking into account that the average $(\mathbf{E} \cdot \mathbf{j})$ has a minimum on the true values of field $\mathbf{E}$ and assuming the values $\langle \mathbf{E} \rangle$ and $\langle \mathbf{j} \rangle$ as trial values of $\mathbf{E}$ and $\mathbf{j}$, we obtain

$$\langle \mathbf{E}\mathbf{j} \rangle = \langle \mathbf{E} \rangle \langle \mathbf{j} \rangle = \sigma_e \langle \mathbf{E} \rangle^2 = \langle \sigma \mathbf{E}^2 \rangle \leq \langle \sigma \rangle \langle \mathbf{E} \rangle^2, \tag{3.1.7}$$

$$\langle \mathbf{E}\mathbf{j} \rangle = \frac{1}{\sigma_e} \langle \mathbf{j} \rangle^2 = \left\langle \frac{1}{\sigma} \mathbf{j}^2 \right\rangle \leq \left\langle \frac{1}{\sigma} \right\rangle \langle \mathbf{j} \rangle^2. \tag{3.1.8}$$

Hence we find the final relation

$$\left\langle \sigma^{-1} \right\rangle^{-1} \leq \sigma_e \leq \langle \sigma \rangle. \tag{3.1.9}$$

The next in complexity and even narrower "bound" can be obtained for the average isotropic medium. Note that the inequalities (3.1.3) describe in the general case the anisotropic medium, when $\hat{\sigma}_e$ is a tensor. Estimates of σ_e for the isotropic medium are called Hashin–Shtrikman "bounds" [12, 13]. To obtain them, one employs a generalized variational principle and finds for σ_e narrower bounds than those given by the relations (3.1.3). A detailed derivation can be found in the work [32]. In particular, for the two-phase material these bounds are determined by inequalities (at $\sigma_1 > \sigma_2$)

$$\sigma_2 + \frac{p}{1/(\sigma_1 - \sigma_2) + (1-p)/3\sigma_2} \leq \sigma_e \leq \sigma_1 + \frac{1-p}{1/(\sigma_2 - \sigma_1) + p/3\sigma_1}. \tag{3.1.10}$$

Hashin and Shtrikman showed that the bounds (3.1.10) cannot be improved, if phase concentrations p are assigned. Figure 3.2 shows the region of "borders" for different σ_1 and σ_2 values. The "borders" "work" well at low values of $\frac{\sigma_1}{\sigma_2}$ ratio, at large $\frac{\sigma_1}{\sigma_2}$ values the double-sided restrictions are practically useless.

In the construction of "borders" one can use a more detailed information on the composite than phase concentration and medium isotropy, for instance, information

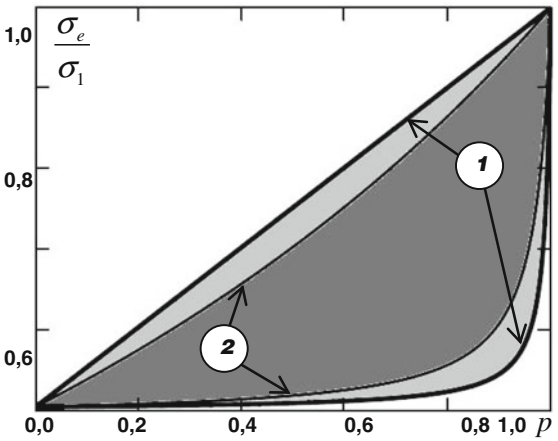

Fig. 3.2 Double-sided restrictions for conductivity: *1* "bound" (3.1.9); *2* Hashin–Shtrikman "bound" (3.1.10)

on the geometry of phase arrangement or the data on three-point correlation function. A review of the respective results is given in [3, 14]. The above-considered variational principle can be extended to the problems of magnetostatics, which allows finding double-sided restrictions for the magnetic field energy and the induction of multicomponent materials [15]. For the case of complex values of phase conductivity (quasi-harmonic case of conductivity on the alternating current) one can also construct the respective "borders" [4, 10]. Their construction is based on the assumption of analyticity of complex conductivity functions.

3.2 Approximations of Maxwell, Garnett, and Bruggeman

The Maxwell approximation. The Maxwell approximation is based on the assumption that concentration of inclusions of one of the phases is low and the inclusions have a correct compact shape, for instance, spherical. Contrary instance is "metal" net in dielectric medium. The conducting phase concentration is low and at the same time the inclusions are not compact.

One can obtain σ_e in the analytical form in the Maxwell approximation only for inclusions of certain shape. The general view of such a shape is a three-axial ellipsoid. Under low concentration is understood such concentration of inclusions $(p \ll 1)$ whereby the effect of one inclusion on the other (neighboring) can be neglected. It means that the problem of distribution of fields and currents can be solved for the case of a single inclusion. The analytical solution of such problem for ellipsoid is well known. Note that the field inside the inclusion in this case proves to be homogeneous. This fact allows finding a good approximation for the effective conductivity in the nonlinear case as well.

Let us consider first the case of spherical inclusions. Let p be concentration of good conducting phase of conductivity σ_1 (for instance, inclusions) in a medium of

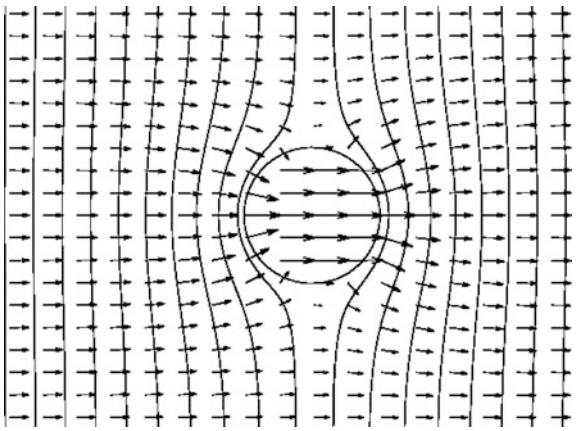

Fig. 3.3 View of equipotential lines and the direction of current density vectors for a secluded cylinder inclusion

conductivity σ_2. As an example, Fig. 3.3 shows current distribution around the cylinder inclusion in a two-dimensional case.

On the infinity, field $\mathbf{E}_\infty$ is finite and for the secluded inclusion coincides with $\langle \mathbf{E} \rangle$. The field inside the inclusion is given by solving stationary electrodynamics equations [18]

$$\mathbf{E}_1 = \frac{3\sigma_2}{2\sigma_2 + \sigma_1} \langle \mathbf{E} \rangle, \tag{3.2.1}$$

and, as is evident from (3.2.1), is coordinate independent. Subsequent derivation of expression for σ_e can be done by several methods interesting in that they yield qualitatively different results. Let us consider the average $\langle \mathbf{j} - \sigma_2 \mathbf{E} \rangle$. On the one hand

$$\langle \mathbf{j} - \sigma_2 \mathbf{E} \rangle = \langle \mathbf{j} \rangle - \langle \sigma_2 \mathbf{E} \rangle = (\sigma_e - \sigma_2) \langle \mathbf{E} \rangle, \tag{3.2.2}$$

on the other hand

$$\begin{aligned} \langle \mathbf{j} - \sigma_2 \mathbf{E} \rangle &= \frac{1}{V} \int (\mathbf{j} - \sigma_2 \mathbf{E}) \mathrm{d}V = \frac{1}{V} \int (\sigma \mathbf{E} - \sigma_2 \mathbf{E}) \mathrm{d}V \\ &= \frac{V_1}{V} (\sigma_1 - \sigma_2) \mathbf{E}_1 = (\sigma_1 - \sigma_2) p \mathbf{E}_1, \end{aligned} \tag{3.2.3}$$

where V is medium volume, V_1 is first-phase volume, $p = V_1/V$.

Equating (3.2.2) and (3.2.3), we obtain

$$\sigma_{BW}^{e} = \sigma_2 \left(1 + 3p \frac{\sigma_1 - \sigma_2}{2\sigma_2 + \sigma_1} \right), \quad p \ll 1. \tag{3.2.4}$$

Here $\sigma_e \equiv \sigma^e_{BW}$ (BW—black in white)—"black" balls in a "white" medium. This is the usual designation of a conductive phase with conductivity σ_1 called "black" phase, in the phase with lower conductivity σ_2, which is called, respectively, "white" phase. Similarly, one can consider a case of low concentration $p_2 = 1 - p \ll 1$ of poorly conducting phase with conductivity σ_2

$$\sigma^e_{WB} = \sigma_1\left(1 + 3p_2\frac{\sigma_2 - \sigma_1}{2\sigma_1 + \sigma_2}\right) = \sigma_1\left(\frac{4\sigma_2 - \sigma_1}{2\sigma_1 + \sigma_2} + 3p\frac{\sigma_1 - \sigma_2}{2\sigma_1 + \sigma_2}\right). \tag{3.2.5}$$

Let us pass to another method of derivation of Maxwell's approximation that gives the expression for σ_e with a wider application area in terms of concentration. Now on the infinity we will not assign filed intensity, but current density $\mathbf{j}_\infty$ which for a secluded inclusion coincides with $\langle \mathbf{j} \rangle$. In so doing, instead of (3.2.1) there will occur $\mathbf{j}_1 = (3\sigma_1/2\sigma_2 + \sigma_1)\langle \mathbf{j} \rangle$. Let us consider the average $\langle \mathbf{E} - \rho_2 \mathbf{j} \rangle$, where $\rho_2 = 1/\sigma_2$ is resistivity of second medium. Repeating computations similar to (3.2.2)–(3.2.4), for the effective resistivity of medium ρ_e with phase inclusions with ρ_1 in phase with ρ_2 we obtain the expression

$$\rho^e_{BW} = \rho_2\left(1 - 3p\frac{\rho_2 - \rho_1}{2\rho_1 + \rho_2}\right), \tag{3.2.6}$$

where $p \ll 1$ is phase concentration with ρ_1. Taking into account that $\sigma_e = 1/\rho_e$, from (3.2.6) we find the relation

$$\sigma^e_{BW} = \frac{\sigma_2}{1 - 3p\frac{\sigma_1 - \sigma_2}{\sigma_1 + 2\sigma_2}}, \tag{3.2.7}$$

which on expansion in small parameter p (to an accuracy of a linear component) coincides with (3.2.4). As will be shown below, the expression (3.2.7) has a wider application area, in particular, includes a peculiarity related to percolation threshold.

Similar to relation (3.2.5), for $p_2 = 1 - p \ll 1$ one can write down

$$\rho^e_{WB} = \rho_1\left(1 - 3(1-p)\frac{\rho_1 - \rho_2}{\rho_1 + 2\rho_2}\right), \tag{3.2.8}$$

or

$$\sigma^e_{WB} = \frac{\sigma_1(\sigma_2 + 2\sigma_1)}{5\sigma_1 - 2\sigma_2 + 3p(\sigma_2 - \sigma_1)}. \tag{3.2.9}$$

Before we analyze the resulting expressions, let us consider the effective characteristics for other inclusion types. In the case when inclusions are ellipsoids with principal semiaxes a, b, c, to find σ_e one should know the field inside a separate inclusion. The field inside inclusions $\mathbf{E}_1$, as before, can be expressed through the average field $\langle \mathbf{E} \rangle$, but now these fields will be, generally speaking, noncollinear, i.e.,

$$\mathbf{E}_1 = \hat{\Omega}\langle \mathbf{E} \rangle. \tag{3.2.10}$$

If coordinate system is related to ellipsoid axes, tensor $\hat{\Omega}$ will assume the simplest, diagonal form

$$\hat{\Omega} = \begin{pmatrix} \Omega_{11} & 0 & 0 \\ 0 & \Omega_{22} & 0 \\ 0 & 0 & \Omega_{33} \end{pmatrix}, \quad \Omega_{ii} = \frac{\sigma_2}{\sigma_2 + (\sigma_1 - \sigma_2)n_i}, \quad i = x, y, z, \tag{3.2.11}$$

and values n_i that are called depolarization factors can be expressed through the elliptical integrals

$$n_x = \frac{abc}{2}\int_0^\infty \frac{\mathrm{d}s}{(s+a^2)R_s}, \quad n_y = \frac{abc}{2}\int_0^\infty \frac{\mathrm{d}s}{(s+b^2)R_s}, \quad n_z = \frac{abc}{2}\int_0^\infty \frac{\mathrm{d}s}{(s+c^2)R_s},$$
$$R_s = \sqrt{(s+a^2)(s+b^2)(s+c^2)}. \tag{3.2.12}$$

Knowing $\mathbf{E}_1$, we obtain the effective conductivity which in the general case is a tensor. If all the inclusions are coaxial, i.e., directions of the respective axes of different ellipsoids coincide, and their centers are located chaotically, then σ_e is a diagonal tensor

$$\sigma_\mathrm{e} = \begin{pmatrix} \sigma_{11} & 0 & 0 \\ 0 & \sigma_{22} & 0 \\ 0 & 0 & \sigma_{33} \end{pmatrix}, \tag{3.2.13}$$

where

$$\sigma_{ii}^\mathrm{e} = \sigma_2 + (\sigma_1 - \sigma_2)\Omega_{ii}p, \quad ii \to xx, yy, zz. \tag{3.2.14}$$

For some partial cases the integrals in (3.2.12) are taken in the explicit form. Thus, for the ball inclusions $n_x = n_y = n_z = 1/3$ and by means of formulae (3.2.11), (3.2.14), for instance, for σ_{xx}^e we obtain

$$\sigma_{xx}^\mathrm{e} = \frac{3\sigma_2^2(\sigma_1 - \sigma_2)p}{2\sigma_2 + \sigma_1},$$

in a similar way one can calculate other tensor components.

For cylinders with the axes along axis x $(a \to \infty)$

$$n_x = 0,\ n_y = n_z = 1/2 \quad \sigma^{e}_{xx} = \sigma_2 + (\sigma_1 - \sigma_2)p$$

For a prolate ellipsoid of revolution $(a > b = c)$

$$n_x = \frac{1-e^2}{e^3}(\operatorname{arth} e - e) \quad n_y = n_z = \frac{1-n_x}{2}, \quad e = \sqrt{1-(b/a)^2}.$$

For an oblate ellipsoid $(a = b > c)$

$$n_x = n_y = \frac{1-n_z}{2}, \quad n_z = \frac{1+e^2}{e^3}(e - \operatorname{arctg} e), \quad e = \sqrt{(a/c)^2 - 1}.$$

Garnett approximation. Under this approximation, moments induced by the external field on secluded inclusions are considered. Here one can do without "dipole" terminology and make calculations similarly to derivation of Maxwell's approximations, using distortions of electric potential created by secluded inclusions (Fig. 3.4), also referred to as scattered potential. Distortion of potential $\delta\varphi$ created by "black" ball (with conductivity σ_1) of radius a in a "white" medium (with conductivity σ_2) is of the form

$$\delta\varphi = \frac{\sigma_2 - \sigma_1}{2\sigma_2 + \sigma_1}\frac{a^3 \cos\theta}{r^2}|\langle \mathbf{E}\rangle|, \tag{3.2.15}$$

where $\delta\varphi$ is additional component in potential expansion for the case when the unperturbed potential part in the homogeneous medium is $\langle \mathbf{E}\rangle z$, and axis oz is directed along $\langle \mathbf{E}\rangle$

$$\varphi = -\langle \mathbf{E}\rangle z + \delta\varphi. \tag{3.2.16}$$

Consider now n "black" inclusions located in the sphere of radius b. The Garnett approximation is based on the assumption that inclusions create beyond the sphere a scattered potential $n\delta\varphi$. To obtain σ_e, let us introduce comparison medium, i.e.,

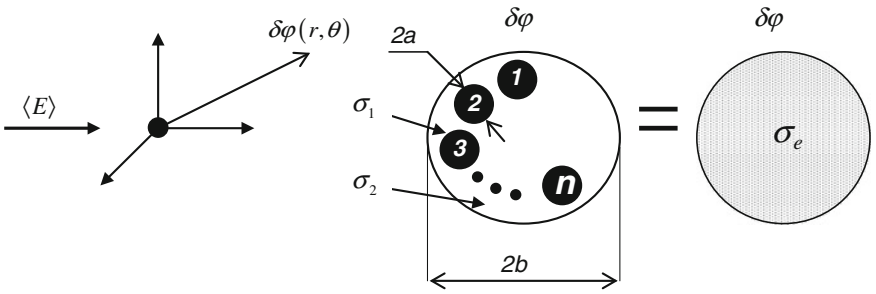

Fig. 3.4 Derivation of the Garnett approximation. The field on the infinity $\langle \mathbf{E}\rangle$ is directed along oz

assume that scattered potential created by n balls of radius a, is equal to scattered potential created by their comprising ball of radius b, provided that its conductivity is σ_e. In other words, $n\delta\varphi = \delta\varphi_e$, (see Fig. 3.4). Then

$$n\frac{\sigma_2-\sigma_1}{2\sigma_2+\sigma_1}\frac{a^3\cos\theta}{r^2}|\langle\mathbf{E}\rangle| = \frac{\sigma_2-\sigma_e}{2\sigma_2+\sigma_e}\frac{b^3\cos\theta}{r^2}|\langle\mathbf{E}\rangle|. \tag{3.2.17}$$

Hence, considering that concentration of "black" phase with conductivity σ_1 is $p = n(a/b)^3$, we obtain

$$\sigma^e_{BW} = \frac{\sigma_2(2\sigma_2+\sigma_1-2p(\sigma_2-\sigma_1))}{2\sigma_2+\sigma_1-p(\sigma_1-\sigma_2)}. \tag{3.2.18}$$

Similarly we also derive σ^e_{WB}, since $p_2 = 1-p$

$$\sigma^e_{WB} = \sigma_1\frac{3\sigma_2+2p(\sigma_2-\sigma_1)}{3\sigma_1-p(\sigma_1-\sigma_2)}. \tag{3.2.19}$$

Note that in the literature one can come across other terms (particularly as applied to dielectric media): "polarization," "polarization factor."

Approximation of self-consistent Bruggeman field. In the literature one can find different names of the Bruggeman approximation: effective medium theory (EMT), self-consistent field theory, Bruggeman–Landauer approximation, etc. This method was considered by many authors (see a review in [32]), to name but [5, 19, 21]. Many examples of using this method are given in the book [24], Chap. 6.

We will illustrate this approximation by an example of a medium with spherical inclusions. Let p is concentration of "black" inclusions, and σ_e is the effective conductivity of medium. Let us place into comparison medium with the effective conductivity σ_e N_1 inclusions with conductivity σ_1 and N_2—with conductivity σ_2, so that $N_1/N_2 = p/(1-p)$. The concentration of "black" and "white" phases in this case will not change, and the effective conductivity will remain the same. At the same time, each inclusion introduces field distortions

$$\delta\mathbf{E}_1 = \mathbf{E}_1 - \langle\mathbf{E}\rangle, \quad \delta\mathbf{E}_2 = \mathbf{E}_2 - \langle\mathbf{E}\rangle, \tag{3.2.20}$$

which we have already considered in the approximation of secluded inclusions

$$\delta\mathbf{E}_1 = \frac{\sigma_e-\sigma_1}{2\sigma_e+\sigma_1}\langle\mathbf{E}\rangle, \quad \delta\mathbf{E}_2 = \frac{\sigma_e-\sigma_2}{2\sigma_e+\sigma_2}\langle\mathbf{E}\rangle. \tag{3.2.21}$$

As long as the effective properties of medium are not changed, field distortions should compensate each other

$$p\delta\mathbf{E}_1 + (1-p)\delta\mathbf{E}_2 = 0, \tag{3.2.22}$$

exactly this is self-consistency condition.

Condition (3.2.22) can be approached otherwise, for instance, the average field is of the form

$$\langle\mathbf{E}\rangle = p\langle\mathbf{E}\rangle_1 + (1-p)\langle\mathbf{E}\rangle_2, \tag{3.2.23}$$

where $\langle\mathbf{E}\rangle_1$ and $\langle\mathbf{E}\rangle_2$ are the average fields in the "black" and "white" phases. Substituting (3.2.20) into (3.2.23), we again obtain self-consistency condition (3.2.22).

Substituting (3.2.21) into (3.2.22), we obtain equation for the determination of σ_e

$$\frac{\sigma_e - \sigma_1}{2\sigma_e + \sigma_1}p + \frac{\sigma_e - \sigma_2}{2\sigma_e + \sigma_2}(1-p) = 0, \tag{3.2.24}$$

whence we find the effective conductivity in EMT approximation

$$\sigma_e = \frac{1}{4}\left[(3p-1)\sigma_1 + (2-3p)\sigma_2 + \sqrt{[(3p-1)\sigma_1 + (2-3p)\sigma_2]^2 + 8\sigma_1\sigma_2}\right]. \tag{3.2.25}$$

Let us analyze in brief the concentration dependences of σ_e for different approximations. At low concentrations of inclusions with conductivity σ_1 $p \ll 1$ or with conductivity σ_2 $(1-p) \ll 1$ the above approximations are in good agreement with the numerical calculation.

So, there are four possible expressions for effective conductivity in approximations of "Maxwell" kind. In canonical Maxwell approximation the homogeneous electrical field is set at the infinity $\mathbf{E}_\infty$ and $\mathbf{E}_\infty = \langle\mathbf{E}\rangle$, as described in numerous monographs, books, and reviews. In this case for $p \ll 1$ effective conductivity of black inclusions in the white phase is described by (3.2.4). At the same time effective conductivity of white inclusions in the black phase at $p_2 = 1 - p \ll 1$ is described by (3.2.5). Border conditions could be different at the infinity: instead of electrical field ($\mathbf{E}_\infty$) it could be conditions for the current: $\mathbf{j}_\infty$ and $\mathbf{j}_\infty = \langle\mathbf{j}\rangle$. For these new border conditions a new expressions for effective conductivity are obtained: expression (3.2.7) for black inclusions in white media ($p \ll 1$) and for white inclusions in the black media (3.2.9). All four dependencies of effective conductivity σ_e and Bruggeman approximation are presented on the Fig. 3.5c. It is clear from Fig. 3.5c that canonical Maxwell approximation is a very good approximation for the case $p \ll 1$ (see 3.2.4) and it is a good fit for even not small values of concentrations p for black inclusions. However, for the opposite case of $p_2 = 1 - p \ll 1$ canonical Maxwell approximation (3.2.5) is much worse than approximation (3.2.9) [28].

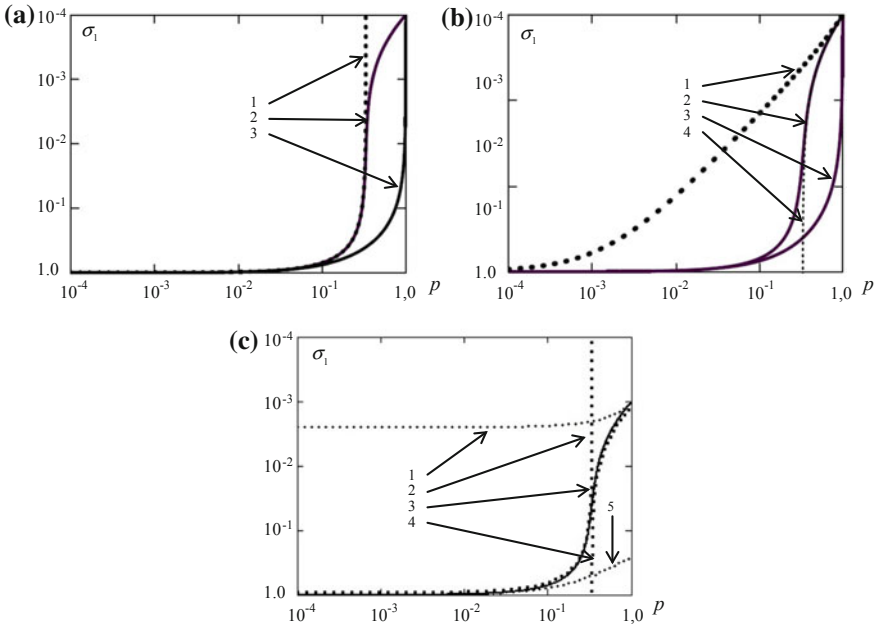

Fig. 3.5 Concentration dependences of the effective conductivity in various approximations: **a** *1* for the Maxwell approximation (3.2.7), *2* Garnett (3.2.18), *3* EMA (3.2.25), it is assumed here $\sigma_1 = 10,000, \sigma_2 = 1$ (in reference units); **b** *1*—for the Maxwell approximation (3.2.5), *2* Garnett (3.2.18), *3* Garnett (3.2.19), *4* EMA (3.2.25), it is assumed here $\sigma_1 = 1000, \sigma_2 = 1$ (in reference units); c -); **c** comparison of Bruggeman approximation—3 (*solid line*) and various Maxwell approximations: σ^e_{WB}(3.2.8)—*1*, σ^e_{BW}(3.2.7)—*2*, σ^e_{WB}(3.2.5)—*4* и σ^e_{BW}(3.2.5)—*5*

It would be useful to stress out two different facts. Approximation (3.2.5) could be obtained from (3.2.4) for small parameter $\sigma_2/\sigma_1 \ll 1$. And, to the contrary, the general approximation (9.2.9) could be obtained from less general (3.2.5) by using approximation Pade for (3.2.5) [28, 29].

Did Maxwell know about percolation threshold? [28] It is extremely surprising fact that the simplest dependence, namely that given by the Maxwell approximation, in the derivation of σ_e through ρ_e (3.2.7) (it can be called as derivation of the Maxwell approximation in ρ-representation) has a peculiarity at $p = \frac{1}{3}$ (percolation threshold). This peculiarity reflects qualitatively truly the really existing transition caused by the origination of infinite cluster—closed path of current flow. It should be noted that derivation of dependence of the Maxwell approximation in σ-representation is related to dependence in ρ-representation, the so-called Pade approximant [29]. Its meaning lies in the polynomial approximation by linear-fractional relation, allowing a good description of real peculiarities of physical dependences. Let us come back to the Maxwell approximation. In σ-representation we have

$$\sigma_{BW}^{\mathrm{e}} = \sigma_2\left(1+3p\frac{\sigma_1-\sigma_2}{2\sigma_2+\sigma_1}\right) = \sigma_2\left(1+3p\frac{1-h}{1+2h}\right) \approx \sigma_2(1+3p), h = \frac{\sigma_2}{\sigma_1} \ll 1, \tag{3.2.26}$$

and in ρ-representation

$$\sigma_{BW}^{\mathrm{e}} = \frac{\sigma_2}{1-3p\frac{\sigma_1-\sigma_2}{2\sigma_2+\sigma_1}} = \frac{\sigma_2}{1-3p\frac{1-h}{1+2h}} \approx \frac{\sigma_2}{1-3p}, h = \frac{\sigma_2}{\sigma_1} \ll 1. \tag{3.2.27}$$

It can be readily seen that in the first approximation in the expansion of σ_{BW}^{e} into a series about p these expressions coincide. However, the Maxwell approximation in ρ-representation (3.2.27) has a specific point wherein an abrupt transition (at $\sigma_1/\sigma_2 \gg 1$) from "dielectric" ($\sigma_{\mathrm{e}} \approx \sigma_2$) to "metal" ($\sigma_{\mathrm{e}} \approx \sigma_1$) behavior occurs (Fig. 3.5). Note that the Bruggeman approximation that "works" well everywhere except for the region close to peculiarity, in the vicinity of peculiarity itself does not coincide with the numerical calculation and the experiment. The region close to peculiarity-percolation threshold (in the approximations under study it is $p = 1/3$) is called critical. Its correct description calls for more complicated mathematical methods and the introduction of deeper representations than a secluded inclusion in the homogeneous external field. The respective research area has separated as so-called percolation theory (from the English "percolation"). The fact, that proposed approximation leads to the percolation threshold, not in any way diminish the importance of the percolation theory. Percolation theory, in addition to the percolation threshold, introduced new concepts such as critical behavior, critical indices, scaling, etc. So, the proper answer to the question in the title is negative: "No, he did not know, but he could have been." One could wonder whether Maxwell would have invented the percolation theory.

Generalizations of approximations described. Consider some generalizations of the approximations described. Up to now we have studied the case of a three-dimensional field (3D). One can find the respective relations in the two-dimensional case (2D). Since the Maxwell approximation is a partial case of the Bruggeman approximation, we will consider the Bruggeman approximation in more detail. The sought-for expression for the 2D case can be obtained by several methods.

1. Within the approach of a self-consistent field one can use the expressions [18]

$$\delta\mathbf{E}_1 = \frac{\sigma_{\mathrm{e}}-\sigma_1}{\sigma_{\mathrm{e}}+\sigma_1}\langle\mathbf{E}\rangle, \quad \delta\mathbf{E}_2 = \frac{\sigma_e-\sigma_2}{\sigma_e+\sigma_2}\langle\mathbf{E}\rangle, \tag{3.2.28}$$

and write down the self-consistency conditions similar to expression (3.2.22).

2. One can use the well known 3D solution for the ellipsoidal inclusions on condition that on the semiaxis $a = b$ and $c \to \infty$. In this case we obtain a set of coaxial cylinder inclusions having sections in the form of circles. The respective solutions represent the 2D case for circular inclusions. Both methods yield the same expression for conductivity σ_e, and self-consistency condition is of the form

$$\frac{\sigma_e - \sigma_1}{\sigma_e + \sigma_1} p + \frac{\sigma_e - \sigma_2}{\sigma_e + \sigma_2} (1 - p) = 0. \tag{3.2.29}$$

The self-consistency conditions can be generalized in one equation suitable for the cases of different dimensions d

$$\frac{\sigma_e - \sigma_1}{(d-1)\sigma_e + \sigma_1} p + \frac{\sigma_e - \sigma_2}{(d-1)\sigma_e + \sigma_2} (1 - p) = 0, \quad d = 1, 2, 3. \tag{3.2.30}$$

Equation (3.2.30) also covers the case $d = 1$ corresponding to conductivity σ_e of composite planar stratified medium. Certainly, in a real world, $d \leq 3$, but in percolation theory the calculation of critical behavior becomes particularly simple for the case $d = 6$ (critical dimension) and can be checked. The situation here is similar to the case of critical dimension $d = 4$ in the theory of second kind phase transitions [18].

The self-consistency condition is also easily generalized for the multiphase media. For instance, for spherical inclusions with conductivities $\sigma_1, \sigma_2, \ldots, \sigma_n$ and the respective concentrations $p_1, p_2, \ldots, p_n$(here, of course, $\sum_{i=1}^{n} p_i = 1$) we have

$$\sum_{i=1}^{n} p_i \frac{\sigma_i - \sigma_e}{\sigma_i + (d-1)\sigma_e} = 0. \tag{3.2.31}$$

Note that for $n > 4$, as is known, there is no general analytical finite expression for solving the expression (3.2.31).

We have already seen that the expression for σ_e in the Bruggeman approximation, just as the Maxwell approximation in ρ-representation, qualitatively describe percolation transition at $p = 1/3$. It is important that though, for instance, in a simple cubic lattice of bonds $p_c \approx 1/3$, in real two-phase composites p_c can have any values in the range $0 < p_c < 1$ [23]. In a modified EMT theory proposed in works [32] p. 188, [22] it is taken into account that close to p_c the concentration of conducting phase p in a local field becomes larger than volume average concentration.

3.3 Periodically Located Inclusions

With low concentrations of inclusions it is not essential whether the inclusions are distributed randomly or orderly, for instance, in periodic lattice nodes. The effective conductivity of such media can be described by means of continual models (secluded inclusion in the external field, see the Maxwell approximation in paragraph 3.2), like in the discrete variant, by introducing a network (random or periodical), see, for instance, "network" derivation of the EMT approximation by Kirkpatrick [17].

With large concentrations, the behavior of the effective conductivity for media with a random and periodic arrangement of inclusions differs considerably. It is already apparent from the qualitative considerations—with a random arrangement of good conducting inclusions in the poor conducting matrix with the inclusion concentration equal and larger than the threshold (p_c), in the medium there is a formed infinite path only along the good conducting phase. For inclusions arranged in cubic lattice sites such a path is created only at maximum possible concentration, when all inclusions will touch each other. Composite with a periodic or close to periodic arrangement of inclusions with large concentration values are called high-filled composites, they are widely used in practice. For instance, it is covered in publications dedicated to high-filled magnetic composites [9].

Investigation of media with periodic inclusions is interesting in many respects. For example, a model problem which in a number of cases can be solved exactly and as in comparison with the results of approximate methods to yield the applicability limits (the error) of the latter.

With large concentration values, there is a big difference between the media that can be described by discrete resistance networks and those for which such discretization is not permissible. With a medium simulation by a network composed of good ("black") and poor conducting ("white") resistances, the information on the shape of inclusions is lost completely. Moreover, concentration of inclusions can assume any value (between zero and unity). The network variant of the Bruggeman approximation gives the same expression for σ_e as the continual variant for spherical inclusions. And though it is clear that concentration of spherical inclusions cannot exceed certain value (depending on the arrangement of particles), such approximate results often agree well with the experiment (see, for instance [19, 20]) for a two-phase alloy, where the shape of phases is far from spherical.

However, in the cases when inclusions have spherical shape (or cylinder in 2D case) and their shape cannot be neglected, at large concentrations of inclusions the dependence of σ_e on concentration and the ratio $\frac{\sigma_2}{\sigma_1}$ will differ considerably from the EMT approximation. Among other things, it is related to the absence of symmetry between the "black" and "white," i.e., a medium with "black" spherical inclusions in a "white" matrix under no concentration will go over to a medium where "white" inclusions are in a "black" matrix. Besides, at large concentration values of inclusions when calculating σ_e the mutual effect of inclusions is essential. In the EMT it was assumed that each inclusion is in the external homogeneous field and

field distortions introduced by inclusions occur only in their own vicinity, whereas now, figuratively speaking, there is no place without distortions of the field.

There are possible at least two basically different cases of media with inclusions the shape of which is essential. First, these are the above-mentioned high-filled polymers with periodically located inclusions (or with close to periodic arrangement). Second, these are the so-called Swiss Cheese Media which are said to exhibit continual percolation [8, 11], and which will be considered below in Chap. 7.

We consider here the effective conductivity of a medium with a periodic arrangement of inclusions—the two-dimensional case—circular shaped inclusions. To emphasize the difference between σ_e obtained from EMT (or by numerical calculation on the two-phase lattice, which also gives concentration dependence σ_e) and σ_e for a medium with periodic inclusions, let us cite Fig. 3.6. Here each type (*BW* and *WB*) has its limiting concentration of inclusions when they touch each other—$p^*_{BW} = \pi/4$ and $p_{WB} = 1 - \pi/4$, the result of EMT coincides with the result of solving a problem with a periodic arrangement of inclusions.

In the works [30, 31] for the periodically arranged circular inclusions by means of physical simulation (dielectric inclusions were obtained by cutting holes in a conducting film) there was obtained concentration dependence σ^e_{WB}. In [1] the expression for σ^e is found in the form of a series quickly converging in concentration, or, which is the same (see Fig. 3.6), in the size parameter R/a. According to [1] for *WB*-medium the effective conductivity σ_e with an accuracy to 1 % can be presented as follows:

$$\sigma^e_{WB} = \sigma_1 \frac{\alpha - \frac{\pi R^2}{4a^2}\delta}{\alpha + \frac{\pi R^2}{4a^2}\delta}, \tag{3.3.1}$$

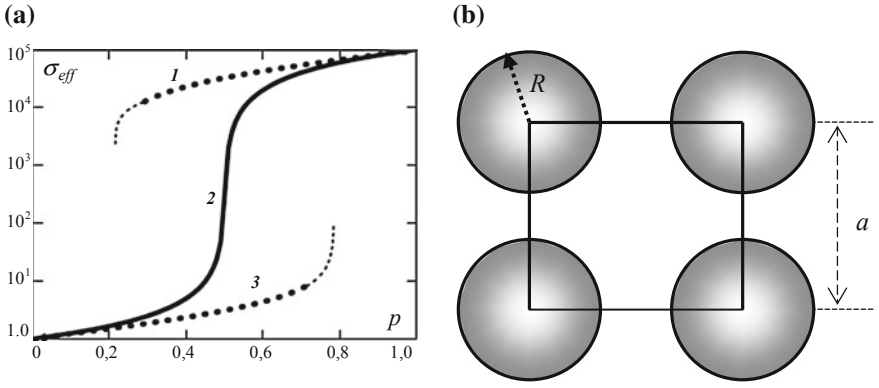

Fig. 3.6 Dependence of effective conductivity of media with periodic inclusions and small concentration of inclusions **a** media **b** for *BW*-case: *1* $(1 - p) \ll 1$ for case *WB* (3.1.1), *2* $p \ll 1$ for case *BW* (3.3.4), *3* results for EMT approximation. Points—result of numerical calculation for circular inclusions [25], thin line—from the work [1], $\frac{\sigma_2}{\sigma_1} = 10^{-5}$

$$\alpha = 1 - \frac{1}{3}\left(gR^4\right)^2\delta^2 - \frac{1}{63}\left(gR^4\right)^4\delta^2 - \frac{5}{9}\left(\delta^2 + \frac{4}{5\cdot 11\cdot 13^2}\right)\left(gR^4\right)^6\delta^2\ldots, \quad (3.3.2)$$

$$\delta = \frac{\sigma_1 - \sigma_2}{\sigma_1 + \sigma_2} = \frac{1-h}{1+h}; \quad h = \frac{\sigma_2}{\sigma_1}; \quad g = \frac{1}{a^4}\left[K\left(\frac{1}{\sqrt{2}}\right)\right]^4, \quad (3.3.3)$$

where $K\left(1/\sqrt{2}\right) = 1.85407\ldots$ is full elliptical integral of the first kind with a modulus.

Concentration of well conducting phase σ_1) has the form $p = 1 - \pi R^2/4a^2$. The expression (3.3.1) is valid: a) in the entire range of changing concentration $p^*_{BW} \le p \le 1$ of good conducting phase at $|\delta| \le 0.7$. For $\sigma_1 > \sigma_2$ the latter condition means $\sigma_1/\sigma_2 \ge 5.67$; b) in the range of concentration $0.29 \le p \le 1$ for any ratio $\sigma_1/\sigma_2 > 1$.

Figure 3.7 shows concentration dependence of the effective conductivity with a periodic arrangement of circular inclusions of poorly conducting phase in a good conducting matrix

As an example, there were selected different values of phase conductivity ratios σ_1/σ_2 (see also Fig. 3.6a). Inclusions touch each other at concentration equal to $p^*_{BW} = 1 - \frac{\pi}{4} \approx 0.21 (R = a/2)$.

The effective conductivity in the opposite case, i.e., "black" inclusions in a "white" matrix, as shown in [1], can be found using the reciprocity relations [7] (see Chap. 6)

$$\sigma_e(p) = \frac{\sigma_1\sigma_2}{\sigma_e(1-p)}. \quad (3.3.4)$$

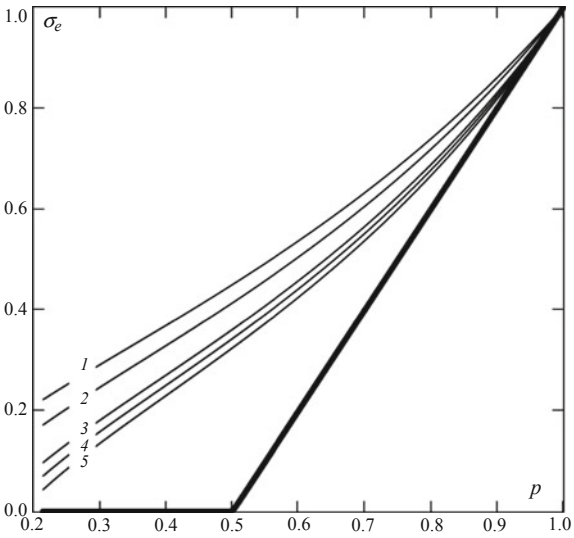

Fig. 3.7 Concentration dependences for different values of ratio σ_2/σ_1: *1* $\sigma_1 = 7$, *2* $\sigma_1 = 10$, *3* $\sigma_1 = 25$, *4* $\sigma_1 = 50$, *5* $\sigma_1 = 10^5$, in all examples $\sigma_2 = 1$; for comparison, *solid line* is concentration dependence of conductivity for randomly inhomogeneous medium within the EMA-approximation

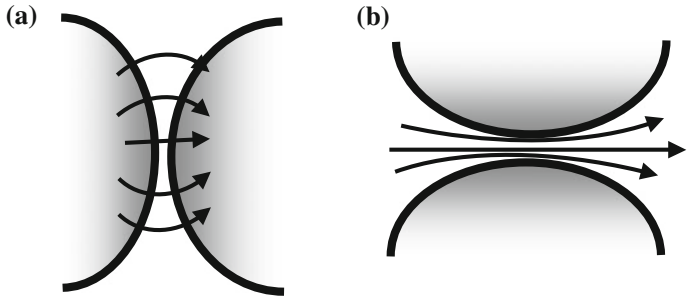

Fig. 3.8 Contact areas where the main resistance is "accumulated": **a** well conducting inclusions in poorly conducting matrix (*BW*); **b** poorly conducting inclusions in well conducting matrix (*WB*). The *arrows* indicate current direction at places of its largest density

In the region of concentrations close to limiting p^*_{BW} and p^*_{WB}, the expression for σ_e with a good precision can be written much simpler. As long as at $R \to a$ the larger part of resistance is accumulated in contact area. For *BW*-system the contact area has the form of interlayer (Fig. 3.8a), and in case of *WB*—the form of constrictions (bridges) (Fig. 3.8b).

Consider, for instance, the problem *WB*. At $R > 0.95a$ the expression (3.3.1) "works no longer." In the calculation using bridge "ideology," for the case of $\sigma_2 = 0$ according to [1] we obtain

$$\sigma^e_{WB} = \sigma_1 \frac{1}{\pi} \sqrt{2\frac{a-R}{R}}, \tag{3.3.5}$$

or in terms of concentration of good conducting phase we have

$$\sigma^e_{WB} = \sigma_1 \frac{\sqrt{2}}{\pi} \sqrt{\frac{\sqrt{\pi}}{2\sqrt{1-p}} - 1}. \tag{3.3.6}$$

Note that in terms of proximity to minimum possible concentration in this case $\tau = p - p^*$, dependence σ^e_{WB} with regard to $\tau \ll 1$ has a power form with exponent 1/2 (see also [16])

$$\sigma^e_{WB} \approx \sigma_1 \frac{2}{\pi^{3/2}} \tau^{1/2}_{WB} \tag{3.3.7}$$

Figure 3.9 shows concentration dependences of the effective conductivity σ^e_{WB} close to p^*_{BW}, here it is assumed $\sigma_1 = 100$, $\sigma_2 = 0$ (in reference units).

Similarly we find the concentration dependence of the effective conductivity in the case of inclusions of well conducting phase in poorly conducting matrix. Close to p^*_{BW} according to (3.3.4) and (3.3.5), or (3.3.6) [1]:

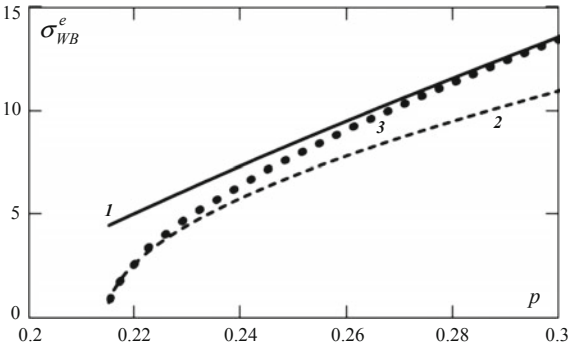

Fig. 3.9 Concentration dependence σ^{e}_{WB}: *1* by the formula (3.3.1); *2* by the formula (3.3.5); *3* direct numerical simulation [26]

$$\sigma^{\mathrm{e}}_{BW} = \sigma_2 \pi \sqrt{\frac{R}{2(a-R)}}, \tag{3.3.8}$$

where now is assumed $\sigma_1 \to \infty$.

If σ^{e}_{BW} (3.3.8) is expressed through concentration, we obtain

$$\sigma^{\mathrm{e}}_{BW} = \sigma_2 \frac{\pi}{\sqrt{2}\sqrt{\frac{1}{2}\sqrt{\frac{\pi}{p}} - 1}}. \tag{3.3.9}$$

From the expression (3.3.9) it follows immediately that in terms of proximity to p^*_{BW}—$\tau = p^*_{BW} - p$ dependence σ^{e}_{BW}, just as σ^{e}_{BW}, has a power form with exponent 1/2 (see also [16])

$$\sigma^{\mathrm{e}}_{BW} \approx \sigma_2 \frac{\pi^{3/2}}{2} \tau^{-1/2}_{BW}. \tag{3.3.10}$$

For the two-dimensional case, the effective conductivity of a medium for the case of ideally conducting balls ($\sigma_1 \to \infty$) periodically arranged in the sites of cubic lattice, close to maximum possible concentration ($p^*_{BW} = \pi/6$) has the form of a logarithmic dependence [16]:

$$\sigma^{\mathrm{e}}_{BW} \approx -\pi/2 \ln(\pi/6 - p). \tag{3.3.11}$$

Thus, if in the two-dimensional case σ_e behaves at $p \to p^*$ similarly to σ_{e} in percolation media (i.e., it has power dependence on proximity to p^*), then in the periodic three-dimensional media (3.3.11) it is not the case.

In real high-filled composites strictly periodic arrangement of inclusions is observed approximately. It seems important to be able to estimate how small structural deviations ("movements") from strict periodicity influence the effective conductivity. In other words, whether σ_{e} of such media is "rigid" or "soft," i.e., will a small structural deviation result in a large change of σ_{e} or not. If the structure is "rigid," the value of precise solution for strictly periodic arrangement of inclusions is of less interest for

practical purposes than "soft" structure. The problem of the influence of "movement" in the two-dimensional structure of periodically arranged cylinders is considered in [26], where it is shown that periodic structure is stable against "movement."

3.4 Plain-Layered Systems

We considered above the approximate methods of describing the effective kinetic coefficients. To establish their applicability limits is often a difficult task. Therefore, it is desirable to have precise expressions of the effective kinetic coefficients at least in some special partial cases. Such expressions are not only interesting in their own right, but can be used for checking the precision of other methods. One of such examples is planar stratified media for which one can get exact solutions for the effective kinetic coefficients.

As an example, we will consider the effective conductivity σ_e. For the planar stratified media the effective conductivity is second-rank tensor. In the calculation of σ_e we will use the so-called method of brackets.[1] Figure 3.10 represents a planar stratified periodic two-phase medium homogeneous on the average.

Locally this medium is isotropic: the conductivities of layers σ_1 and σ_2 are isotropic, and the effective conductivity σ_e is a tensor. To find σ_e, we write down the following equations:

$$\operatorname{div} \mathbf{j} = 0, \tag{3.4.1}$$

$$\operatorname{curl} \mathbf{E} = 0, \tag{3.4.2}$$

$$\mathbf{j} = \sigma(z)\ \mathbf{E}. \tag{3.4.3}$$

As usual, we assign a field on the infinity equal to $\langle \mathbf{E} \rangle$. From expressions (3.4.1) and from $\sigma = \sigma(z)$ it follows that j_z = const, and it is evident that this constant is equal to $\langle j_z \rangle$, where under the mean the following expression is meant (the origin of coordinates is at any point of oz axis)

$$\langle \ldots \rangle = \frac{1}{\delta} \int_0^{\delta} \ldots \mathrm{d}z,$$

where δ is a size of a two-layer package (Fig. 3.10).

From Eqs. (3.4.1), (3.4.2) it follows that on the bounds

$$j_z|_1 = j_z|_2,\ E_z|_1 = E_z|_2,$$

$$E_x = \langle E_x \rangle = \text{const}. \tag{3.4.4}$$

[1]The authors did not manage to trace the reference.

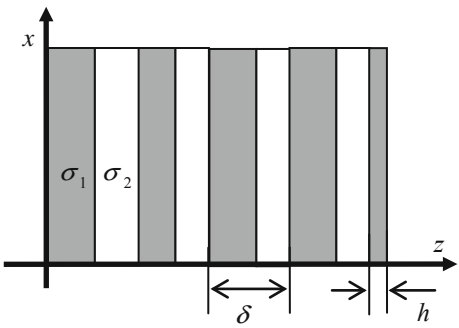

Fig. 3.10 Two-phase planar stratified periodic medium with the layer conductivities σ_1 and σ_2

According to (3.4.3) and (3.4.4) one can construct the following chain:

$$\begin{aligned} j_x = \sigma(z)E_x \to j_x = \sigma(z)\langle E_x\rangle \to \langle j_x = \sigma(z)\langle E_x\rangle\rangle \\ \to \langle j_x\rangle = \langle\sigma(z)\rangle\langle E_x\rangle, \end{aligned} \tag{3.4.5}$$

Then, by determination of the effective coefficient of conductivity $\langle j_x\rangle = \sigma^{\mathrm{e}}_{xx}\langle E_x\rangle$ we have

$$\sigma^{\mathrm{e}}_{xx} = \langle\sigma(z)\rangle. \tag{3.4.6}$$

For another current component $j_z = \sigma(z)E_z$ a similar chain (with regard to $j_z = \langle j_z\rangle$) will be as follows

$$E_z = \frac{j_z}{\sigma(z)} \to E_z = \frac{\langle j_z\rangle}{\sigma(z)} \to \left\langle E_z = \frac{\langle j_z\rangle}{\sigma(z)}\right\rangle \to \langle E_z\rangle = \langle j_z\rangle\langle 1/\sigma(z)\rangle, \tag{3.4.7}$$

and hence

$$\sigma^{\mathrm{e}}_{xx} = \langle 1/\sigma(z)\rangle^{-1}. \tag{3.4.8}$$

Thus, the effective conductivity of a planar stratified medium is a tensor which in the coordinate system in question can be written as

$$\widehat{\sigma}_{\mathrm{e}} = \begin{pmatrix} \langle\sigma\rangle & 0 \\ 0 & \langle 1/\sigma\rangle^{-1} \end{pmatrix}, \tag{3.4.9}$$

as it should be, the medium has different conductivities in different directions.

For a two-layer package shown in Fig. 3.10 we have

$$\sigma^{\mathrm{e}}_{xx} = p\sigma_1 + (1-p)\sigma_2, \quad \sigma^{\mathrm{e}}_{xx} = \frac{\sigma_1\sigma_2}{(1-p)\sigma_1 + p\sigma_2}, \tag{3.4.10}$$

where phase concentration is related to layer sizes as follows: $p = \delta_1/\delta$, $1 - p = \delta_2/\delta$.

It can be said that (3.4.9) is just a parallel and series connection of resistances.

Similarly one can also consider more complicated cases, for instance, the case of anisotropic conductivity of layers, when each layer is an anisotropic media. Here we will consider another case—the case of two-flux systems [27]. Thermoelectric material can serve as an example. Let there be given two fluxes **j** and **w** and two fields **E** and **g**. In other words, there are given two thermodynamic fluxes and two thermodynamic forces. The fluxes obey the laws of conservation

$$\operatorname{div}\mathbf{j}=0,\quad \operatorname{div}\mathbf{w}=0, \tag{3.4.11}$$

and the fields are potential

$$\operatorname{curl}\mathbf{E}=0,\quad \operatorname{curl}\mathbf{g}=0. \tag{3.4.12}$$

For the thermoelectric case **j** is electric current density, **w** is energy flux density, **E** is electric field intensity, $\mathbf{g}=-\operatorname{grad}T$, T is temperature [18].

In the framework of a linear nonequilibrium thermodynamics, the fluxes and forces are related by linear relations (the so-called material equations)

$$\begin{aligned}\mathbf{j}&=A^{11}\mathbf{E}+A^{12}\mathbf{g},\\ \mathbf{w}&=A^{21}\mathbf{E}+A^{22}\mathbf{g},\end{aligned} \tag{3.4.13}$$

where $A^{\alpha\delta}$ is second-rank tensor in space $\{E,g\}$.

In coordinate notation material Eqs. (3.4.13) are of the form

$$\begin{aligned}j_1&=(A_{ik})^{11}E_k+(A_{ik})^{12}g_k,\ j_i=A_{ik}^{11}E_k+A_{ik}^{12}q_k,\\ w_i&=(A_{ik})^{21}E_k+(A_{ik})^{22}g_k.\end{aligned} \tag{3.4.14}$$

For planar stratified media components of tensor $A^{\alpha\delta}$ are functions of coordinate z $A_{ik}^{\alpha\delta}=A_{ik}^{\alpha\delta}(z)$. We will introduce new (generalized) fluxes and fields

$$i_x=\begin{pmatrix}j_x\\ w_x\end{pmatrix},\ i_y=\begin{pmatrix}j_y\\ w_y\end{pmatrix},\ i_z=\begin{pmatrix}j_z\\ w_z\end{pmatrix},\ p_x=\begin{pmatrix}e_x\\ g_x\end{pmatrix},\ p_y=\begin{pmatrix}e_y\\ g_y\end{pmatrix},\ p_z=\begin{pmatrix}e_z\\ g_z\end{pmatrix}. \tag{3.4.15}$$

Now ratio (3.4.13) can be written down in compact form

$$\mathbf{i}=\widehat{\Omega}\mathbf{p},\quad i_k=\Omega_{km}^{\alpha\beta}p_m \tag{3.4.16}$$

where

$$\Omega_{km}=\begin{pmatrix}A_{km}^{11}A_{km}^{12}\\ A_{km}^{21}A_{km}^{22}\end{pmatrix}. \tag{3.4.17}$$

To find the effective kinetic coefficient means to determine coefficients interrelating the average fluxes and fields $\langle \mathbf{i} \rangle \equiv \mathbf{I}$, $\langle \mathbf{p} \rangle \equiv \mathbf{\Pi}$. According to the Onsager principle, in the absence of a magnetic field tensor $\widehat{\Omega}$ is symmetric. It means, for instance, that $A_{xy}^{12} = A_{yx}^{21}$. Based on the above-described schematic, the expressions (3.4.5) and (3.4.7) will be written as

$$i_x = \Omega_{xx}^{\alpha\beta}\Pi_x + \Omega_{xz}^{\alpha\beta}p_z,\ I_z = \Omega_{zx}^{\alpha\beta}\Pi_x + \Omega_{zz}^{\alpha\beta}p_z. \tag{3.4.18}$$

Solving the second Eq. (3.4.18) for p_z and averaging it by terms, we obtain (omitting indices α β)

$$\langle p_z \rangle = \left\langle (\Omega_{zz})^{-1} \right\rangle I_z - \left\langle (\Omega_{zz})^{-1}\Omega_{zx} \right\rangle \Pi_x = \Pi_x, \tag{3.4.19}$$

whence we have

$$I_z = \left\langle (\Omega_{zz})^{-1} \right\rangle^{-1} \Pi_z + \left\langle (\Omega_{zz})^{-1} \right\rangle^{-1} \left\langle (\Omega_{zz})^{-1}\Omega_{zx} \right\rangle \Pi_x. \tag{3.4.20}$$

Similarly by means of Π_x and Π_z, we find I_x, hence, the effective tensor $\widehat{\Omega}^{\mathrm{e}}$ [27]:

$$\begin{aligned}
(\Omega_{xx})^{\mathrm{e}} &= \langle \Omega_{xx} - \Omega_{xz}\Omega_{zz}\Omega_{zx} \rangle + \left\langle \Omega_{xz}(\Omega_{zz})^{-1} \right\rangle \left\langle (\Omega)^{-1} \right\rangle \left\langle (\Omega_{zz})^{-1}\Omega_{zx} \right\rangle, \\
(\Omega_{xz})^{\mathrm{e}} &= \left\langle \Omega_{xz}(\Omega_{zz})^{-1} \right\rangle \left\langle (\Omega_{zz})^{-1} \right\rangle^{-1}, \\
\Omega_{zx} &= \left\langle (\Omega_{zz})^{-1} \right\rangle \left\langle (\Omega_{zz})^{-1}\Omega_{zx} \right\rangle, \\
\Omega_{zz} &= \left\langle (\Omega_{zz})^{-1} \right\rangle^{-1}.
\end{aligned} \tag{3.4.21}$$

A medium with periodically changing properties is idealization. A real medium always has finite sizes. A question arises: how the finiteness of medium dimensions affects the possibilities of practical use of planar stratified media. The error introduced to the effective kinetic coefficient by the medium finiteness for planar stratified media can be estimated as in follows [2]. Figure 3.10 shows part of infinite planar stratified medium where a portion finite along the oz axis is separated. This portion includes n packages (n periods) and incomplete part $n+1$ of layer of dimension h. With a large n value, portion of dimension h will not affect the effective conductivity value along the oz axis. By the value of deviation of medium effective conductivity (with a finite h value) from the effective conductivity of infinite σ_{zz}^{e} one can judge of the applicability of expression for σ_{zz}^{e}.

For the infinite medium (3.4.8) we have

$$\sigma_{zz}^{\mathrm{e}} = \langle 1/\sigma(z) \rangle^{-1} = \lim_{n\to\infty} \left(\frac{1}{n\delta} \int_0^{n\delta} \frac{\mathrm{d}z}{\sigma(z)} \right)^{-1} = \left(\frac{1}{\delta} \int_0^{\delta} \frac{\mathrm{d}z}{\sigma(z)} \right)^{-1}, \tag{3.4.22}$$

where the last equality takes into account periodicity in z with period δ.

Similarly for the finite medium it can be written

$$\sigma_{zz}(h,n) = \left(\frac{1}{n\delta+h}\int_0^{n\delta+h}\frac{\mathrm{d}z}{\sigma(z)}\right)^{-1} = \left(\frac{n\delta}{n\delta+h}\frac{1}{\delta}\int_0^{\delta}\frac{\mathrm{d}z}{\sigma(z)} + \frac{\delta}{n\delta+n}\frac{1}{\delta}\int_0^{h}\frac{\mathrm{d}z}{\sigma(z)}\right)^{-1} \tag{3.4.23}$$

At $n \to \infty$ $\sigma_{zz}(h,n) \to \sigma^{\mathrm{e}}_{zz}$, and at $n \gg 1$ one can approximately find

$$\sigma_{zz}(h,n) \approx \left(\frac{1}{\sigma^{\mathrm{e}}_{zz}} + \frac{1}{n\delta}\int_0^{h}\frac{\mathrm{d}z}{\sigma(z)}\right)^{-1}. \tag{3.4.24}$$

Thus, it is exactly the ratio of $\frac{n\delta}{\int_0^{\delta}\frac{dz}{\sigma(z)}}$ to σ^{e}_{zz} that shows (at $n \gg 1$) how essential is the fact that the medium is finite (Fig. 3.11)

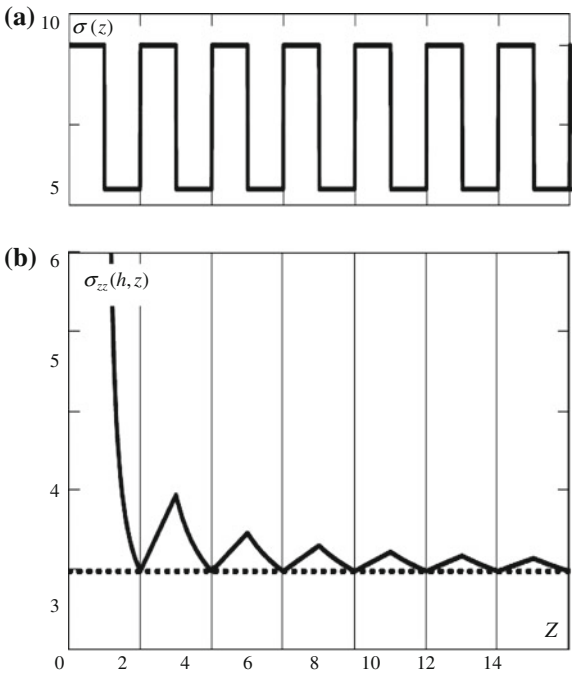

Fig. 3.11 Dependence of the effective conductivity on the size of planar stratified medium **a** for $\sigma(z)$ from z, **b** for $\sigma_{zz}(h,z)$ along oz, *dotted line* σ^{e}_{zz}

References

1. Balagurov BY, Kashin VA (2000) Conductivity of a two-dimensional system with a periodic distribution of circular inclusions. Sov Phys JETP 90:850–860
2. Belozki E, Snarskii A, Trofimov C (1982) Investigation of artificial anizotropic media Ukrain. Fiz Jur 27:91–95 (in Russian)
3. Beran M (1974) Application of statistical theories for the determination of thermal, electrical and magnetic properties of heterogeneous materials. In: Sendeckyj GP (ed) Mechanics of composite materials. Academic Press, New York, vol 2, pp 209–249
4. Bergman DJ, Stroud D (1992) Physical properties of macroscopically inhomogeneous media. Solid State Phys 46:147–269
5. Bruggeman DAG (1936) Berechnung verschiedener physikalischer Konstanten von heterogenen Substanzen. II Ann Physik 25:645–672
6. Dykhne AM (1967) Calculation of the kinetic coefficients of media with random inhomogeneities. Sov Phys JETP 25:170–171
7. Dykhne AM (1970) Conductivity of a two-dimensional two-phase system. Sov Phys JETP 32:63–64
8. Feng S, Halperin BI, Sen PN (1987) Transport properties of continuum systems near the percolation threshold. Phys Rev B 35:197–214
9. Fishke TJ, Gokturk HS, Kalyon DM (1993) Electric and magnetic properties of low density polyethylene filled with ferromagnetic powders. Soc Plastic Eng ANTEG Tech Pap 39:614–617
10. Golden K (1986) Bounds on the complex permittivity of a multicomponent material. J Mech Phys Sol 34:333–358
11. Halperin BI, Feng S, Sen PN (1985) Differences between lattice and continuum percolation transport exponents. Phys Rev Lett 54:2391–2394
12. Hashin Z, Strikman S (1962) On some variational principles in anisotropic and nonhomogeneous elasticity. J Appl Phys 35:3125–3131
13. Hashin Z, Strikman S (1963) A variational approach to the theory of the elastic behavior of multiphase materials. J Mech Phys Solid 11:127–140
14. Kazancev V (1983) Variational estimates in electrostatic of insulators. Tech Phys 53:449–457 (in Russian)
15. Kazancev V (1987) Variational principles of magnetostatics college communications. Physics 7:70–75 (in Russian)
16. Keller JB (1963) Conductivity of a medium containing a dense array of perfectly conducting spheres or cylinders or nonconducting cylinders. J Appl Phys 34:991–993
17. Kirpatrick S (1973) Percolation and conduction. Rev Mod Phys 45:574–588
18. Landau LD, Lifshitz EM (1984) Electrodynamics of continuous media, 2nd ed, vol 8. Butterworth-Heinemann, Oxford 460 p
19. Landauer R (1952) The electrical resistance of binary metallic mixtures. J Appl Phys 23:779–784
20. Landauer R (1978) Electrical conductivity in inhomogeneous media electrical transport and optical properties of inhomogeneous media. In: Proceedings of American Institute of Physics conference, vol 40, pp 2–45
21. Odelevsky VI (1951) Calculation of generalized conductivity. Tech Phys 21:667–677, 678–685, 1379–1382 (in Russian)
22. Sarychev AK, Vinogradov AP (1981) Drop model of infinite cluster for 2D percolation. J Phys C 14:L487–L490
23. Shklovskii BI, Efros AL (1984) Electronic properties of doped semiconductors. Springer, Berlin 388 p
24. Shvidler M (1985) Statistical hydromechanics of porous media. Nedra, Moscow 288 p. (in Russian)

25. Snarskii AA, Shamonin MV, Zhenirovsky MI (2003) The effective properties of macroscopically nonuniform ferromagnetic composites: theory and numerical experiment. Sov Phys JETP 96:66–77
26. Snarskii AA, Shamonin MV, Zhenirovskyy MI (2005) Effect of disorder on the conductivity of two-phase strongly inhomogeneous highly filled composites. Tech Phys 50:11–18
27. Snarskii AA, Tomchuk PM (1987) Kinetic phenomena in macroscopic inhomogeneous media (Review) Ukrain. Fiz Jur 32:66–92 (in Russian)
28. Snarskii AA (2007) Did Maxwell know about the percolation threshold? (On the fiftieth anniversary of percolation theory). Phys Uspechi 50:1239–1242
29. Stanley E (1971) Introduction to phase transition and critical phenomena. Oxford University Press, Oxford 308 p
30. Tolmachev CT (1975) Calculation of effective conductivity of two-phase media with cylindrical inclusions. Electricity 2:39–43 (in Russian)
31. Tolmachev CT, Danilejko OK (1976) Calculation of flat potential field in the ordered system of circular cylinders. Electromech, Coll Commun 2:139–144 (in Russian)
32. Vinogradov AP (2001) Electrodynamics of composite materials URSS. Moscow 208 p. (in Russian)

Chapter 4
Elements of Geometrical Theory of Percolation

4.1 Percolation Problem

Initially percolation problem had been formulated by Broadbent and Hammersly in [2]. Let us consider a porous medium, where pores are distributed randomly, for instance, in activated coal in a filter of a gasmask. What is the dependence of the length of the path of floating air on pores number density (relative volume). It is obvious that the greater is this path, the cleaner the air is. How much is this path branched up and paralleled? If the number density of pores gets smaller then, effectively air path becomes shorter and, obviously, we can face a situation that the air may not at all be able to get through the filter. What would be critical number density which will bring this situation about? This critical number corresponds to the so-called percolation threshold.

The simplest abstract formulation of this problem is following

There exists a ladder of random connections, random part of them p "black"—conducting, and a rest of them—$(1 - p)$ "white"—nonconducting (broken connections). One has to determine p_c "black" connections, when there exists at least one nonvanishing conducting path. Similarly, one can formulate this problem for vertices of the ladder. This threshold number density has been called percolation threshold. For the first time this problem was formulated by Broandbent and Hammersley [2]. The existence of such critical threshold is the main marker of theory of percolation. Physical properties of this kind of system drastically change while getting though this threshold of percolation (Fig. 4.1).

We use here "electric picture"—"black" connections (bonds) conduct current, "white" (broken ones) do not conduct (in more advanced theory of percolation they still conduct but not that effective (Fig. 4.2).

It turns out that the problem of finding the percolation threshold happened to be a very nontrivial problem of the theory of probability and while trying to solve it

A.A. Snarskii et al., *Transport Processes in Macroscopically Disordered Media*, DOI 10.1007/978-1-4419-8291-9_4

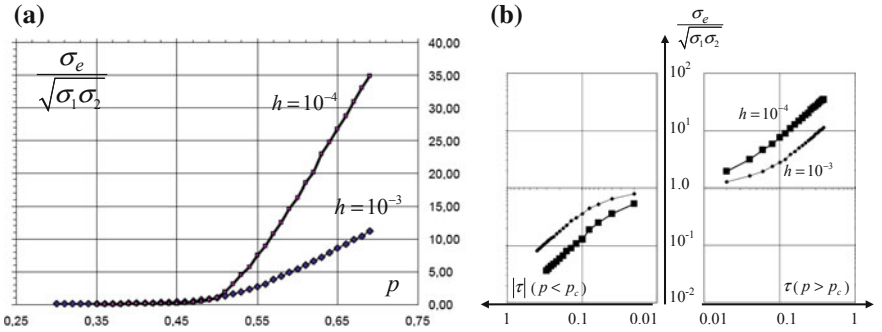

Fig. 4.1 Dependencies of effective conductivity $\sigma_e/\sqrt{\sigma_1\sigma_2}$ for two-dimensional lattice of resistors for different values of $h = \sigma_2/\sigma_1$: **a** upon conducting phase concentration p, **b** upon proximity to the percolation threshold $\tau = (p - p_c)/p_c$

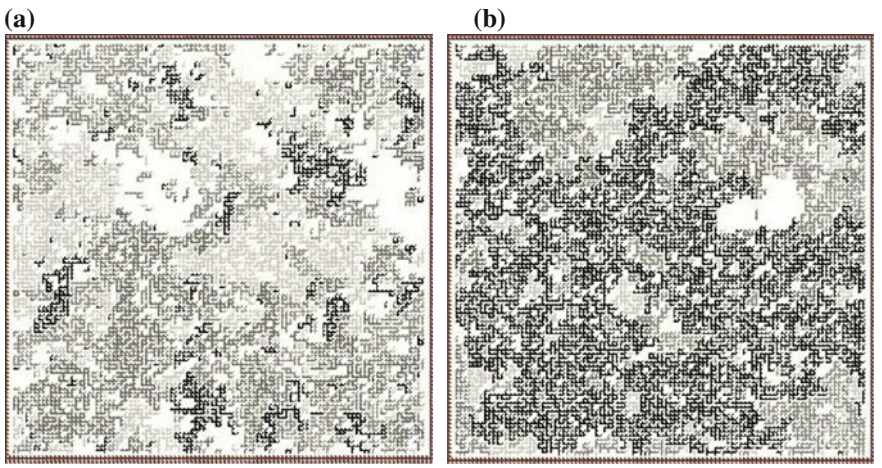

Fig. 4.2 The view of percolation system in vicinity of percolation threshold. **a** below threshold, without percolation. **b** above threshold, with percolation

mathematicians and physicists come up with quite a number of new and original ingenious techniques and methods termed today as the theory of percolation.

Conditionally one subdivides theory of percolation into geometric and physical ones. The former one investigates questions of structure, statistics, and connectivity of "black and white" sites or areas, finite, or infinite clusters in the spaces of different dimensionality. (see, for example, [11]) and we will not consider these topic in this book. The physical part of the theory of percolation usually deals with various physical processes such as conduction of electric current, thermoelectric phenomena, elastic as well as nonelastic deformations in the media with two- and greater number of phases of this media with number density in the vicinity of percolation threshold.

4.2 Basic Concepts of Geometric Percolation

Here we will introduce some important concepts of the geometrical theory of percolation, which will be significant in our later discussions of the physical aspects of the phenomenon of percolation.

In the theory of percolation typically one considers dimensionless quantity which indicate closeness to the threshold of percolation instead of number density

$$\tau = \frac{p - p_c}{p_c}, \tag{4.2.1}$$

characteristically, methods of the percolation theory applicable in the vicinity of the threshold. $|\tau| \ll 1$.

The set of "black" connections (bonds), connecting "left infinity" with the "right" one, are called infinite cluster. At $\tau > 0$ infinite cluster exists, though at $\tau < 0$ it is missing. Appearance (creation) of the infinite cluster at the transition of number density through the threshold of percolation can be considered to be analogous to the emergence of geometrical analog of new state, new order parameter. This fact makes it possible to see here second-order phase transition, where order parameters possess so-called scaling and, specifically, while approaching to threshold they feature power behavior. Thus, the power of infinite "black" cluster P_∞ (the probability of getting randomly "black" connections or knot belonging to this cluster) takes up following values

$$P_\infty \sim \tau^\beta, \quad \tau > 0, \quad \beta_2 \approx 0.15, \quad \beta_3 \approx 0.4. \tag{4.2.2}$$

where β—so-called critical index, universal number, which depends only on dimensionality of the problem, having a unique value for all lattices (for example, in two-dimensional case for quadratic, triangular, hexagonal, disordered, etc.); lower index at β points out to the number of dimensions of the system under consideration.

Of course, the notion of infinite cluster, and, subsequently, P_∞ exists only above threshold of percolation at $p > p_c$, $\tau > 0$.

Below the percolation threshold ($p < p_c$) there are clusters of "black" phase only of finite size.

One of characteristics of such clusters—the average number of "black" connections (nodes) that belong to these clusters

$$S \sim |\tau|^{-\gamma}, \quad \gamma_2 \approx 2.4, \quad \gamma_3 \approx 1.7. \tag{4.2.3}$$

One more, a very important characteristic of a disordered medium is so-called correlation ξ. It represents a typical length along which intensity of correlations falls off accordingly to the vicinity of threshold τ:

$$\xi \approx a_0|\tau|^{-\nu}, \quad \nu_2 = \frac{4}{3}, \quad \nu_3 \approx 0.9, \tag{4.2.4}$$

where ν—critical index of correlation length.

In the area with sizes ξ there exists only one cluster.

The characteristics of percolation system P_∞, S, ξ behave nonanalytically, having power dependence on τ, and a power—critical index—is a noninteger number. Therefore, ether dependence itself or some of its derivatives with respect to τ are going to infinity at $\tau \to 0$. Critical indices do not depend on the type of lattice and this fact is called universality of critical indices. Notice that for systems of different dimensions (two-dimensional, three-dimensional) the critical indices are, of course, different.

In what follows, while describing critical phenomena most prominent role would belong to percolation. Apart from P_∞ (4.2.2) and S (4.2.3), it depends on many other characteristics such as, for instance, number of nodes of infinite cluster with characteristic sizes r

$$M(r) \sim r^{\alpha_f}, \quad (r < \xi), \quad \alpha_f = \alpha - \beta/\nu. \tag{4.2.5}$$

In infinite cluster one can recognize (1) "isle" of a cluster (back bone)—when we talk about current flow along "black" connections, then it is currant-conducting part; (2) "dead ends"—parts of infinite parts, along which current does not flow; (3) "red connections" (red bounds)—single connections, located in a such manner so that elimination of only one of them prevent current flow in infinite; (4) "skeleton" cluster—it is a set of shortest paths from the given knot to all other for the particular length.

Each of given characteristics is defined by its critical index. Their values can be found in. [3, 11].

In order to describe behavior of different physical properties (for example, σ_e) in percolation media there exist a number of geometrical models: Skul-Shklovsky [8], similar to it de Gennes [5], fractal model of Given-Mandelbrot [7], model of Arcahelis-Redner-Caniglio [1], droplet model of Stanley and Coniglio [4, 10], droplet model of Vinogradov and Sarichev [12], Luk'yanets-Snarsky [6], and many others.

For some prolonged time it was a general belief that critical indices of basic physical phenomena (effective conductivity, effective thermoEMF, etc.) could be expressed only through geometrical critical indices—ν, β, …. Though, as was mentioned in [9], "*it is quite possible that it is false.*" Since that time of publication of [9], most specialists believe into it. In spite of this, the concrete models of the percolation structure proved to be useful theoretical tools, allowing researchers in this field simplify and clarify basic quantitative (sometimes even qualitative) characteristics of kinetic phenomena in percolation media.

References

1. de Arcangelis L, Redner S, Coniglio A (1985) Anomalous voltage distribution of random resistor networks and new model for the backbone at the percolation threshold. Phys Rev B 31:4725–4727
2. Broadbent SR, Hammersley JM (1957) Percolation processes. 1. Crystals and mazes. Proc Camb Phyl Soc 53:629–633
3. Bunde A, Havlin S (1996) Fractals and disordered systems, 2nd edn. Springer, 412 p
4. Coniglio A (1982) Cluster structure near the percolation threshold. J Phys A 15:3829–3844
5. de Gennes PGJ (1976) On relation between percolation theory and the elasticity of gels. Phys Lett 37:L1–L2
6. Luk'yanets SP, Snarskii AA (1988) Model of macroscopically inhomogeneous mixtures of a perfect conductor and an insulator near the mobility edge. Sov Phys JETP 67:1467–1470
7. Mandelbrot BB, Given JA (1984) Physical properties of a new fractal model of percolation clusters. Phys Rev Lett 52:1853–1856
8. Skal AS, Shklovskii BI (1974) Topology of infinite cluster in the theory of percolation and hopping conduction. Sov Phys Semicond 8:1586–1592 (in Russian)
9. Sokolov IM (1986) Dimensionalities and other geometric critical exponents in percolation theory. Phys Usp 29:924–945
10. Stanley HE (1977) Cluster shapes at the percolation threshold: an effective cluster dimensionality and its connection with critical-point exponents. J Phys A 10:L211–L220
11. Tarasevich Yu (2002) Percolation: theory, applications and algorithms. URSS, Moscow, 112 p. (in Russian)
12. Vinogradov AP, Sarychev AK (1983) Structure of percolation channels and the metal-insulator transition in composites. Sov Phys JETP 58:665–669

Chapter 5
Effective Conductivity of Percolation Media

5.1 Analogy with the Phenomenological Theory of Second-Order Phase Transitions. Scaling and Critical Exponents

Once Broadbent and Hammersly [4] had introduced the percolation threshold and discovered that various geometrical and physical characteristics of percolation systems depend on the proximity to percolation threshold τ and this is a power dependence and critical indices describing it are universal (see Chap. 4), it could not but suggest the idea that percolation systems behave similarly to systems with second-order phase transitions. This idea was first put forward and realized in [15, 54]. To describe the results of these works and their subsequent development, it is necessary to give some brief information, the basic terms and relationships of the phenomenological theory of second-order phase transitions detailed, for instance, in [25, 30, 39].

The trend in the theory of phase transitions is to use the so-called proximity to phase transition point (temperature)$t = T - T_c$ or $t = (T - T_c)/T_c$. In the latest definition t is dimensionless; the order parameter η—the value characterizing the properties of system as a whole, changes considerably with a phase transition, i.e. in passing through T_c. In the case of ferromagnetics, the order parameter is ferromagnetic magnetization, and then T_c is the Curie temperature.

Correlation radius (length) r_c, which is also frequently designated as ξ, shows the order of magnitude of distances where correlation between the order parameter fluctuations decreases considerably. This magnitude appears in the correlation function [compare to (2.2.5)]:

$$G(\mathbf{r}) \sim \mathrm{e}^{-\frac{r}{\xi}},$$

A.A. Snarskii et al., *Transport Processes in Macroscopically Disordered Media*, DOI 10.1007/978-1-4419-8291-9_5

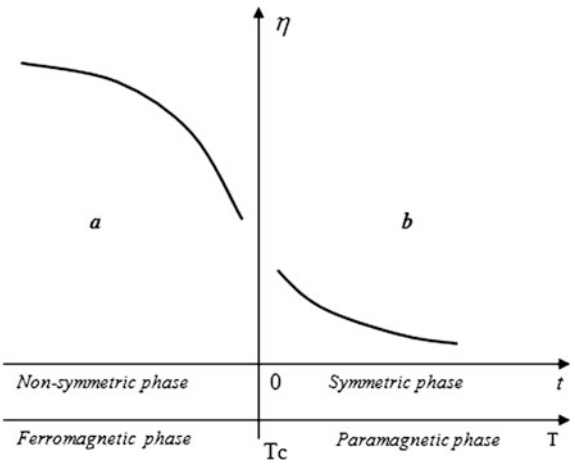

Fig. 5.1 Dependence of the order parameter η on the proximity to phase transition point T_c

and shows a power dependence on the proximity to the transition point

$$\xi \sim |t|^{-\nu}, \tag{5.1.1}$$

where ν is critical index of correlation length. Above and below the transition point, the order parameter, just like the correlation length, has power-mode behavior (Fig. 5.1):

$$\eta \sim h|t|^{-\gamma}, \quad t > 0 (T > T_c), \quad \gamma > 0, \tag{5.1.2}$$

$$\eta \sim |t|^{\beta}, \quad t < 0 (T < T_c), \quad \beta > 0, \tag{5.1.3}$$

where γ and β are certain critical indices, h is an external field (dimensionless), its nature is different for various order parameters η, in the case of ferromagnetism it is a magnetic field. In the area of $t < 0$, $T < T_c$ (Fig. 5.1a) $\eta \sim t^{\beta}$ there is a spontaneous magnetization separating some direction (hence the name—nonsymmetric phase).

In the area of $t > 0$, $T > T_c$ (Fig. 5.1b) $\eta \sim h\,|t|^{-\gamma}$ the spontaneous magnetization occurs in the presence of an external magnetic field. Note that at $T > T_c$ the order parameter is different from zero only in the presence of an external field h.

The external field (its dimensionless value is designated as h) "*smears the phase transition," "the discrete point of the phase transition disappears"* [25]. There is some t-dependent characteristic h_t, such that in the "weak" ($h \ll h_t$) fields its effect on the order parameter behavior can be neglected, and in the "strong" ($h \gg h_t$) fields this effect becomes dominant, and the order parameter, just like the correlation length, depends not on t, but rather on h:

$$\eta \sim h^{\frac{1}{\delta}}, \quad \xi \sim h^{-\mu}. \tag{5.1.4}$$

With an arbitrary relationship between t and h (however, remember that the system is in the vicinity of the phase transition point, i.e.$|t| \ll 1$), one can formulate for η the so-called scaling relationship (scaling function, scale invariance) incorporating as particular cases (5.1.2)—(5.1.4):

$$\eta = h^{\frac{1}{\delta}} f\left(\frac{t}{h^{\frac{1}{\beta\delta}}}\right), \quad h > 0. \tag{5.1.5}$$

Here at $h < 0$ one should make a substitution $h \to -h$, $\eta \to -\eta$. Note that from (5.1.5) immediately follows the characteristic value h_t which determines the magnitude of dimensionless field (weak–strong):

$$h_t^{\frac{1}{\beta\delta}} \sim |t|. \tag{5.1.6}$$

Scaling function $f(z)$ depending on one variable $z = t/h^{\frac{1}{\beta\delta}}$ behaves within different limits as follows:

$$f(z) \sim \begin{cases} z^{-\gamma}, & z \to +\infty, (\text{a}), \\ \text{const}, & z \to 0, \quad (\text{c}), \\ |z|^{\beta}, & z \to -\infty, (\text{b}). \end{cases} \tag{5.1.7}$$

Not all of the above used critical indices are independent. Some of them relate the so-called equalities. For instance, one of them–

$$\beta\delta = \beta + \gamma, \tag{5.1.8}$$

written here in a somewhat unusual form, is known as the Widom relation.

On separating the main factor from $f(z)$, the remaining part has no peculiarities and can be expanded in the small parameter z or $1/z$ depending on the limit kind in (5.1.7). It is considered in more detail in [25]. For the case (5.1.7b) at $h \neq 0$, $\eta \neq 0$ both for $t < 0$ and for $t > 0$. Thus, the case $t = 0$ is "in no way remarkable" physically, which means that $f(z)$ is expanded in the integer powers z:

$$\eta \approx h^{\frac{1}{\delta}}\left(B_0 + B_1 h^{-\frac{1}{\beta\delta}} t + B_2 h^{-\frac{2}{\beta\delta}} t^2 + \ldots\right). \tag{5.1.9}$$

Similarly to cases (5.1.7a) и (5.1.7c), η (t, h) can be expanded in the integer powers h (with regard to different factors $z^{-\gamma}$ and $|z|^{\beta}$, respectively). For expression (5.1.7a) we get

$$\begin{aligned} \eta &= h^{\frac{1}{\delta}} f\left(\frac{t}{h^{\frac{1}{\beta\delta}}}\right) = h^{\frac{1}{\delta}} \left(\frac{t}{h^{\frac{1}{\beta\delta}}}\right)^{-\gamma} f\left(\frac{t}{h^{\frac{1}{\beta\delta}}}\right) \\ &= h t^{-\gamma} \varphi_+\left(\frac{t}{h^{\frac{1}{\beta\delta}}}\right) \approx h t^{-\gamma}\left(A_0 + A_1 h t^{-\beta\delta} + A_2 h^2 t^{-2\beta\delta} + \ldots\right), \end{aligned} \tag{5.1.10}$$

where the Widom relation is taken into account (5.1.8), and in the function $f(z)$ the variable is raised to the—$\delta\beta$ power.

For the case (5.1.7b) we have

$$\eta = h^{\frac{1}{\delta}} f\left(\frac{t}{h^{\frac{1}{\delta\beta}}}\right) = h^{\frac{1}{\delta}}\left(\frac{|t|}{h^{\frac{1}{\delta\beta}}}\right)^{\beta} f\left(\frac{t}{h^{\frac{1}{\delta\beta}}}\right) = |t|^{\beta}\varphi_{-}\left(\frac{h}{|t|^{\beta\delta}}\right) \approx$$
$$\approx |t|^{\beta}\left(C_0 + C_1 h|t|^{-\delta\beta} + C_2 h^2|t|^{-2\delta\beta} + \ldots\right). \tag{5.1.11}$$

Summarizing (5.1.9), (5.1.10), and (5.1.11), we write down

$$\eta = \begin{cases} h\,t^{-\gamma}\left(A_0 + A_1\,h\,t^{-\delta\,\beta} + A_2\,h^2\,t^{-2\,\delta\,\beta} + \ldots\right), & t > 0, \quad \frac{h}{t^{\delta\beta}} \ll 1, \qquad (a) \\ h^{\frac{1}{\delta}}\left(B_0 + B_1\,h^{-\frac{1}{\delta\beta}}t + B_2\,h^{-\frac{2}{\delta\beta}}t^2 + \ldots\right), & \frac{h}{t^{\delta\beta}} \geq 1, \qquad (c) \\ |t|^{\beta}\left(C_0 + C_1\,h\,|t|^{-\delta\,\beta} + C_2\,h^2\,|t|^{-2\,\delta\,\beta} + \ldots\right), & t<0, \quad \frac{h}{|t|^{\delta\beta}} \ll 1 \quad (b). \end{cases} \tag{5.1.12}$$

The constants A_i, B_i, C_i remain of the order of unity, among them there are both positive and negative.

Up to now it has been supposed that the system sizes L wherein the phase transition occurs are much in excess of the correlation length $L \gg \xi$. In this case the properties of system as a whole do not depend on the instantaneous realization of local properties (with regard to fluctuations) that takes place at given time moment. At the same time, it means that the properties of system do not depend on the system size$L$. In the opposite case, when $L \leq \xi$, at each time moment due to fluctuations (the characteristic size of which is now of the order of system sizes) the values of the order parameter are different and all subsequent relationships are certainly written for the time average. The order parameter in this case is a function of system size L, this dependence becoming minor with increase in L, when condition $L \gg \xi$ is satisfied. To determine the dependence $\eta = \eta\ (L)$, one must use a relation between the proximity to transition point t and the correlation length (5.1.1):

$$|t| \sim \xi^{-\frac{1}{\nu}}, \tag{5.1.13}$$

moreover, $|t| \sim (\xi/a_0)^{-\frac{1}{\nu}}$, where a_0 is characteristic microscopic size, such as interatomic distance, which, in the subsequent discussion will be omitted for simplicity.

A technique leading to dependence $\eta = \eta\ (L)$ for systems with $L \leq \xi$ lies in the substitution of ξ by L in (5.1.13). Thus, substituting (5.1.13) into (5.1.2) and (5.1.3) and replacing ξ by L, we get

$$\eta \sim h\,L^{\frac{\gamma}{\nu}}\ (T > T_c), \quad \eta \sim L^{-\frac{\beta}{\nu}}\ (T < T_c). \tag{5.1.14}$$

The infinite cluster $P_\infty(\tau)$ can serve as the analog of the order parameter η in the geometrical percolation theory, see (4.2.2). In so doing, the analog of variable T in

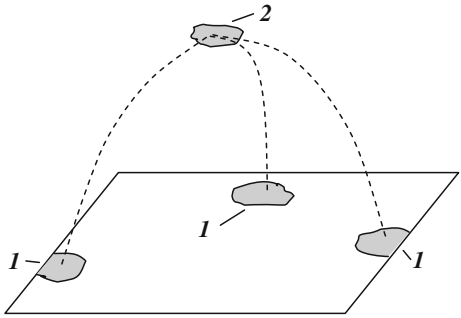

Fig. 5.2 Schematic of combination of finite clusters of the "black" phase *1* finite "black" clusters *2* Kastellein-Fortuine demon

the theory of phase transitions is $1 - p$, where p is concentration of "black" nodes (or bonds). According to (4.2.2), $P_\infty(\tau) \neq 0$ only at $\tau > 0$, i.e. in the case of the infinite cluster. To draw an analogy, one should introduce the concept of infinite cluster power $P_\infty(\tau)$ below the percolation threshold, when there is not infinite cluster, but there are single finite clusters of the "black" phase. Such a paradoxical requirement can be met by interrelating finite clusters in artificial way. For this purpose Kastellein and Fortuine [22] (see also a detailed presentation in [45]) introduced the so-called Kastellein-Fortuine demon (Fig. 5.2a) "black" node beyond the lattice to which with a probability $1 - e^{-h}$ is related each of the "black" lattice nodes (dashed line), where h is the analog of the external magnetic field in the theory of phase transitions.

At $\tau \ll 1\,(p > p_c)$ and $h \ll 1\, P_\infty(p) \sim h$, i.e. just like the order parameter η in the theory of phase transitions is proportional to the external field, and at $p = p_c\, P(\tau = 0, h) \sim h^{\frac{1}{\delta}}$ [compare to (5.1.4)].

As we will see below, in the description of physical effects, such as conductivity, in percolation structure, when the effective conductivity σ_e can be assumed as the order parameter, the introduction of analog to the external magnetic field does not require the use of the above described artificial technique.

5.2 Effective Conductivity as an Order Parameter. Phenomenological Description

In this paragraph, we use the analogy with the theory of second-order phase transitions (see 5.1). The role of proximity to phase transition point $t = (T - T_c)/T_c$ is now played by the value $\tau = (p - p_c)/p_c$. Like before, p is the concentration of good conducting ("black") phase, and as p increases (passes through the percolation threshold p_c), the medium goes over to a conducting state (the analog of non-symmetric ferromagnetic phase in the theory of phase transitions), however, in the theory of phase transitions such a transition takes places with a reduction of t. Thus, if we draw an analogy, the T and p axes are directed in opposite directions.

Above and below the percolation threshold p_c the effective conductivity σ_e, as established by numerous experiments (full-scale and numerical [51]), shows a power dependence on τ:

$$\left.\begin{array}{l}\sigma_e \approx \sigma_1 \tau^t, \quad \tau > 0, \quad p > p_c \\ \sigma_e \approx \sigma_2 |\tau|^{-q}, \quad \tau < 0, \quad p < p_c\end{array}\right\} \tag{5.2.1}$$

or in a dimensionless form:

$$\frac{\sigma_e}{\sigma_1} \approx \tau^t, \quad \tau > 0, \quad \frac{\sigma_e}{\sigma_1} \approx \frac{\sigma_2}{\sigma_1} |\tau|^{-q}, \quad \tau < 0, \tag{5.2.2}$$

where t and q are critical indices of conductivity above and below p_c.

From Eqs. (5.2.2) and (5.2.1), it can be seen that role of field h in the theory of phase transitions is played by the relationship of phase conductivities

$$h = \frac{\sigma_2}{\sigma_1}. \tag{5.2.3}$$

Theory of critical behavior of σ_e, based on the analogy with the theory of phase transitions, was constructed in the works [15, 54]. In this theory, the analog of scaling relationship for the order parameter (5.1.6) is scaling relationship for the effective conductivity

$$\sigma_e = \left(\sigma_1^q \sigma_2^t\right)^{\frac{1}{t+q}} f\left(\frac{\tau}{h^{\frac{1}{t+q}}}\right), \tag{5.2.4}$$

where for the sum of $t + q$ the designation $\varphi = t + q$—the so-called scaling factor, is often introduced.

Scaling relationship (5.2.4) can be written in a dimensionless form as follows:

$$\frac{\sigma_e}{\sigma_1} = h^{\frac{t}{\varphi}} f\left(\frac{\tau}{h^{\frac{1}{\varphi}}}\right), \quad \varphi = t + q, \tag{5.2.5}$$

Scaling function (compare to (5.1.7)) has the following asymptotes: [15]:

$$f(z) \sim \left\{\begin{array}{ll} z^t, & z \to +\infty, \quad (a), \\ \text{const}, & z \to 0, \quad (c), \\ |z|^{-q}, & z \to -\infty, \quad (b). \end{array}\right. \tag{5.2.6}$$

Remind that the T and p axes are directed oppositely, therefore, in (5.2.6) as compared to (5.1.7) the a and b dependences (drop and increase with a reduction of z) have changed their places. According to [25] (paragraph 5.1) from (5.2.4) and (5.2.6) follow three types of different behaviurs of σ_e and expansion of $f(z)$ in three different areas of parameters. At $z \to \infty$, i.e. when $\tau > 0$ and $\tau h^{-\frac{1}{\varphi}} \gg 1$, from (5.2.4) and (5.2.6) we get $\sigma_e = \sigma_1 h^{\frac{t}{\varphi}} f\left(\frac{\tau}{h^{\frac{1}{\varphi}}}\right)\Big|_{\tau h^{-\frac{1}{\varphi}} \gg 1} \approx \sigma_1 h^{\frac{t}{\varphi}} \left(\tau h^{-\frac{1}{\varphi}}\right)^t f_1\left(\frac{\tau}{h^{\frac{1}{\varphi}}}\right)$.

When the main factor (singular part z^t) is singled out from $f(z)$, the remaining factor has no peculiarities, $\tau \neq 0$, therefore, the function $f_1\left(\tau/h^{\frac{1}{\varphi}}\right)$ can be expanded in the integer powers h:

$$f_1\left(\frac{\tau}{h^{\frac{1}{\varphi}}}\right) \equiv f_2\left(\frac{h}{\tau^{\varphi}}\right) \approx A_0 + A_1\, h\, \tau^{-\varphi} + A_2\, h^2 \tau^{-2\,\varphi} + \ldots.$$

Finally, for σ_e we get

$$\sigma_e \approx \sigma_1 \tau^t \left(A_0 + A_1\, h\, \tau^{-(t+q)} + A_2\, h^2 \tau^{-2(t+q)} + \ldots\right). \tag{5.2.7}$$

Similarly, for the case $z \to -\infty$, i.e. at $\tau < 0$ и $|\tau| h^{-\frac{1}{\varphi}} \gg 1$, we have

$$\begin{aligned}\sigma_e &\approx \left(\sigma_1^q \sigma_2^t\right)^{\frac{1}{\varphi}} \left(\frac{|\tau|}{h^{\frac{1}{\varphi}}}\right)^{-q} f_3\left(\frac{h}{|\tau|^{\varphi}}\right) \\ &\approx \sigma_2 |\tau|^{-q} \left(C_0 + C_1\, h |\tau|^{-(q+t)} + C_2\, h^2 |\tau|^{-2(t+q)} + \ldots\right).\end{aligned} \tag{5.2.8}$$

For the case $z \to 0$ and $h \neq 0$ scaling function can be expanded in the integer powers τ:

$$\sigma_e \approx \left(\sigma_1^q\, \sigma_2^t\right)^{\frac{1}{\varphi}} \left(B_0 + B_1\, \tau\, h^{-\frac{1}{\varphi}} + B_2\, \tau^2\, h^{-\frac{2}{\varphi}} + \ldots\right). \tag{5.2.9}$$

The A_i, B_i, C_i coefficients need not be positive. Later we shall see that from physical considerations one can determine a sign for some of them. Note that when describing behavior of σ_e close to percolation threshold by analogy to theory of phase transitions there is no need in the structure of the Kastellein-Fortuine demon type that interrelates finite "black" clusters. For the conductivity the analog of external field h is the ratio between phase conductivities σ_2/σ_1, i.e., at nonzero "field" h $(\sigma_2 \neq 0)$ "black" clusters (with conductivity σ_1) are connected through "white" (σ_2) bonds. Transition to the geometrical percolation theory lies in the fact that $\sigma_2 \to 0$, and, hence, one has to introduce special addition kind of "black" cluster bonding—the Fortuin–Kasteleyn demon.

The large field area (phase transition blurring area) in the theory of phase transitions (5.1.12c) is referred to as smearing region in the percolation theory (5.2.9). Its size—Δ, like in the theory of phase transitions, can be determined from two considerations. First, according to (5.2.6), a change in a and b: modes $|z| \gg 1$ (5.2.6a, b) by $z \ll 1$ mode (5.2.6c) occurs at $z \approx 1$. Replacing in z $|\tau|$ by Δ, we get

$$\Delta/h^{\frac{1}{\varphi}} = 1, \quad \Delta = h^{\frac{1}{\varphi}}, \quad \varphi = t + q. \tag{5.2.10}$$

Second, since (5.2.7) and (5.2.8) are valid at $\tau \gg \Delta$, and (5.2.9)—at $\tau \ll \Delta$, the value of Δ can be found from the condition of violation of convergence of series (5.2.7–5.2.9), i.e., when the next expansion member becomes of the order of the preceding one. Assuming that constants A_i, B_i, C_i have the values of the order of unity, we get the same value of Δ (5.2.10).

Summing up (5.2.7), 5.2.8), and (5.2.9), we write down [15]:

$$\sigma_e = \begin{cases} \sigma_1 \tau^t \left(A_0 + A_1 h \tau^{-(t+q)} + A_2 h^2 \tau^{-2(t+q)} + \ldots\right), & \Delta \ll \tau \ll 1, \quad \tau > 0, \quad \text{(a)} \\ \left(\sigma_1^q \sigma_2^t\right)^{\frac{1}{t+q}} \left(B_0 + B_1 \tau h^{-\frac{1}{t+q}} + B_2 \tau^2 h^{-\frac{2}{t+q}} + \ldots\right), & |\tau| \le \Delta, \quad \text{(c)} \\ \sigma_2 |\tau|^{-q} \left(C_0 + C_1 h |\tau|^{-(q+t)} + C_2 h^2 |\tau|^{-2(t+q)} + \ldots\right), & \Delta \ll |\tau| \ll 1, \quad \tau < 0. \quad \text{(b)} \end{cases} \tag{5.2.11}$$

In many cases (but not all!) we can restrict ourselves to the first term in (5.2.11), then beyond the smearing region σ_e behaves according to (5.2.1), and in the smearing region [15]:

$$\sigma_e = \left(\sigma_1^q \sigma_2^t\right)^{\frac{1}{t+q}}. \tag{5.2.12}$$

Note that under this approximate description, the smearing region is the value of τ whereby the conductivity realized in the "black" (σ_1) phase $\sigma_e = \sigma_2 \tau^t$ is compared to the conductivity determined by the "white" (σ_2) phase $\sigma_e = \sigma_2 |\tau|^{-q}$:

$$\sigma_1 \tau^t|_{\tau=\Delta} = \sigma_2 |\tau|^{-q}|_{\tau=\Delta}. \tag{5.2.13}$$

From expression (5.2.13) it follows immediately that $\Delta = (\sigma_2/\sigma_1)^{\frac{1}{t+q}}$, and on substituting Δ to any relation from (5.2.1), we get the expression σ_e in the smearing region (5.2.12). Qualitatively, behavior of $\sigma_e = \sigma_e(p)$ is represented in Fig. 5.3. Here Δ is the size of smearing region, a is the area of concentration above the percolation threshold (the analog of the nonsymmetric phase in the theory of phase transitions), b is the area below the percolation threshold, c is the region of phase transition smearing (the analog of the symmetric phase in the theory of phase transitions.

In Fig. 5.3 it is difficult to see the behavior of σ_e in smearing region. On the one hand, percolation theory is valid at $h \ll 1$, on the other—this condition means infinitesimality of Δ. Qualitatively, the existence of smearing region means (for example, for $\tau > 0$) in logarithmic coordinates $(\ln \sigma_e, \ln \tau)$ the saturation of $\ln \sigma_e$ with a reduction of τ.

Surprisingly, this transition for the two-dimensional case is qualitatively described already by EMT (Bruggeman approximation). Figures 5.4a, b show dependences obtained from the EMT-approximation in the two-dimensional case. In the limiting case $h \to 0$ ($\sigma_1 \to \infty$ or $\sigma_2 \to 0$) there is no smearing region, qualitatively the behavior of σ_e and ρ_e is shown in Fig. 5.5.

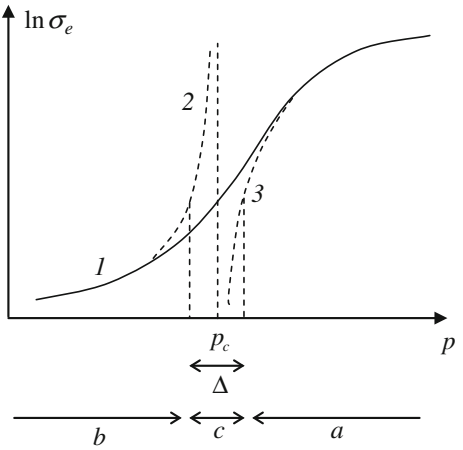

Fig. 5.3 General view of effective conductivity dependence $\sigma_e = \sigma_e(p)$ in the critical area: *1* $\sigma_e(p)$ at $h \neq 0$; *2* $\sigma_e(p)$ at $h = 0$, $\sigma_2 \neq 0$, $\sigma_1 = \infty$; *3* $\sigma_e(p)$ at $h = 0$, $\sigma_2 = 0$,$\sigma_1 \neq \infty$

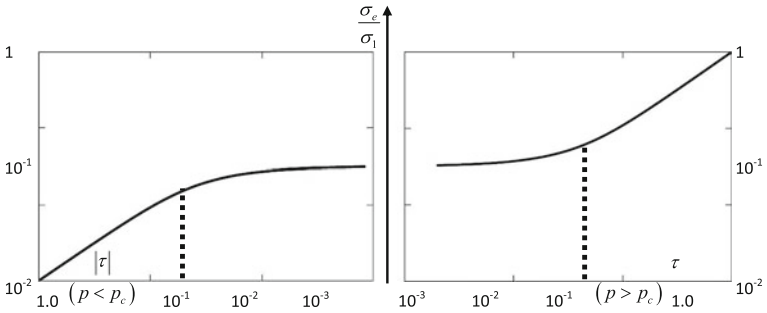

Fig. 5.4 The saturation of effective conductivity σ_e/σ_1 in smearing region Δ and its behavior far from percolation threshold

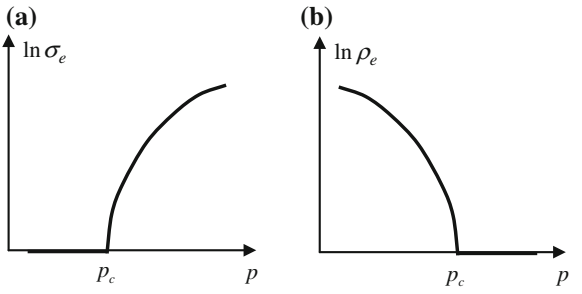

Fig. 5.5 Dependence of σ_e and ρ_e in the limiting case $h = 0$. **a** one of the phases is an ideal isolator, $\sigma_2 = 0$; **b** one of the phases is an ideal conductor $\sigma_1 = \infty, \rho_1 = 1/\sigma_1 = 0$.

One would think that so small area Δ inside an already small region $|\tau| \ll 1$ should not "manifest" itself during real experiments. However, as will be shown below, for instance, in Chap. 8 where strongly inhomogeneous systems with exponentially broad spectrum are described, the concept of smearing region is crucial and necessary.

5.3 Calculation of Critical Indices

Up to now, by analogy to theory of phase transitions, it has been assumed that at $p > p_c$ ($|\tau| \gg \Delta$) the region in Fig. 5.3, i.e., the region with infinite "black" phase cluster, is the analog to nonsymmetric phase in theory of phase transitions. Conductivity in this region is also available at zero "field" $h = 0$, similar to theory of phase transitions where the order parameter $\eta \neq 0$ at $h = 0$. And vice versa, in the region $|\tau| < \Delta$ the effective conductivity is proportional to "field" (5.2.2) and is zero in the zero field. However, in the percolation theory, unlike theory of phase transitions, the "field" can be zero both due to $\sigma_2 = 0$ (what happens in this case is described above), and with $\sigma_1 = \infty$. In the former case a medium of one of the phases is an ideal isolator; in the latter case a medium comprises an ideal conductor. Behavior of σ_e at $\sigma_1 = \infty$ is shown by dashed line in Fig. 5.3. Thus, $h = 0$ means the possibility of two ideal cases that can be conveniently represented as behavior of σ_e at $h = 0$, $\sigma_2 = 0$ and $\rho_e = 1/\sigma_e$, at $h = 0$, $\sigma_1 = 0$ (see Fig. 5.4).

Up to now, in the description of behavior of various physical values close to percolation threshold p_c the numerical values of critical indices have not been considered. The task of their theoretical determination is a considerable challenge. Suffice it to recall that for the development of theoretical methods of calculating critical indices in the theory of second-order phase transitions K. Wilson won a Nobel Prize.

At first, for the description of system behavior close to p_c few critical indices were employed—ν, β, t, q. Later on, the number of critical indices describing both the geometrical and physical properties of percolation system was increased. In the geometrical percolation theory, the number of critical indices was largely increased due to the fact that an infinite cluster at the percolation threshold is of fractal nature and, accordingly, has a large set (generally speaking, infinite) of fractal dimensions describing various structure details. For instance, outside perimeter, inside perimeter, distribution of "dead" ends, parallel bonds and so on. In the description of physical processes for each physical effect—conductivity, thermoelectricity, elasticity, etc., special critical indices are introduced as well.

It turned out that some of them are "secondary," i.e., expressed through the basic "primary" indices. Thus, the percolation theory has come against two main tasks: (1) to obtain the numerical values of critical indices and (2) to establish relations

between critical indices describing various physical processes in percolation systems. The first task will be described in the next paragraph, and the second task—in what follows.

There are a great number of more or less appropriate methods for determination of critical indices. From some simple and obvious methods, such as the Skal-Shklovsky model [47], [13] to such mathematically refined as field theory methods with the use of continual integration [3]. For the calculation of critical indices the percolation theory employs the same methods that were elaborated in second-order phase transition theory, in particular, series expansion [1, 17], expansion about critical dimension $d_c = 6$ in parameter $\varepsilon = d_c - d$ [18, 19, 28], renormalization group method [24, 53], fractal approach (drop model) [29, 58] (see details in [57]). Many papers (their number continues to increase) are dedicated to numerical simulation on large lattices (with size L larger than correlation radius) and on the lattices with $L < \xi$ (the so-called finite scaling). The first numerical calculation of critical index of conductivity t was made in [23]. The review [21] cites over 40 references dedicated to calculation of critical indices.

Here, we consider only several models which will be used in the modified form hereafter for a qualitative and quantitative description of different kinetic effects in percolation media. Prior to discussing these models, let us cite the numerical values of critical indices according to monograph [51]. From this point on, we will call these values canonical. Table 5.1 represents the numerical values of canonical critical indexes that will be used in the calculation of other critical indices.

The Last-Thouless model of percolation structure [26] is the simplest model above the percolation threshold. Figure 5.6 shows conducting channels along one of the three equivalent directions in the $\xi \times \xi \times \xi$ cube. All conducting bonds belong to infinite cluster, with the same current passing through each of them.

Table 5.1 Numerical values of canonical critical indices

Relationship with a critical index	Critical index	Lattice dimension d		
		$d = 2$	$d = 3$	$d = d_c = 6$
Correlation length $\xi \sim \lvert\tau\rvert^{-\nu}$	ν	$\frac{4}{3} \approx 1.33$	0.88	$\frac{1}{2}$
Power of infinite cluster $P_\infty \sim \tau^\beta$	β	$\frac{5}{36} \approx 0.14$	0.41	1
Effective conductivity at $p > p_c$ $\sigma_e \sim \tau^t$	t	1.30	2.0	3
Effective conductivity at $p < p_c$ $\sigma_e \sim \lvert\tau\rvert^{-q}$	q	1.30	0.73	0

Note ν_2 and β_2 are precise values. Critical indices at $d = d_c$ are calculated on the Bethe lattice ("Cayley tree") and also are established precisely. The remaining indices are calculated with certain error which is different in different works

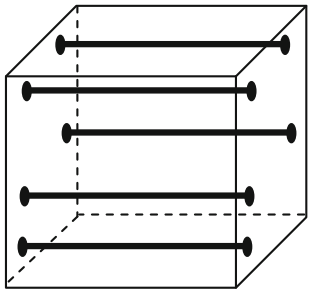

Fig. 5.6 Last-Thouless model of percolation structure

In this model the entire infinite cluster is current-carrying. In the cube of dimension $\xi \times \xi \times \xi$ the number of bonds in the infinite cluster is equal to $P_\infty(p)(\xi/a_0)^3$, where a_0 is a bond length. The number of conducting channels along one of the three equivalent directions is equal to

$$\frac{1}{3}\frac{P_\infty(p)(\xi/a_0)^3}{\xi/a_0} = \frac{1}{3}P_\infty(p)(\xi/a_0)^2. \tag{5.3.1}$$

The effective conductivity $\sigma_e = 1/\rho_e$ can be determined with regard to the fact that, on the one hand, for cube $\xi \times \xi \times \xi$ the resistance

$$R = \rho_e \frac{\xi}{\xi^2}, \tag{5.3.2}$$

and on the other hand,

$$R = \frac{1}{\sigma_1}\frac{\xi}{\frac{1}{3}P_\infty(p)\left(\frac{\xi}{a_0}\right)^2}. \tag{5.3.3}$$

Equating these expressions to each other we get

$$\sigma_e = \frac{1}{R\,\xi} \sim \sigma_1 P_\infty(p) \sim \sigma_1 \tau^\beta. \tag{5.3.4}$$

Of course, this model is oversimplified. It assumes that all the bonds of infinite cluster are electric current conductors and form a very simple structure—all conducting channels have the length ξ. Nevertheless, this model does reflect the essence of the process. The effective conductivity depends on the proximity to percolation threshold as a power function. The numerical value of critical index of conductivity t obtained in this model is equal to critical index β, in the three-dimensional case equal to $\beta_3 = 0.41$ (see Table 5.1), which is considerably different from the canonical value $t_3 = 2.0$. The assumption that all the bonds of the infinite cluster are current conductors did "undermined" for this model. Indeed,

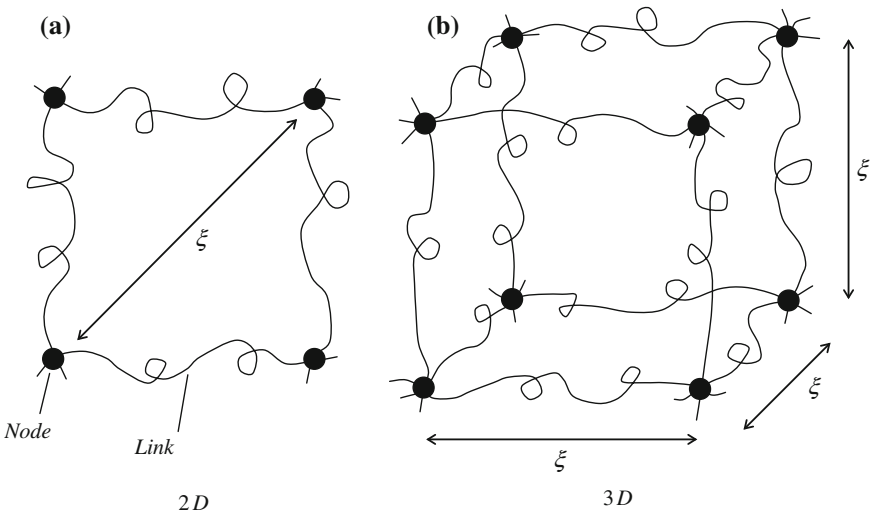

Fig. 5.7 Skal-Shkovsky model of percolation structure above the percolation threshold in the two-dimensional (**a**) and three-dimensional (**b**) cases

some of them, as is known, for example, from the numerical simulation, are dead ends and at $\sigma_2 = 0$ do not participate in current transfer.

A more complicated model that takes into account the presence of dead ends is the Skal-Shklovsky model [45, 47] (see also [13]). The authors themselves call this model a single-conductor network model. To construct it, let us assume that in the infinite cluster one can single out a single-scale current-carrying network with a characteristic dimension equal to correlation length ξ (Fig. 5.7).

To calculate σ_e, like in the Last-Thouless model, one must know the length of a link. Let it have a power dependence on τ:

$$\ell \approx a_0 \tau^{-\zeta}, \tag{5.3.5}$$

where ζ is critical index that can be found from the following considerations. If the network bond is broken with a probability $(p - p_c)/p$, the fraction of integral bonds will be surely equal to $p[1 - (p - p_c)/p] = p_c$. As long as in the assumed model a link is single-conductor, it will be broken already with breaking a single bond. Thus, the probability of breaking each link is proportional to its length and equal to $(\ell/a_0)(p - p_c)/p_c$. With a certain value of fraction of broken links y_c, the network of links will be broken as well $y_c = [(p - p_c)/p]\,(\ell/a_0)$, hence

$$\ell \sim (p - p_c)^{-1}, \tag{5.3.6}$$

i.e., in the designations of (5.3.5) $\zeta = 1$.

Knowing ℓ, similar to the way it was done in the Last-Thouless model, one can determine critical index of the effective conductivity

$$\frac{1}{\sigma_1}\frac{\ell}{a_0^{d-1}} = \frac{1}{\sigma_e}\frac{\xi}{\xi^{d-1}}, \quad \sigma_e \sim \frac{\sigma_1}{\ell\xi^{d-2}}, \tag{5.3.7}$$

where d is problem dimension.Substituting $\xi = a_0\tau^{-\nu}$ and ℓ from (5.3.6) into (5.3.7) gives

$$\sigma_e = \sigma_1\tau^{1+\nu(d-2)}, \quad t_2 = 1, \quad t_3 = 1+\nu_3 = 1.88. \tag{5.3.8}$$

The critical indices of conductivity found for the two-dimensional t_2 and three-dimensional t_3 cases are closer to the canonical, however, in the two-dimensional case the critical index $\zeta_2 = 1$ leads to a controversy. With a reduction in τ (on approximation to percolation threshold) due to the fact that $\nu_2 > \zeta_2$, the correlation length grows faster than the length of link ℓ, i.e., at some value of $\tau > 0\,(p > p_c)$ the link should have been broken. And this contradicts the condition of $p > p_c$. Such a controversy, of course, is due to the fact that the model takes no account of doubling the bonds in a link.

Further model development and account of parallel bonds lead to creation of the so-called Nodes-Links-Blobs model (NLB) [50]. In this model, the two elements, namely nodes and single-conductor links (see Fig. 5.7) are supplemented with "blobs"—parts of the network comprising many parallel bonds (Fig. 5.8).

Now the controversy that appeared in the Skal-Shklovsky model is removed. The link (single-conductor with $\ell \sim \tau^{-1}$) need not be longer than ξ, the missing part being added by "blobs."

The NLB model is also approximate. According to this model, a "blob" is supposed to include so many parallel bonds that "blob" resistance as compared to

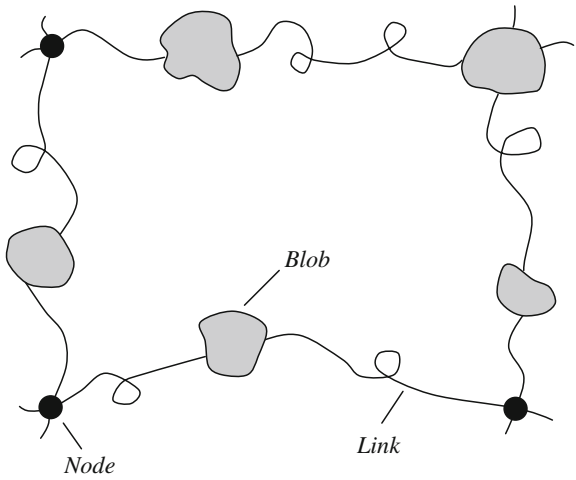

Fig. 5.8 Nodes–Links–Blobs model (dead ends are not indicated)

link resistance can be ignored. Thus, the entire system resistance is governed by the so-called single connected bonds (SCB), i.e., such bonds when a breakdown of any of them will result in current cut-off. It is exactly SCB that form a link in the Skal-Shklovsky model and a link in the NLB model. In the works [9, 10, 40] it was shown that the number of SCB bonds between two N_{SCB} nodes has in the context of NLB model a critical index equal to -1 (compare to (5.3.6)

$$N_{\mathrm{SCB}} \sim \tau^{-\zeta_R}, \quad \zeta_R = 1 \tag{5.3.9}$$

where the sign R will be explained a little bit later.

From the formula (5.3.9) it immediately follows [let us repeat the reasoning of (5.3.6)→(5.3.8)] that critical index of the effective conductivity:

$$\sigma_{\mathrm{e}} = \sigma_1 \tau^{\zeta_R + (d-2)\nu}, \quad \zeta_R = 1. \tag{5.3.10}$$

Both in the two- and three-dimensional cases critical index t in the NLB model coincides with critical index of the Skal-Shklovsky model:

$$t_{\mathrm{NLB}} = 1 + (d-2)\nu, \quad t_2 = 1, \quad t_3 = 1.88, \ldots, \quad t_6 = 3, \tag{5.3.11}$$

in particular, for critical dimensions $d_{\mathrm{c}} = 6$ critical index assumes an exact value (see Table 5.1).

Up to this point we have considered the models of percolation structure above the percolation threshold $p > p_c$ and assumed that only good conducting phase with electric conductivity σ_1 takes part in conduction, and $\sigma_2 = 0$. Below the percolation threshold there is no infinite cluster, and the model of percolation conducting structure should comprise small conducting bonds. Now, specifically these bonds determine in the first approximation ($\sigma_1 = \infty, \sigma_2$ is finite) the complete system resistance (see Table 5.1).

Of vital importance here are those places between the parts of good conducting phase that are maximum close—"at the distance" of one bad conducting bond. Such bonds (see Fig. 5.9) are called Single DisConnected Bonds (SDCB). The SCB bonds are arranged in succession. A breakdown of any of them (i.e., substitution of the "black" bond (σ_1) by the "white"(σ_2)) results in system transition from $p > p_c$ to $p < p_c$ state. The number of such bonds is governed by critical index ζ_R (5.3.9), where index R is a logical consequence of the fact that SCB resistance is a sum of resistances of the "black" phase bonds. The SDCB, on the contrary, are arranged in parallel to each other. A breakdown of any of them (substitution of the "white" bond (σ_2) by the "black (σ_1)) results in system transition from $p < p_c$ to $p > p_c$. Their number is also governed by critical index designated as ζ_G, where index G logically follows from the fact that the sum of conductances of these bonds yields SDCB conductance:

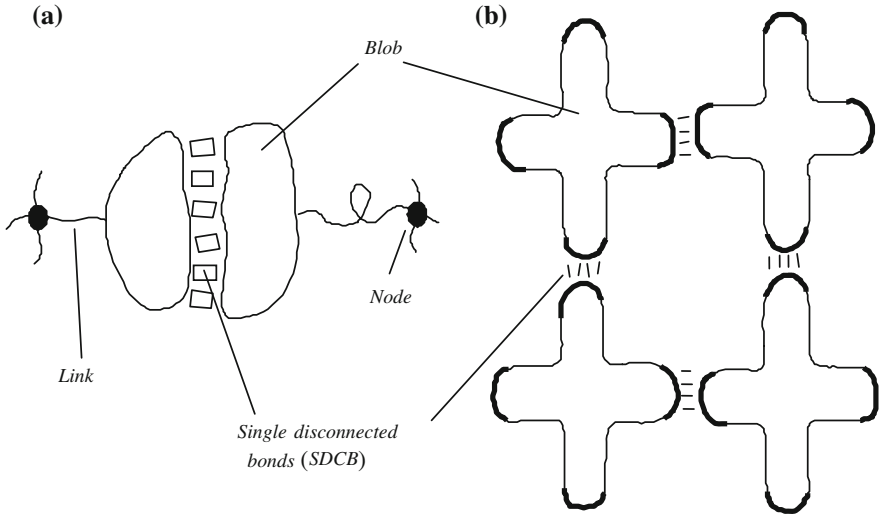

Fig. 5.9 Model of percolation structure below the percolation threshold: **a** case including "blobs," nodes, SCB-single connected bonds and shorted bonds of bad connecting phase, the so-called single disconnected bonds (SDCB); **b** schematic according to work [11]

$$N_{\mathrm{SDCB}} \sim |\tau|^{-\zeta_G}. \tag{5.3.12}$$

In the work [60] it is shown that $\xi_G = 1$.

Knowing N_{SDCB}, it is easy to find critical index of effective conductivity σ_{e} below the percolation threshold. On the one hand, conductance G of the cube ξ^d is equal to

$$G = \sigma_{\mathrm{e}} \frac{\xi^{d-1}}{\xi} = \sigma_{\mathrm{e}} \xi^{d-2} = \sigma_{\mathrm{e}} |\tau|^{-\nu(d-2)} a_0^{d-2}, \tag{5.3.13}$$

on the other hand,

$$G = \sigma_2 \, a_0^{d-2} \, N_{SDCB} = \sigma_2 \, a_0^{d-2} \, |\tau|^1, \tag{5.3.14}$$

when

$$\sigma_{\mathrm{e}} = \sigma_2 |\tau|^{-(1-\nu(d-2))}, \quad q = 1 - \nu(d-2). \tag{5.3.15}$$

Thus, in the two- and three-dimensional cases according to this model we have

$$q_2 = 1, \quad q_3 = 0.22. \tag{5.3.16}$$

It is clear that the above models yield critical indices t and q with little accuracy. However, a lot of credit must go to these models because they allowed pointing out the main elements of percolation structure in the problem of current flow. Critical indices describing the elements of these structures obtained in the context of the above-considered approach, are approximate and sometimes lead to a controversy, for example, according to (5.3.15) $q_6 = 1$ instead of the canonical (see Table 5.1) $q_6 = 0$. More strict reasoning within the same models [38, 60] yields only the inequalities

$$t \geq 1 + \nu(d-2), \quad q \geq 1 - \nu(d-2).$$

"First principle" calculation of critical indices by analogy with the theory of second-order phase transitions will be called a microscopic approach. The description of kinetic phenomena in percolation systems can be also attacked on the other side: to construct certain generalized phenomenological model of percolation structure, whose geometry elements have critical indices that are supposed to be known, and to use this model for the description of various kinetic effects. Such an approximate approach, of course, where it "works," would allow to describe in a unified manner various kinetic processes in percolation media and to indicate the relation between critical indices of these processes. Exactly this model will be dealt with in the following paragraph.

5.4 Hierarchical Model of Percolation Structure

In this paragraph, we consider a hierarchical model (HM) of percolation structure which afterwards will be used to describe various physical processes in percolation media.

1. First we consider an ideal case for $p > p_c$: good conducting phase has finite conductivity σ_1, and bad conducting phase is an ideal dielectric, $\sigma_2 = 0$. Let us modify the NLB model given in Fig. 5.10. The resistance of a bridge (thus, of the entire system on dimensions ξ) is determined by its length $a_0 \cdot N_1$, where a_0, like before, is a minimum dimension in the system, for instance, bond length. We will ignore the resistance of blobs, just like in the NLB model, and select the

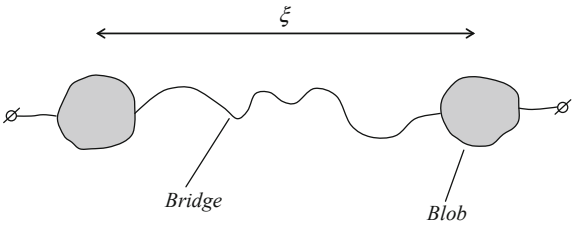

Fig. 5.10 Schematic of the first step of hierarchical model above the percolation threshold $(p > p_c)$

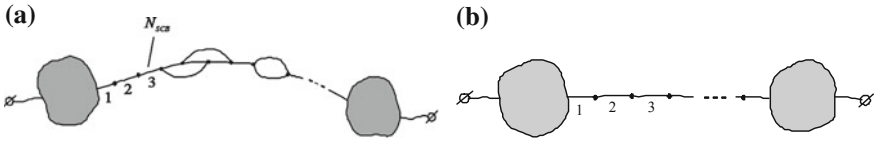

Fig. 5.11 Schematic of the first step of HM (**b**) and NLB model (**a**)

resistance of the bridge such that the resulting critical index of conductivity coincides with the canonical one. The resistance of the bridge R_1 and of the entire system on ξ is governed by its length which is assigned by the number of bonds in the bridge N_1. The law for N_1 will be chosen as

$$N_1 = \tau^{-\alpha_1}. \tag{5.4.1}$$

This law is different from a similar for NLB (see Fig. 5.11). In the percolation structure apart from "blobs" including many parallel bonds, there are portions with two or three parallel bonds. The number of parallel bonds—SCB, $N_{\mathrm{SCB}} \sim \tau^{-1}$. In the first step of HM the bridge lacks any bonds, except for unparallel, but their number is a function of τ by a different law $N_1 \sim \tau^{-\alpha_1}$.

Let us determine critical index α_1 through critical index of conductivity t which will be assumed to be known. On the one hand, system resistance on the dimensions ξ is of the form

$$R_1 = \frac{N_1}{\sigma_1\, a_0^{d-2}} = \frac{\tau^{-\alpha_1}}{\sigma_1\, a_0^{d-2}}, \tag{5.4.2}$$

on the other hand,—$(\xi = a_0\, \tau^{-\nu})$ it can be written as

$$R_1 = \frac{1}{\sigma_{\mathrm{e}}\, \xi^{d-2}} = \frac{\tau^{\nu\,(d-2)}}{\sigma_{\mathrm{e}}\, a_0^{d-2}}, \tag{5.4.3}$$

and, since $\sigma_e = \sigma_1\, \tau^t$, from (5.4.2) and (5.4.3) we get

$$\alpha_1 = t - \nu(d-2) = \zeta_R. \tag{5.4.4}$$

This index ζ_R has been already encountered in percolation theory, it governs system resistance on the dimensions ξ [60]:

$$R_\xi \sim \tau^{-\zeta_R}. \tag{5.4.5}$$

Here it is used to determine the bridge parameters. A bridge can be represented as a combination of bonds, each having the resistance $r_1 = (1/\sigma_1)\left(a_0/a_0^{d-1}\right)$. In fact, separate parts of the bridge are scattered among the blobs, but in the model under consideration (see Fig. 5.11b all of them are connected together in a single

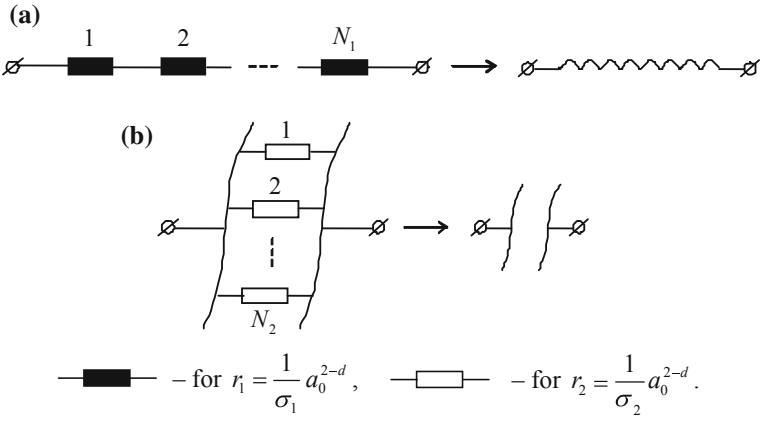

Fig. 5.12 Schematic of the main elements of percolation structure **a** bridge, **b** interlayer

link. Thus, at $p > p_c$ and $\sigma_2 = 0$, (where σ_1 is finite) a model of percolation structure is a bridge and "blobs," and the resistance of the latter can be ignored. The bridge will be designated by a wavy line (see Fig. 5.12a).

2. Consider now an ideal case at $p < p_c$: bad conducting phase σ_2 has finite conductivity, and good conducting phase is an ideal conductor $\rho_1 = 1/\sigma_1 = 0$. The main role in the determination of system resistances is played by SDCB consisting of small conducting phase and connected in parallel [44, 55], see also [38, 60]. Here, unlike the referred works, in the HM of the percolation structure we assign

$$N_2 = |\tau|^{-\alpha_2}, \tag{5.4.6}$$

so that critical index governing behavior of σ_e at $p < p_c$ is equal to q. For this purpose we note that, on the one hand, system conductance on the dimensions of order ξ [38, 60] is of the form:

$$G_\xi \sim |\tau|^{\zeta_G}, \tag{5.4.7}$$

and on the other hand—(see Fig. 5.12b):

$$G_\xi = \sigma_2 N_2. \tag{5.4.8}$$

Comparing (5.4.6), (5.4.7), and (5.4.8) and taking into account that $\sigma_e(p < p_c) = \sigma_2 |\tau|^{-q}$, for N_G we get [38, 48]:

$$\alpha_2 = q + \nu(d-2) \equiv \zeta_G. \tag{5.4.9}$$

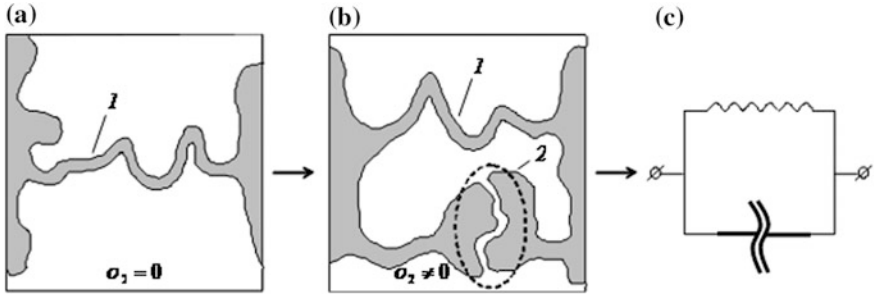

Fig. 5.13 Model of percolation structure above the percolation threshold: **a** ideal case $\sigma_2 = 0$, the only element of percolation structure which is essential for determination of system resistance is bridge *1*; **b** case $\sigma_2 \neq 0$, one should take into account one more element of percolation structure—interlayer *2* that shunts the bridge; **c** percolation structure in terms of bridge and interlayer

Thus, at $p < p_c, \sigma_2 \neq 0, \rho_1 = 1/\sigma_1 = 0$, a model of percolation structure is an interlayer (Fig. 5.12b) and blobs with bridges whose resistance $(\rho_1 = 0)$ does not contribute to system resistance.

3. Let us now move from "idealization" of $h = \sigma_2/\sigma_1 = 0\,(\sigma_2 = 0\,\text{or}\,\rho_1 = 0)$ and consider a more realistic case when both above and below the percolation threshold $h = \sigma_2/\sigma_1 \neq 0$. In particular, it means that above the percolation threshold (Fig. 5.13) part of the current (of course, minor—by virtue of $h \ll 1$) can pass through the interlayer—the element of percolation structure consisting of bad conducting phase. The bridge in this case is shunted by the interlayer (see Fig. 5.13b).

Schematic below the percolation threshold (Fig. 5.14), when at $h \neq 0$ the bridge adds its small part of resistance to the interlayer resistance is similar and presented in Fig. 5.14b [32, 33].

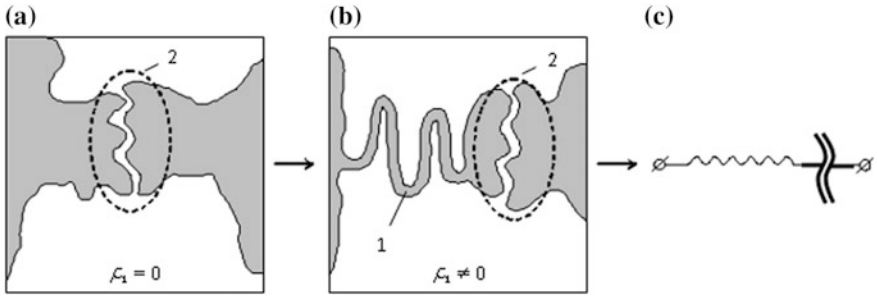

Fig. 5.14 Model of percolation structure below the percolation threshold: **a** ideal case $\rho_1 = 0$, the only element of percolation structure which is essential for determination of system resistance is interlayer *2*; **b** case $\rho_1 \neq 0$, one should take into account one more element of percolation structure, namely, bridge *1*. **c** schematic representation of part of percolation structure in terms of bridge and interlayer

The schemes 5.4.10 and 5.4.11 show the first corrections to the ideal case of $h = \sigma_2/\sigma_1 = 0$ ($\sigma_2 = 0$ in Fig. 5.13b and $\rho_1 = 1/\sigma_2 = 0$ in Fig. 5.14b. This specification alone allowed qualitative and in some cases quantitative [33] explanation of the regularities of various physical processes in percolation media. Prior to showing it, we continue constructing the following IM of percolation structure [34] above the percolation threshold:

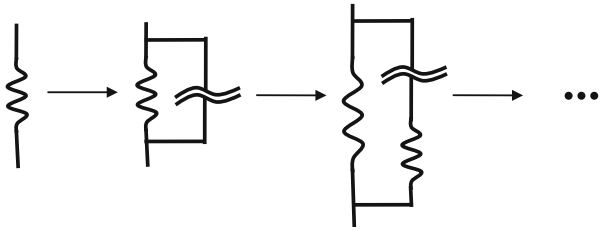

(5.4.10)

and below the percolation threshold

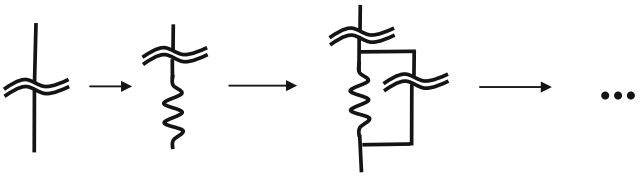

(5.4.11)

Graphical schemes (5.4.12) and (5.4.13) consecutively show the first, second and other hierarchy levels of percolation structure hierarchical model. Each of them in their own approximation, if we are dealing, for instance, with conductivity problems, yields the value of full resistance R or conductance $G = 1/R$ of system for the dimensions of orderξ. These schemes for the conductivity problem (and not only) should be logically replaced by the equivalent electric circuits:

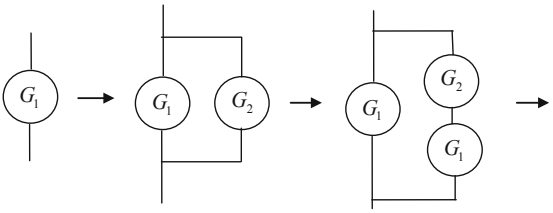

(5.4.12)

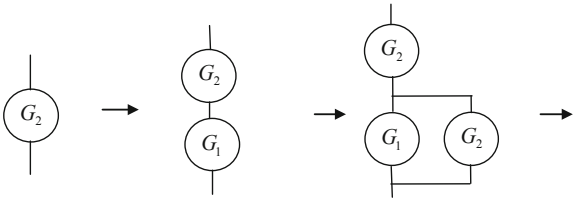

(5.4.13)

where G_1 is bridge conductance (5.4.1)–(5.4.4):

$$G_1 = 1/R_1 = 1/r_1\, N_1 = \sigma_1\, a_0^{d-2}/N_1 = \sigma_1\, a_0^{d-2}|\tau|^{\alpha_1}, \quad \alpha_1 = \zeta_R, \tag{5.4.14}$$

and G_2 is interlayer conductance (5.4.5)–(5.4.8):

$$G_2 = 1/R_2 = \sigma_2\, a_0^{d-2}\, N_2 = \sigma_2\, a_0^{d-2}|\tau|^{-\alpha_2}, \quad \alpha_2 = \zeta_G. \tag{5.4.15}$$

The bridge and interlayer conductances can appear in the expressions (5.4.12) and (5.4.13) with their weights. If we ignore this, then for a full (effective) conductance of system G_e on dimensions of order ξ one can write down a closed equation (an analog of the Dyson equation), solution of which gives G_e with regard to all hierarchy levels. Indeed, from (5.4.12) it follows

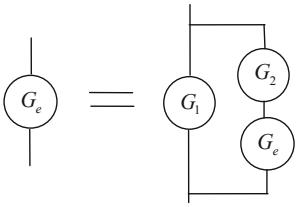

(5.4.16)

and from (5.4.13) we have

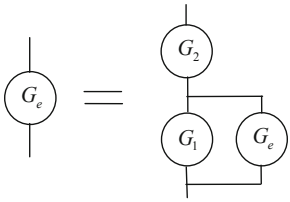

(5.4.17)

in this case, of course, (5.4.12) and (5.4.13) are supposed to converge. Equations (5.4.16) and (5.4.17), written in symbolic form, are conventional quadratic equations:

$$G_e^2 - G_1\, G_e - G_1\, G_2 = 0, \quad p > p_c; \quad G_e^2 + G_1\, G_e - G_1\, G_2 = 0, \quad p < p_c. \tag{5.4.18}$$

Note that the ratio G_2/G_1 according to (5.4.14) and (5.4.15) is of the form

$$\frac{G_2}{G_1} = \frac{\sigma_2}{\sigma_1}|\tau|^{-(\zeta_R+\zeta_G)} = \frac{\sigma_2}{\sigma_1}|\tau|^{-(t+q)} = \left(\frac{\Delta}{|\tau|}\right)^{t+q}, \tag{5.4.19}$$

and is a small parameter, since beyond smearing region [see (5.2.1)] $|\tau| \gg \Delta$, which means infinitesimality of the right side in (5.4.19). Expanding solution of Eqs. (5.4.18) in the small parameter G_2/G_1, we obtain

$$\begin{aligned} G_e &= G_1\left[1 + G_2/G_1 - (G_2/G_1)^2 + \ldots\right], \quad p > p_c, \\ G_e &= G_2\left[1 - G_2/G_1 + 2(G_2/G_1)^2 - \ldots\right], \quad p < p_c. \end{aligned} \tag{5.4.20}$$

With regard to $G_e = \sigma_e\, \xi^{\alpha-2} = \sigma_e\, a_0^{d-2}|\tau|^{-\nu(d-2)}$, and taking into account (5.4.13), (5.4.14), and (5.4.19), we find expressions (5.4.20) passing to known expressions (5.2.11a), (5.2.11c) [15] for σ_e.

Thus, the hierarchical model of percolation structure yields all the expansion members of scaling function of the effective conductivity σ_e to an accuracy of numerical values of factors A_i and C_i, however, allows to determine their sign. These signs can be also found based on simple physical reasons. Thus, adding an interlayer to the second hierarchy level above the percolation threshold [(5.4.10) and (5.4.12) second schematic] can only increase the effective conductivity, therefore, $A_1 > 0$ (5.2.11), and adding a bridge to the second level of hierarchical model below the percolation threshold can only reduce σ_e, therefore, $C_1 < 0$ (5.1.11c).

4. Smearing region. At first sight, a simple model of percolation structure in smearing region (sometimes it is said—on the percolation threshold) is impossible, since at $p = p_c$ the correlation length is infinite and the model should include an infinite number of elements of various structure. Indeed, infinite cluster of good conducting phase on the percolation threshold has a fractal structure [16, 41]. Fractality feature is used in many models of percolation structure (see, for instance, [12, 31, 43, 58], many models are considered in the review [8]). However, all these models consider only good conducting phase structure, i.e., the case of $\sigma_2 = 0$. Therefore, they deal with calculation of critical indices of various values, in particular, the effective conductivity t above the percolation threshold. As regards the model of percolation structure in smearing region for the effective conductivity, it should result in the expression $\sigma_e = \left(\sigma_1^q\, \sigma_2^t\right)^{\frac{1}{t+q}}$, i.e., include structural elements of bad conducting phase (with $\sigma_2 \neq 0$) alongside with good conducting one.

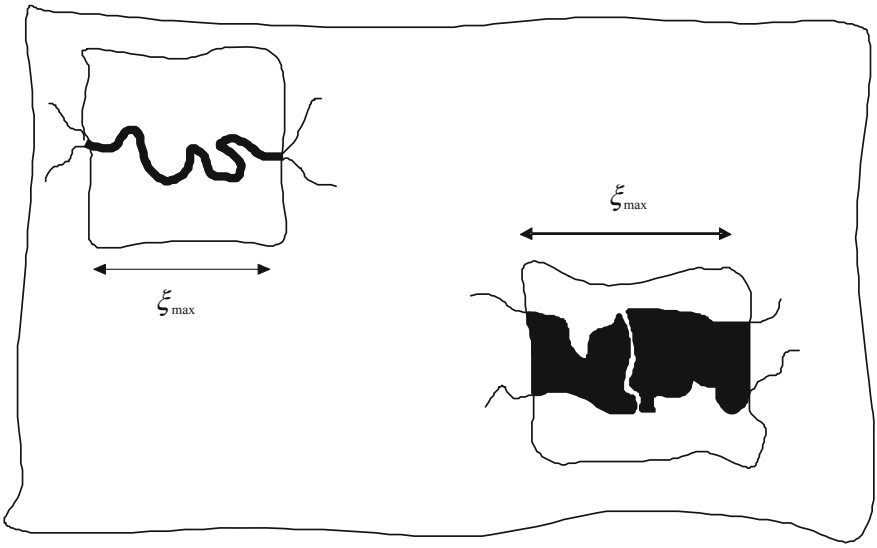

Fig. 5.15 Structure of percolation system in smearing region: In different regions with dimensions of order ξ_{max} one can come across both a bridge and an interlayer. These regions have the same resistance values

By definition, smearing region is such a range of τ values where the contributions to σ_e of the good conducting (σ_1) and bad conducting (σ_2) phases become equalized [see (5.1.13)]. The correlation length in this case $(-\Delta \leq \tau \leq +\Delta)$ is finite,

$$\Delta = (\sigma_2/\sigma_1)^{\frac{1}{t+q}} \neq 0, \quad \xi_{max} = \xi(\Delta) = a_0\, \Delta^{-\nu} = a_0(\sigma_2/\sigma_1)^{-\frac{\nu}{t+q}} \neq \infty.$$

Finiteness of ξ and equality of contribution of phases to Δ means that in smearing region on the dimensions of order ξ one can come across different structures. It can be both the bridge and the interlayer type (see Fig. 5.15). Both of them will make approximately equal contribution to resistance.

In Ref. [49], a model of percolation structure in smearing region is proposed that includes both a bridge and an interlayer. Such a model is given in Fig. 5.16. In this model the bridge and interlayer resistances at $|\tau| = \Delta$ are as follows:

$$R_1 = \frac{N_1(\tau = \Delta)}{\sigma_1\, a_0^{d-2}} = \frac{\Delta^{-\alpha_1}}{\sigma_1\, a_0^{d-2}}, \quad \alpha_1 = \zeta_R, \tag{5.4.21}$$

$$R_2 = \frac{1}{\sigma_2\, a_0^{d-2} N_2(\tau = \Delta)} = \frac{\Delta^{\alpha_2}}{\sigma_2\, a_0^{d-2}}, \quad \alpha_2 = \zeta_G. \tag{5.4.22}$$

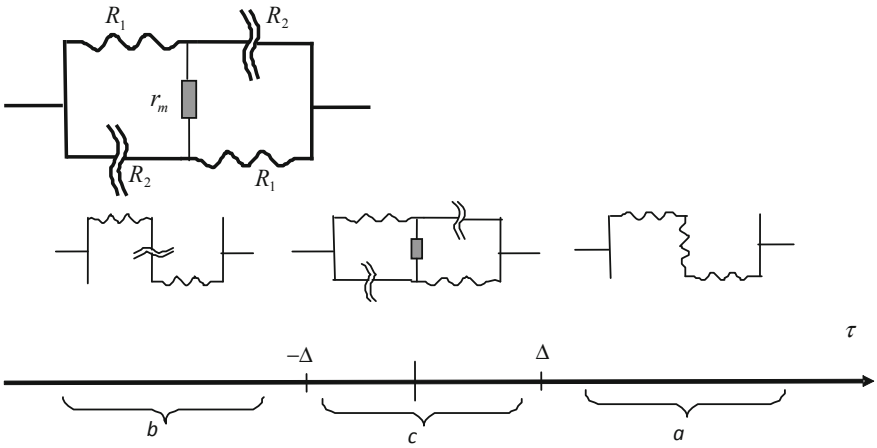

Fig. 5.16 Model of percolation structure in smearing region: **a** $p > p_c$ there is a path along the good conducting phase (bridges); **b** $p < p_c$ current will necessarily flow through bad conducting phase (interlayers); **c** $|\tau| < \Delta$ smearing region, bridges, and interlayers make equal contribution to resistance

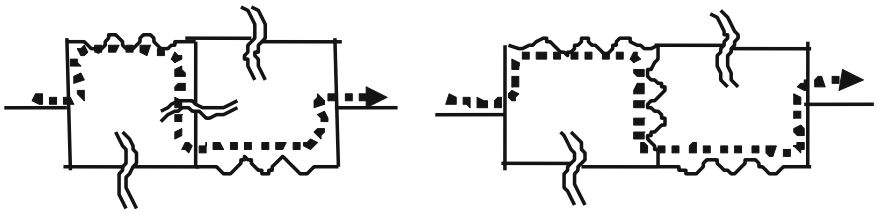

Fig. 5.17 Model of smearing region for two extreme cases: **a** $a - \tau = \Delta, r_m = r_1$, current can flow only through the bridges (good conducting phase), interlayers (bad conducting phase) only shunt the bridges; **b** $b - \tau = -\Delta, r_m = r_2$, current must flow through the interlayer (bad conducting phase)

Note that $R_1(\Delta) = R_2(\Delta)$. Resistance r_m in the schematic of Fig. 5.16a should be such that in going from area c to area a, the model would pass to a model of percolation structure above the percolation threshold (where bridge is the main element), and in going from c to b it would pass to a model of percolation structure below the percolation threshold (where interlayer is the main element). Such requirements can be met on the assumption that with probability P_Δ the resistance $r_m = r_1$, and with probability $1 - P_\Delta$—it is equal to $r_m = r_2$, where

$$P_\Delta = \frac{\Delta + \tau}{2\Delta}, \quad 1 - P_\Delta = \frac{\Delta - \tau}{2\Delta}. \tag{5.4.23}$$

In other words, if r_m is a bridge, the schematic of a model of percolation structure in smearing region (Fig. 5.16c) goes over to a series connection of

bridges, and the interlayers are just shunting the bridges (see Fig. 5.16a). And on the contrary, if $r_m = r_2$, current must necessarily flow along the interlayer. With $\tau \to \Delta$, the probability is increased, the closer τ is toΔ, and the system—to the boundary between the areas c and a in Fig. 5.16, the larger is the probability of a bridge occurring on the dimensions of order ξ. With $\tau = \Delta$, the interlayer as the main element of percolation structure disappears (see Fig. 5.17a). And on the contrary, for $\tau \to -\Delta$, interlayers are seen more frequently, and, for $\tau = -\Delta$, bridges as the main element of percolation structure disappear. Current must necessarily flow through the interlayers (see Fig. 5.17b).

Thus, on the whole, the percolation structure of a medium is as follows:

- beyond smearing region, above the percolation threshold ($|\tau| \gg \Delta, \tau > 0$) the system resistance is governed by bridges with resistance $R_1 = r_1\tau^{-\alpha_1}, r_1 = 1/\sigma_1 a_0^{d-2}, \alpha_1 = \zeta_R = t - \nu(d-2)$.
- beyond smearing region, below percolation threshold ($|\tau| \gg \Delta, \tau < 0$) the system resistance is governed by interlayers with resistance $R_2 = r_2\tau^{+\alpha_2}, r_2 = 1/\sigma_2 a_0^{d-2}, \alpha_2 = \zeta_G = q + \nu(d-2)$.
- in smearing region (including the percolation threshold itself for $p = p_c$) the correlation radius ξ and the resistances of bridges and interlayers no longer depend on τ, so $R_1 = R_1(\Delta)$, $R_2 = R_2(\Delta)$, $\xi = \xi_{\max} = \xi(\Delta)$, and the main element of percolation structure with certain probability P_Δ is a bridge, and with probability $1 - P_\Delta$—an interlayer.

Hereafter, we shall see that the described model of percolation structure provides for a simple, illustrative, and unified means of describing a plurality of various physical processes in the media with percolation threshold. In particular, a model of percolation structure in smearing region allowed obtaining the basic regularities of finite scaling at $\sigma_2/\sigma_1 \neq 0$ and the effective conductivity in systems with the so-called exponentially wide spectrum of local conductivity distribution.

5.5 Examples of Applications of Percolation Theory

Many different theoretical models based on the percolation and explain different transport phenomena (hopping transport in disordered materials—[2], transport properties of bilayer graphene [42], kinetic properties of polymer composites—[35], properties of tunneling resistor networks—[36], conductivity of acids—[56], thermal conductivity—[5, 27].

Application of percolation theory in porosity media considered in works [20, 37, 46]. Application of percolation theory for the description of ionic conductors was described in [6, 14], 61].

Nonstandard modification or applications of percolation theory considered in [7, 52] (a mechanism of nonuniversality of critical component for conductivity in composites). Two percolation thresholds were observed in the paper [59].

References

1. Adler J, Meir Y, Harris AB, Klein L (1990) Low-concentration series in general dimension. J Stat Phys 58:511–538
2. Baranovskii SD, Rubel O, Thomas P (2005) Theoretical description of hopping transport in disordered materials. Thin Solid Films 487:2–7
3. Barthelemy M (2000) Path-integral approach to strongly nonlinear composites. Phys Rev B 62:8576–8579
4. Broadbent SR, Hammersley JM (1957) Percolation processes. In crystals and mazes. Proc Camb Phyl Soc 53:629–633
5. Bulat LP, Osvenskii VB, Pshenai-Severin DA (2013) Influence of grain size distribution on the lattice thermal conductivity of Bi_2Te_3-Sb_2Te_3-based nanostructured materials. Phys Solid State 55:2442–2449
6. Bunde A, Heitjans P, Sylvio IS et al (2007) Anomalous transport and diffusion in percolation systems. Diffus Fundam 6:9.1–9.17
7. Cai W, Tu S, Gong J (2006) A physically based percolation model of the effective electrical conductivity of particle filled composites. J Compos Mater 40:2131–2142
8. Clerc JP, Giraud G, Laugier JM, Luck JM (1990) The electrical conductivity of binary disordered systems, percolation clusters, fractals and related models. Adv Phys 39:191–309
9. Coniglio A (1981) thermal phase transition of the dilute s-State potts and n-Vector models at the percolation threshold. Phys Rev Lett 46:250–253
10. Coniglio A (1982) Cluster structure near the percolation threshold. J Phys A 15:3829–3844
11. Coniglio A, Stanley HE (1984) Screening of deeply invaginated clusters and the critical behavior of the random superconducting network. Phys Rev Lett 52:1068–1071
12. de Arcangelis L, Redner S, Coniglio A (1985) Anomalous voltage distribution of random resistor networks and new model for the backbone at the percolation threshold. Phys Rev B 31:4725–4727
13. de Gennes PGJ (1976) On relation between percolation theory and the elasticity of gels. Phys Lett 37:L1–2
14. Dieterich W, Durr O, Pendzig P et al (1999) Percolation concepts in solid state ionics. Phys A 266:229–237
15. Efros AL, Shklovskii BI (1976) Critical behaviour of conductivity and dielectric constant near the metal-non-metal transition threshold. Phys Stat Sol B 76:475–485
16. Feder J (1988) Fractals. Plenum Press, New York, 283 p
17. Fisch R, Harris AB (1978) Critical behavior of random resistor networks near the percolation threshold. Phys Rev B 18:416–420
18. Harris B (1987) Field-theoretic formulation of the randomly diluted nonlinear resistor network. Phys Rev B 35:5056–5065
19. Harris AB, Lubensky TC (1987) Randomly diluted xy and resistor networks near the percolation threshold. Phys Rev B 35:6964–6986
20. Hunt A, Ewing R, Ghanbarian B (2014) Percolation theory for flow in porous media. Springer, Berlin
21. Isichenko MB (1992) Percolation, statistical topography, and transport in random media. Rev Mod Phys 64:961–1043
22. Kasteleyn PW, Fortuin CM (1969) Phase transition in lattice systems with random local properties. J Phys Soc Jpn Suppl 26:11
23. Kirkpatrick S (1973) Percolation and conduction. Rev Mod Phys 45:574–588
24. Kirkpatrick S (1977) Percolation thresholds in Ising magnets and conducting mixtures. Phys Rev 15:1533–1538
25. Landau LD, Lifshitz EM (1980) Statistical physics,vol 5, 3rd edn. Butterworth-Heinemann, Oxford, 544 p
26. Last BJ, Thouless DJ (1977) Percolation theory and electrical conductivity. Phys Rev Lett 27:1719–1721

27. Liang LH, Wei YG, Li Baowen (2008) Thermal conductivity of composites with nanoscale inclusions and size-dependent percolation. J Phys Condens Matter 20:365201
28. Lubensky TC, Harris B (1987) Potts-model formulation of the random resistor network. Phys Rev B 35:6987–6996
29. Luk'yanets SP, Snarskii AA (1988) Model of macroscopically inhomogeneous mixtures of a perfect conductor and an insulator near the mobility edge. Sov Phys JETP 67:1467–1470
30. Ma Shang-Keng (1980) Modern theory of critical phenomena. Westview Press, New York, 561 p
31. Mandelbrot BB, Given JA (1984) Physical properties of a new fractal model of percolation clusters. Phys Rev Lett 52:1853–1856
32. Morozovsky AE, Snarskii AA (1988) Critical behaviour of 1/f noise in percolation systems Preprint IMF AN USSR, 31.88 p. 15 (in Russian)
33. Morozovsky AE, Snarskii AA (1989) Critical behaviour of 1/f noise in percolation systems. Sov Phys JETP 68:1066–1069
34. Morozovsky AE, Snarskii AA (1992) Multiscaling in randomly inhomogeneous media: effective conductivity, relative spectral density of 1/f noise, and higher-order moments. Sov Phys JETP. 75:366–371
35. Morsli M, Bonnet A, Samir F (1996) Electrical conductivity and thermoelectric power of polybithiophene-polystyrene composites. Synth Met 76:273–276
36. Nigro B, Ambrosetti G, Grimaldi C et al (2011) Transport properties of nonhomogeneous segregated composites. Phys Rev B 83:064203-1–064203-10
37. Ofir A, Dor S, Grinis L et al (2008) Porosity dependence of electron percolation in nanoporous TiO2 layers. J Chem Phys 128:064703
38. Ohtsuki T, Keyes T (1984) Conduction in random networks on super-normal conductors: geometrical interpretation and enhancement of nonlinearity. J Phys A 11:L559–L563
39. Patashinskii AZ, Pokrovskii VL (1979) Fluctuation theory of phase transitions. Pergamon, Oxford, 321 p
40. Pike R, Stanley HE (1981) Order propagation near the percolation threshold. J Phys A 14: L169–L177
41. Reynolds PS, Klein W, Stanley HE (1977) A real-space renormalization group for site and bond percolation. J Phys C 10:L167–L172
42. Rossi E, Sarma SD (2011) Inhomogenous electronic structure, transport gap, and percolation threshold in disordered bilayer graphene. Phys Rev Lett 107: 155502-1–155502-5
43. Sarychev AK, Vinogradov AP (1981) Drop model of infinite cluster for 2D percolation. J Phys C 14:L487–L490
44. Shklovskii BI (1977) Critical behavior of the Hall coefficient near the percolation threshold. Sov Phys JETP 45:152–156
45. Shklovskii BI, Efros AL (1984) Electronic properties of doped semiconductors. Springer, Berlin, 388 p
46. Skaggs TH (2011) Assessment of critical path analyses of the relationship between permeability and electrical conductivity of pore networks. Adv Water Resour 34:1335–1342
47. Skal AS, Shklovskii BI (1974) Topology of infinite cluster in the theory of percolation and hopping conduction. Sov Phys Semicond 8:1586–1592 (in Russian)
48. Snarskii AA (1986) Effective conductivity of strongly inhomogeneous media near the percolation threshold. Sov Phys JETP 64:828–831
49. Snarskii AA, Morozovsky AE (1995) Percolation structure model in the smearing region. Int J Electron 78:135–137
50. Stanley HE (1977) Cluster shapes at the percolation threshold: an effective cluster dimensionality and its connection with critical-point exponents. J Phys A 10:L211–L220
51. Stauffer D, Aharony A (1992) Introduction to percolation theory, 2nd edn. Taylor & Francis, 181
52. Stenull O, Janssen H (2008) Conductivity of continuum percolating systems. Phys Rev E 64:056105-1–056105-14

53. Stinchcombe RB, Watson BP (1976) Renormalization group approach for percolation conductivity. J Phys C 9:3221–3248
54. Straley JP (1976) Critical phenomena in resistor networks. J Phys C 9:783–796
55. Straley P (1980) Dimensionality-dependent scaling relations for conduction exponents. J Phys C 13:819–822
56. Ukshe AE, Shmygleva LV, Pisareva AV et al (2013) Percolation model of conductivity of calix[n]arene-*p*-sulfonic acids. Russ J Electrochem 49:807–812
57. Vinogradov AP (2001) Electrodynamics of composite materials. URSS, Moscow 208 p (in Russian)
58. Vinogradov AP, Sarychev AK (1983) Structure of percolation channels and the metal-insulator transition in composites. Sov Phys JETP 58:665–669
59. Wei Y, Li Z (2013) Observation of double percolation transitions in Ag-SnO2 nanogranular films. Appl Phys Lett 102:131911
60. Wright DC, Bergman DJ, Kantor Y (1986) Resistance fluctuations in random resistor networks above and below the percolation threshold. Phys Rev B 33:396–401
61. Wu Z, Liu M (1997) Modelling of ambipolar transport properties of composite mixed ionic-electronic conductors. Solid State Ionics 93:65–84

Chapter 6
Self-dual Media

6.1 Locally Isotropic Media

Exact solutions for the effective conductivity σ_e are interesting for many reasons. In particular, an exact solution allows estimating the validity of different approximations applied in the derivation of σ_e. By the exact solution, we mean a finite analytical expression with one or several parameters that can be varied over the entire range of their values. Let us remind ourselves that (see Chap. 1) there is an infinite number of various composite structures. With a slight inhomogeneity (the degree of inhomogeneity is determined by the ratio σ_2/σ_1), a great number of structures have not only about the same value of σ_e, but even the same concentration dependence $\sigma_e(p)$. With a strong inhomogeneity $h = \sigma_2/\sigma_1 \ll 1$, it is no longer the case, at least, for large concentrations. Thus, as it seems at first sight, at $h \ll 1$ and a large concentration, each composite with given structure will have its own σ_e. In other words, the effective conductivity will be sort of "mark," "label" of this structure, similar to fractal dimension of given Koch snowflake [9], and no more than that. It turned out to be even more surprising that there exists an infinite and rather versatile set of two-dimensional structures with half concentration of phases for which the effective conductivity has the same expression, and no restrictions are imposed on the inhomogeneity value, the case $\sigma_1/\sigma_2 \to \infty$ taking place. These are the so-called self-dual media (D-media). The expression for the effective conductivity σ_e for the D-medium was first obtained in [5] for a very general case. In the same work there were introduced, in the general form, symmetry transformations for the local fields and currents, generalized and used thereafter for solving many problems. A concept of conjugate harmonic functions (potentials) that are a particular case of transformations in [5] was introduced in [10]. From this point on, like in nearly all papers using self-duality, we will employ these symmetry transformations [5].

Let us consider a two-dimensional two-phase medium with such an arrangement of phases that

A.A. Snarskii et al., *Transport Processes in Macroscopically Disordered Media*, DOI 10.1007/978-1-4419-8291-9_6

Fig. 6.1 Examples of a self-dual (on the average) medium: phase arrangement is self-dual, i.e., substitution $\sigma_1 \Leftrightarrow \sigma_2$ in figure **a** results in medium **b**, but does not change the effective conductivity σ_e

(1) the effective conductivity is isotropic;
(2) the interchange of phases does not change σ_e. The latter means that the phases are in geometrically equivalent positions and have half concentration. Examples of such phase arrangement are given in Fig. 6.1. Figure 6.2 shows an example of "basic" medium and its dual.

For the two-dimensional randomly inhomogeneous media at the percolation threshold, on sizes larger than correlation length, different phases are also in a geometrically equivalent (on the average) position, interchanging $\sigma_1 \Leftrightarrow \sigma_2$ does not change σ_e. Thus, these are also the *D*-media.

According to [5], let us introduce symmetry transformations

$$\begin{aligned} \tilde{\mathbf{j}} &= \Lambda \mathbf{n} \times \mathbf{E}, \\ \tilde{\mathbf{E}} &= \Lambda^{-1} \mathbf{n} \times \mathbf{j}, \end{aligned} \tag{6.1.1}$$

where (see Fig. 6.2) $\mathbf{E}$ and $\mathbf{j}$ are local fields and current in the "basic" medium, and $\tilde{\mathbf{E}}$ and $\tilde{\mathbf{j}}$—in its "dual" medium, $\mathbf{n}$ is normal unit vector.

It must be emphasized that fields $\tilde{\mathbf{E}}$ and points $\tilde{\mathbf{j}}$ are "real," i.e., obey the same equations $\operatorname{div} \tilde{\mathbf{j}} = 0$, $\operatorname{curl} \tilde{\mathbf{E}} = 0$ as the fields and currents in the basic medium. It can be easily shown: for instance, $\operatorname{curl} \tilde{\mathbf{E}} = \nabla \times \tilde{\mathbf{E}} = \Lambda^{-1} \nabla \times (\mathbf{n} \times \mathbf{j}) = \Lambda^{-1} \mathbf{n} (\nabla \cdot \mathbf{j}) = \Lambda^{-1} \mathbf{n} \operatorname{div} \mathbf{j}$ and from $\operatorname{div} \mathbf{j} = 0$ it follows that $\operatorname{curl} \tilde{\mathbf{E}} = 0$.

The possibility of div transformation into rot, and vice versa, at symmetry transformation (6.1.1) exists only in the two-dimensional case. In the three-dimensional case one equation $\operatorname{div} \mathbf{j} = 0$ can in no way be transformed into three equations $-\operatorname{curl} \mathbf{E} = 0$.

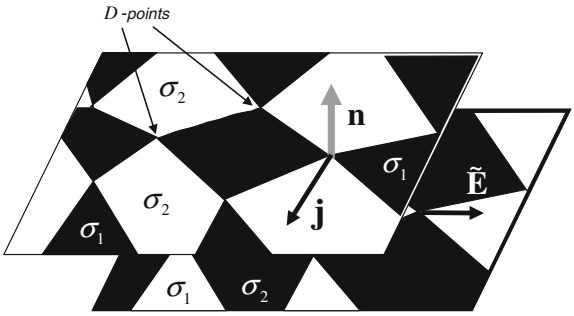

Fig. 6.2 Two-phase self-dual medium: on *top* is "basic" medium, at the *bottom*—its dual, **n** is normal unit vector

Local Ohm's law in the "basic" medium after transformations (6.1.1) will pass into Ohm's law in the "dual" medium

$$\mathbf{j} = \sigma(x,y)\mathbf{E} \quad \rightarrow \quad \tilde{\mathbf{j}} = \frac{\Lambda^2}{\sigma(x,y)}\tilde{\mathbf{E}}, \tag{6.1.2}$$

where $\Lambda^2/\sigma(x,y)$, apparently, is local conductivity in the dual medium:

$$\tilde{\sigma}(x,y) = \frac{\Lambda^2}{\sigma(x,y)}. \tag{6.1.3}$$

By virtue of duality, at the coordinate values (x,y) whereby the conductivity $\sigma(x,y)$ is equal to σ_1, the conductivity of the dual medium $\tilde{\sigma}(x,y)$ must be equal to σ_2, and vice versa:

$$\sigma(r) = \begin{cases} \sigma_1, & r \in O_1, \\ \sigma_2, & r \in O_2, \end{cases} \quad \tilde{\sigma}(r) = \begin{cases} \sigma_2, & r \in O_1, \\ \sigma_1, & r \in O_2. \end{cases} \tag{6.1.4}$$

Conditions (6.1.4) can be satisfied on setting

$$\Lambda^2 = \sigma_1 \cdot \sigma_2 \tag{6.1.5}$$

For medium-volume fields and currents in the isotropic case

$$\langle \mathbf{j} \rangle = \sigma_e \langle \mathbf{E} \rangle, \quad \langle \tilde{\mathbf{j}} \rangle = \tilde{\sigma}_e \langle \tilde{\mathbf{E}} \rangle, \tag{6.1.6}$$

one can use averaged in volume symmetry transformation (6.1.1)

$$\langle \tilde{\mathbf{j}} \rangle = \Lambda \mathbf{n} \times \langle \mathbf{E} \rangle, \quad \langle \tilde{\mathbf{E}} \rangle = \Lambda^{-1} \mathbf{n} \times \langle \mathbf{j} \rangle. \tag{6.1.7}$$

Then from expressions (6.1.5), (6.1.6) and (6.1.7) it follows

$$\tilde{\sigma}_e = \frac{\sigma_1 \sigma_2}{\sigma_e}. \tag{6.1.8}$$

Since the media under consideration are self-dual, i.e.,

$$\sigma_e = \tilde{\sigma}_e, \tag{6.1.9}$$

from (6.1.8) immediately follows the Dykhne formula for σ_e:

$$\sigma_e = \sqrt{\sigma_1 \sigma_2}. \tag{6.1.10}$$

The expression for σ_e is also valid for the two-dimensional randomly inhomogeneous medium on the percolation threshold, and it is exactly this expression that percolation theory leads to at $p = p_c = 1/2$.

For a net problem with bond resistances r_1 and r_2 there exists an analog (6.1.10) in the form

$$r_e = \sqrt{r_1 r_2}. \tag{6.1.11}$$

The continual variants of the D-media are certain to include the so-called D-points. One of them is shown in Fig. 6.2. The conductivity of this point (if at all one can speak of point conductivity) is neither σ_1 nor σ_2. It would seem that this point can be equally considered conductive with σ_1 or σ_2 depending on the history of this medium formation. For instance, if a medium of chessboard type with $p = 1/2$ was formed with a growth of "black" (σ_1) squares in a "white" (σ_2) matrix, then the D-point conductivity is, certainly,σ_2, and if, on the contrary, with a growth of "white" squares, then its conductivity is, certainly, σ_1. Indeed, as is easily seen from the analysis of the net D-medium considered below, the D-point conductivity is $\sqrt{\sigma_1 \sigma_2}$. For a continual realization the conductivity of one (or even many) point is minor, however, at large inhomogeneity $\sigma_1/\sigma_2 \gg 1$ it is exactly the D-point neighborhood that determines the conductivity of the entire system. Soderberg and Grimvall [15] deals with the distribution of current and Joule heat release in the D-medium which has the structure of a chessboard. With a large inhomogeneity, the behavior of current lines in the D-point neighborhood is as shown in Fig. 6.3.

In a bad conducting (σ_2) phase, current lines in the D-point neighborhood are actually a part of concentric circles, i.e., have the only component $\mathbf{j}_\theta$ and can be approximately written as [15]

$$\mathbf{j}_\theta(r, \theta) \sim \langle \mathbf{j} \rangle \frac{\sqrt{\sigma_2/\sigma_1}}{r^{1-\sqrt{\sigma_2/\sigma_1}}}, \tag{6.1.12}$$

i.e., current density quickly ($\sim 1/r$) reduces with distance from the D-point.

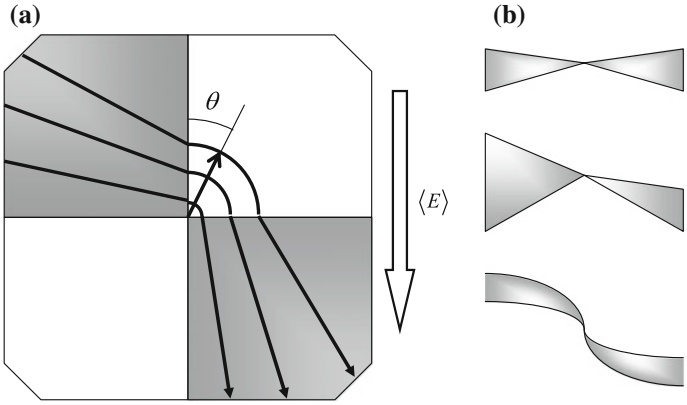

Fig. 6.3 View of the *D*-point neighborhood: **a** current line distribution in the *D*-point neighborhood at $\sigma_1 \gg \sigma_2$, *black color* is used to denote the good conducting phase; **b** different kinds of the *D*-point neighborhood

The Joule heat release is reduced still more quicker, and since the effective conductivity σ_e is nothing more than normalized Joule heat release ($\sigma_e \sim \langle \sigma \mathbf{E}^2 \rangle$), the region in the *D*-point neighborhood determines the value of σ_e. More detailed calculations show [15], that, for instance, at $\sigma_2/\sigma_1 = 10^{-2}$, half of the entire Joule heat is released in approximately 0.1 % of its volume.

There is known [8] an exact solution of mathematical physics problem on the potential distribution in a strictly periodical inhomogeneous structure of chessboard type, however, it is clear that for any other realization (for instance, periodic only on the average or when sides intersect at the *D*-point not only at a right angle) the solution will be different. But the conclusion itself on current concentration and Joule heat distribution in the *D*-point neighborhood and the basic dependencies, such as $j_\theta \sim r^{-\alpha}$, $\alpha \approx 1$ ($\sigma_2/\sigma_1 \ll 1$) that govern the resistance of the entire medium, persist.

With unequal phase concentration, self-duality is impossible. Then from (6.1.8) follows only the relation between σ_e of the basic medium and its dual (but no longer self-dual):

$$\sigma_e(p)\tilde{\sigma}_e(p) = \sigma_1\sigma_2. \tag{6.1.13}$$

For the randomly inhomogeneous media and some other (periodic) structures, the substitution $\sigma_1 \Leftrightarrow \sigma_2$ is equivalent to the substitution $p \Leftrightarrow 1 - p$, i.e.

$$\tilde{\sigma}_e(p) = \sigma_e(1 - p). \tag{6.1.14}$$

For such media from (6.1.13) follows the so-called reciprocity relation [5, 10]

$$\sigma_e(p)\sigma_e(1 - p) = \sigma_1\sigma_2. \tag{6.1.15}$$

Fulfillment of (6.1.15) imposes certain restrictions on the geometry of phase arrangement [1], thus, for a medium consisting of "black" round inclusions in a "white" matrix there is no reciprocity relation (6.1.15).

Hereafter we will use one specific realization of the *D*-medium. This medium is "built" using the so-called mixing procedure [11–13], i.e., step by step, when homogenization takes place during each step, minimal characteristic length tends to zero and the description of its properties passes from local to averaged by means of the effective values, which, in turn, becomes local for the next step. During the first step (Fig. 6.4a) the medium is constructed of equally thick stripes with conductivities σ_1 and σ_2. The first white arrow indicates to homogenization process, dimension a_0 tends to zero and planar stratified medium "passes" into a monocrystal with the principal values of conductivity tensor $\sigma_{||}^{(1)}$ and $\sigma_{\perp}^{(1)}$, the second white arrow shows how a new planar stratified medium is assembled of these anisotropic layers.

Letting stripe thickness a_0 to zero, i.e., homogenizing the medium, we pass over to a primary "single crystal," the conductivity of which is described by the effective conductivity tensor

$$\tilde{\sigma}^{(1)} = \begin{pmatrix} \sigma_{||}^{(1)} & 0 \\ 0 & \sigma_{\perp}^{(1)} \end{pmatrix}, \quad \sigma_{||}^{(1)} = \frac{\sigma_1 + \sigma_2}{2}, \quad \sigma_{\perp}^{(1)} = 2\frac{\sigma_1 \sigma_2}{\sigma_1 + \sigma_2}. \tag{6.1.16}$$

During the second step, equally thick stripes are cut of primary "single crystal" (Fig. 6.4b) along and across the initial layers and a new stratified medium is composed of them (Fig. 6.4c). Tending the stripe thickness to zero, we pass over to the secondary "single crystal" with the basic components of conductivity tensor

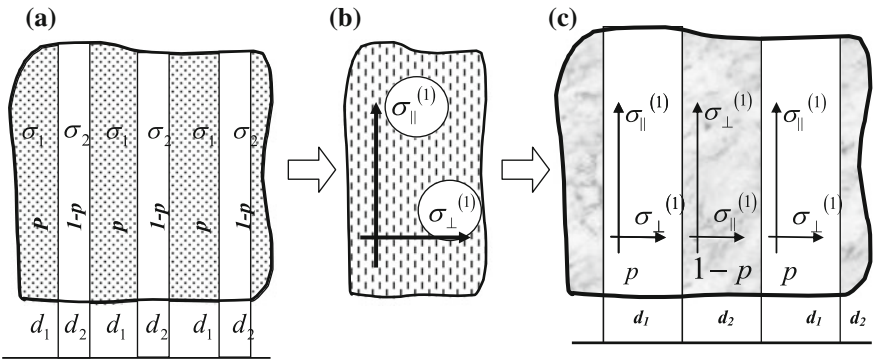

Fig. 6.4 Schematic of the first steps of mixing procedure: **a** planar stratified medium of equally thick stripes with conductivities σ_1 and σ_2. **b** Equally thick layers are cut of primary "single crystal" along the quasi-crystalline axes; **c** a new planar stratified medium is assembled of these anisotropic layers

$$\sigma_{||}^{(2)} = \frac{\sigma_{||}^{(1)} + \sigma_{\perp}^{(1)}}{2}, \quad \sigma_{\perp}^{(2)} = 2\frac{\sigma_{||}^{(1)}\sigma_{\perp}^{(1)}}{\sigma_{||}^{(1)} + \sigma_{\perp}^{(1)}}. \tag{6.1.17}$$

Further mixing (when good and bad conducting directions $\sigma_{||}$ and $\sigma_{\perp}$ are permanently alternating, i.e., mixed), for $n+1$ step yields

$$\sigma_{||}^{(n+1)} = \frac{\sigma_{||}^{(n)} + \sigma_{\perp}^{(n)}}{2}, \quad \sigma_{\perp}^{(n+1)} = 2\frac{\sigma_{||}^{(n)} \cdot \sigma_{\perp}^{(n)}}{\sigma_{||}^{(n)} + \sigma_{\perp}^{(n)}}. \tag{6.1.18}$$

The iteration procedure (6.1.18) possesses invariant J of the kind

$$\sigma_{||}^{(n+1)} \cdot \sigma_{\perp}^{(n+1)} = \sigma_{||}^{(n)}\sigma_{\perp}^{(n)} = \cdots = \sigma_1\sigma_2 = J. \tag{6.1.19}$$

If the iteration procedure is converged, then

$$\lim_{n\to\infty} \sigma_{||}^{(n)} = \lim_{n\to\infty} \sigma_{\perp}^{(n)} = \sigma_e, \tag{6.1.20}$$

and from (6.1.19) immediately follows $\sigma_e^2 = \sigma_1 \cdot \sigma_2$, i.e., the effective conductivity of the D-medium (6.1.10) (the Dykhne formula).

One can trace the convergence of the procedure having written the first equation from (6.1.14) with regard to the fact that $\sigma_{\perp}^{(n)} = \sigma_1\sigma_2/\sigma_{||}^{(n)}$ (6.1.19) in the form of a one-dimensional representation:

$$\sigma_{||}^{(n+1)} = \frac{1}{2}\left(\sigma_{||}^{(n)} + \frac{J}{\sigma_{||}^{(n)}}\right), \quad J = \sigma_1\sigma_2, \tag{6.1.21}$$

or in simplified designations

$$x_{n+1} = f(x_n), \quad f(x) = \frac{1}{2}\left(x + \frac{J}{x}\right). \tag{6.1.22}$$

Figure 6.5 shows the Lamerey ladder for the representation (6.1.22). With any initial value $x_0 \neq 0$, consecutive iterations lead to a fixed point x^*, $x^* = \frac{1}{2}(x^* + J/x^*)$, т.о. $(x^*)^2 = J$.

This procedure allows obtaining the D-medium. Indeed, (1) the substitution $\sigma_1 \Leftrightarrow \sigma_2$ does not change σ_e; (2) the phase concentration is half one; (3) the effective conductivity is isotropic.

Mixing method (Fig. 6.4) is easily generalized for the case of $p \neq 1/2$. Now, instead of the iteration procedure (6.1.18), we have

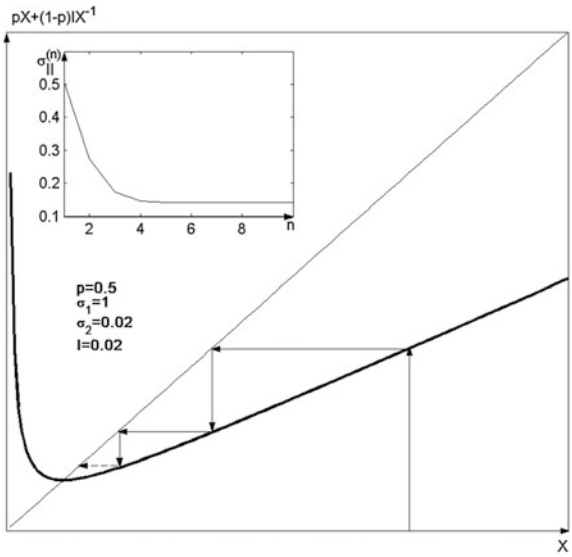

Fig. 6.5 The Lamerey ladder for one-dimensional representation $x \to \frac{1}{2}\left(x + \frac{J}{x}\right)$; *on the insert* consecutive values of $\sigma_{||}^{(n)}$ for $n = 1, 2, \ldots$ for $\sigma_1 = 1$, $\sigma_2 = 0.02$

$$\sigma_{||}^{(1)} = p\sigma_1 + (1-p)\sigma_2,\ \sigma_\perp = \frac{\sigma_1\sigma_2}{(1-p)\sigma_1 + p\sigma_2}, \tag{6.1.23}$$

with the invariant J of the kind

$$J = \sigma_1\sigma_2\frac{p\sigma_1 + (1-p)\sigma_2}{(1-p)\sigma_1 + p\sigma_2}, \tag{6.1.24}$$

and one-dimensional representation (6.1.21) can be written

$$\sigma_{||}^{(n+1)} = p\sigma_{||}^{(n)} + (1-p)\frac{J}{\sigma_{||}^{(n)}}. \tag{6.1.25}$$

The fixed point of representation (6.1.25) where $\sigma_{||}^{(n)}$ and $\sigma_\perp^{(n)}$ are converged at $n \to \infty$ leads to

$$\sigma_e(p) = \sqrt{\sigma_1\sigma_2}\sqrt{\frac{p\sigma_1 + (1-p)\sigma_2}{(1-p)\sigma_1 + p\sigma_2}}. \tag{6.1.26}$$

As it immediately follows from (6.1.26), for the obtained procedure of medium mixing the following reciprocity relation is met: $\sigma_e(p)\sigma_e(1-p) = \sigma_1\sigma_2$.

Symmetry transformations can be applied not only to the two-phase D-medium, but also to numerous particular cases of multiphase media and media with a smooth coordinate dependence of local conductivity. As is shown in [5], for this purpose

the multi-point function of local conductivity distribution must be an even function of variables

$$\chi(x,y) = \ln\,\sigma(x,y) - \langle \ln\,\sigma(x,y)\rangle. \tag{6.1.27}$$

Now constant Λ in symmetry transformations (6.1.1) is of the form $\Lambda = \exp(\langle \ln\,\sigma\rangle)$, and Ohm's law in the basic medium with conductivity $\sigma(x,y) = \exp(\langle \ln\,\sigma\rangle + \chi)$:

$$j = \mathrm{e}^{\langle \ln\,\sigma\rangle + \chi}. \tag{6.1.28}$$

Substituting in (6.1.28) $\chi \to -\chi$ and using the parity of local conductivity distribution function, we find that the dual medium is macroscopically equivalent to the basic one, i.e., it is self-dual. Using averaged symmetry transformations (6.1.7) with

$$\Lambda = \exp(\langle \ln\,\sigma\rangle), \tag{6.1.29}$$

we find that $\sigma_\mathrm{e} = \Lambda$, i.e.

$$\sigma_\mathrm{e} = \mathrm{e}^{\langle \ln\,\sigma\rangle}. \tag{6.1.30}$$

Examples of local conductivity distributions, even in χ, are shown in Fig. 6.6. In a particular two-phase case we have

$$f(\sigma) = p\delta(\sigma - \sigma_1) + (1-p)\delta(\sigma - \sigma_2), \quad p = 1/2, \tag{6.1.31}$$

and (see Fig. 6.6a) in the logarithmic axes the peaks of δ-functions are symmetrical with respect to $\ln\,\sigma_\mathrm{e}$. A similar symmetry is also observed for a multiphase case

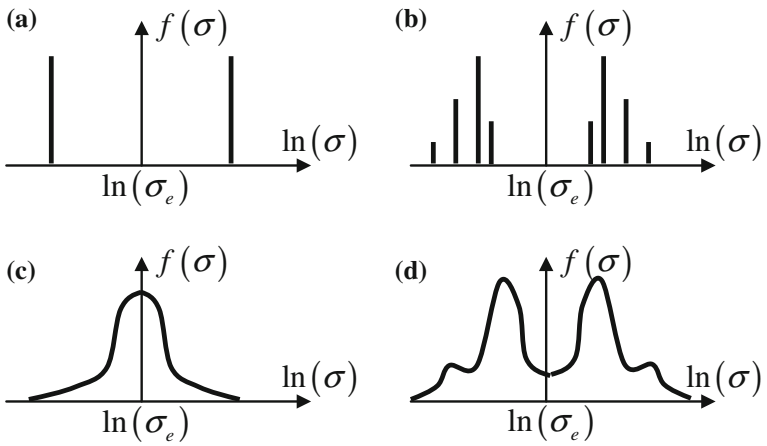

Fig. 6.6 Examples of local conductivity distribution functions of self-dual media: **a** two-phase medium with phase conductivities σ_1 and σ_2; **b** eight-phase medium with conductivities $\sigma_1,\ \sigma_2 \ldots \sigma_8$; **c**, **d** examples of continuous phase distribution

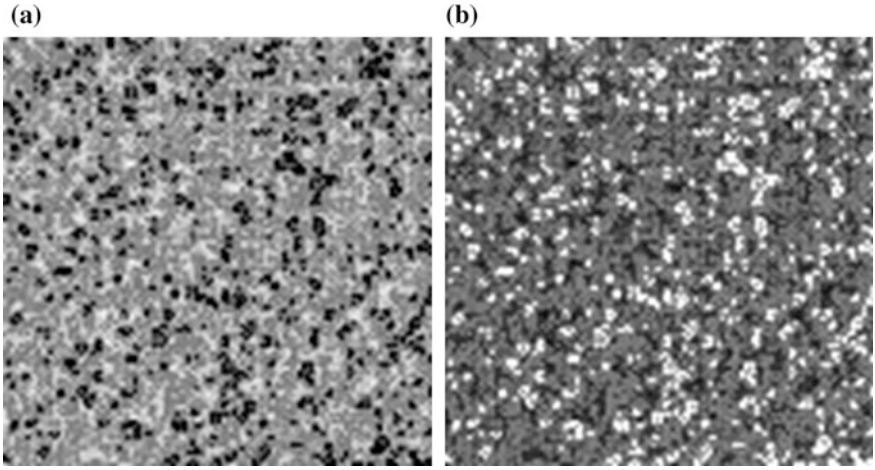

Fig. 6.7 Example of a self-dual medium with a continuous distribution of local conductivity. **a** basic medium (positive), **b** its dual (negative)

(see Fig. 6.6b) and for each pair of phases the relation of the type $\ln \sigma_1 - \ln \sigma_e = \ln \sigma_e - \ln \sigma_5$ is met.

With a continuous distribution of local conductivity, a self-dual medium can be easily imagined as such that will not differ (on the average) from the basic medium in the case when in the basic medium (positive) the value of local conductivity is matched with "black" colored intensity, then its dual medium will be a negative (Fig. 6.7).

For the Gaussian distribution (see Fig. 6.6c) with a mean square fluctuation of conductivity logarithm $\Delta = \sqrt{\langle \chi^2 \rangle}$ the effective conductivity according to (6.1.30) can be written as

$$\sigma_e = \langle \sigma \rangle e^{-\Delta/2}. \tag{6.1.32}$$

Mixing procedure (Fig. 6.4) which in the two-phase case leads to σ_e of the self-dual media, can be extended to n-phase and three-dimensional media that will be self-dual no more, however [12, 13].

6.2 Locally Anisotropic Media

Consider a two-dimensional polycrystal [5], the local conductivity of which in plane XOY at given point $\mathbf{r}$ is described by tensor $\hat{\sigma}(\varphi(\mathbf{r}))$, where

$$\hat{\sigma}(\varphi(\mathbf{r})) = \hat{P}_\varphi \, \hat{\sigma} \, \hat{P}_{-\varphi}, \tag{6.2.1}$$

Here $\hat{P}_{\varphi}$ is operator of rotation by angle φ in plane xoy, $\hat{\sigma}$ is conductivity tensor in crystallographic coordinate system, angle φ, thus, assigns the direction of principal crystallographic axes in this coordinate system. Using the Dykhne transformations written here in a somewhat different form

$$\tilde{\mathbf{j}} = \Lambda\, \hat{P}_{\pi/2}\, \mathbf{E}, \quad \mathbf{E} = \Lambda^{-1} \hat{P}_{\pi/2} \mathbf{j}, \tag{6.2.2}$$

we will pass from Ohm's law for the basic medium

$$\mathbf{j} = \hat{\sigma}(\varphi)\mathbf{E}, \tag{6.2.3}$$

to Ohm's law for the dual medium

$$\tilde{\mathbf{j}} = \hat{\tilde{\sigma}}(\varphi)\tilde{\mathbf{E}}, \tag{6.2.4}$$

where

$$\hat{\tilde{\sigma}} = \Lambda^2\, \hat{P}_{\pi/2}\, \hat{\sigma}^{-1}\, \hat{P}_{-\pi/2} \tag{6.2.5}$$

is local conductivity tensor in the dual medium.

Using the identity

$$\hat{P}_{\pi/2}\hat{\sigma}^{-1}(\varphi)\hat{P}_{-\pi/2} = \frac{\hat{\sigma}(\varphi)}{\det\hat{\sigma}(\varphi)}, \tag{6.2.6}$$

we get

$$\hat{\tilde{\sigma}}(\varphi) = \frac{\Lambda^2\hat{\sigma}(\varphi)}{\det\hat{\sigma}(\varphi)} \tag{6.2.7}$$

By applying to averaged Ohm's laws for the basic and dual media

$$\langle \mathbf{j} \rangle = \sigma_e \langle \mathbf{E} \rangle, \ \langle \tilde{\mathbf{j}} \rangle = \hat{\tilde{\sigma}}_e \langle \tilde{\mathbf{E}} \rangle \tag{6.2.8}$$

the averaged in volume transformations (6.2.2), we find a relation between the effective conductivities of the basic $\bar{\sigma}_e$ and dual $\bar{\tilde{\sigma}}_e$ media

$$\hat{\tilde{\sigma}}_e = \frac{\Lambda^2\hat{\sigma}_e}{\det\hat{\sigma}_e}. \tag{6.2.9}$$

Now consider a case for such a polycrystalline medium where $\det\hat{\sigma}(\varphi)$ is coordinate independent. Choosing constant Λ equal to

$$\Lambda^2 = \det\hat{\sigma}(\varphi), \tag{6.2.10}$$

from (6.2.7) we find that the basic and dual media are identical

$$\hat{\tilde{\sigma}}(\varphi) = \hat{\sigma}(\varphi). \tag{6.2.11}$$

Consequently, their effective values are also identical

$$\hat{\tilde{\sigma}}_{\mathrm{e}} = \hat{\sigma}_{\mathrm{e}}, \tag{6.2.12}$$

which leads to a precise (applicable for however large anisotropy) relation for a determinant of the effective conductivity of such polycrystalline medium

$$\det\hat{\sigma}_{\mathrm{e}} = \det\hat{\sigma}(\varphi) = \det\hat{\sigma}. \tag{6.2.13}$$

If crystals are located in a polycrystal such that the medium on the whole is isotropic, i.e., the effective conductivity is a scalar, then from (6.2.13) follows the Dykhne expression [5]:

$$\sigma_{\mathrm{e}} = \sqrt{\det\hat{\sigma}}. \tag{6.2.14}$$

The simplest example of such a polycrystal consists of identical monocrystals with a chaotic spread in the angles of axes of local conductivity tensor

$$\hat{\sigma} = \begin{pmatrix} \sigma_{\parallel} & 0 \\ 0 & \sigma_{\perp} \end{pmatrix}, \tag{6.2.15}$$

where $\sigma_{\parallel}$ and $\sigma_{\perp}$ are principal values of local conductivity tensor that are coordinate independent. In this case from expression (6.2.14) we get

$$\sigma_{\mathrm{e}} = \sqrt{\sigma_{\parallel}\sigma_{\perp}}. \tag{6.2.16}$$

Formula (6.2.16) can be derived as simply as possible [13] based on the exact solution for a two-phase D-medium [5]. For this purpose let us imagine that each crystallite with conductivity tensor (6.2.15) is a limiting case of the two-phase planar stratified medium with the values of layer conductivities σ_1 and σ_2 with identical phase concentration (Fig. 6.8).

For such a two-phase medium having a specific structure all conditions required by the D-medium are met (the medium is on the average isotropic, the phase concentration **is** $p = (1-p) = 0.5$, and interchanging $\sigma_1 \rightleftarrows \sigma_2$ does not change the effective conductivity value) and, hence, on the one hand,

$$\sigma_{\mathrm{e}} = \sqrt{\sigma_1\sigma_2}, \tag{6.2.17}$$

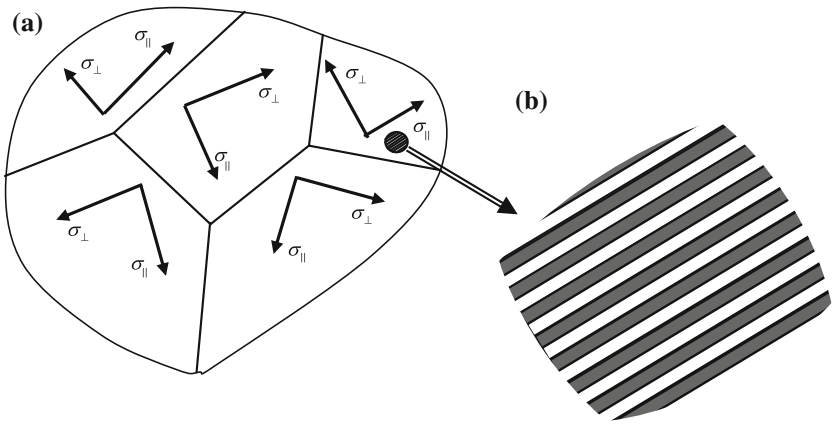

Fig. 6.8 Polycrystal structure as the limiting case of planar stratified media: **a** polycrystal: *arrows* are used to indicate the directions of principal axes of crystallite conductivity tensor; **b** crystallite "microstructure"—two-phase planar stratified medium

on the other hand, for $\sigma_{\parallel}$ and $\sigma_{\perp}$ of such planar stratified medium the equality is met

$$\sigma_{\parallel}\sigma_{\perp} = \sigma_1\sigma_2, \tag{6.2.18}$$

whence on substituting (6.2.18) to (6.2.17) follows the Dykhne expression for the effective conductivity of a two-dimensional polycrystal (6.2.16).

The expression (6.2.16) for the effective conductivity is valid for however strong anisotropy. In so doing, as can be seen from (6.2.16), the "good" $\sigma_{\parallel}$ and "bad" $\sigma_{\perp} \ll \sigma_{\parallel}$ conductivities contribute to σ_e equally. The nontriviality of σ_e behavior at $\sigma_{\parallel} \gg \sigma_{\perp}$ lies in the fact that current that should have avoided directions with bad conductivity $\sigma_{\perp}$ on passing through polycrystal, in fact, flows not only along "easy" directions ($\sigma_{\parallel}$), but also along "difficult" ones ($\sigma_{\perp}$), with equal resistance accumulated along both directions.

A similar situation in a two-phase isotropic strongly inhomogeneous D-medium ($\sigma_e = \sqrt{\sigma_1\sigma_2}$) (current in the bad conducting phase is met with the same resistance as in the good conducting phase) is due to the presence of the D-points. As was mentioned above, it is exactly current behavior in the D-point neighborhood that governs (at $\sigma_1 \gg \sigma_2$) the resistance of the entire medium. A specific geometric structural element exists in a polycrystalline medium, too.

As was shown in [3], the reason for "equality" of $\sigma_{\parallel}$ and $\sigma_{\perp}$ lies in the existence of the so-called current traps. When current lines get into the area near the apex of three crystallites, where directions with good conductivity $\sigma_{\parallel}$ cross the converging

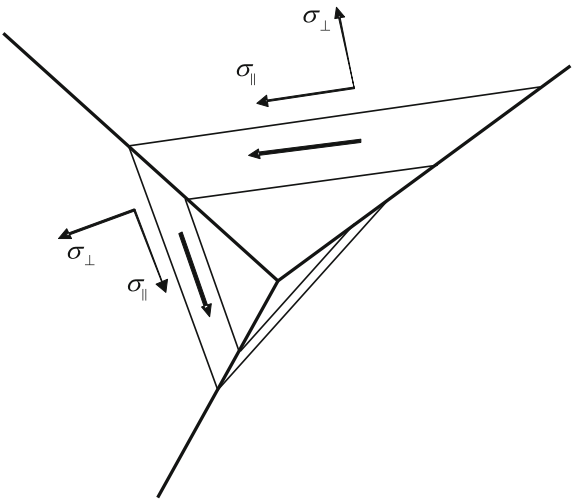

Fig. 6.9 Good conducting lines (along $\sigma_\parallel$) close to the apex of three crystallites: *solid arrows* are used to indicate current direction

boundaries, the line of good conductivity together with current line ($\sigma_\parallel \gg \sigma_\perp$) will "wind" around this apex (Fig. 6.9).

According to [3] (see also [6, 7]), the trap cross section is of the order of crystal size, and the probability that good conducting lines will pass the polycrystal past all the traps is exponentially little.

Current bundle, wound around the apex after the good conductivity line, will be compressed (Fig. 6.9). Current density in this case will increase, and the resistance per bundle unit length along the good conductivity line will increase accordingly. Finally, this resistance will become so large that for the current it will be "advantageous" to cross the good conductivity line and "unwind" in the reverse direction along the adjacent good conductivity line. In [3], the trap resistance R was estimated using the variational principle, formulated in [4], $R \sim 1/\sqrt{\sigma_\parallel \sigma_\perp}$.

A good trap model can be represented by a quasi-crystallographic medium with the axes running along the logarithmic spiral (Fig. 6.10). Such an approach to calculation of current trap resistance and, thus, the effective conductivity, was proposed and partially realized in [6]. In the intrinsic crystallographic axes $\{X,\ Y\}$ (Fig. 6.10) the conductivity tensor is of the form (6.2.5), whereas in the laboratory polar system $\{r,\ \psi\}$ its components are as follows:

$$\begin{aligned} &\sigma_{rr} = \sigma_\parallel \cos^2\theta + \sigma_\perp \sin^2\theta, \quad \sigma_{r\psi} = \sigma_{\psi r} = \left(\sigma_\perp - \sigma_\parallel\right)\cos\theta\ \sin\theta \\ &\sigma_{\psi\psi} = \sigma_\parallel \sin^2\theta + \sigma_\perp \cos^2\theta, \end{aligned} \tag{6.2.19}$$

Note that with such a choice of crystallographic axes in the form of a logarithmic spiral, components of local conductivity tensor (6.2.19) are coordinate independent, therefore the equation for potential $\varphi(r, \psi)$ $\mathrm{dir}(\hat{\sigma}\ \mathrm{grad}\varphi) = 0$ has a simple form

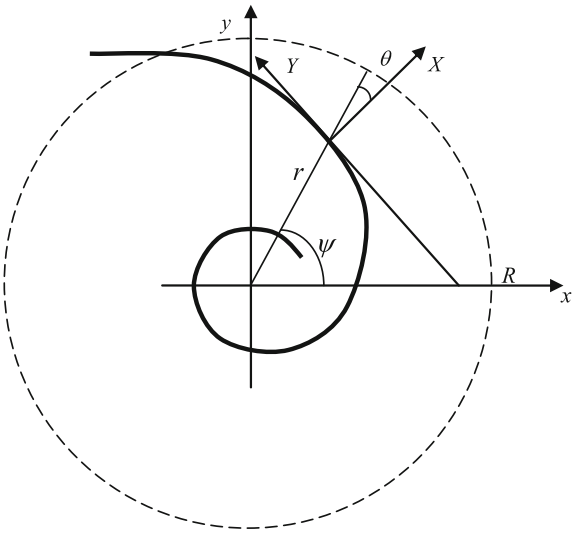

Fig. 6.10 Current trap model —quasi-crystallographic medium with the axes in the form of a logarithmic spiral: *solid line* is used to show one of the crystallographic axes, angle θ is spiral parameter

$$\sigma_{rr}\frac{\partial}{\partial r}\left(r\frac{\partial\varphi}{\partial r}\right)+2\sigma_{r\psi}\frac{\partial^2\varphi}{\partial r\,\partial\psi}+\frac{1}{r}\sigma_{\psi\psi}\frac{\partial^2\varphi}{\partial\psi^2}=0. \tag{6.2.20}$$

Choosing its solution in the form

$$\varphi(r,\psi)=Ar^{\alpha}\mathrm{e}^{i\psi}, \tag{6.2.21}$$

for α we have

$$\alpha=\omega-i\gamma,\ \omega=\sqrt{\sigma_{\parallel}\sigma_{\perp}}/\sigma_{rr}. \tag{6.2.22}$$

Thus,

$$\varphi(r,\psi)=Ar^{\omega}\cos(\psi-\gamma\,\ln r). \tag{6.2.23}$$

As long as with a strong anisotropy the main resistance is accumulated close to the trap center, at some distance of radius R from it one can replace the locally anisotropic medium by the isotropic one with the effective conductivity σ_{e}, demanding satisfaction of standard boundary conditions that follow from continuity equation ($\mathrm{div}\mathbf{j}=0$) and field potentiality

$$j_r(r=R)=j_r^{+}(r=R),\quad \varphi(r=R)=\varphi^{+}(r=R), \tag{6.2.24}$$

where index "+" is used to denote the outer problem in the region of $r>R$.

Solution in the outer region will be selected as

$$\varphi^{+}(r,\psi) = B\,r\,\cos(\psi-\theta). \tag{6.2.25}$$

Writing down the expressions for current density $j_r = \sigma_{rr}E_r + \sigma_{r\psi}E_\psi$ in the inner and outer regions

$$j_r = Ar^{\omega-1}\sigma_{rr}\omega\,\cos(\psi-\gamma\,\ln r),\ j_r^{+} = \sigma^{\mathrm{e}}B\,\cos(\psi-\theta) \tag{6.2.26}$$

and satisfying the boundary conditions (6.2.24), for the effective conductivity, as was to be expected, we get $\sigma^{\mathrm{e}} = \omega\sigma_{rr} = \sqrt{\sigma_{\|}\sigma_{\perp}}$.

Different generalizations of (6.2.14) and (6.2.16) are possible. Reference [2] deals with such a two-dimensional anisotropic medium wherein the direction of principal axes of local conductivity tensor $\hat{\sigma}(r)$ does not depend on coordinates, i.e., at any r we have

$$\hat{\sigma}(r) = \begin{pmatrix} \sigma_{\|}(r) & 0 \\ 0 & \sigma_{\perp}(r) \end{pmatrix}. \tag{6.2.27}$$

For a two-phase case: $\hat{\sigma}(r) = \hat{\sigma}_1(r)$—in the first phase and $\hat{\sigma}(r) = \hat{\sigma}_2(r)$—in the second phase, with the first phase concentration equal to p, one can write down the following reciprocity relations:

$$\begin{aligned} &\sigma_{\|}^{\mathrm{e}}\left(p;\sigma_{\|1},\sigma_{\perp1};\sigma_{\|2},\sigma_{\perp2}\right)\sigma_{\perp}^{\mathrm{e}}\left(p;\sigma_{\|1},\sigma_{\perp2};\frac{\sigma_{\|1}\sigma_{\perp1}}{\sigma_{\|2}},\frac{\sigma_{\|2}\sigma_{\perp2}}{\sigma_{\perp2}}\right) = \sigma_{\|1}\sigma_{\perp1}, \\ &\sigma_{\perp}^{\mathrm{e}}\left(p;\sigma_{\|1},\sigma_{\perp1};\sigma_{\|2},\sigma_{\perp2}\right)\sigma_{\|}^{\mathrm{e}}\left(p;\sigma_{\|1},\sigma_{\perp1};\frac{\sigma_{\|1}\sigma_{\perp1}}{\sigma_{\|2}},\frac{\sigma_{\|2}\sigma_{\perp2}}{\sigma_{\perp2}}\right) = \sigma_{\|1}\sigma_{\perp1}. \end{aligned} \tag{6.2.28}$$

If the distribution of the anisotropic phases is geometrically isotropic, then

$$\begin{aligned} \sigma_{\|}^{\mathrm{e}}\left(p;\sigma_{\|1},\sigma_{\perp1};\sigma_{\|2},\sigma_{\perp2}\right) &= \sigma_{\|}^{\mathrm{e}}\left(p;\sigma_{\perp1},\sigma_{\|1};\sigma_{\perp2},\sigma_{\|2}\right), \\ \sigma_{\perp}^{\mathrm{e}}\left(p;\sigma_{\|1},\sigma_{\perp1};\sigma_{\|2},\sigma_{\perp2}\right) &= \sigma_{\|}^{\mathrm{e}}\left(p;\sigma_{\perp1},\sigma_{\|1};\sigma_{\perp2},\sigma_{\|2}\right), \end{aligned} \tag{6.2.29}$$

and for the randomly inhomogeneous medium

$$\sigma_{\|,\perp}^{\mathrm{e}}\left(p;\sigma_{\|1},\sigma_{\perp1};\sigma_{\|2},\sigma_{\perp2}\right) = \sigma_{\perp}^{\mathrm{e}}\left(1-p;\sigma_{\|2},\sigma_{\perp2};\sigma_{\|1},\sigma_{\perp1}\right). \tag{6.2.30}$$

Reference [14] deals with a polycrystal consisting of two types of single crystals $\widehat{\sigma}_1$ and $\widehat{\sigma}_2$, such that

$$\hat{\sigma}_2 = \alpha\hat{\sigma}_1,\ \alpha = \mathrm{const}, \tag{6.2.31}$$

then with a mutually dual geometry of their arrangement and equal concentration ($p = 1/2$)

$$\det\hat{\sigma}_e = \sqrt{\det\hat{\sigma}_1 \det\hat{\sigma}_2} = \sqrt{\alpha}\det\hat{\sigma}_1. \tag{6.2.32}$$

For $p \neq 1/2$ the reciprocity relation is met

$$\hat{\sigma}_e(1-p)\det\hat{\sigma}_e(p) = \hat{\sigma}_e(p)\sqrt{\det\hat{\sigma}_1 \det\hat{\sigma}_2}. \tag{6.2.33}$$

For a continuous distribution, when $\sigma_\parallel(r)$ and $\sigma_\perp(r)$ are scalar random fields having identical polynomial distribution functions even in χ.

$$\chi = \left(\ln\sigma_\parallel - \left\langle\ln\sigma_\parallel\right\rangle, \ln\sigma_\perp - \left\langle\ln\sigma_\perp\right\rangle\right), \tag{6.2.34}$$

it is possible [14] to generalize the Dykhne expression

$$\det\hat{\sigma}_e = e^{2\left\langle\ln\sigma_\parallel\right\rangle} = e^{2\langle\ln\sigma_\perp\rangle}. \tag{6.2.35}$$

However, if the fields $\sigma_\parallel(r)$ and $\sigma_\perp(r)$ are not correlated, the effective conductivity tensor will degenerate into a scalar

$$\sigma_e = e^{\left\langle\ln\sigma_\parallel\right\rangle} = e^{\langle\ln\sigma_\perp\rangle}. \tag{6.2.36}$$

References

1. Balagurov BY (1981) Reciprocity relations in two-dimensional percolation theory. Sov Phys JETP 54:355–358
2. Balagurov BY (1982a) On the conductivity of anisotropic inhomogeneous media. Sov Phys JETP 55(C), 1180–1188(1982)
3. Dreizin YA, Dykhne AM (1983) A qualitative theory of the effective conductivity of polycrystals. Sov Phys JETP 57:1024–1026
4. Dykhne AM (1967) Calculation of the Kinetic coefficients of media with random inhomogeneities. Sov Phys JETP 25:170–171
5. Dykhne AM (1970) Contluctivity of a two-dimensional two-phase system. Sov Phys JETP 32:63–64
6. Dykhne AM (1990) Theor Phys Inst, Univ. Minnesota, Prep. TPI-MINN-90/59-T (1990)
7. Dykhne AM, Kaganova IM (1997) The electrodynamics of polycrystals. Phys Rep 288:263–290
8. Emets YuP (1989) Symmetry transformations of 2D binary electrically conducting system. Sov Phys JETP 69:397–402
9. Feder J (1988) Fractals. Plenum Press, New York 283 p
10. Keller JB (1964) A theorem on the conductivity of a composite medium. J Math Phys 5:548–549
11. Luk'yanets SP, Morozovskii AE, Snarskii AA (1999) Transition to chaotization and loss of self-averagability in two-dimensional two-phase media at the percolation threshold. Tech Phys Lett 44:458–461
12. Morozovsky AE, Snarskii AA (1983) An effective conductivity of nonuniform media Ukrain. Fiz. Jur 28:1023–1028 (in Russian)

13. Schulgasser K (1977) Bounds on the conductivity of statistically isotropic polycrystals. J Phys C 10:407–417
14. Shvidler MI (1983) Effective conductivity of two-dimensional anisotropic media. Sov Phys JETP 57:688–690
15. Soderberg M, Grimvall G (1983) Current distributions for a two-phase material with chequer-board geometry. J Phys C 16:1085–1088

Chapter 7
Continual Percolation Problem

7.1 Types of Continual Percolation Problems

So far we have considered percolation problems that might be logically reduced to solving network problems, i.e., two-phase medium was simulated by a network of resistances r_1 and r_2. On the one hand, it means that there exists a certain characteristic linear size a_0 of the network, on the other—that in the calculation of impedance, spectral density of $1/f$-noise, etc., the shape of resistances is not important, it is only resistance rating that matters. In other words, in all the resistances the spatial distribution of current is homogeneous. In particular, it means that resistance of the bridge (see Chap. 5) is just a sum of equal resistances r_1 forming this bridge. However, a different case is possible, when the problem lacks a minimum length, and then the shape of given phase inclusions becomes vital. One of such important cases is Swiss Cheese Media [4, 6, 14], the simplest example of which is a medium that represents a conducting matrix (σ_1) with nonconducting ($\sigma_2 = 0$) spherical inclusions, i.e., porous medium. When the concentration of inclusions is close to threshold value, current has to flow through contractions formed by the nonconducting media (Fig. 7.1).

Current flow in such media can differ from that described by a standard network model. As is evident from Fig. 7.1, in different points the contraction size can be different, including arbitrarily small one. In so doing, current lines are contracted in the area of a neck and the resistance of this contraction is essentially dependent on the size δ, which, unlike a_0, is not fixed, different for different contractions, and has no characteristic (minimum) value.

Thus, on the one hand, the problem of calculation, for instance, of the effective conductivity σ_e is, as usual, the percolation problem, and, hence, there exist: (1) percolation threshold, (2) two phases $\sigma_1 \gg \sigma_2$, (3) standard elements of

A.A. Snarskii et al., *Transport Processes in Macroscopically Disordered Media*, DOI 10.1007/978-1-4419-8291-9_7

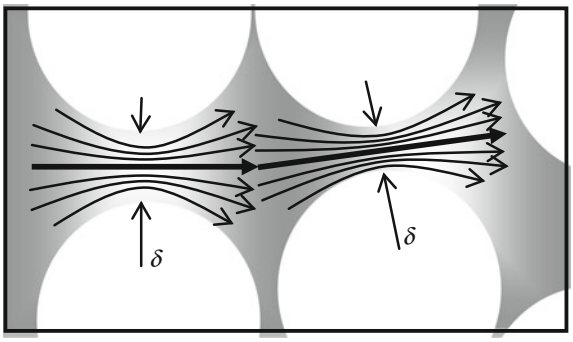

Fig. 7.1 Contractions (*necks*) in the percolation structure, on which the main voltage drop can be observed. For simplicity, the two-dimensional case is shown

percolation structure (bridge, interlayer), and on the other hand—the "elementary resistance" r_1 is not a constant, but rather depends in a certain way on parameter δ: $r = r(\delta)$. To emphasize both the similarity and difference of these two problems—standard percolation and Swiss Cheese problem, Fig. 7.2 qualitatively shows the main element of percolation structure—bridge—for these two problems.

To determine the effective conductivity in the case of $p > p_c$ one should be able to calculate the resistance of the bridge. To do this, in a standard percolation problem it is sufficient to know the number of resistances r_1 in a bridge N_1. In Swiss Cheese problem the resistance of the bridge depends not only on N_1, but also on the law of distribution of parameter δ.

The research on network models but with distributed values of r_1 (or, which is the same, δ) was originated in [2, 8, 18], where the following distribution function for local conductivity δ was assumed:

$$D(\delta) = (1-p)\delta(\sigma) + Ap\sigma^{-\alpha}. \tag{7.1.1}$$

Here α is the distribution parameter.

The problems similar to those described above are commonly called continual. Let us describe three of them

(1) Swiss Cheese problems (see Fig. 7.1)—intersecting voids ($\sigma_2 = 0$) in a continuous conducting (σ_1) medium [4, 6]. This problem is also called the problem of voids.

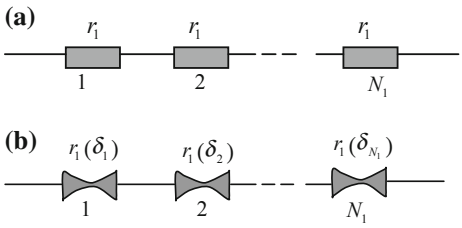

Fig. 7.2 The main element of percolation structure—a bridge: **a** for a standard (network) percolation problem, **b** for Swiss Cheese problem

(2) Problem of spheres or inverted Swiss Cheese problem—intersecting good conducting spheres (σ_1) in a nonconducting matrix ($\sigma_2 = 0$) [13, 16].
(3) Another type of percolation-similar problems with a continuous distribution of local conductivity that will be discussed in Chap. 8—conductivity of a medium with exponentially wide spectrum of local conductivity.

The geometric aspect of the Swiss Cheese and inverted Swiss Cheese problems is detailed in the books [3, 15] and a review [7]. We only note here that correlation length, like in an ordinary network problem, is determined by a standard critical index ν [1, 5].

7.2 Swiss Cheese Media

Let us show how to calculate the effective conductivity σ_e in Swiss Cheese model. According to [4, 6], an assumption is made that for $\delta \ll a$, where a is the radius of voids, the distribution is uniform—see Fig. 7.3. In so doing, each $\tau = (p - p_c)/p_c$ value has its own $\delta_{\min}$ (certainly, different from zero, since $p > p_c$). The resistance of irregular shaped neck (for the three-dimensional case this shape is given in Fig. 7.4) is found by replacing this shape by a simple one—parallelepiped having the same dependence on δ:

$$r \sim \delta^{-(1+y)},\ g_i = \frac{1}{r_i},\ y = \frac{\alpha}{1-\alpha}. \tag{7.2.1}$$

Here parameter y is found from qualitative considerations and can be obtained by solving a boundary value problem of mathematical physics. Thus, for the three-dimensional case we have

$$g \sim \delta^{3/2},\ y = \frac{1}{2},\ \alpha = \frac{1}{3}, \tag{7.2.2}$$

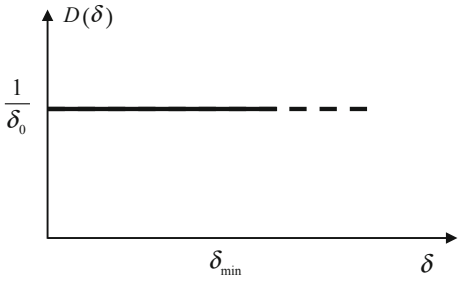

Fig. 7.3 Distribution of parameter δ in the case when δ is much less than the radius of voids, $\delta \ll a$ (with their inclusion conductivity $\sigma_2 = 0$)

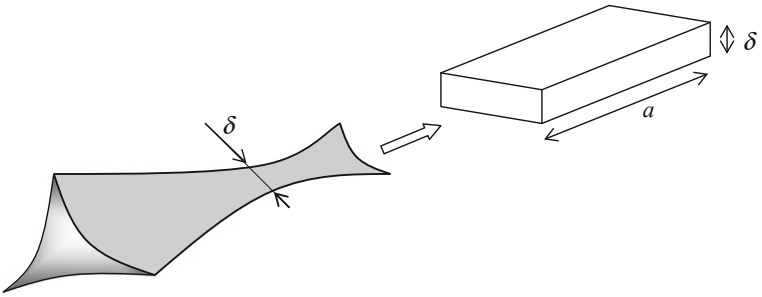

Fig. 7.4 View of a neck in the three-dimensional case and its approximation

for the two-dimensional case

$$g \sim \delta^{1/2},\ y = -\frac{1}{2},\ \alpha = -1. \tag{7.2.3}$$

By definition, a bridge always comprises maximum of all possible resistances, therefore its resistance values are expressed through r and $D(\delta)$ as follows:

$$R_1 = r(\delta_{\min}) + N_1 \int\limits_{\delta_{\min}} r(\delta) D(\delta) \mathrm{d}\delta + N_1 r_1 \approx r_1 \left(\delta_{\min}^{-(1+y)} + N_1 \delta_{\min}^{-y} \right) + N_1 r_1. \tag{7.2.4}$$

The last term in (7.2.4) is a standard percolation term which is universally present (at large δ, when the neck shape is of no significance). This term will matter, if the resistance $r_{\max} \sim 1/\delta_{\min}$ included into the bridge and will make a lesser contribution to the bridge resistance than the sum of the other resistances $N_1 r_1$.

Minimal size $\delta_{\min}$ (for given τ value) is found from the following considerations: the probability of the bridge having no resistance larger than $r_{\max}$ (i.e., there are no δ lesser than $\delta_{\min}$) can be written as

$$\left(1 - \int\limits_0^{\delta_{\min}} D(\delta) \mathrm{d}\delta \right)^{N_1} \sim \mathrm{e}^{-\frac{\delta_{\min}}{\delta_0} N_1}, \tag{7.2.5}$$

where it is taken into account that $1/\int_0^{\delta_{\min}} D(\delta)\mathrm{d}\delta \to \infty$ at $\delta_{\min} \to 0$.

Since this probability should not depend on τ, we have

$$\frac{\delta_{\min}}{\delta_0} N_1 \sim \tau^0, \tag{7.2.6}$$

whence it follows that

$$\delta_{\min} \sim N_1^{-1}. \tag{7.2.7}$$

Thus, the larger is N_1, i.e., the closer is the system to percolation threshold, the lower $\delta_{\min}$ and the larger $r_{\max}$ will be included into the bridge. The value of δ_0 does not affect the calculation results.

Substituting $\delta_{\min}$ from (7.2.7) to the expression for R_1 (7.2.4) yields

$$R_1 \sim r_1\left(N_1^{1+y} + N_1\right) = r_1 N_1\left(N_1^y + 1\right). \tag{7.2.8}$$

Passing from the bridge resistance R_1 to the effective resistivity $\rho_e = R_1 N_1^{\nu(d-2)}$, we find (all the calculations are made within the NLB-model)

$$\rho_e \approx R_1 N_1^{1+\nu(d-2)}\left(N_1^y + 1\right), \tag{7.2.9}$$

and taking into account that within the NLB-model $N_1 \sim \tau^{-1}$ and $t = 1 + \nu(d-2)$, from (7.2.9) we have

$$\rho_e \simeq \rho_1 |\tau|^{-(t+y)} + \rho_1 |\tau|^{-t}. \tag{7.2.10}$$

The last expression is valid close to percolation threshold, i.e., at $\tau \to 0$, therefore, depending on the value of y this or other term will "win" in it. In the three-dimensional case, at $y = 1/2$, the first term is considerably larger than the second one, therefore critical index of the effective conductivity in Swiss Cheese problem $\bar{t}_3$ is of the form

$$\bar{t}_3 = t_3 + y, \tag{7.2.11}$$

and in the two-dimensional case, as long as $y = -1/2$, the second term will take over, we have

$$\bar{t}_2 = t_2. \tag{7.2.12}$$

The effective conductivity of inverted Swiss Cheese problem is found similarly. If in Swiss Cheese model renormalization of critical index t was related to the fact that current lines had to pass through a contraction that was called a neck (see Figs. 7.1, 7.4), here current lines pass through a contraction (see Fig. 7.5), that is commonly called a bottle neck. As is shown in [4], both in the two-dimensional and the three-dimensional case parameter $y<0$: $y_2 = -1$, $y_3 = -1/2$, therefore critical index of conductivity in the inverted Swiss Cheese problem does not differ from such in the network problem (see also [11]).

Similar to Swiss Cheese and inverted Swiss Cheese problems describing continual percolation problem above the percolation threshold, one can also consider

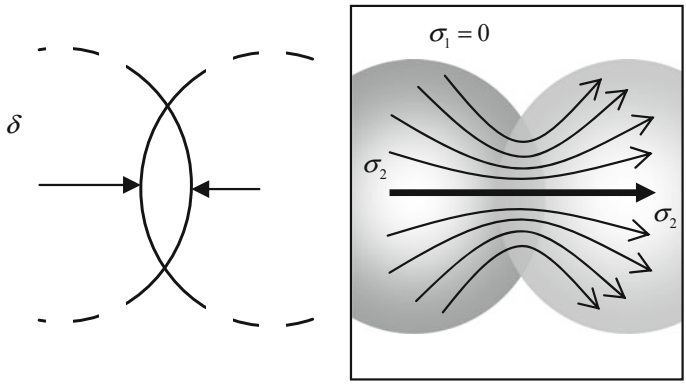

Fig. 7.5 Schematic of inverted Swiss Cheese problem: **a** geometrical parameters of contraction; **b** qualitative view of current lines in the contraction. Concentration of conducting (σ_1) phase above the percolation threshold

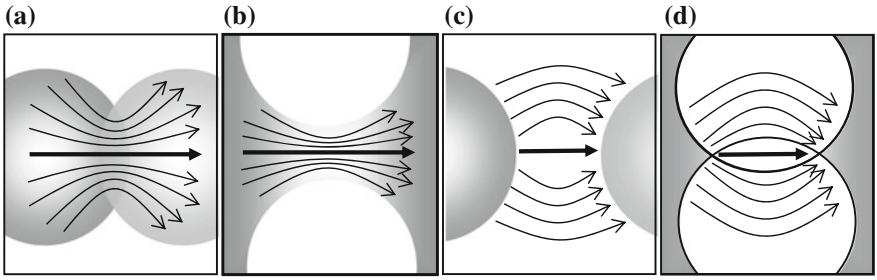

Fig. 7.6 Schematic of four possible continual Swiss Cheese problems: **a** Swiss Cheese model ($\sigma_2 = 0$); **b** inverted Swiss Cheese- ($\sigma_2 = 0$); **c** and **d** percolation system below the percolation threshold ($1/\sigma_1 = 0$). *Dark color* is for a phase with conductivity σ_1

problems below the percolation threshold. Schematically all the four continual problems are given in Fig. 7.6. The elements on which the main voltage drop occurs include the bridge (Fig. 7.6a, b) and the interlayer (Fig. 7.6c, d).

In work [17] one more type of continual percolation problem is proposed, close to Swiss Cheese, and named by the author as Blue Cheese. The shape of non-conducting inclusions ($\sigma_2 = 0$) in this problem is strongly different from the spherical one in Swiss Cheese—one of inclusion sizes is considered equal to zero (Fig. 7.7).

Blue Cheese problem is a good model of fractured media and allows determining critical behavior and critical indices of the effective conductivity, elasticity, etc., in such media. Critical indices of the effective conductivity in Blue Cheese problem for the three-dimensional case do not differ from the network ones, and in the three-dimensional case they differ logarithmically. However, for other problems (elasticity, $1/f$-noise) these indices are different.

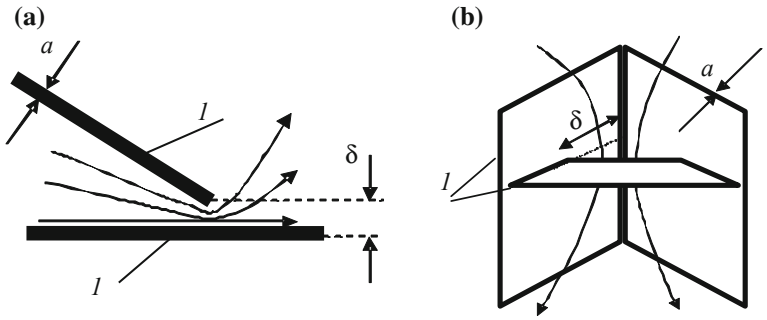

Fig. 7.7 Contraction model in Blue Cheese problem: *1*—nonconducting inclusions, $a \ll \delta$: **a** two-dimensional case, **b** three-dimensional case

In the study [12] the Swiss Cheese and inverted Swiss Cheese models were generalized for the case of more complicated (but still convex) inclusion surfaces.

Let us note, without going into details, several works that describe the experiments. In work [9] for a composite consisting of conductive balls (indium balls of diameter about 20 μm) in a glass matrix the critical index of conductivity was obtained as $\bar{t}_3 \simeq 3.1 \pm 0.3$ which is in agreement with the theoretical value $\bar{t}_3 = t + 1/2 \approx 2 + 0.5 = 2.5$. In work [10] an experiment was performed with a metal plate with openings drilled in it. As theoretically predicted, for the two-dimensional case the resultant critical index $\bar{t}_2 = 1.24 \pm 0.13$ coincides with the network one.

References

1. Balberg I (1987) Recent development in continuum percolation. Phil Mag 57:991–1003
2. Ben-Mizrahi A, Bergman DJ (1981) Non-universal critical behavior of random resistor networks with a singular distribution of conductances. J Phys C 14:909–922
3. Efros AL (1986) Physics and geometry of disorder. Mir, Moscow, p 259
4. Feng S, Halperin BI, Sen PN (1987) Transport properties of continuum systems near the percolation threshold. Phys Rev B 35:197–214
5. Gawlinski ET, Stanley HE (1981) Continuum percolation in two dimensions: Monte Carlo tests of scaling and universality for non-interacting discs. J Phys A 14:L291–L298
6. Halperin BI, Feng S, Sen PN (1985) Differences between lattice and continuum percolation transport exponents. Phys Rev Lett 54:2391–2394
7. Isichenko MB (1992) Percolation, statistical topography, and transport in random media. Rev Mod Phys 64:961–1043
8. Kogut PM, Straley JP (1979) Distribution-induced non-universality of the percolation conductivity exponents. J Phys C 12:2151–2160
9. Lee SI, Song Y, Noh TW, Chen XD, Gaines JR (1986) Experimental observation of nonuniversal behavior of the conductivity exponent for three-dimensional continuum percolation systems. Phys Rev B 34:6719–6724
10. Lobb CJ, Forrester MG (1987) Measurement of nonuniversal critical behaviour in a two-dimensional continuum percolating system. Phys Rev B 35:1899–1901

11. Lobb CJ, Hui PM, Stroud D (1987) Nonuniversal breakdown behaviour in superconducting and dielectric composites. Phys Rev B 36:1956–1961
12. Miyazima S (1987) Percolation transport exponents in a generalized Swiss-Cheese model and a generalized inverted Swiss-Cheese model for a conductive substance. J Phys Soc Jap 56:1268–1270
13. Pike R, Stanley HE (1981) Order propagation near the percolation threshold. J Phys A 14: L169–L177
14. Sen PN, Roberts JN, Halperin BI (1985) Nonuniversal critical exponents for transport in percolating systems with a distribution of bond strengths. Phys Rev B 32:3306–3308
15. Shklovskii BI, Efros AL (1984) Electronic properties of doped semiconductors. Springer, Berlin, p 388
16. Skal AS, Shklovskii BI (1974) Topology of infinite cluster in the theory of percolation and hopping conduction. Sov Phys Semicond 8:1586–1592 (in Russian)
17. Sornette D (1988) Critical transport and failure in continuum crack percolation. J Phys Fr 49:1365–1377
18. Straley JP (1982) Non-universal threshold behaviour of random resistor networks with anomalous distributions of conductances. J Phys C 15:2343–2346

Chapter 8
Media with Exponentially Broad Spectrum of Local Properties

8.1 Formulation of the Problem and Approximate Calculation of the Effective Conductivity

Hitherto we have considered percolation media that can be represented as a network of randomly scattered strongly different resistances $r_2 \gg r_1$, with the concentration p of the lower of resistances (r_1) being close to the threshold p_c. The distribution function $f(r)$ in the case when there are only two resistance types: "metal"—r_1 and "dielectric"—r_2 is of the form

$$f(r) = p\delta(r - r_1) + (1 - p)\delta(r - r_2). \tag{8.1.1}$$

No less interesting and important is the problem of calculation of the effective conductivity of media, when the spectrum of resistance values is continuous on retention of a strong inhomogeneity, i.e., the "worst" $(r_{\max})$ of all possible resistances are much larger than "the best" $(r_{\min})$, $r_{\max} \gg r_{\min}$. One of the examples of such distribution is exponentially wide distribution, when

$$r = r_0 \mathrm{e}^{-\lambda x}, \quad \lambda \gg 1. \tag{8.1.2}$$

Here x is a random variable lying in the interval $(0, 1)$ and having a smooth distribution function $D(x)$. In the simplest case $D(x)$ is a uniform distribution,

$$D(x) = \begin{cases} 1, & 0 \le x \le 1, \\ 0, & x < 0, x > 1. \end{cases} \tag{8.1.3}$$

The resistance distribution function $f(r)$ according to (8.1.3) in this case is of the form

$$f(r) = \frac{1}{\lambda r}, \quad r_0 \mathrm{e}^{-\lambda} \le r \le r_0. \tag{8.1.4}$$

A.A. Snarskii et al., *Transport Processes in Macroscopically Disordered Media*, DOI 10.1007/978-1-4419-8291-9_8

The problem of calculation of the effective conductivity σ_e of such randomly inhomogeneous medium with exponentially wide spectrum of resistance distribution is of great significance in various applications, in particularly, it is a type of sample conductivity determination problem for hopping conductivity [2, 11, 12]. According to [12], the electron conductivity of a sample, if hopping conductivity happens to be the case, amounts to "*calculating conductivity of a random network, where each node coincides with one of the donors, and a resistance is included between a pair of nodes,"* one of possible, taken from (8.1.4). Such network is called Miller-Abrahams network [7].

Resistance between i and j nodes for hopping conductivity depends on the distance between the nodes l_{ij} and the difference in energies at the donor levels ε_{ij} (see details in [12]), the latter at relatively high temperatures can be neglected, and then

$$r_{ij} \sim e^{\frac{2l_{ij}}{a}}, \tag{8.1.5}$$

where a is effective Bohr radius.

In the specific cases of weakly doped semiconductors the resistances r_{ij} are essentially dependent on l_{ij} and can be different by many orders of magnitude (10^5 and more). In [12] an example is given when $r_{ij}(2l_{ij})$ is different from $r_{ij}(l_{ij})$ by a factor of $10^5 - 10^{10}$.

On the face of it, the problem of determination of σ_e for a network with exponentially wide resistance spectrum is not percolation—there is no percolation threshold, on reaching which, one of the phases forms infinite cluster, since there are no phases as such. However, a technique proposed in [5] and [11] allows in a certain approximation reducing this problem to a standard percolation one. To demonstrate how this technique works, let us make the following construction. "Remove" from the Miller-Abrahams network all the resistances, keeping in mind their positions and begin consecutively "inserting" them in their places, starting the process from the minimum $(r_{\min})$ (Fig. 8.1). All the resistances included at this moment will be considered a "metal" phase. When the "metal" phase reaches the threshold concentration, an infinite cluster will appear in the system—the last inserted resistance r_c will close the bridge. Since with exponentially wide resistance spectrum each subsequent inserted resistance is much larger compared with the preceding one, the resistance of resultant infinite cluster is practically determined, to an accuracy of pre-exponential factor, by the last inserted resistance. Further addition of shunting resistances will not change anything, since their values are much larger than the critical r_c.

Critical resistance r_c can be easily found from the following condition: it "appears" at the threshold concentration

$$\int_{x_c}^{1} D(x)\mathrm{d}x = p_c. \tag{8.1.6}$$

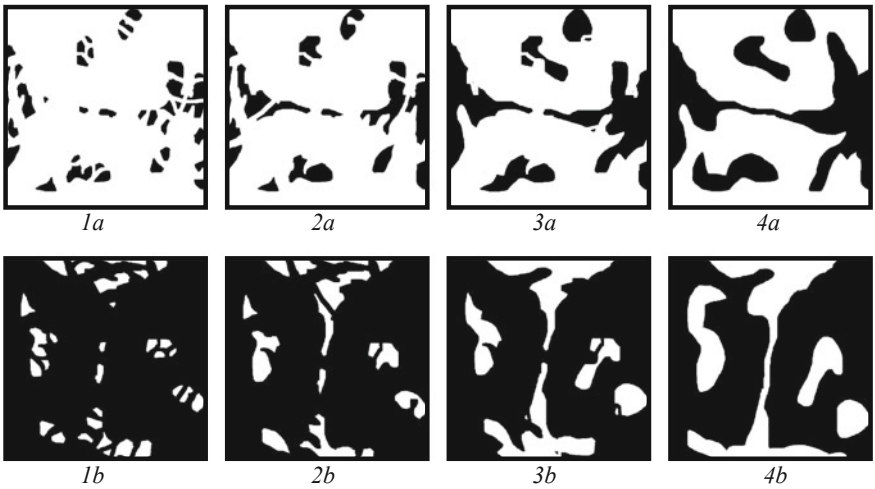

Fig. 8.1 System view with a consecutive insertion of "metal" and "dielectric" inclusions: *1a–4a*—arrangement of "metal" resistances as they are inserted, in *4a* there appears a bridge; *1b–4b*—arrangement of "metal" resistances as "dielectric" resistances are inserted, in *4b* there appears an interlayer

Whence, with regard to (8.1.3), we obtain $x_c = 1 - p_c$.

Thus, we have

$$r_c = r_0 e^{-\lambda x_0} = r_0 e^{-\lambda(1-p_c)}, \tag{8.1.7}$$

or in terms of specific conductivity:

$$\sigma_e = \sigma_0 e^{\lambda x_c} = \sigma_0 e^{\lambda(1-p_c)}. \tag{8.1.8}$$

8.2 Correlation Length and Pre-exponential Factor

Such an approach—insertion of consecutively growing resistances—yields a good approximation for σ_e. Though, a series of unsolved problems remain. The first one is related to correlation length ξ.

Unlike the two-phase system with $\sigma_2/\sigma_1 = 0$ for which ξ is infinite on the percolation threshold, the correlation length for a system with exponentially wide resistance spectrum is finite. However, it is not clear which considerations can lead one to obtain its value, since the approach employed lacks the concept of smearing region. There is also an alternative way of reducing the problem to percolation one

[8], [9]. According to the above-described method, during the first stage (Fig. 8.11a), the system was completely nonconducting, i.e., one can say that practically all the network was filled with infinite resistances that were consecutively replaced by $r_{\min} \le r \le r_c$. According to the alternative approach, at first (Fig. 8.11b), practically all the network is filled with zero resistances that are consecutively replaced by $r_c \le r \le r_{\max}$, i.e., the largest resistances are inserted first. As the threshold concentration is approached, there comes a moment when the inserted resistance blocks the zero resistance channels, and then the entire system will possess finite resistance. Since each subsequent resistance is much less that the preceding one, it is exactly the last inserted resistance r_c that will govern current in the system. Thus, like in the first approach, $\sigma_e = \sigma_0 e^{\lambda x_c}$. One can say that in the first approach a "metal" phase was closed in a medium with infinite resistance, and in the second approach a "dielectric" phase disconnected the current flowing in a perfect conductor. Both approaches give the same σ_e, but to an accuracy of exponential factor. As can be readily seen in Fig. 8.1, the finite percolation structure Fig. 8.14a, 4b in both approaches is quite different. And this certainly leads [9], as will be shown below, to different pre-exponential factors. Write down σ_e as follows [3, 14]:

$$\sigma_e = \frac{A}{a_0^{d-2} r(x_c)} \left(\frac{D(x_c)}{\lambda} \right)^y = \frac{A}{a_0^{d-2}} \frac{D(x_c)^y}{r_0} \lambda^{-y} e^{\lambda x_c} \sim \lambda^{-y} e^{\lambda x_c}. \tag{8.2.1}$$

To determine the critical index, we begin with considering the ***first approach***: i.e., all the resistances $r \le r(x_c) \le r_c$ are "metal," and the rest have infinite resistance. We will use the NLB and HM models described earlier in Chap. 5. Let the concentration of "metal" phase be p, then, with regard to

$$\tau = \frac{p - p_c}{p_c},\ x - x_c = (1 - x_c)\tau, \tag{8.2.2}$$

one can estimate the average value of resistances that form the bridge

$$\langle r \rangle_1 = \int_{x_1}^{1} r(x) P_1(x) \mathrm{d}x \approx \frac{r(x_1)}{1 - x_1} \lambda^{-1},\ x_1 > x_c,\ \lambda \gg 1 \tag{8.2.3}$$

where $r(x_1)$ is the largest resistance in the bridge; renormalization of distribution

$$P(x_1) = \frac{D(x)}{\int_{x_1}^{1} D(x) \mathrm{d}x} \tag{8.2.4}$$

is related to the fact that the largest bridge resistance is $r(x_1)$.

The resistance of the bridge, hence of the entire system on correlation dimensions, is of the form

$$R_1 = N_1 \langle r \rangle_1. \tag{8.2.5}$$

Passing from the system resistance $R = R_1$ to specific conductivity $\sigma_e = 1/R\xi^{d-2}$, for the first approach we find

$$\sigma_I^e = \frac{1 - x_1}{r(x_1) a_0^{d-2}} \tau^{\alpha_1 + \nu(d-2)}, \tag{8.2.6}$$

where $\alpha_1 = 1$ in the NLB-model and $\alpha_1 = \xi_R = t - \nu(d-2)$ in the HM.

In perfect analogy we find system resistance in the ***second approach***. The average bond resistance in the interlayer, provided all of them are located in parallel, can be estimated as follows:

$$\langle 1/r \rangle_2 = \int_0^{x_2} \frac{P_2(x)}{r(x)} \mathrm{d}x \approx \frac{1}{\lambda x_2 r(x_2)}, \tag{8.2.7}$$

where [compare to (8.2.4)] the renormalization of distribution

$$P_2(x) = \frac{D(x)}{\int_0^{x_2} D(x) \mathrm{d}x} \tag{8.2.8}$$

is due to the fact that the lowest resistance in the interlayer is $r(x_2)$.

The resistance of interlayer, hence the resistance of the entire correlation volume is of the form

$$R_2 = \frac{1}{N_2 \langle 1/r \rangle_2}. \tag{8.2.9}$$

Passing to specific conductivity, for the second approach we find

$$\sigma_{II}^e = \frac{\tau^{-\alpha_2 + \nu(d-2)}}{x_2 r(x_2) a_0^{d-2}} \lambda^{-1}. \tag{8.2.10}$$

Comparing the values of σ_I^e from (8.2.6) and σ_{II}^e from (8.2.10), we see that even if we assume $x_1 = x_2 = x_c$, they will contradict each other; dependence on λ (remind that $\lambda \gg 1$) will be exactly opposite: λ^{+1} in σ_I^e and λ^{-1} in σ_{II}^e. Moreover, σ_I^e and σ_{II}^e have also dependence on the proximity to percolation threshold τ, which was introduced conventionally [11], it is not a free parameter whose values can be selected at will, as it is done for the two-phase media, changing the concentration of

one of the phases, and should not be present in the final expression for the effective conductivity.

The above contradictions can be removed [9], further assuming by analogy to the two-phase system that a system with exponentially wide resistance spectrum is the smearing region. It is the more natural since if in the two-phase systems in extreme cases $\sigma_2 = 0$ or $\sigma_1 = \infty$ the magnitude of smearing region can be equal to zero, then in systems with exponentially wide resistance spectrum the ratio of local conductivities, even if very small, is always finite.

To determine the magnitude of smearing region Δ, like in the two-phase case, equating σ_I^{e} and σ_{II}^{e}, we obtain

$$\sigma_I^{\mathrm{e}}(\tau = \Delta) = \sigma_{II}^{\mathrm{e}}(\tau = -\Delta), \tag{8.2.11}$$

and take into account that according to (8.2.2)

$$x_1 = x_c + (1 - x_c)\Delta, \; x_1 = x_c - (1 - x_c)\Delta. \tag{8.2.12}$$

Substituting now (8.2.6), (8.2.10) and (8.2.12) to (8.2.11), we find the equation for determination of the magnitude of smearing region

$$\mathrm{e}^{-2(1-x_c)\Delta\lambda} = [x_c - (1 - x_c)\Delta][1 - x_c - (1 - x_c)\Delta]\Delta^{\alpha_1 + \alpha_2} \cdot \lambda^2. \tag{8.2.13}$$

As is shown by numerical solution (8.2.13) at $\alpha_1 = \xi_R$ and $\alpha_2 = \xi_G$ for $10^2 < \lambda < 10^7$ the values of Δ lie in the range of $10^{-6} < \Delta < 2 \cdot 10^{-2}$, in this case $1 < \Delta\lambda < 6$. Thus, $|\ln \Delta| > \ln \lambda\Delta$, which enables to obtain an approximate solution of the equation. Ignoring the summand $(1 - x_c)\Delta$ as compared to x_c and $1 - x_c$, from expression (8.2.13) we find

$$\Delta \approx -\lambda^{-1} \frac{\ln\left[\sqrt{x_c(1 - x_c)}\lambda^{1 - \frac{\alpha_1 + \alpha_2}{2}}\right]}{1 - x_c}. \tag{8.2.14}$$

From this we have

$$\sigma_{\mathrm{e}} = \frac{A}{a_0^{d-2}} \lambda^{-y} \mathrm{e}^{\lambda x_c}, \tag{8.2.15}$$

where A is weakly dependent on λ ($A \sim (\ln \lambda)^{\alpha_1 + \alpha_2 + \nu(d-2)}$), and critical index of percolation factor [9]:

$$y = \frac{\alpha_1 - \alpha_2 + 2\nu(d - 2)}{2}. \tag{8.2.16}$$

To determine the numerical value of critical index y, one should assign the values of indices α_1 and α_2, which, in turn, will govern the number of the so-called

SCB- and SDCB-bonds (see Chap. 5). For the two-phase systems in the HM it was assumed that $\alpha_1 = \xi_R$, $\alpha_2 = \xi_G$. In this case

$$y(\alpha_1 = \xi_R, \alpha_2 = \xi_G) = \frac{t-q}{2} \tag{8.2.17}$$

However, if $\alpha_1 = \alpha_2 = 1$ (NLB-model),

$$y(\alpha_1 = 1, \alpha_2 = 1) = \nu(d-2). \tag{8.2.18}$$

As can be seen, in the two-dimensional case, both (8.2.17) and (8.2.18) imply that $y_2 = 0$.

This $y_2 = 0$ assertion is rigorous, following immediately from considerations of duality and available in work [1]. Indeed, in case of continuous distribution according to [1] we have

$$\sigma_e = e^{\langle \ln \sigma \rangle}, \tag{8.2.19}$$

and in case of exponentially wide resistance spectrum (8.1.2) the effective conductivity can be written as

$$\sigma = \sigma_0 e^{-\lambda x}. \tag{8.2.20}$$

In case of uniform distribution (8.1.3) the distribution function $f(\sigma)$ is [compare to (8.1.4)]

$$f(\sigma) = -\frac{1}{\lambda \sigma}. \tag{8.2.21}$$

Then $(x_0 = 0,\ x_1 = 1)$ we have

$$\langle \ln \sigma \rangle = \int_{x_0}^{x_1} f(\sigma) \ln \sigma d\sigma = \ln \sigma_0 - \frac{1}{2}\lambda. \tag{8.2.22}$$

Substituting $\langle \ln \sigma \rangle$ to (8.2.19), we find

$$\sigma = \sigma_0 e^{-\lambda x} = e^{-\lambda x_c},\ x_c = \frac{1}{2}, \tag{8.2.23}$$

which is to say that at $d = 2$ [see (8.2.15)] $y_2 = 0$.

Table 8.1 gives the numerical values of critical index in the three-dimensional case with the HM (8.2.17) and NLB-model (8.2.18) and according to numerical simulation.

Work [6] analyzes the use of different theoretical methods when solving the problem of determination of critical index y, such as renormalization group and

Table 8.1 The numerical values of critical index y_3 (the three-dimensional case)

HM: $y_3(\alpha_1 = \xi_R, \alpha_2 = \xi_G)$ (8.2.17)	0.635
NLB: $y(\alpha_1 = 1, \alpha_2 = 1)$ (8.2.18)	0.88
Numerical simulations:	
[5]	0.6 ± 0.25
[14]	0.6 ± 0.1
[4]	0.76 ± 0.04
[13]	0.74 ± 0.01

finite size scaling methods, field-theoretical method (expansion close to critical dimension $d_c = 6$) and so on. All these methods according to [6] result in (8.2.18). However, work [13] summarizes arguments against it, since according to [13] all conclusions have been obtained within the limit $\lambda \to \infty$, which is impossible both in real systems and in numerical simulation alike. As is evident from Table 8.1, the numerical values (8.2.17) better agree with numerical simulation. It means that in the three-dimensional case $y < v$, rather than $y = v$ [6]. As we will see below, in Chap. 13, in the calculation of higher moments of current distribution (in the calculation of σ_e the second moment was calculated) it appears necessary to come back to determination of α_1 and α_2 within the NLB-model. The distribution of the Joule dissipation in such media (see Chap. 14) is considered in [10].

References

1. Dykhne AM (1970) Contluctivity of a two-dimensional two-phase system. Sov Phys JETP 32:63–64
2. Gantmakher VF (2005) Electrons and disorder in solids. Clarendon Press, Oxford, p 240
3. Halperin BI (1989) Remarks on percolation and transport in networks with a wide range of bond strengths. Phys D 38:179–183
4. Kolek A, Snarskii AA, Morozovskii AE (1995) Structure of the percolation cluster and excess 1/f noise in systems with an exponentially broad spectrum of resistances. Sov Phys JETP 81:490–495
5. Kurkijarvi J (1974) Conductivity in random systems. II. Finite-size-system percolation. Phys Rev B 96:770–774
6. Le Doussal P (1989) Percolation like exponent for the conductivity of highly disordered resistor networks. Phys Rev B 39:881–884
7. Miller A, Abrahams E (1960) Impurity conduction at low concentration. Phys Rev 120:745–755
8. Morozovsky AE, Snarskii AA (1992) Multiscaling in randomly inhomogeneous media: effective conductivity, relative spectral density of 1/f noise, and higher-order moments. Sov Phys JETP 75:366–371
9. Morozovsky AE, Snarskii AA (1993) Percolation description of the conductivity of random networks with a broad spectrum of the distribution of resistances. Sov Phys JETP 77:959–965
10. Roux S, Rigord P, Hansen A, Hinrichsen L (1991) Power dissipation in random resistor networks with a broad distribution of conductivities. Phys Rev B 43:10984–10998
11. Shklovskii BI, Efros AL (1975) Preexponential factor in hopping conduction. Tech Phys Lett 1:174–177 (in Russian)

12. Shklovskii BI, Efros AL (1984) Electronic properties of doped semiconductors. Springer, Berlin, p 388
13. Skaggs TH (2003) Effects of finite system—size and finite inhomogeneity on the conductivity of broadly distributed resistor networks. Phys Rev B 338:266–269
14. Tyč S, Halperin BI (1989) Random resistor networks with exponentially wide distribution of bond conductances. Phys Rev B 39:877–880

Chapter 9
Finite Scaling

9.1 Properties of Percolation Systems with Dimensions Lesser Than Their Correlation Length

Up to now, in the description of geometrical or physical properties of media located close to percolation threshold, we have implied that sample size L for which, for example, conductance G or effective conductivity $\sigma_e = GL^{d-1}/L$ are determined, is much larger than the correlation length ξ, i.e., $L \gg \xi$. In this case the value G (or σ_e) is self-averaged over realizations of a random structure, i.e., does not depend on the way this or other resistance will "fit" at creation of a random medium [1].

When $L < \xi$, this, of course, is not the case, and the value G (or σ_e) will change from one realization to another one, and its fluctuations (due to structure realizations) will be the larger, the lower value of L. It would seem that at $L < \xi$ it is difficult to count on revealing of simple regularities—after all, each medium realization is random. However, in the critical region, close to percolation threshold, the main feature of percolation structure is infinite cluster with fractal dimensions. One of the main properties of fractal objects is the fact that any intensive X value that characterizes a fractal, for instance, its density (volume unit mass) [2] depends on L as follows:

$$X(L, \xi) = x(L/\xi) \cdot \xi^{\chi/\nu} \sim \begin{cases} \xi^{\chi/\nu}, & L \gg \xi, \\ L^{\chi/\nu}, & L < \xi, \end{cases} \tag{9.1.1}$$

where $x(L/\xi)$ is scaling function, ν is critical index of correlation length, χ is critical index describing behavior of $X(L, \xi)$ value. Certainly, in the case of $L < \xi$, by $X(L, \xi)$ is meant an average over realizations $\{X(L, \xi)\}$, though in the literature this essential remark is often omitted.

As long as $\xi \sim \tau^{-\nu}$, with increasing L the value X is no longer dependent on dimension, but on the other hand the dimension becomes dependent on concentration $X \sim |\tau|^{-\chi}$. And averaging over realizations is not required any more.

A.A. Snarskii et al., *Transport Processes in Macroscopically Disordered Media*, DOI 10.1007/978-1-4419-8291-9_9

Surprisingly, the regularity of passing from one, concentration type of dependence, to another, namely dimensional, has a perfect analogy in the theory of second-order phase transitions in going from temperature dependence of the order parameter to dimensional dependence, averaged over time (thereby, over realizations).

The use of the term "finite-size scaling" is attributable to the fact that we are dealing with scaling dependences of systems with finite size $L<\xi$. Starting from $L > \xi$, the system properties are no longer dependent on L.

It should be specified what is meant by percolation structure in the case of $L<\xi$. One of the basic parameters of percolation medium is percolation threshold p_c which is strictly determined only at $L \gg \xi$. For a sample with a finite size, as detailed in [7, 9], the name of percolation threshold for a sample of given size L can be given to such concentration of "black" nodes (bonds), averaged over realizations, whereby for the first time there appears an "infinite cluster", i.e., percolation through the whole system of given size. By this concentration is meant (1) relative number of "black" nodes (bonds) in the network where "white" nodes (bond) randomly "change color" before the onset of percolation—p_c (microcanonical distribution)—$p_c(MC)$ or (2) apriori probability of the fact that a node (bond) is "black", and percolation p_c (canonical distribution)—$p_c(C)$ has occurred in the system. Both definitions are identical for a system with $L \gg \xi$, but for a finite case at $L<\xi$ they result in different values of percolation threshold.

In the former case we are dealing with a microcanonical assembly, i.e., the concentration of "black" bonds (nodes) in the sample is strictly equal to $p_c(MC)$; in the latter case—with a canonical assembly.

In [7] the numerical simulation was used to find the distribution function $f(p_c(C))$ for a canonical assembly of the problem of nodes that proved to be very close to the Gaussian function. The dispersion of this distribution $W = \sqrt{\{p_c^2\} - \{p_c\}^2}$ (from here on the sign K will be omitted) is determined by the critical index of correlation length

$$W \approx BL^{-1/\nu} \sim L^{-1/\nu}, \tag{9.1.2}$$

where B is a certain constant of the order of unity, in the two-dimensional case in [7] it was obtained as $B \approx 0.54$. As one would expect, W is reduced with increasing L.

Percolation threshold averaged over realizations $\{p_c(L)\}$ for a system of size $L<\xi$ is larger than the threshold of "infinite" system with $p_c = p_c(L \gg \xi)$.

$$\{p_c(L)\} - p_c = AL^{-1/\nu} \sim L^{-1/\nu}, \tag{9.1.3}$$

where A is a certain constant. These regularities are true both for the two- and three-dimensional cases [12].

Numerical experiments show "*...quite nontrivial, well appreciable ... excess of mean-square fluctuation W over the shift of maximum point of distribution function* $\{p_c(L)\}$ (i.e., *the average value*)" [7, 9]. Thus, for the distribution function of percolation thresholds in the finite ($L<\xi$) system one can write down

$$f(p_c) = \frac{1}{\sqrt{2\pi}W} \mathrm{e}^{-\frac{\left[p_c(L)-p_c-AL^{-1/\nu}\right]^2}{2W^2}}, \tag{9.1.4}$$

or, ignoring the excess of W over the shift and passing on to afterwards more convenient variable $\tau_c = (p_c(L) - p_c)/p_c$ (Fig. 9.1), we have

$$f(\tau_c) = \frac{1}{\sqrt{2\pi}W} \mathrm{e}^{-\frac{p_c^2}{2W^2}\tau_c^2}. \tag{9.1.5}$$

Come back now to finite-size scaling of the effective conductivity. According to (9.1.1) we write down

$$\{\sigma_\mathrm{e}\} = \sigma_1 \left(L/a_0\right)^{-\frac{t}{\nu}} \sim \sigma_1 L^{-\frac{t}{\nu}}, \tag{9.1.6}$$

Later on in this chapter, for simplicity of notation, we will use dimensionless unit and therefore omit a_0 everywhere.

In formula (9.1.6) it is meant that the system is in the critical region and that $\sigma_2 = 0$. Realizations where no percolation occurs do not contribute to an average over realizations. Numerical experiments in this case (see references in [12]) with a good precision confirm the power dependence $\{\sigma_\mathrm{e}\}$ and these dependences are used to determine the numerical value t/ν. Such numerical experiments employed rather high-power (at that time) computers, up to Cray [8] and Sun 4/280 [5].

In the case when bad conducting medium has a finite resistance $\rho_2 \neq \infty$, and good conducting medium is a perfect conductor ($\sigma_1 = \infty$), the average over realizations conductivity is no longer an appropriate characteristic, since one percolation realization (which is always available) is enough for $\{\sigma_\mathrm{e}\} = \infty$. An appropriate characteristic here will be the average over realizations resistivity

$$\{\rho_\mathrm{e}\} = \rho_2 L^{q/\nu}, \tag{9.1.7}$$

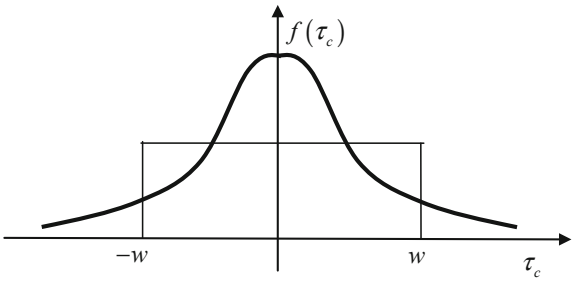

Fig. 9.1 The distribution function of percolation thresholds for the size $L<\xi$, the thin line is its uniform approximation

in so doing, realizations with percolation, where $\{\sigma_e\} = \infty$, will fall out of averaging, since for them $\rho_e = 0$.

Formally, dependences (9.1.6) and (9.1.7) were obtained from the first approximations over concentration $\sigma_e = \sigma_e(\tau)$ above $\sigma_e = \sigma_1 \tau^t$ and below $\sigma_e = \sigma_2 |\tau|^{-q}$ the percolation threshold by simple substitution $\tau \to \xi^{-1/\nu} \to L$. It is clear that with arbitrary sets of parameters σ_1, σ_2, τ and L such formal technique does not allow answering the question of finite-size scaling at $\sigma_2/\sigma_1 \neq 0$.

With sizes $L < \xi$, i.e., in the fractal region both above and below the percolation threshold, realizations with and without the percolation will occur (see Fig. 9.2). In other words, in the assembly of systems with sizes $L < \xi$ and given value τ, with certain probability P_L there will occur systems lying above the percolation threshold (percolation ones)—I and with probability $1 - P_L$—below the percolation threshold (non-percolation ones)—II. The probability P_L is of the form

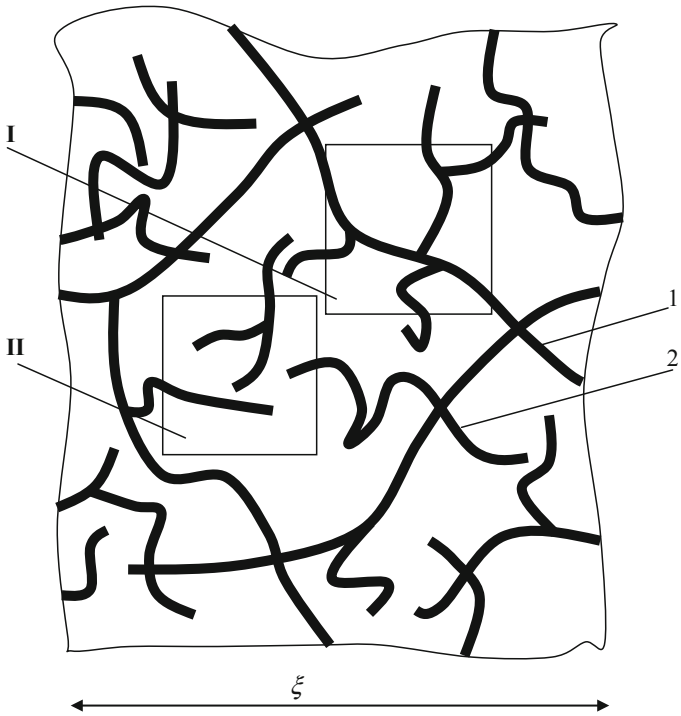

Fig. 9.2 Schematic of percolation system above the percolation threshold: *Solid lines* a combination of conducting bonds. *1* part of infinite cluster, *2* finite clusters. *I* region of size $L < \xi$ lying above the percolation threshold, *II* region of size $L < \xi$ lying below the percolation threshold

$$P_L = \int_{-\infty}^{0} f(\tau_c) d\tau_c. \tag{9.1.8}$$

To obtain simple analytical expressions for P_L, function $f(\tau_c)$ can be conveniently approximated by a uniform function. Then ignoring constant W and introducing the notation

$$\tau_L = L^{-1/\nu}, \tag{9.1.9}$$

for P_L and $1 - P_L$ we get

$$P_L = \frac{\tau_L + \tau}{2\tau_L}, \quad 1 - P_L = \frac{\tau_L - \tau}{2\tau_L}. \tag{9.1.10}$$

The situation when both percolation and non-percolation parts are found in the system has been already encountered in smearing region. Indeed, if at $L < \xi$ the system is in the smearing region ($|\tau| \le \Delta$), then with probabilities $P_\Delta = (\Delta + \tau)/2\Delta$ and $1 - P_\Delta = (\Delta - \tau)/2\Delta$ one can (within the order of ζ^d) come across both percolation and non-percolation situations (see Chap. 5). Using this analogy (the role of Δ—smearing region—is now played by τ_L) between $\{\sigma_e\}$ at $L < \xi$ ($\xi = \tau^{-\nu}$, i.e., $|\tau| \le \tau_L$) and σ_e at $L < \xi$ and $|\tau| \le \Delta$; $\sigma_e(|\tau| \le \Delta) \approx \sigma_1 \frac{\Delta+\tau}{2\Delta} + \sigma_2 \frac{\Delta-\tau}{2\Delta} \Delta^{-q}$ $\approx \frac{1}{2}(\sigma_1 \Delta^t + \sigma_2 \Delta^{-q}) = \left(\sigma_1^q \sigma_2^t\right)^{\frac{1}{t+q}}$, we write down

$$\{\sigma_e\} = \sigma_1 \frac{\tau_L + \tau}{2\tau_L} \tau_L^t + \sigma_2 \frac{\tau_L - \tau}{2\tau_L} \tau_L^{-q}, \tag{9.1.11}$$

or, distinguishing the main multipliers with L, we get

$$\{\sigma_e\} = \sigma_1 \frac{\tau_L + \tau}{2\tau_L} L^{-t/\nu} + \sigma_2 \frac{\tau_L - \tau}{2\tau_L} L^{q/\nu}. \tag{9.1.12}$$

In perfect analogy one can write down the expression for the average over realizations resistivity

$$\{\rho_e\} = \rho_1 \frac{\tau_L + \tau}{2\tau_L} L^{t/\nu} + \rho_2 \frac{\tau_L - \tau}{2\tau_L} L^{-q/\nu}. \tag{9.1.13}$$

Note at once that expressions (9.1.6) and (9.1.7) follow from (9.1.12) and (9.1.13) as particular cases (for $\sigma_2/\sigma_1 = 0$). For instance, at $\tau > 0$ and $\sigma_2 = 0$ from (9.1.12) and (9.1.13) we find

$$\{\sigma_e\} = \sigma_1 \frac{\tau_L + \tau}{2\tau_L} L^{-t/\nu}, \quad \{\rho_e\} = \infty, \tag{9.1.14}$$

with due regard here that in the fractal region $0<\tau<\tau_L$ and $P_L \sim 1$. Similarly, for the case $\tau<0$ and $\rho_1 = 0$ ($\sigma_1 = \infty$) we have

$$\{\rho_e\} = \rho_2 \frac{\tau_L - \tau}{2\tau_L} L^{-q/\nu}, \quad \{\sigma_e\} = \infty. \tag{9.1.15}$$

For the analysis of general case (9.1.12) and (9.1.13) it is convenient to use the space of parameters with the axes $1/\tau_L$ and $1/\Delta$ (Fig. 9.3). The first quadrant is matched with $\tau > 0$, the second—with $\tau<0$. Since percolation behavior implies larger inhomogeneity ($\sigma_1 \gg \sigma_2$), then the area close to axis $1/\tau_L$ (shaded in Fig. 9.3) is excluded from consideration of $\{\sigma_e\}$ with finite-size scaling, since in this area the condition $\sigma_2/\sigma_1 \ll 1$ is not met. The area immediately surrounding the axis $1/\Delta$ is not considered either, since the size of system L must be larger than minimum size a_0.

Fractal behavior ($\sim L$) is matched with the areas I and II, where the average over realizations $\{\sigma_e\}$ and $\{\rho_e\}$ have power dependence on the system size L. In the area I_a (except for the part immediately adjacent with the axis $1/\Delta$) $\{\sigma_e\} \sim L^{-t/\nu}$, $\{\rho_e\} \sim L^{-q/\nu}$ At the boundaries between the areas I and III and I and IV $\{\sigma_e\}$ and $\{\rho_e\}$ pass over to expressions for smearing region $\sigma_e = \left(\sigma_1^q \sigma_2^t\right)^{\frac{1}{t+q}}$. In the area V the effective conductivity is conductivity at $\tau > 0$ and $L \gg \xi$ ($\sigma_e = \sigma_1 \tau^t$) in the area VI

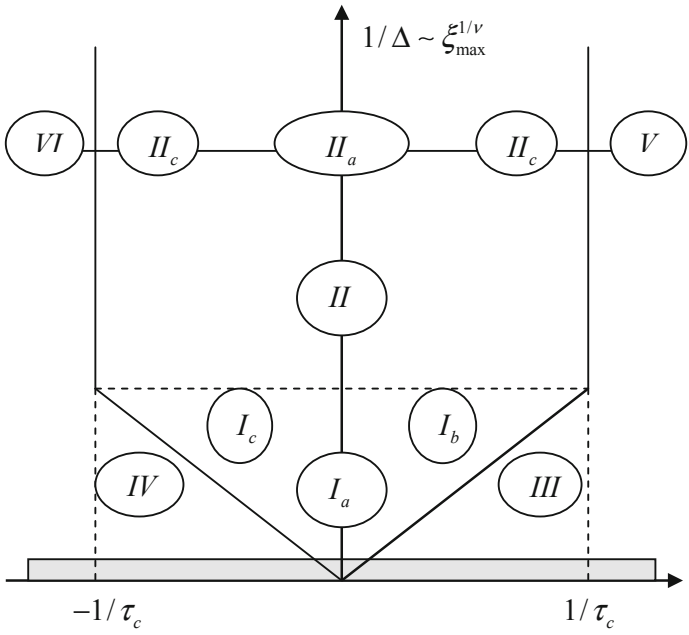

Fig. 9.3 Schematic of space partition $(1/\tau_L, 1/\Delta)$

at—$\tau < 0$ and ($\sigma_e = \sigma_2|\tau|^{-q}$). Inside the fractal region (finite-size scaling), (I and II —the shaded area in Fig. 9.3) $\{\sigma_e\}$ and $\{\rho_e\}$ behave as follows.

The area I_a $1/\tau_L \ll 1/|\tau|$, i.e.$\tau_L \gg |\tau|$, moreover, the area II is much lower than the dashed line in Fig. 9.3, it means $\tau_L \gg \Delta$. Account of these two inequalities for (9.1.12) and (9.1.13) results in the following:

$$\{\sigma_e\} \approx \sigma_1 \tau_L^t = \sigma_1 L^{-t/\nu},\ I_a, \tag{9.1.16}$$

$$\{\rho_e\} \approx \rho_2 \tau_L^q = \rho_2 L^{-q/\nu},\ I_a. \tag{9.1.17}$$

Thus, in the area I_a

$$\{\sigma_e\} \neq \frac{1}{\{\rho_e\}}. \tag{9.1.18}$$

With increasing system dimension L (or, which is the same, $1/\tau_L$) $I_a \to I_b$ and $I_a \to I_c$, the expressions (9.1.16) remain in force, but close to transition lines $1/\tau_L \approx 1/\Delta$, hence, $\sigma_1 \Delta^t \approx \sigma_2 \Delta^{-q}$, so now already

$$\{\sigma_e\} \approx \frac{1}{\{\rho_e\}},\ I_b, I_c. \tag{9.1.19}$$

Similar partitioning in the space temperature-size for metal-insulator mixtures is presented in [3, 4].

9.2 Finite-Size Scaling for Self-dual Media

For the two-dimensional samples with $L < \xi$ the reciprocity relation (Chap. 6) can be generalized [11]. As was shown in [1], if $L \gg \xi$, then in the two-dimensional case we have

$$\sigma_e(\tau) \cdot \sigma_e(-\tau) = \sigma_1 \sigma_2. \tag{9.2.1}$$

A similar relation is also possible for $L < \xi$. Consider a rectangular shaped two-dimensional sample with the sides $L_\parallel$ and $L_\perp$, where $L_\parallel$ is sample size along ox, and $L_\perp$—along oy. We apply current contacts to this sample: one time along the parallel sides, so that the average current is $\langle \mathbf{j} \rangle \parallel ox$, another time along oy. In so doing, Ohm's law can be written as

$$I_{\parallel,\perp} = G_{\parallel,\perp} \cdot U_{\parallel,\perp}, \tag{9.2.2}$$

where $G_{\parallel,\perp}$ is sample conductance along ox and perpendicular to ox. The Dykhne symmetry transformations (Chap. 6), expressed through full current, in terms of full current $I_{\parallel,\perp}$ and voltage drop $U_{\parallel,\perp}$ are as follows

$$I_{\parallel,\perp} = -\Lambda \tilde{U}_{\parallel,\perp}, U_{\parallel,\perp} = -\Lambda^{-1} \tilde{I}_{\parallel,\perp}, \tag{9.2.3}$$

where $\Lambda = \sqrt{\sigma_1 \sigma_2}$.

Note that determination of conductance G or resistance $R = 1/G$ of finite sample implies assignment of specific boundary conditions. For instance, ideal current contacts on some surfaces and ideal isolation on the other. The Dykhne transformations change boundary conditions so that ideal current contacts pass into ideally isolated surfaces, and vice versa. Indeed (see Chap. 6), an ideal current contact, in particular, implies that current density has only normal to it component (see Fig. 9.4a), and symmetry transformations rotate this vector by $\pi/2$, "turning" it by means of multiplication by constant Λ to the electric field intensity (Fig. 9.4b), which is now tangent to the edge with an ideal isolation.

Substituting (9.2.3) to (9.2.2), we find

$$\tilde{I}_{\parallel,\perp} = \tilde{G}_{\parallel,\perp} \tilde{U}_{\parallel,\perp}, \tag{9.2.4}$$

where

$$\tilde{G}_{\parallel,\perp} = \frac{\Lambda^2}{G_{\parallel,\perp}}. \tag{9.2.5}$$

One can select such special arrangement of phases or resistances in the network, that, for instance, with a half concentration of their phases the valid expression will be $\tilde{G}_{\parallel,\perp} = G_{\parallel,\perp} = G$, see, for instance, [6, 14, 13], later on we will come back to such examples.

In the case when squares $L \times L$ are cut of randomly inhomogeneous medium and its dual medium ($\sigma_1 \rightleftarrows \sigma_2$), averaging should be made over possible realizations. From the expression (9.2.5) we have

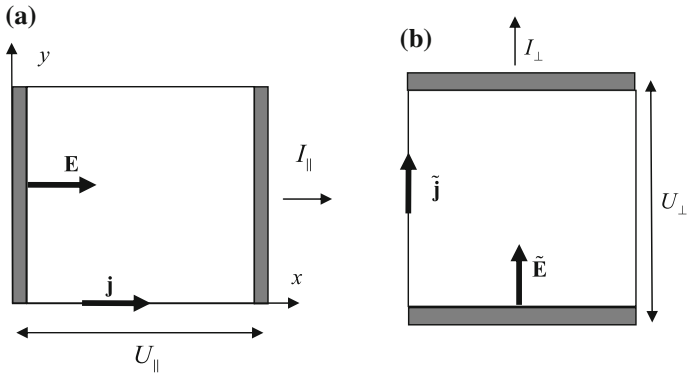

Fig. 9.4 Basic and dual media and their boundary conditions: **a** current contacts are arranged in the basic medium vertically; **b** in the dual medium—horizontally

$$\frac{\{\tilde{G}_{\parallel,\perp}\}}{\{1/G_{\parallel,\perp}\}} = \Lambda^2 = \sigma_1\sigma_2. \tag{9.2.6}$$

Taking into account that $L_\parallel = L_\perp$ and passing on to specific characteristics, we get

$$\frac{\{\sigma_e(p,L)\}}{\{\tilde{\rho}_e(p,L)\}} = \sigma_1\sigma_2, \tilde{\rho}_e = \frac{1}{\sigma_e}. \tag{9.2.7}$$

The following is valid for randomly inhomogeneous media

$$\{\tilde{\rho}_e(p,L)\} = \{\rho_e(1-p,L)\}, \tag{9.2.8}$$

and then from (9.2.7) follows the reciprocity relation

$$\frac{\{\sigma_e(p,\ L)\}}{\{\rho_e(1-p,\ L)\}} = \sigma_1\sigma_2, L<\xi. \tag{9.2.9}$$

With $L \gg \xi$ the need for averaging over realizations disappears and then (9.2.9) passes into a well-known reciprocity relation [1], and at $p = 1/2$—to the Dykhne formula for the effective conductivity $\sigma_e = \sqrt{\sigma_1\sigma_2}$.

Since the operations of division and averaging over realizations are not commutated, then at $L<\xi$ the expression similar to the Dykhne formula no longer follows from (9.2.9). Its analog can be obtained by finding the logarithm of (9.2.5)

$$\ln\tilde{G}_{\parallel,\perp} + \ln G_{\parallel,\perp} = 2\ln\sqrt{\sigma_1\sigma_2}, \tag{9.2.10}$$

and then averaging over realizations with regard to the fact that $\{\ln\tilde{G}_{\parallel,\perp}\} = \{\ln G_{\parallel,\perp}\} = \{\ln\sigma_e(p=1/2,\ L)\}$.

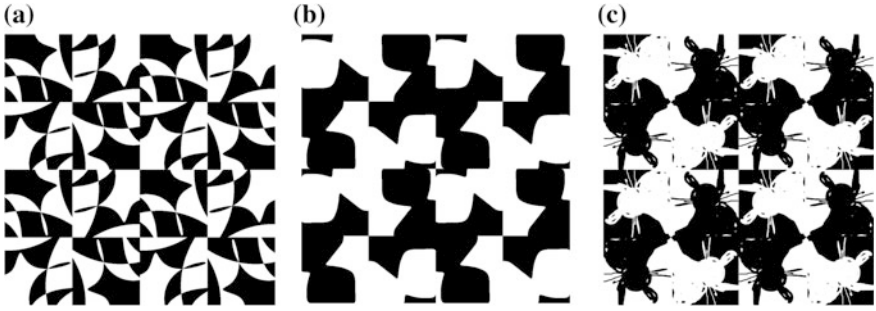

Fig. 9.5 Example of deterministic two-dimensional two-phase self-dual media. *Black color* is for phase σ_1, *white* is for σ_2

Then from (9.2.10) it follows

$$\{\ln \sigma_e(p = 1/2, L)\} = \ln \sqrt{\sigma_1 \sigma_2}, \tag{9.2.11}$$

which for the case $L < \xi$ is the analog of the Dykhne formula. In [11] the relation (9.2.11) is verified by numerical simulation on the networks.

There can be also such phase arrangements that at $L < \xi$ a medium is self-dual and no averaging over realizations is required for conductance determination [11]. Numerous examples of such phase arrangement are given in [10], some of them are represented in Fig. 9.5. The effective conductivity σ_e of any such media is $\sqrt{\sigma_1 \sigma_2}$ and will not change with substitution $\sigma_1 \rightleftarrows \sigma_2$ or transfer of contacts from one pair of parallel sides to the other.

References

1. Dykhne AM (1970) Contluctivity of a two-dimensional two-phase system. Sov Phys JETP 32:63–64
2. Feder J (1988) Fractals. Plenum Press, New York, 283 p
3. Gantmakher VF (2005) Electrons and disorder in solids. International Series of Monographs on Physics (Book 130) Oxford University Press, 240 p
4. Gantmakher VF, Dolgopolov VT (2008) Localized-delocalized electron quantum phase transitions. Phys Usp 51:3–22
5. Gingold DB, Lobb CJ (1990) Precolative conduction in three dimensions. Phys Rev B 42:8220–8224
6. Helsing J, Grimvall G (1990) Conductance in random inductance-capacitance networks. Phys Rev B 16:11364–11367
7. Levinshtein ME, Shklovskii BI, Shur MS (1975) The relation between the critical exponents of percolation theory. Sov Phys JETP 42:197–200
8. Normand JM, Herrmann HJ, Hajjar M (1988) Precise calculation of the dynamical exponent of two-dimensional. J Stat Phys 52:441–446
9. Shklovskii BI, Efros AL (1984) Electronic properties of doped semiconductors. Springer, Berlin, 388 p
10. Snarskii AA (2004) Effective conductivity of 2D Macroscopic heterogeneous self-dual media (review). Laser Phys 14:337–343
11. Snarskii AA, Slipchenko KV, Bezsudnov IV (1998) Reciprocity relations for the effective electrical conductivity of randomly inhomogeneous media in the fractal regime. Sov Phys JETP 86:811–814
12. Stauffer D, Aharony A (1992) Introduction to percolation theory, 2nd edn. Taylor & Francis, p 181
13. Straley JP (1977) Critical exponents for the conductivity of random resistor lattices. Phys Rev B 15:5733–5737
14. Söderberg M, Grimvall G (1986) Conductivity of inhomogeneous materials represented by discrete resistor networks. J Appl Phys 59:186–190

Chapter 10
Conductivity of Percolation Layer

10.1 Effective Conductivity of the Percolation Systems in the Cases with Some Sizes Are Lesser and the Other Greater Than Percolation Length. Definition of the Problem

In the case when size L of a sample cut of randomly inhomogeneous medium is much larger than the correlation length ξ, the effective characteristics of the medium, such as the effective conductivity, are well-defined entities. In the case when $L \leq \xi$, sample conductance changes from one realization to another realization and the well-defined value is conductance $\{G\}$ averaged over realizations, or effective conductivity $\{\sigma_e\}$ averaged over realizations (see Chap. 9).

In practice (see, for instance, [1, 3]) the situation is not infrequent, when one of sample sizes exceeds the correlation length, and the others—not. Figure 10.1 shows an example when along two directions the sample length is $H \gg \xi$, and along the third direction—$L < \xi$.

Such a layer, on the one hand, does not behave as a three-dimensional sample, i.e., for instance, for σ_e no standard percolation dependence of the type $\sigma_e = \sigma_1 \tau^t$ will be met, and on the other hand, despite its seeming two-dimensionality ($H \gg L$), the necessary condition of two-dimensionality—no absence of z-components of fields and currents—is not met. However, by virtue of the fact that $H \gg \xi$, the effective properties are well defined. The layer conductance both along ox and oy, and oz directions requires no averaging over realizations.

At $L \to a_0$ the medium becomes two-dimensional, at $L \gg \xi$—three-dimensional. Thus, a layer in the case when $H \gg \xi$ and $L \leq \xi$, occupies intermediate position between the two- and three-dimensional cases. Hereafter, for brevity, we will call this case $2.5D$-media. One can also speak about $1.5D$-media, however, they represent much less interesting possibility.

A.A. Snarskii et al., *Transport Processes in Macroscopically Disordered Media*, DOI 10.1007/978-1-4419-8291-9_10

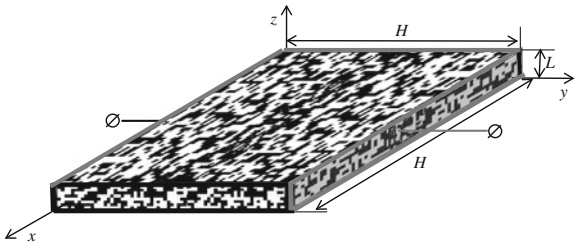

Fig. 10.1 Percolation layer. Layer sizes along *ox* and *oy* axes—$H \gg \xi$, and along *oz*—$L < \xi$

Depending on the concentration of phases, the sizes and the ratio of phase conductivities, 2.5*D*-media show a large variety of regularities [1, 4]. Here we will consider the effective conductivity of 2.5*D*-media—σ_e along *xoy* (position of contacts see in Fig. 10.1). Later on we will consider that we deal with a "deeply" fractal mode:

$$a_0 \ll L \ll \xi_{3\max}. \tag{10.1.1}$$

To avoid confusion, we will write down the index denoting problem dimensionality; here $\xi_{3\max}$ is maximum value of correlation length in the three-dimensional case:

$$\xi_{3\max} = \Delta_3^{-\nu_3} = (\sigma_2/\sigma_1)^{-\frac{\nu_3}{t_3+q_3}}. \tag{10.1.2}$$

Here and afterwards, like in Chap. 9, for simplicity of notation, where convenient, we will assume $a_0 = 1$.

Condition (10.1.1) with regard to (10.1.2) simultaneously means

$$\sigma_1 \tau_L^{t_3} \gg \sigma_2 \tau_L^{-q_3}, \tag{10.1.3}$$

where $\tau_L = L^{-1/\nu_3}$, while $\sigma_1 \tau_L^{t_3}$ and $\sigma_2 \tau_L^{-q_3}$ are the average over realizations effective conductivities of a sample of $L \times L \times L$ sizes in the case of percolation and non-percolation realization, respectively.

Introduce the following designations:

$$\tilde{\sigma}_1 = \sigma_1 \tau_L^{t_3}, \quad \tilde{\sigma}_2 = \sigma_2 \tau_L^{-q_3}. \tag{10.1.4}$$

As was shown in Chap. 9, the probabilities to come across the percolation (P_L) and non-percolation—$(1 - P_L)$ realizations can be written down as follows:

$$P_L = \frac{\tau_L + \tau_3}{2\tau_L}, \quad 1 - P_L = \frac{\tau_L - \tau_3}{2\tau_L}, \quad \tau_L = L^{-1/\nu_3}. \tag{10.1.5}$$

10.2 Solution Technique

The main idea [2] that allows to find approximately the expressions for conductance and effective conductivity $\sigma_e^{2.5D}$ of a layer being in a "deeply" fractal mode. This idea consists of roughening inhomogeneous structure with characteristic size a_0 to size L. The layer after this roughening is a two-dimensional film with a typical inhomogeneity size L.

This two-dimensional inhomogeneous medium (its characteristics will be denoted by tilde sign) is characterized by proximity to percolation threshold

$$\tilde{\tau}_2 = \frac{P_L - P_{c_2}}{2P_{c_2}}, \tag{10.2.1}$$

which with regard to (10.1.5) and the fact that $P_{c_2} = 1/2$ can be written as follows:

$$\tilde{\tau}_2 = \tau_3/\tau_2. \tag{10.2.2}$$

In going from a three-dimensional $H \times H \times L$ layer with $L < \xi$ to a three-dimensional medium the following approximation was implicitly made. A good conducting element $\tilde{\sigma}_1$ (Fig. 10.2) of a medium roughened to size L, was selected as the average over realizations (10.1.4) of $L \times L \times L$ cube. Now the characteristic size of inhomogeneity $\tilde{a}_0 = L$. Percolation element with $\tilde{\sigma}_1$ and non-percolation element with $\tilde{\sigma}_2$ differ considerably from each other in conductivity $\tilde{\sigma}_1 \gg \tilde{\sigma}_2$. However, the conductance of $L \times L \times L$ cube for given concrete realization with percolation structure and the average over realizations conductance $\{G\} = \tilde{\sigma}_1$ differ from each other in that the former can have percolation structure along one direction and not have it along the other. Thus, it should be taken into account that in a more precise approximation the "roughened" layer in Fig. 10.2 consists of randomly scattered strongly anisotropic elements, rather than of two isotropic phases. We consider below the simplest approximation: the layer in Fig. 10.2 will be thought as one to consist of two isotropic phases.

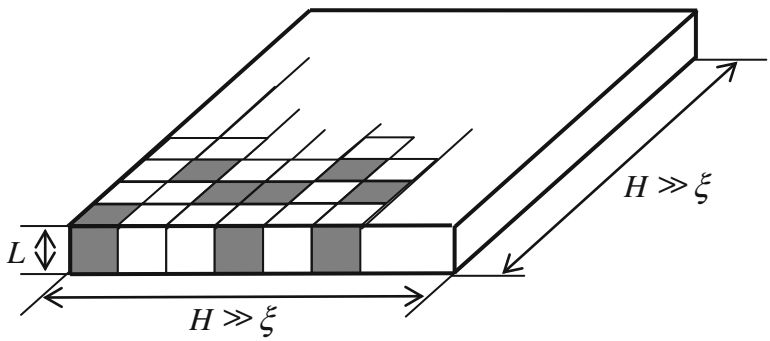

Fig. 10.2 View of inhomogeneous layer after "roughening" (renormalization): *Black color* is for percolation realizations with conductivity $\tilde{\sigma}_1$, *white color*—for non-percolation realizations with conductivity $\tilde{\sigma}_2$

We require the following condition to be satisfied

$$|\tilde{\tau}_2| \ll 1, \tag{10.2.3}$$

only in this case the percolation description of the "two-dimensional" medium in Fig. 10.2 is possible.

From (10.2.3) it follows that $|\tau_3| \ll L^{-1/\nu_3}$, and since the minimum value $\tau_3 - \Delta_3$ (see Sect. 5.1), then the inequality (10.2.3) leads to $L \ll \xi_{3\max}$ or to (10.1.2), and, hence, under the assumed conditions of a "deeply" fractal mode the inequality (10.2.3) is met automatically.

Therefore, in the description of layer conductivity one can use the two-dimensional percolation relationships

$$\sigma_e^{2.5D} \approx \tilde{\sigma}_1 \tilde{\tau}_2^{t_2}, \quad |\tilde{\tau}_2| > 0, \quad \tilde{\Delta}_2 \ll \tilde{\tau}_2 \ll 1, \quad \text{I}, \tag{10.2.4}$$

$$\sigma_e^{2.5D} \approx \tilde{\sigma}_1 |\tilde{\tau}_2|^{-q_2}, \quad |\tilde{\tau}_2| < 0, \quad \tilde{\Delta}_2 \ll |\tilde{\tau}_2| \ll 1, \quad \text{II}, \tag{10.2.5}$$

$$\sigma_e^{2.5D} \approx \sqrt{\tilde{\sigma}_1 \tilde{\sigma}_2}, \quad |\tilde{\tau}_2| \le \tilde{\Delta}_2, \quad \text{III}, \tag{10.2.6}$$

where smearing region $\tilde{\Delta}_2$, like in the ordinary two-dimensional case (see Chap. 5), is found from condition $\sigma_1 \Delta_2^{t_2} = \sigma_2 \Delta_2^{-q_2}$ and is of the following form:

$$\tilde{\Delta}_2 = (\tilde{\sigma}_2 / \tilde{\sigma}_1)^{\frac{1}{t_2 + q_2}}. \tag{10.2.7}$$

Substituting $\tilde{\tau}_2$ and $\tilde{\sigma}_1$, $\tilde{\sigma}_2$ to (10.2.4)–(10.2.7), we find the dependence of the effective conductivity of percolation layer

$$\sigma_e^{2.5D} = \sigma_1 \tau_3^{t_2} \tau_L^{t_3 - t_2} = \sigma_1 \tau_3^{t_2} L^{-\frac{t_3 - t_2}{\nu_3}}, \quad \text{I}, \tag{10.2.8}$$

$$\sigma_e^{2.5D} = \sigma_2 |\tau_3|^{-q_2} \tau_L^{q_2 - q_3} = \sigma_2 |\tau_3|^{-q_2} L^{-\frac{q_2 - q_3}{\nu_3}}, \quad \text{II}, \tag{10.2.9}$$

$$\sigma_e^{2.5D} = \sqrt{\sigma_1 \sigma_2} \tau_L^{\frac{t_3 - q_3}{2}} = \sqrt{\sigma_1 \sigma_2} L^{\frac{t_3 - q_3}{2\nu_3}}, \quad \text{III}, \tag{10.2.10}$$

where the areas I, II, III, in (10.2.8)–(10.2.10) are the same as in (10.2.4)–(10.2.6). Obtained in (10.2.8)–(10.2.10) three types of $\sigma_e^{2.5D}$ behavior, namely above, below and the percolation threshold itself, are met in quite certain concentration ranges of good conducting phase $p(\tau_3)$. For instance, in III (10.2.6) or (10.2.10) $|\tilde{\tau}_2| \le \Delta_2$, whence according to (10.2.2) we have

$$|\tau_3| \le \Delta_2 \tau_L^{\frac{t_2 + q_2 - (t_3 + q_3)}{t_2 + q_2}} = \Delta_2 L^{\frac{t_3 + q_3 - 2t_2}{2t_2 \nu_3}} \equiv \tau_{3\min}, \tag{10.2.11}$$

where $\Delta_2 = (\sigma_2/\sigma_1)^{1/2t_2}$ is smearing region in the ordinary two-dimensional case, and in (10.2.11) it is considered that $q_2 = t_2$, and for convenience the designation of characteristic value $\tau_{3\min}$ is introduced

$$\tau_{3\,\min} = \Delta_2 L^{\frac{t_3+q_3-2t_2}{2t_2\nu_3}}, \quad \frac{t_3+q_3-2t_2}{2t_2\nu_3} = 0.057. \tag{10.2.12}$$

Let's note a weak dependence of $\tau_{3\min}$ on L.

In all the three modes—I, II, and III, the effective conductivity of the layer $\sigma_e^{2.5D}$ is decreased with increase of L [see (10.2.8)–(10.2.10)]. However, from general considerations it follows that the layer resistance $R = \sigma_e^{2.5D} H/HL$ should decrease at $H = \text{const}$ and with increase of L. And, certainly, dependences (10.2.8)–(10.2.10) must satisfy this requirement. Indeed, (10.2.8)–(10.2.10) imply

$$R \sim L^{\alpha},\ \alpha_{\mathrm{I}} = \frac{t_3 - t_2}{\nu_3} - 1,\ \alpha_{\mathrm{II}} = \frac{q_2 - q_3}{\nu_3} - 1,\ \alpha_{\mathrm{III}} = \frac{t_3 - q_3}{2\nu_3} - 1, \tag{10.2.13}$$

where index y α denotes belonging to mode I, II, III in (10.2.8)–(10.2.10).

Substituting into (10.2.13) the canonical values of critical indices, from Table 5.1 we find

$$\alpha_{\mathrm{I}} = -0.2,\ \alpha_{\mathrm{II}} = -0.35,\ \alpha_{\mathrm{III}} = -0.28, \tag{10.2.14}$$

With increasing layer thickness, its resistance drops.

In dependences of R on the layer thickness, critical indices of two- and three-dimensional problem of percolation theory have "united" in a manner unusual for percolation, which resulted, in particular, in the unexpected inequalities. Requirement of condition $\alpha < 0$ according to (10.2.13) necessitates fulfillment of two inequalities:

$$t_3 - t_2 < \nu_3,\ q_2 - q_3 < \nu_3. \tag{10.2.15}$$

It is easy to derive the expressions for the effective conductivity, similar to (10.2.8)–(10.2.10), for the two-dimensional stripe $\sigma_e^{1.5D}$. Moreover, for the case of stripe one can indicate a class of media for which the reciprocity relations are met [5].

So far we have dealt primarily with a "deeply" fractal mode, when the condition (10.1.1) or (10.1.3) was supposed to be valid. It means, among other things, that $(L/a_0)^{-1/\nu} \ll 1$, i.e. $L \gg a_0$. If such a strong inequality is not fullfilled, i.e., the system leaves the "deeply" fractal mode, one must take into account [1, 4], that percolation threshold of percolation layer $p_{c\|}$ is different from that of three-dimensional sample:

$$p_{c\|} = p_{c_3} + (p_{c_2} - p_{c_3}) L^{-1/\nu_3}. \tag{10.2.16}$$

In a "deeply" fractal mode the second term in (10.2.16) is minor, it can be ignored.

Account of percolation threshold shift (10.2.16) allows at $L \to a_0$ passing to a two-dimensional case in the expressions for $\sigma_e^{2.5D}$:

$$p_{c\|}(L \to a_0) \to p_{c_2}. \tag{10.2.17}$$

In [4] a large number of particular cases are considered, as well as the dielectric ($\omega \neq 0$) properties of percolation layer.

References

1. Clerc JP, Giraud G, Alexander S, Guyon E (1980) Conductivity of a mixture of conducting and insulating grains: dimensionality effects. Phys Rev B 22:2489–2494
2. Dziedzic A, Snarskii AA, Buda SI (2000) Nonlinear properties of two-phase composite films with a fractal structure. Tech Phys 45:334–338
3. Kapitulnik A, Deutscher G (1983) 2D to 3D percolation crossover in the resistivity of co-evaporated Al-Ge mixture films. J Phys A 16:L255–L257
4. Neimark AV (1990) Electrophysical properties of a percolation layer of finite thickness. Sov Phys JETP 71:341–349
5. Snarskii AA, Buda SI (1998) Reciprocity relations for the nonlinear conductivity of fractal resistors. Tech Phys 41:1381–1384

Part II
Processes

Chapter 11
AC Conductivity

11.1 EMT-Approximation

So far we have considered direct current problems, abbreviated as DC-problems (DC—direct current). For an alternating current (AC-problem, AC—alternating current) and in the case of low frequencies as compared to frequencies necessary for establishing the electrical and magnetic polarizations [3], then the conductivity can be described using complex resistance $Z(\omega)$—the so-called conductor impedance. The value inverse to $Z(\omega)$, is called a conductance $G(\omega) = 1/Z(\omega)$. In this chapter, we will provide brief discussion (see monograph [1, 4]) of the effective properties of the so-called "bad" conductors [3]. For this case both conductivity and dielectric constant (or inductance) can be simultaneously introduced for the media.

Specific conductance $\sigma(\omega)$ in this case can be written as

$$\sigma(\omega) = \sigma' + \mathrm{i}\sigma'' = \sigma + \frac{\omega\varepsilon}{\mathrm{i}4\pi}, \tag{11.1.1}$$

where σ is "ordinary" conductivity (i.e., conductivity at direct current), and ε is dielectric constant.

Consider a two-phase composite, where one of the phases is metal and the other is a "bad" conductor, i.e., a dielectric having low conductivity at direct current as follows:

$$\sigma_1(\omega) = \sigma_1, \quad \sigma_2(\omega) = \frac{\omega\varepsilon_2}{\mathrm{i}4\pi} + \sigma_2. \tag{11.1.2}$$

Here we ignore the imaginary part of the metal phase conductivity and assume that the medium is strongly inhomogeneous: $\sigma_1 \gg \sigma_2$, and in the case of an ideal dielectric $\sigma_2 = 0$.

A.A. Snarskii et al., *Transport Processes in Macroscopically Disordered Media*, DOI 10.1007/978-1-4419-8291-9_11

Accordingly, for the effective coefficients we have

$$\sigma_e(\omega) = \sigma'_e + \sigma''_e = \sigma_e + \frac{\omega\varepsilon_e}{i4\pi}. \tag{11.1.3}$$

The concentration dependences $\sigma_e(p)$ and $\varepsilon_e(p)$ can be found in the EMT approximation (see Sect. 3.2). For the three-dimensional case

$$\frac{\sigma_e(\omega) - \sigma_1(\omega)}{2\sigma_e(\omega) + \sigma_1(\omega)} p + \frac{\sigma_e(\omega) - \sigma_2(\omega)}{2\sigma_e(\omega) + \sigma_2(\omega)} (1 - p) = 0. \tag{11.1.4}$$

Figure 11.1 is a plot of the concentration dependence of the real and imaginary parts of the effective conductivity $\sigma_e(\omega) = \sigma_e + \omega\varepsilon_e/i4\pi$ versus the metal phase concentration p.

The real part of the effective conductivity $\mathrm{Re}\,\sigma_e(\omega) = \sigma'_e$ (hereafter the prime will be omitted) behaves in an ordinary (see Chap. 5) monotonous manner, drastically changing its behavior close to $p_c = 1/3$, as it should be with a large

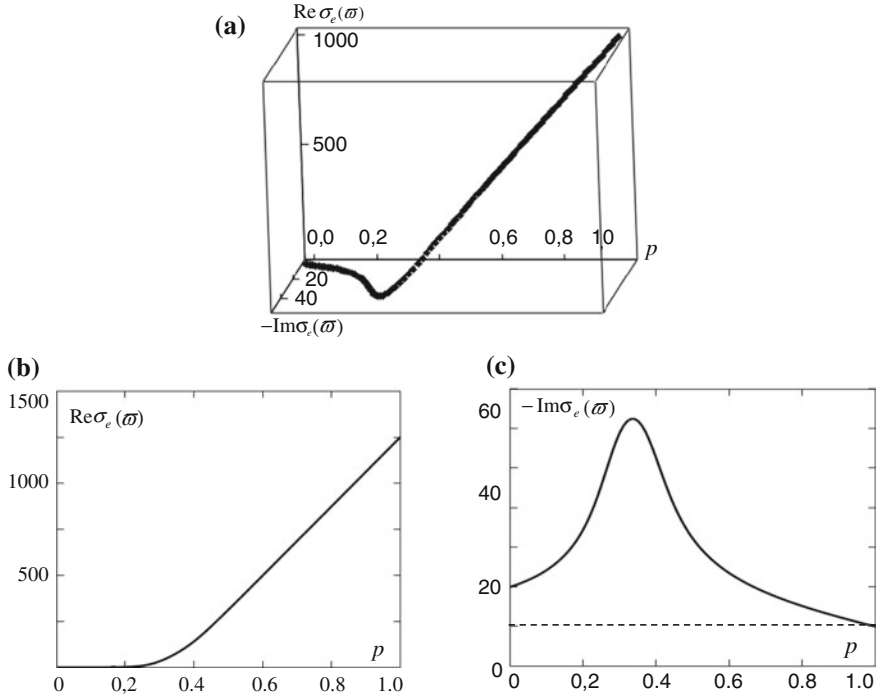

Fig. 11.1 Concentration dependence of the real and imaginary parts of the effective conductivity: **a** the plot of $\sigma_e(\omega)$. **b** dependence of $\mathrm{Re}\,\sigma_e(\omega)$ on the metal phase concentration, projection to real plane. **c** dependence of $\mathrm{Im}\,\sigma_e(\omega)$—dielectric constant on the metal phase concentration, projection to imaginary plane for $\sigma_1 = 1000$, $\sigma_2 = 0$, $\varepsilon_1 = 0$, $\omega\varepsilon_2/4\pi = 10$ (in arbitrary units)

inhomogeneity ($\sigma_1 \gg \sigma_2$ or $\sigma_2 = 0$). The imaginary part describing the behavior of the effective dielectric constant, as is seen from Fig. 11.1c, has a maximum close to p_c, the value of this maximum (with selected parameter values in Fig. 11.1c $\varepsilon_e\omega/4\pi \approx 50$) being much in excess of the phase itself ($\varepsilon_2\omega/4\pi = 10$). Thus, if σ_e is monotonously increasing with growth in p, then ε_e has a maximum close to p_c, i.e., on approaching p_c it increases "on both sides." From expression (11.1.4) it also appears that maximum of the effective dielectric constant $\varepsilon_e(p_e)$ is proportional to the metal phase conductivity σ_1.

11.2 The Method of Percolation Theory

In the case of large inhomogeneity, as already mentioned before (Sect. 3.2), close to percolation threshold the EMT predictions become only qualitative, and for a quantitative determination of the behavior of σ_e, critical indices describing the behavior of $\mathrm{Re}\,\sigma_e(\omega)$ and $\mathrm{Im}\,\sigma_e(\omega)$ one should apply to percolation theory.

Percolation analysis of AC-problem was made in [2], where several possible particular cases are considered. One of them: $\mathrm{Im}\,\sigma_1(\omega) = 0,\ \mathrm{Re}\,\sigma_2(\omega) = 0$,—when good conducting phase—metal—has no imaginary part, and bad conducting phase is a perfect dielectric, in this case the direct current conductivity is zero:

$$\sigma_1(\omega) = \sigma_1,\ \sigma_2(\omega) = \omega\varepsilon_2/\mathrm{i}4\pi. \tag{11.2.1}$$

At $\omega = 0$ below the percolation threshold in such a medium current cannot flow $\sigma^e(\omega = 0, \tau < 0) = 0$. However, at $\omega \neq 0$ this is no longer the case. According to [2], infinitesimality parameter h which in the "ordinary" ($\omega = 0$) case is $h = \sigma_2/\sigma_1$, at $\omega \neq 0$ should be replaced by

$$h = \omega\varepsilon_2/4\pi\sigma_1. \tag{11.2.2}$$

Now, using h from (11.2.2) and the analogy to the effective conductivity, at $\omega = 0$ below the percolation threshold we get

$$\begin{aligned} &\mathrm{Re}\,\sigma_e(\omega, p) = \frac{\omega^2\varepsilon^2}{4\pi\sigma_1}|\tau|^{-(2q+t)}, \quad \tau < 0, \\ &\varepsilon_e(\omega, p) = \varepsilon_2|\tau|^{-q}, \quad \tau < 0. \end{aligned} \tag{11.2.3}$$

In smearing region we have

$$\mathrm{Re}\,\sigma_c(\omega, p_e) = \sigma_1\left(\frac{\omega\varepsilon_2}{4\pi\sigma_1}\right)^{\frac{t}{t+q}}, \quad \varepsilon_e(\omega, p_c) = \varepsilon_2\left(\frac{4\pi\sigma_1}{\varepsilon_2\omega}\right)^{\frac{q}{t+q}}. \tag{11.2.4}$$

This, among other things, implies that $\varepsilon_e \sim \sigma_1$, as was qualitatively predicted by EMT.

In the case when a dielectric is imperfect, we write down

$$\sigma_2(\omega) = \frac{\omega\varepsilon_2}{\mathrm{i}4\pi} + \sigma_2, \quad \sigma_2 \neq 0. \tag{11.2.5}$$

Instead of expression (11.2.4) we have

$$\varepsilon_{\mathrm{e}}(\omega, p_{\mathrm{c}}) = \varepsilon_2 \left(\frac{\sigma_1}{\sigma_2}\right)^{\frac{q}{t+q}}. \tag{11.2.6}$$

These and some other regularities are described by scaling relationship [2]:

$$\sigma_{\mathrm{e}}(\omega, \tau) = \sigma_1(\omega) h^{\frac{t}{t+q}} \Psi\left(\frac{\tau}{h^{\frac{1}{t+q}}}\right), \tag{11.2.7}$$

formally repeating scaling relationship (5.2.5), however, now $h = \sigma_2(\omega)/\sigma_1(\omega)$ and will be a complex quantity.

A combination of these regularities, and in particular, such a strange at first sight fact that the effective dielectric constant above the percolation threshold is described by index q which had been earlier introduced for the description of σ_{e} below the percolation threshold, can be explained on the basis of a hierarchical model of percolation structure (Sect. 5.4).

Consider first a hierarchical model above the percolation threshold. The first phase will be assumed to be a metal $\operatorname{Im}\sigma_1(\omega) = 0$, and the second—a perfect dielectric $\operatorname{Re}\sigma_2(\omega) = 0$, i.e., $\sigma_2 = 0$ see (11.1.2). According to (5.4.12), for the second hierarchy degree we have

$$G_{\mathrm{e}} = G_1 + G_2, \tag{11.2.8}$$

where according to (5.4.14), (5.4.15)

$$\begin{aligned} &G_1 = \sigma_1 a_0^{d-2} \tau^{\alpha_1}, \; G_2 = \sigma_2 a_0^{d-2} \tau^{-\alpha_2}, \\ &G_{\mathrm{e}} = \sigma_{\mathrm{e}}(\omega) a_0^{d-2} \tau^{\nu(d-2)}, \; \alpha_1 = t - \nu(d-2), \; \alpha_2 = q + \nu(d-2). \end{aligned} \tag{11.2.9}$$

Whence

$$\sigma_{\mathrm{e}}(\omega) = \sigma_1 \tau^t + \sigma_2(\omega)\tau^{-q}, \; \tau > 0. \tag{11.2.10}$$

On dividing $\sigma_{\mathrm{e}}(\omega)$ into real and imaginary parts, we find

$$\begin{aligned} \operatorname{Re}\sigma_{\mathrm{e}}(\omega) &= \sigma_1 \tau^t + \operatorname{Re}\sigma_2(\omega)\tau^{-q}, \\ \operatorname{Im}\sigma_{\mathrm{e}}(\omega) &= \operatorname{Im}\sigma_2(\omega)\tau^{-q}. \end{aligned} \tag{11.2.11}$$

In this case, when $\mathrm{Re}\,\sigma_2(\omega) = 0$, from (11.2.11) it follows

$$\sigma_e = \sigma_1 \tau^t, \ \tau > 0. \tag{11.2.12}$$

And, since $\varepsilon_2 = -(4\pi/\omega)\mathrm{Im}\,\sigma_2(\omega)$, $\varepsilon_e = -(4\pi/\omega)\mathrm{Im}\,\sigma_e(\omega)$, for the effective dielectric constant

$$\varepsilon_e = \varepsilon_2 \tau^{-q}, \ \tau > 0. \tag{11.2.13}$$

The schematic of hierarchical model (11.2.8) immediately implies qualitative explanation of the appearance of critical index q in the case of $\tau > 0$. Indeed, whereas for the real part of conductivity its main element is an ordinary resistance $R_1 = 1/G_1$ of the bridge, for the imaginary part which exists only at $\omega \neq 0$, the main element is interlayer (capacitor) which is a good conductor of the alternating current. Thus, a bridge, hence index t, is responsible for $\mathrm{Re}\,\sigma_e(\omega)t$, and interlayer, hence index q, is responsible for $\mathrm{Im}\,\sigma_e(\omega)$. With the alternating current, an interlayer is an element of percolation structure which at $p > p_c$ and $\omega = 0$ gives just a slight correction to the effective conductivity (5.2.11a), for the imaginary part σ_e is the main element.

For the same case ($\sigma_1(\omega) = \sigma_1$, $\sigma_2(\omega) = \omega\varepsilon_2/\mathrm{i}4\pi$) below the percolation threshold according to the second degree of hierarchical model (5.4.13) we have

$$G_e = \frac{G_1 G_2}{G_1 + G_2}, \tag{11.2.14}$$

where G_1, G_2, and G_e are determined as before according to (11.2.9).

Hence

$$\sigma_e(\omega) = \frac{\sigma_1 \left(\frac{\omega\varepsilon_2}{4\pi}\right)^2 \tau^{t-2q}}{\sigma_1^2 \tau^{2t} + \left(\frac{\omega\varepsilon_2}{4\pi}\right)^2 \tau^{-2q}} + \frac{\sigma_1^2 \left(\frac{\omega\varepsilon_2}{\mathrm{i}4\pi}\right) \tau^{2t-q}}{\sigma_1 \tau^{2t} + \left(\frac{\omega\varepsilon_2}{4\pi}\right)^2 \tau^{-2q}}. \tag{11.2.15}$$

For the case of direct current conductivity ($\omega \to 0$), $\mathrm{Re}\,\sigma_e(\omega) \to 0$. The interlayer serving as a capacitor (11.2.14) "locks" the current. Thus, $\mathrm{Re}\,\sigma_e(\omega)$ should be proportional to ω and, as is seen from (11.2.15), it is possible on meeting the inequality

$$|\tau|^{t+q} \gg \frac{\omega\varepsilon_2}{4\pi\sigma_1}, \tag{11.2.16}$$

and then (11.2.15) takes on the form

$$\sigma_e(\omega) \approx \sigma_1 \left(\frac{\omega\varepsilon_2/4\pi}{\sigma_1}\right)^2 |\tau|^{-(t+2q)} + \frac{\omega\varepsilon_2}{\mathrm{i}4\pi} |\tau|^{-q}, \tag{11.2.17}$$

which, on dividing into real and imaginary parts, yields the expression

$$\operatorname{Re}\sigma_{\mathrm{e}}(\omega)\approx\sigma_1\left(\frac{\omega\varepsilon_2/4\pi}{\sigma_1}\right)^2|\tau|^{-(t+2q)},\ \varepsilon_{\mathrm{e}}=\varepsilon_2|\tau|^{-q}. \tag{11.2.18}$$

Smearing region, like in the DC-problem, is determined from equality $\sigma_{\mathrm{e}}(\Delta,p>p_{\mathrm{e}})=\sigma_{\mathrm{e}}(\Delta,p<p_{\mathrm{e}})$. Indeed, equating (11.2.10) and (11.2.16), we have

$$\sigma_1\Delta^t+\frac{\omega\varepsilon_2}{4\pi\mathrm{i}}\Delta^{-q}=\sigma_1\left(\frac{\omega\varepsilon_2/4\pi}{\sigma_1}\right)^2\Delta^{-(t+2q)}+\frac{\omega\varepsilon_2}{\mathrm{i}4\pi}\Delta^{-q} \tag{11.2.19}$$

from the equality of both real (11.2.19) and imaginary parts, we obtain smearing region [2]:

$$\Delta=\left(\frac{\omega\varepsilon_2}{4\pi\sigma_1}\right)^{\frac{1}{t+q}}. \tag{11.2.20}$$

Note that according to (11.2.20) condition (11.2.16) means $|\tau|\gg\Delta$, i.e., condition of $\sigma_{\mathrm{e}}(\omega)$ from (11.2.17) describing the behavior of the effective conductivity and dielectric constant beyond smearing region [2].

In the case of imperfect dielectric (11.2.5) instead of (11.2.15) from (11.2.14) it follows

$$\sigma_{\mathrm{e}}(\omega)=\frac{\sigma_1\tau^t\cdot\sigma_2(\omega)\tau^{-q}}{\sigma_1\tau^t+\sigma_2(\omega)\tau^{-q}},\quad \sigma_2(\omega)=\sigma_2+\frac{\omega\varepsilon_2}{\mathrm{i}4\pi}. \tag{11.2.21}$$

On the assumption of $\sigma_2\gg\omega\varepsilon_2/4\pi$ and $\sigma_1\gg\sigma_2$ (strong inhomogeneity) [2] and condition that the system is beyond smearing region $\sigma_1\tau^t\gg\sigma_2\tau^{-q}$, from (11.2.21) one can approximately write down $\sigma_{\mathrm{e}}(\omega)$ as

$$\sigma_{\mathrm{e}}(\omega)=\sigma_2\tau^{-q}+\frac{\omega\varepsilon_2}{\mathrm{i}4\pi}\tau^{-q},\tau<0. \tag{11.2.22}$$

Equating (11.2.22) to (11.2.10) at $|\tau|=\Delta$, we find smearing region for the case of imperfect dielectric $(\sigma_2\neq0)$:

$$\Delta=\left(\frac{\sigma_2}{\sigma_1}\right)^{\frac{1}{t+q}}. \tag{11.2.23}$$

Whence follows the expression for the effective dielectric constant in smearing region

$$\varepsilon_{\mathrm{e}}(\Delta)=\varepsilon_2\left(\frac{\sigma_2}{\sigma_1}\right)^{-\frac{q}{t+q}}. \tag{11.2.24}$$

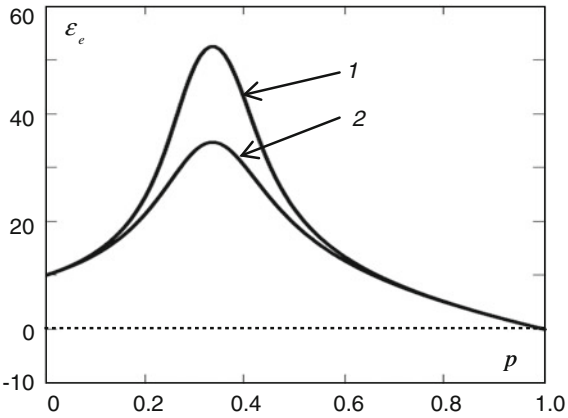

Fig. 11.2 Effective dielectric constant $\varepsilon_e(p)$: *1*—$\sigma_1 = 1000,\ \varepsilon_1 = 0,\ \sigma_2 = 0,\ \omega\varepsilon_2/4\pi = 10$, *2*—$\sigma_1 = 1000,\ \varepsilon_1 = 0,\ \sigma_2 = 10,\ \omega\varepsilon_2/4\pi = 10$.

Thus, depending on the fact which inequality holds true: $\sigma_2 \gg \omega\varepsilon_2/4\pi$ or the opposite one—the maximum value $\varepsilon_e(\Delta)$ will have the form (11.2.19) or (11.2.4). Figure 11.2 schematically, on the basis of EMT—approximation, shows both cases (a similar schematic figure is given in [2]).

Another case is also possible—when the metal phase conductivity includes a small imaginary part

$$\sigma_1(\omega) = \sigma_1 - \frac{\omega\varepsilon_1}{\mathrm{i}4\pi}, \quad \frac{\omega\varepsilon_1}{4\pi} \ll \sigma_1, \tag{11.2.25}$$

where ε_1 is called the dielectric constant of metal.

Note that since the sign of the imaginary part in $\sigma_1(\omega)$ is opposite to the sign of the imaginary part of dielectric phase $\sigma_2(\omega) = \omega\varepsilon_2/\mathrm{i}4\pi$, one can speak of the imaginary addition in (11.2.25) not as of "dielectric" or capacitive, but as of inductive one. In conformity with this, above the percolation threshold, with increasing concentration of the first phase, the imaginary part of the effective conductivity can change its sign from positive to negative. The medium in general will become "inductive," rather than "capacitive." Figure 11.3 shows a calculation of the dependence of the imaginary part of the effective conductivity made within the EMT-approximation for the case of nonzero imaginary part of the first (metal) phase: $\sigma_1(\omega) = \sigma_1 - \omega\varepsilon_1/\mathrm{i}4\pi,\ \sigma_2(\omega) = \omega\varepsilon_2/\mathrm{i}4\pi$.

In critical region from (11.2.8) and (11.2.10) immediately follows [2]

$$\varepsilon_e = \varepsilon_2\tau^{-q} - \varepsilon_2\tau^t. \tag{11.2.26}$$

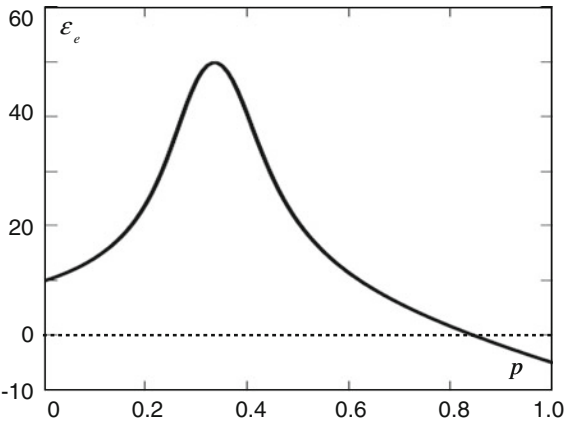

Fig. 11.3 Concentration dependence of the effective dielectric constant $\varepsilon_e(p)$: $\sigma_1 = 1000$, $\sigma_2 = 1$, $\omega\varepsilon_1/4\pi = -5$, $\omega\varepsilon_2/4\pi = 10$ (in arbitrary units). Concentration whereby ε_e changes its sign, $p^* \approx 0.86$

And from condition $\varepsilon_e(p^*) = 0$ one obtains

$$p^* = p_c + p_c \left(\frac{\varepsilon_2}{\varepsilon_1}\right)^{\frac{1}{t+q}}. \tag{11.2.27}$$

In so doing, certainly, the following inequality should be satisfied

$$\tau^* = \frac{p^* - p_c}{p_c} \ll 1. \tag{11.2.28}$$

As was shown above, the derivation of all considered cases of the effective conductivity behavior in critical region was based on the previously established percolation expressions $\sigma_e(\tau, \omega = 0)$ (5.2.4), (5.2.11) or, which is the same, on the hierarchical model of percolation structure. One can say that the resulting expressions for $\sigma_e(\omega)$ are valid as much as the schemes of percolation model, in other words, until bridges and interlayers are the main governing elements at current flow in the system. As long as there is strong inhomogeneity $\mathrm{Re}\,\sigma_1(\omega) \gg \mathrm{Re}\,\sigma_2(\omega)$—this is probably so. However, other cases are possible, for instance, systems with low dissipation, when $\mathrm{Re}\,\sigma_1(\omega)$ and $\mathrm{Re}\,\sigma_2(\omega)$ are small (ideally, tend to zero), and the imaginary parts $\mathrm{Im}\,\sigma_1(\omega)$ and $\mathrm{Im}\,\sigma_2(\omega)$ have different signs. Figuratively speaking, this is a case, when a medium is a mixture of capacitive and inductive elements with an ultimately low dissipative part. Such a case goes beyond the standard percolation theory and will be dealt with in Chap. 20.

References

1. Dyre JC, Schröder T (2000) Universality of AC conduction in disordered solids. Rev Mod Phys 72:873–892
2. Efros AL, Shklovskii BI (1976) Critical behaviour of conductivity and dielectric constant near the metal-non-metal transition threshold. Phys Stat Sol b 76:475–485
3. Landau LD, Lifshitz EM (1984) Electrodynamics of continuous media, vol 8, 2nd edn. Butterworth-Heinemann, Oxford p 460
4. Vinogradov AP (2001) Electrodynamics of composite materials URSS, Moscow, p 208 (in Russian)

Chapter 12
Galvanomagnetic Properties of Macroscopically Disordered Media

12.1 Introduction

On introducing a medium into a magnetic field, an "ordinary" Ohm's law for the isotropic medium $\mathbf{j} = \sigma\mathbf{E}$ (σ is a scalar) states that

$$\mathbf{j} = \hat{\sigma}(H)\mathbf{E}, \tag{12.1.1}$$

where $\hat{\sigma}(H)$ is conductivity tensor,

$$\hat{\sigma} = \begin{pmatrix} \sigma_s & \sigma_a & 0 \\ -\sigma_a & \sigma_s & 0 \\ 0 & 0 & \sigma_z \end{pmatrix}, \tag{12.1.2}$$

where magnetic field intensity $\mathbf{H} \parallel oz$.

Hereafter, for the dependence of the diagonal σ_s, σ_z and nondiagonal σ_a tensor components on the field H (12.1.2) we will use standard expressions

$$\sigma_s = \frac{\sigma}{1+\beta^2}, \quad \sigma_a = \frac{\sigma\beta}{1+\beta^2}, \tag{12.1.3}$$

where $\sigma = \sigma(H = 0)$, dimensionless magnetic field $\beta = \mu H/c$, μ is current carrier mobility in a medium, c is velocity of light. In so doing, it is common practice to recognize two cases, a weak field:

$$\beta \ll 1, \quad \sigma_s = \sigma, \quad \sigma_a = \beta, \tag{12.1.4}$$

and a strong field:

$$\beta \gg 1, \quad \sigma_s = \sigma\beta^{-2}, \quad \sigma_a = \sigma\beta^{-1}. \tag{12.1.5}$$

A.A. Snarskii et al., *Transport Processes in Macroscopically Disordered Media*, DOI 10.1007/978-1-4419-8291-9_12

Other designations are also of frequent use, e.g.

$$\mathbf{E} = \rho\mathbf{j} + \mathbf{j} \times \mathbf{b}, \quad \mathbf{b} \parallel \mathbf{H}, \tag{12.1.6}$$

or

$$\sigma\mathbf{E} = \mathbf{j} - \mathbf{j} \times \boldsymbol{\beta}, \quad \boldsymbol{\beta} \parallel \mathbf{H}, \tag{12.1.7}$$

where σ is the same as in (12.1.3), $\rho = 1/\sigma, \beta = -\sigma b$.

The Hall constant R in these designations is of the form

$$R = -\frac{b}{H} = \frac{\beta}{\sigma H}. \tag{12.1.8}$$

As such, a complicated problem of determination of the effective conductivity σ_e, becomes even more complicated at $H \neq 0$, and this additional complexity is due to two factors: the conductivity which is a scalar at $H = 0$, becomes a tensor when $H \neq 0$. Second, on application of a magnetic field, the electrical field and current distortions around a secluded inclusion are changed considerably. At $\beta \gg 1$, current distortion occurs not only at the distance of the order of inclusion with size a, but at a much larger distance of the order of value β_a (Fig. 12.1).

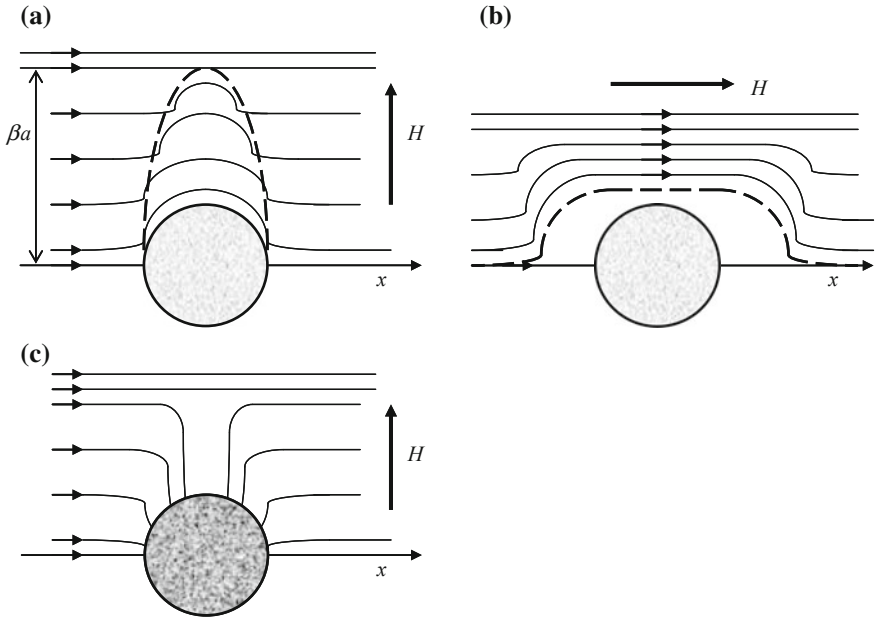

Fig. 12.1 Qualitative pattern of current distortion around spherical inclusion in the three-dimensional case: Magnetic field H is oriented: **a** perpendicular to undistorted current density lines, inclusion—a perfect dielectric $\hat{\sigma}_2 = 0$; **b** along current lines, inclusions—a perfect dielectric $\hat{\sigma}_2 = 0$; **c** perpendicular to current lines, inclusion—a perfect conductor $\hat{\sigma}_1 = \infty$

However, at $\beta \gg 1$ and $p\beta \gg 1$ (p is concentration of inclusions) and $p \ll 1$, EMA "works" no longer. There is no solution of "initialization" problem for EMA—the problem of field and current distribution in and around a secluded inclusion, since there is no secluded inclusion itself. Many works disregarding this fact have unclear applicability limits.

When the distance β_a "reaches" the neighboring inclusions (becomes comparable to the distance between the neighboring inclusions), there appear many size effects. In particular, there is a possibility in the case when $p\beta \gg 1, \sigma_s^e$ becomes proportional to the odd degree of field $\sigma_s^e \sim \beta^{-1}$, at the same time the longitudinal σ_z^e becomes dependent on a magnetic field in an odd way: $\sigma_z^e \sim \beta^{-1}$.

In the case of large fields ($\beta \gg 1$) it becomes essential that $\sigma_a > \sigma_s$ and, even with small inhomogeneities, when $\delta\sigma/\sigma \ll 1$ and $\delta\beta/\beta \ll 1$, fluctuations of σ_a can be much in excess of σ_s itself, and the use of perturbation theory is impossible. The elaborated methods that made it possible to go beyond the limits of conventional perturbation theory in the case of $\beta \gg 1$ have shown that at weak fluctuations of $\sigma(\delta\sigma/\sigma \ll 1)$:

$$\hat{\sigma} = \sigma(r)\begin{pmatrix} \beta^{-2} & \beta^{-1} & 0 \\ -\beta^{-1} & \beta^{-2} & 0 \\ 0 & 0 & 1 \end{pmatrix}, \quad \beta \gg 1, \tag{12.1.9}$$

the effective values $\sigma_a^e \sim \beta^{-1}$ and $\sigma_z \sim \beta^0$ show a standard magnetic field dependence, however, a diagonal component of the effective conductivity tensor σ_s^e depends on the field unexpectedly (the law of Dykhne-Dreizin):

$$\sigma_s^e \sim H^{-4/3} \tag{12.1.10}$$

Qualitative description of result (12.1.10) (obtained in [57]) was given in [55]. Account of the limitations of medium sizes along the magnetic field L_z in large magnetic fields can change the effective conductivity considerably. Thus, as is shown in [18], in the ultimately strong fields we have

$$\sigma_s^e \sim H^{-1}L_z^{-1/2}, \quad \beta \to \infty. \tag{12.1.11}$$

There is no exact solution for effective magnetoresistance properties. However, for some specific cases—exact solutions (specific for two-dimensional models) and approximations exist and continued to be developed.

Particularly, for media with two-dimensional microstructure new results developed in papers [7–9, 11, 21, 22]. Another simplified structure that allows obtaining new results is a periodical media. Interesting results for periodical media described in the article [23].

The behavior of magnetotransport in high field in percolation media discussed in papers [5, 19]. Another approaches (effective medium approximation, two-dimensional media with equal area fractions) for determining magnetotransport in high field considered in papers [10, 17].

There is no possibility to consider the entire variety of inhomogeneous media behavior in a magnetic field. Therefore, we will dwell on some of them

1. One-dimensional case—layered media in a magnetic field.
2. Two-dimensional *D*-media and two-dimensional polycrystalline media.
3. Strongly inhomogeneous two-phase media ($\sigma_1(H=0) \gg \sigma_2(H=0)$) close to percolation threshold in the two-dimensional and three-dimensional cases.

12.2 Layered Media in the Magnetic Field

Let us consider the case when oz axis is directed along a magnetic field, $oz \parallel \mathbf{H}$, ox axis—along the layers, and oy—across the layers. In this case (12.1.2) is written down as

$$\left.\begin{aligned} j_x &= \sigma_s(y)E_x + \sigma_a(y)E_y \\ j_y &= -\sigma_a(y)E_x + \sigma_s(y)E_y \end{aligned}\right\}, \tag{12.2.1}$$

and account of the boundary conditions (similar to the case of layered media without a magnetic field, Chap. 3.4) leads to expressions

$$j_y = \langle j_y \rangle, \quad E_x = \langle E_x \rangle. \tag{12.2.2}$$

Using a conventional "parentheses" method (see Sect. 3.4) one can obtain the following effective conductivity tensor:

$$\sigma_e = \begin{pmatrix} \sigma^e_{xx} & \sigma^e_{xy} \\ \sigma^e_{yx} & \sigma^e_{yy} \end{pmatrix}, \quad \sigma^e_{yx} = -\sigma^e_{xy}, \tag{12.2.3}$$

where

$$\sigma^e_{xx} = \langle \sigma \rangle - \frac{\langle \beta^2 \rangle}{\left\langle \frac{1+\beta^2}{\sigma} \right\rangle}, \quad \sigma^e_{xy} = \frac{\langle \beta \rangle}{\left\langle \frac{1+\beta^2}{\sigma} \right\rangle}, \quad \sigma^e_{yy} = \frac{1}{\left\langle \frac{1+\beta^2}{\sigma} \right\rangle}. \tag{12.2.4}$$

Note that in the local conductivity tensor $\sigma_{xx} = \sigma_{yy}$, while in the effective conductivity tensor it is no longer the case: $\sigma^e_{xx} \neq \sigma^e_{yy}$. Certainly, it is due to the fact that a layered medium is on the average anisotropic even in the absence of a magnetic field.

12.3 Dual Media in the Magnetic Field

The problem of calculation of σ_e in two-dimensional self-dual media (see [13] also [1, 2, 20] was generalized in [14] for the case when magnetic field is perpendicular to the gradient of inhomogeneity.

Then for $H \neq 0$ it is possible to obtain an exact solution of the problem for any value of inhomogeneity (see Chap. 6). Two different cases were considered in [14]: (1) $\beta_1 = \beta_2, \sigma_1 \neq \sigma_2$ and (2) $\sigma_1 = \sigma_2, \beta_1 \neq \beta_2$. Generalizations were given in [1, 20], where the most general situation was considered in [1].

Generalization of transformations Dykhne presented in (12.3.1) using notations from [1]:

$$\left.\begin{aligned} \mathbf{j} &= \tilde{a}\left(\tilde{\mathbf{j}} + \tilde{b}\mathbf{n} \times \tilde{\mathbf{E}}\right) \\ \mathbf{E} &= \tilde{a}\left(\tilde{c}\tilde{\mathbf{E}} + \tilde{d}\mathbf{n} \times \tilde{\mathbf{j}}\right) \end{aligned}\right\}, \tag{12.3.1}$$

Ohm's law in the presence of magnetic field could be written as:

$$\mathbf{j} + \mathbf{j} \times \boldsymbol{\beta} = \sigma \mathbf{E} \tag{12.3.2}$$

Let us note that β in (12.3.2) has different sign in comparison to (12.1.7). That, however, does not influence the final result.

Substituting (12.3.1) into (12.3.2) for fields and fluxes with tilde, it is possible to obtain the same expression (but with tilde field and flux) as in (12.3.2), where

$$\tilde{\sigma} = \frac{\tilde{b}^2 + \left(\sigma\tilde{c} - \beta\tilde{b}\right)^2}{\sigma\left(\tilde{c} + \tilde{b}\tilde{d}\right)}, \quad \tilde{\beta} = \frac{\left(\beta + c\tilde{d}\right)\left(\sigma\tilde{c} - \beta\tilde{b}\right) - \tilde{b}}{\sigma\left(\tilde{c} + \tilde{b}\tilde{d}\right)} \tag{12.3.3}$$

The media with tilde values would be dual to the main media when for the first phase

$$\sigma = \sigma_1, \quad \beta = \beta_1, \quad \tilde{\sigma} = \sigma_2, \quad \tilde{\beta} = -\beta_2, \tag{12.3.4}$$

and for the second phase:

$$\sigma = \sigma_2, \quad \beta = \beta_2, \quad \tilde{\sigma} = \sigma_1, \quad \tilde{\beta} = -\beta_1, \tag{12.3.5}$$

It is possible to obtain values $\tilde{a}, \tilde{b}, \tilde{c}, \tilde{d}$ from (12.3.3), (12.3.4), and (12.3.5).

Using the same analysis for average quantities $\langle \mathbf{E} \rangle, \langle \mathbf{j} \rangle$, it is possible to get for $p = 1/2$:

$$\sigma_e^2 \tilde{d} + 2\beta_e \tilde{\sigma}_e - \left(1 + \beta_e^2\right)\tilde{b} = 0 \tag{12.3.6}$$

It is necessary to have one more expression with σ_e and β_e in order to get these values.

Let us consider one more transformation similar to (12.3.1) for the new double tilde media that will be exactly like the original media, but with the opposite sign of the magnetic field.

It means that instead of (12.3.4) and (12.3.5) the following expressions should be considered:

for the first phase:

$$\sigma = \sigma_1, \quad \beta = \beta_1, \quad \tilde{\tilde{\sigma}} = \sigma_1, \quad \tilde{\tilde{\beta}} = -\beta_1, \tag{12.3.7}$$

and for the second:

$$\sigma = \sigma_2, \quad \beta = \beta_2, \quad \tilde{\tilde{\sigma}} = \sigma_2, \quad \tilde{\tilde{\beta}} = -\beta_2, \tag{12.3.8}$$

Finally, it is possible to find for the two tilde media

$$\sigma_e^2 \tilde{\tilde{d}} + 2\beta_e \sigma_e - \left(1 + \beta_e^2\right)\tilde{\tilde{b}} = 0 \tag{12.3.9}$$

After substituting $\tilde{a}, \tilde{b}, \tilde{c}, \tilde{d}$ into (12.3.6) and (12.3.9), it is possible to find σ_e and β_e:

$$\left.\begin{aligned} \sigma_e &= \frac{\sqrt{\sigma_1\sigma_2}}{\sqrt{1 + \left(\frac{\sigma_1\beta_2 - \sigma_2\beta_1}{\sigma_1 + \sigma_2}\right)^2}}, \\ \beta_e = \sigma_e \frac{\beta_1 + \beta_2}{\sigma_1 + \sigma_2} &= \sqrt{\sigma_1\sigma_2}\, \frac{\beta_1 + \beta_2}{\sqrt{(\sigma_1 + \sigma_2)^2 + (\sigma_1\beta_2 - \sigma_2\beta_1)^2}} \end{aligned}\right\} \tag{12.3.10}$$

Let us note that expression (12.3.9) is correct for arbitrary distribution of phases and their concentrations (however, only for isotropic media on the average) [1]. Otherwise, it will not be possible to obtain effective kinetic coefficients. For example, if one phase is a dielectric ($\hat{\sigma}_2 = 0$), it is possible to obtain from (12.3.9):

$$\frac{\beta_e}{\sigma_e} = \frac{\beta_1}{\sigma_1}, \quad p > 1/2, \tag{12.3.11}$$

It means, that effective Hall coefficient is equal to R_1 for weak magnetic fields [1]:

$$R_e = R_1, \tag{12.3.12}$$

i.e., effective Hall coefficient is not equal to zero (even with $\hat{\sigma}_2 = 0$) and R_e is a constant quantity, not dependent on concentration [1].

For D-media, it is possible to write equations for effective coefficients above and below the percolation threshold for magnetic field, similar to case when $H = 0$.

The values of $\sigma_e(H \neq 0)$ could be obtained for different regular structures, for example for the net of narrow of periodic dielectric inclusions, or periodic squares of one phase that do not touch each other, etc. [16]. These values could be obtained mostly by the methods of theory of complex variables.

The range of applicability of such expression is not clear in advance, especially in strong magnetic fields, when currents' changes spreading for long distance. It is not clear if the solution is stable for small changes of structure (for example, in case of small deviations from periodicity).

Generalized transformations Dykhne has been considered for the case when two-dimensional media is locally anisotropic even for $H = 0$ [4].

For the case when magnetic field is perpendicular to the two-dimensional media, it is possible to obtain

$$\hat{\sigma}(r) = \begin{pmatrix} \sigma_{11} & \sigma_{12} \\ \sigma_{21} & \sigma_{22} \end{pmatrix} = \begin{pmatrix} \sigma_{11} & \sigma_{\Lambda} \\ \sigma_{\Lambda} & \sigma_{22} \end{pmatrix} + \begin{pmatrix} 0 & \sigma_a \\ -\sigma_a & 0 \end{pmatrix} \tag{12.3.13}$$

where for initially isotropic media $\sigma_\Lambda = 0$. Particularly, these generalized transformations are helpful for obtaining effective conductivity for the two-dimensional polycrystalline media

$$\left.\begin{aligned} \sigma_e = \begin{pmatrix} \sigma_s^e & \sigma_a^e \\ -\sigma_a^e & \sigma_s^e \end{pmatrix}, \\ \sigma_s^e = \sqrt{\sigma_{11}\sigma_{22} - \frac{(\sigma_{12}+\sigma_{21})^2}{4}}, \quad \sigma_a^e = \frac{\sigma_{12}-\sigma_{21}}{2} \end{aligned}\right\} \tag{12.3.14}$$

There is also a simple way for obtaining the same expressions using different considerations [15].

In this case, polycrystalline is "built" from two-phase media. Let us assume that anisotropy (12.3.13)"not real," but artificially created—local media consists of parallel infinite stripes with different conductivities:

$$\hat{\sigma}_1(H) = \begin{pmatrix} a_1 & b_1 \\ -b_1 & a_1 \end{pmatrix}, \quad \hat{\sigma}_2(H) = \begin{pmatrix} a_2 & b_2 \\ -b_2 & a_2 \end{pmatrix} \tag{12.3.15}$$

Connections between stripes' conductivities a_i, b_i and conductivities of single crystals considered above (12.2.4), in our two-phase case they are:

$$\sigma_{11} = 2\frac{a_1 a_2}{a_1 + a_2}, \quad \sigma_{22} = \frac{(a_1 + a_2)^2 + (b_1 - b_2)^2}{2(a_1 + a_2)}, \quad \sigma_{12} = -\sigma_{21} = \frac{a_1 b_2 + a_2 b_1}{a_1 + a_2} \tag{12.3.16}$$

The tensor of the effective conductivity of the two-phase media in the magnetic field (12.3.10) could be expressed in the following way:

$$\sigma_s^e = \sqrt{a_1 a_2}\sqrt{1+\left(\frac{b_1-b_2}{a_1+a_2}\right)^2}, \quad \sigma_a^e = \frac{a_1 b_2 + a_2 b_1}{a_1 + a_2} \tag{12.3.17}$$

In order to obtain the tensor of the effective conductivity of polycrystal, it is necessary to present a_i and b_i from (12.3.16) as the function of tensor components σ_{ik} from (12.3.14). It follows from (12.3.16) and (12.3.17),

$$\sigma_{11}\sigma_{22} = \left(\sigma_s^e\right)^2, \quad \sigma_{12} = \sigma_a^e, \tag{12.3.18}$$

From here it is possible to derive expressions for the tensor of effective conductivity of polycrystall in the magnetic field (12.3.13).

The same result could be obtained using the generalization of the idea of trap model (see Chap. 6) for the case of not equal to zero of the magnetic field [15].

12.4 Strongly Inhomogeneous Media in the Vicinity of the Percolation Threshold, Two-Dimensional Case

Consider galvanomagnetic properties with the initial (without a magnetic field) considerable inhomogeneity, $\sigma_1(H=0)/\sigma_2(H=0) \gg 1$. In this case, percolation structure is of great importance in current distribution, and magnetic field "plays its game" in its background. Galvanomagnetic phenomena in percolation structures were considered in many papers, see for example [3, 6–12, 19, 20–23, 27–31, 34, 36, 39-54].

Connection between effective Hall constant Re and σ_e(H=0) was determined for two-dimensional case for all concentration in the paper [20], see also [25]. In papers [3, 4] isomorphism method was introduced for galvanomagnetic phenomena (see chap. 15 specifically – for thermoelectric phenomena). The case of the strong magnetic fields was considered in paper [3]. Particularly, (see [45, 20]), critical behavior of R_e is quite non-trivial as well as the critical behavior of magnetoresistance. In [3] different cases are considered: 1. The case when the first phase is an ideal conductor σ_1 ->∞. 2. The case when the first phase is an ideal isolator σ_2=0. Two particular cases: (1) the first phase—a perfect conductor $\hat{\sigma}_1 = \infty$, (2) the second phase—a perfect dielectric $\sigma_2 = 0$.

In the first case [3]:

$$\sigma_s^e = \sigma_{s2} f_2(p), \quad \sigma_a^e = \sigma_{a2}, \quad \tau < 0, \tag{12.4.1}$$

where $f_2(p)$ is a function that determines the concentration behavior of the effective conductivity below the percolation threshold at $H = 0$,

$$f_2(p) = \sigma_e(H = 0, p)/\sigma_2, \quad \tau < 0, \tag{12.4.2}$$

for $|\tau| \ll 1$ this function, as is known from the percolation threshold (Chap. 5), is $f_2(\tau) = |\tau|^{-q}$.

In the second case [3], at $\hat{\sigma}_2 = 0$ we have

$$\sigma_s^e = \sigma_{s1} \frac{\sigma_{s1}^2 + \sigma_{a1}^2}{\sigma_{s1}^2 + \sigma_{a1}^2 f_1(\tau)} f_1(\tau), \quad \sigma_a^e = \sigma_{a1} \frac{\sigma_{s1}^2 + \sigma_{a1}^2}{\sigma_{s1}^2 + \sigma_{a1}^2 f_1(\tau)} f_1^2(\tau), \quad \tau > 0, \tag{12.4.3}$$

where $f_1(\tau)$ is introduced similarly $f_2(\tau)$:

$$f_1(p) = \sigma_e(H = 0, p)/\sigma_1, \quad \tau > 0, \tag{12.4.4}$$

and at $\tau \ll 1$

$$f_1(\tau) = \tau^t, \quad \tau > 0. \tag{12.4.5}$$

Thus, close to percolation threshold Eq. (12.4.3) assume the form

$$\sigma_s^e = \sigma_1 \frac{\tau^t}{1 + \beta_1^2 \tau^{2t}}, \quad \sigma_a^e = \sigma_1 \beta_1 \frac{\tau^{2t}}{1 + \beta_1^2 \tau^{2t}}, \tag{12.4.6}$$

these expressions, for $\beta_1 \tau^t \ll 1$, are simplified:

$$\sigma_s^e = \sigma_1 \tau^t, \quad \sigma_a^e = \sigma_1 \beta_1 \tau^{2t}, \quad \beta_1 \tau^t \ll 1. \tag{12.4.7}$$

In so doing, the diagonal component of the effective conductivity tensor behaves as if a magnetic field were equal to zero. Note that since $\tau^t \ll 1$, the smallness of $\beta_1 \tau^t$ is by no means the smallnessy of a dimensionless magnetic field β_1.

In the case of a large field, so much large that not only $\beta_1 \gg 1$, but also $\beta_1 \tau^t \gg 1$, from (12.4.6) it follows

$$\sigma_s^e = \sigma_1 \beta^{-2} \tau^{-t}, \quad \sigma_a^e = \sigma_1 \beta^{-1} \tau^0, \quad \tau > 0. \tag{12.4.8}$$

As can be seen from (12.4.8), the diagonal component of the effective conductivity tensor behaves in the unusual way on approaching the percolation threshold, when a bridge becomes increasingly longer, and its resistance—increasingly larger, the diagonal component is not reduced, but $\sigma_s^e \sim \tau^{-t}$ is increased. The effective Hall constant R_e, as is evident from (12.4.6), does not depend on a magnetic field

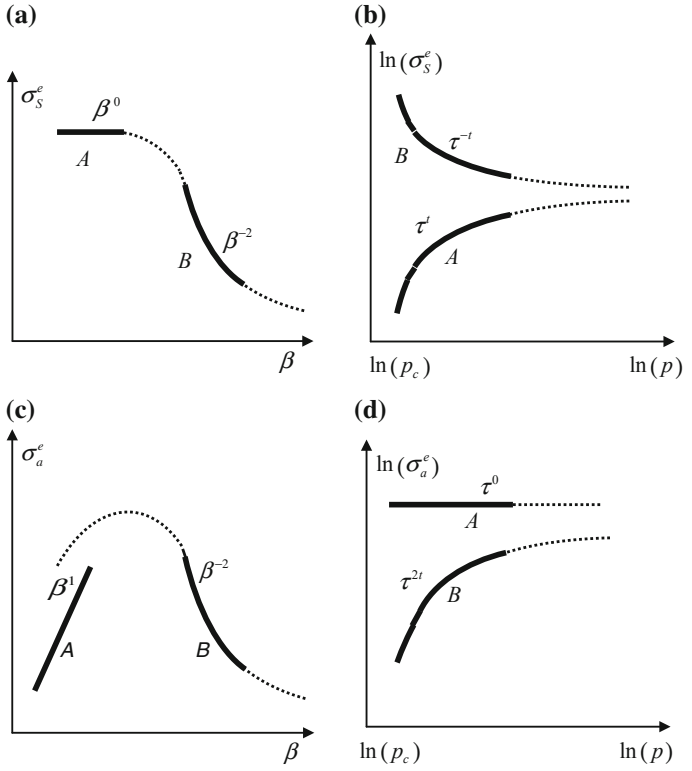

Fig. 12.2 Field **a**, **b** and concentration **c**, **d** dependences of σ_s^e and σ_a^e in the two-dimensional case above the percolation threshold, in the case when the second phase is a perfect dielectric $\hat{\sigma}_2 = 0$: Magnetic field ranges: $A\ 1 \ll \beta_1 \ll \tau^{-t}, \sigma_s^e = \sigma_1 \tau^t, \sigma_a^e = \sigma_1 \tau^{2t} \beta_1$, $B\ \beta_1 \gg \tau^{-t}, \sigma_s^e = \sigma_1 \tau^{-t} \beta_1^{-2}$, $\sigma_a^e = \sigma_1 \beta_1^{-1}$

$$R_e = \frac{\sigma_a^e}{\left(\sigma_s^e\right)^2 H} = R_1. \tag{12.4.9}$$

It is interesting to note (see [3]) that in a sufficiently strong magnetic field the boundary condition at $\hat{\sigma}_2 = 0$ in the second phase becomes the same as for $\hat{\sigma}_1 = \infty$ in the first phase, i.e., at $\hat{\sigma}_1 = \infty$ the boundary of the first ("metal"!) phase behaves as a dielectric. Figures 12.2 and 12.3 show the schematic concentration and field dependences of σ_s^e and σ_a^e in the two-dimensional case above and below the percolation threshold, respectively.

Let us note that though with a change of magnetic field in $\sigma_{s1} = \sigma_1 / \left(1 + \beta_1^2\right)$ a transition from $\sigma_{s1} \sim \beta^0$ dependence to $\sigma_{s1} \sim \beta_1^{-2}$ dependence occurs at $\beta_1 \sim 1$, for σ_s^e it is "extended". Indeed, since $\sigma_s^e \sim \left(1 + \beta_1^2 \tau^{2t}\right)^{-1}$, and now this transition takes

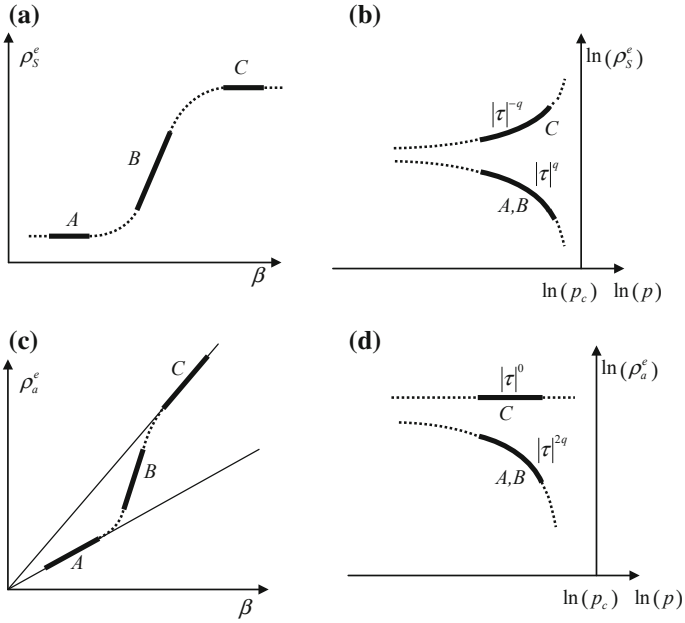

Fig. 12.3 Field **a**, **b** and concentration **c**, **d** dependences of ρ_s^e and ρ_a^e in the two-dimensional case below the percolation threshold, in the case when the second phase is a perfect conductor $\hat{\sigma}_2 = \infty$: Magnetic field ranges: *A* $\beta_2 \ll 1, \rho_s^e = \rho_s|\tau|^q, \rho_a^e = \rho_2|\tau|^{2q}\beta_2$, *B* $1 \ll \beta_1 \ll \tau^{-q}, \rho_s^e = \rho_s|\tau|^q\beta_2^2, \rho_a^e = \rho_2|\tau|^{2q}\beta_2^3$, *C* $\beta \gg |\tau|^{-q}, \rho_s^e = \rho_2|\tau|^{-q}, \rho_a^e = \rho_2\beta_2$

place at $\beta_1 \sim \tau^{-2t} \gg 1$, i.e., with a much larger field. The same "extension" of transition from one field dependence to the other is also observed for σ_a^e.

The general case, when the first phase is not a perfect conductor, but has finite conductivity, and the second phase which is not a perfect dielectric also has finite conductivity, though much lower than the first phase, was described in [3]. This solution clarifies the particular cases mentioned above, and mainly describes the system behavior in smearing region (in ideal cases this region degenerates into a point $p = p_c$). As it turns out, when magnetic field is not equal to 0, the standard smearing region Δ is modified. For a particular case, when $\beta_1 = \beta_2$, we have

$$\Delta_H = \frac{\Delta}{\left(1+\beta^2\right)^{\frac{1}{t+q}}} = \left(\frac{\sigma_2/\sigma_1}{1+\beta^2}\right)^{\frac{1}{t+q}}, \tag{12.4.10}$$

i.e., the larger is a magnetic field, the narrower is smearing region Δ_H. Thus, a situation is possible when a system that was inside smearing region Δ, on application of a magnetic field, leaves smearing region (now Δ_H). The expressions for σ_s^e and σ_a^e (12.4.6) were derived on the basis of similar expressions for the effective

conductivity in the absence of a magnetic field and beyond smearing region $|\tau| \gg \Delta$. Inside smearing region the effective conductivity has, certainly, a different dependence on the values of phase conductivities. While applying a magnetic field, two different cases are possible at $|\tau| \gg \Delta : |\tau| \gg \Delta_H$ and $|\tau| \ll \Delta_H$. Then we have for area A

$$\beta \gg \tau^{-t}, \quad \sigma_s^e = \sigma_1 \tau^{-t} \beta^{-2}, \quad \sigma_a^e = \sigma_1 \beta^{-1}, \quad |\tau| \gg \Delta_H, \tag{12.4.11}$$

for area B

$$\tau^{-t}\sqrt{\sigma_2/\sigma_1} \ll \beta \ll \tau^t, \quad \sigma_s^e = \sigma_1 \tau^t, \quad \sigma_a^e = \sigma_1 \tau^{2t} \beta, \quad |\tau| \gg \Delta_H, \tag{12.4.12}$$

for area C

$$1 \ll \beta \ll \tau^{-t}\sqrt{\sigma_2/\sigma_1}, \quad \sigma_s^e = \sqrt{\sigma_1 \sigma_2}\beta^{-1}, \quad \sigma_a^e = 2\sigma_2 \beta^{-1}, \quad |\tau| \ll \Delta_H, \tag{12.4.13}$$

for area D

$$\beta \ll 1, \quad \sigma_s^e = \sqrt{\sigma_1 \sigma_2}, \quad \sigma_a^e = 2\sigma_2 \beta, \quad |\tau| \ll \Delta_H. \tag{12.4.14}$$

The inequalities for dimensionless field β given in (12.4.11)–(12.4.14), also follow from the restrictions on τ, for instance, from $|\tau| \gg \Delta_H = \Delta_0/\left(1+\beta^2\right)^{\frac{1}{t+q}}, t_2 = q_2$ immediately follows the inequality $\beta \gg \tau^{-t}\sqrt{\sigma_2/\sigma_1}$ (12.4.12).

Apparently, Fig. 12.3 shows the field dependences of σ_s^e and σ_a^e in the two-dimensional case below the percolation threshold.

As it is evident from (12.4.13) (region C in Fig. 12.4a) the field dependence $\sigma_s^e \sim \beta^{-1}$ is abnormal, and even when the field dependences of σ_{s1} and σ_{s2} are even the effective dependence of σ_s^e from the field is odd.

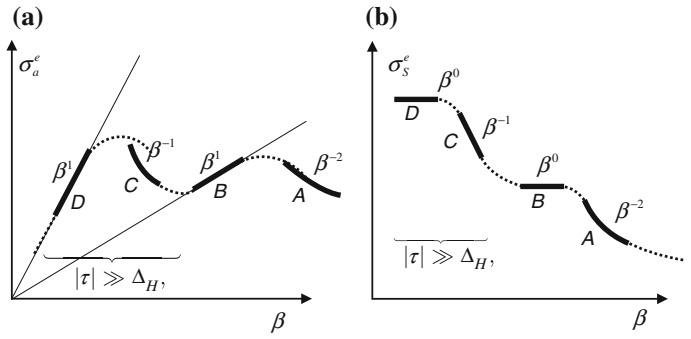

Fig. 12.4 Field dependences of σ_s^e and σ_a^e in smearing region: magnetic field ranges A, B, C, and D correspond to expressions (12.4.11)–(12.4.14)

The general case also described in [3].

The main regularities of the field and concentration behavior of $\hat{\sigma}_e(H)$ in the two-dimensional case beyond smearing region are easily explained and derived within the models of NLB and HM types. Thus, for instance, below the percolation threshold along the ox axis current flow occurs similar to situation without a magnetic field, so we immediately get $\sigma_s^e = \sigma_{s2}(\beta)|\tau|^{-q}$, which coincides with the first expression from (12.4.1), allowing for the fact that beyond smearing region $f_2(p) \sim |\tau|^{-q}$. For the nondiagonal component σ_a^e, (Fig. 12.5) the effective value is determined as such that it connects average over the volume current $\langle j_y \rangle$ and field $\langle E_x \rangle$:

$$\langle j_y \rangle = -\sigma_a^e \langle E_x \rangle, \tag{12.4.15}$$

in so doing, potential difference $\Delta\varphi = \langle E_x \rangle / \xi$, $\langle E_x \rangle \approx \langle E \rangle$ is applied along ox to the volume with dimensions of the order of correlation radius ξ. As long as voltage drop almost completely occurs on the interlayer (with characteristic dimension a_0), the field inside the interlayer is much larger than the average value $\langle E_x \rangle$ and is of the form

$$E' = \langle E \rangle \cdot \xi / a_0. \tag{12.4.16}$$

Exactly this field "creates" the main Hall current directed along the interlayer

$$j_y = -\sigma_a E' \approx -\sigma_a \langle E \rangle \xi / a_0, \tag{12.4.17}$$

Here, (in (12.4.17) and in Fig. 12.5) a case is shown when the interlayer is elongated along oy, however, account of its convolution changes nothing. When field E' rotates, the Hall current which is perpendicular to the field will rotate simultaneously (Fig. 12.5).

The average Hall current is found on condition that this current in the interlayer $j_y \cdot a_0$ is the entire Hall current $\langle j_y \rangle \xi$:

$$\langle j_y \rangle = -j_y \cdot a / \xi = -\sigma_a \langle E \rangle, \tag{12.4.18}$$

which immediately implies $\sigma_a^e = \sigma_a$, since $\langle j_y \rangle = -\sigma_a^e \langle E_x \rangle$ [see the second expression in (12.4.1)]. The absence of concentration dependence of σ_a^e is readily explained in HM—the Hall current is "accumulated" in the interlayer, in the presence of the field E', which is many times larger than the average one, however, the interlayer cross-section is less than correlation size ξ by the same magnitude. Similarly, it is possible to find galvanomagnetic properties above the percolation threshold, using HM [37]. There are many different situations when two-dimensional media is located in inclined magnetic field: see [4,37,48].

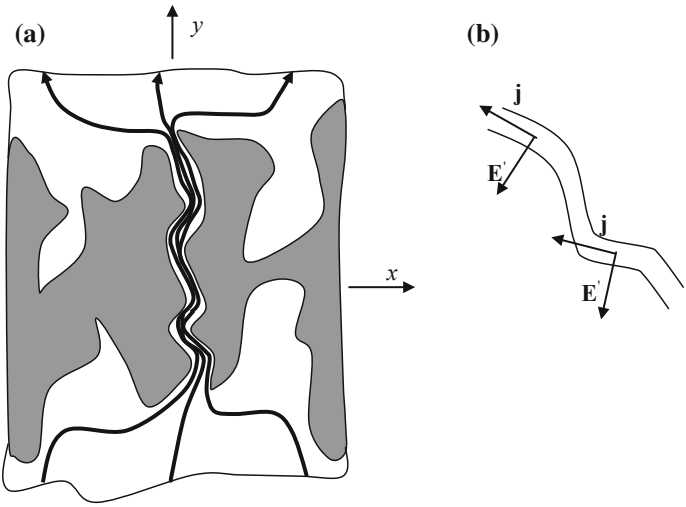

Fig. 12.5 Schematic of the first HM stage (interlayer) for the determination of the nondiagonal component oft the effective conductivity tensor $\sigma^e(H)$ in the two-dimensional case: **a** for the case below the percolation threshold the resistance of the first phase (*shaded*) is ignored (an ideal conductor); **b** part of interlayer with indication of current and the electrical field direction

12.5 Strong Disorder, Three-Dimensional Case

Three-dimensional case is much more complicated than two-dimensional one. At $H = 0$ the behavior of σ_e (see scaling relations in Chap. 5) differs only in the numerical values of critical indexes, whereas at $H \neq 0$, as we will see below, it is not the case. In the three-dimensional case, there can appear regularities that are mostly different from the two-dimensional case.

Particular emphasis in the three-dimensional case was placed on the behavior of the effective Hall constant. Using a percolation model, for $\tau > 0$ one can write down

$$R_e \sim R_1 \tau^g, \quad g = 0.6 \div 1. \tag{12.5.1}$$

Numerical calculations on different nets give close values for g – for example, in [30] - g = 0.25±0.05, [29]- g = 0.49±0.06, [32] – g3/ν3 = 0.4, it means that if ν3 = 0.88, g = 0.35, [42] – g = 0.6±0.1. In granular films [27] the following value of g = 0.49±0.07 was obtained, and in composites GeAu [12] – g = 0.38 when concentration of Ge is close to the percolation threshold, and g = 3.8 when Au is close to the percolation threshold. Based on the phenomenological consideration, for R_e it was obtained

$$R_e = h^2 R_2 \left(\frac{\sigma_e(H=0)}{\sigma_1(H=0)}\right)^{-2} + \left[R_1 - h^2 R_2\right]\Re(p,h), \tag{12.5.2}$$

where

$$h = \frac{\sigma_2(H=0)}{\sigma_1(H=0)}, \quad \Re(p,h) = \varphi(p,h)\cdot\left(\frac{\sigma_2(H=0)}{\sigma_1(H=0)}\right)^{-1}, \tag{12.5.3}$$

and $\varphi(p,h)$ appears in the relationship

$$\sigma_a^e = \sigma_{a2} + (\sigma_{a1} - \sigma_{a2})\varphi(p,h), \tag{12.5.4}$$

In the critical area we have

$$\Re(p,h) = h^{-k} F\left(\frac{\tau}{h^{\frac{1}{t+q}}}\right), \tag{12.5.5}$$

and at

$$\tau > 0, \quad \Delta \ll \tau \ll 1, \quad \Re \sim \tau^{-q}, \tag{12.5.6}$$

$$\tau < 0, \quad \Delta \ll |\tau| \ll 1, \quad \Re \sim |\tau|^{-q}, \tag{12.5.7}$$

$$|\tau| \ll \Delta, \quad \Re \sim h^{-k}, \tag{12.5.8}$$

where

$$k = g/(t+q). \tag{12.5.9}$$

In the two-dimensional case $g_2 = 0$ and, thus, dependence of R_e can be only smooth.

The simplified version of formula (12.5.2) was suggested in [20]):

$$R_e = h^2 R_2 \left(\frac{\sigma_e(H=0)}{\sigma_1(H=0)}\right)^{-2} + [R_1]\Re(p,h), \quad \Re(p,h) = (\tau^2 + \Delta^2)^{-g/2} \tag{12.5.10}$$

Similar expression were obtained in [6]

$$R_e = B_1 R_2 h^2 \tau^{-2t} + A_1 R_1 \tau^{-q}, \quad \tau > 0, \quad 1 \gg \tau \gg \Delta_0, \tag{12.5.11}$$

$$R_e = B_2 R_2 |\tau|^{2q} + A_2 R_1 \tau^{-g}, \quad \tau < 0, \quad 1 \gg |\tau| \gg \Delta_0, \tag{12.5.12}$$

$$R_e = B_3 R_2 h^{\frac{2q}{t+q}} + A_3 R_1 h^{-\frac{q}{t+q}}, \quad |\tau| < \Delta_0, \tag{12.5.13}$$

where A_1, B_1, A_2, B_2, A_3, and B_3 are constants.

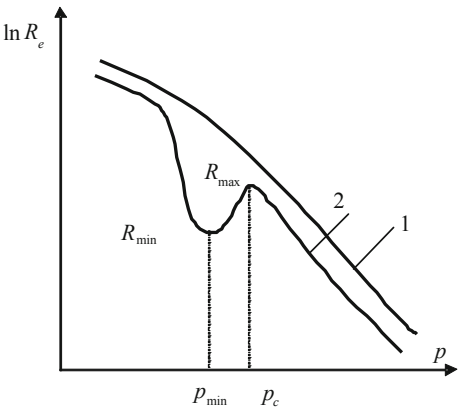

Fig. 12.6 Concentration dependences of the effective Hall constant R_e in critical region $|\tau| \ll 1$: *1* $(R_1/R_2)^{\frac{t+q}{2q+g}} < \sigma_2/\sigma_1$; *2* $(R_1/R_2)^{\frac{t+q}{2q+g}} > \sigma_2\sigma_1$

Let us note that (12.5.11)–(12.5.13) from [6] were obtained under scaling assumptions, but (12.5.2) were obtained for any values of parameters (in linear H approximation).

Formula (12.5.10) explains why different values of critical exponent g measured in [12].

Condition of experiment from [12] are such that for the case $g \sim 0.38$ the second term from (12.5.11) is dominant, and for the second case the dominant is the first term. In the second case not the index g is measured, but an index of the first term ($2t \sim 4$, in experiment ~ 3.8).

Figure 12.6 shows qualitative behavior of R_e [6]. Concentration dependence of R_e in the case $(R_1/R_2)^{\frac{t+q}{2q+g}} < \sigma_2/\sigma_1$ is smooth, but for $(R_1/R_2)^{\frac{t+q}{2q+g}} < \sigma_2/\sigma_1$ - there is a maximum at $p = p_c$ and a minimum at $p_{\min} = p_c - (R_1/R_2)^{\frac{1}{2q+g}}$, accordingly, $R_{e\max} = R_e(p_c) = R_1(R_2/R_1)^{\frac{g}{t+q}}$ and $R_{e\min} = R_e(p_{\min}) = R_1(R_2/R_1)^{\frac{g}{2q+g}}$.

In the two-dimensional case $g_2 = 0$, therefore concentration dependence of R_e is smooth.

Everything stated above for the three-dimensional case refers to a weak magnetic field. In strongly inhomogeneous media, for a strong magnetic field mostly new dependences are possible. In a strongly inhomogeneous medium [56] , i.e., when the second phase is dielectric inclusions with a low concentration, the transverse and longitudinal (with respect to a magnetic field) components of conductivity at $H \to \infty$ abnormally ($\sim H^{-1}$) depend on a magnetic field:

$$\sigma_s^e \sim 1/H, \quad \sigma_{ze} \sim 1/H, \quad \beta(1-p) \gg 1, \quad 1-p \ll 1, \tag{12.5.14}$$

where p, as a rule, is concentration of the first good conducting phase.

It is shown in [40] that at $H \to \infty$ the magnetoresistance exhibits nontrivial magnetic field dependence in the form

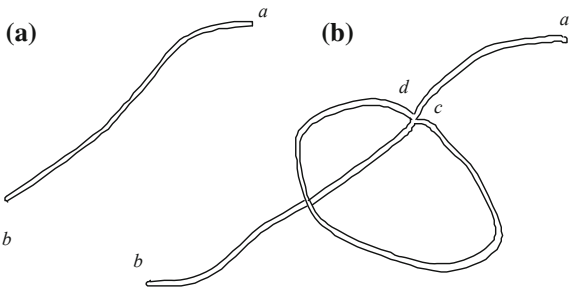

Fig. 12.7 The main element of percolation structure above the percolation threshold—a bridge: **a** portion of a bridge without a loop; **b** a bridge with a loop creating additional Hall voltage in the bridge

$$\rho_e(H)/\rho_e(H=0) \sim H^{0.5}. \tag{12.5.15}$$

Structural details of percolation cluster, though insignificant in small fields, can have important consequences for the magnetoresistance behavior in strong fields. As an example, let us consider a portion of a bridge with and without a loop (Fig. 12.7).

Let a bridge consist of material with a magnetoresistance that is independent of a magnetic field. In the absence of a magnetic field, the resistance of bridge portion between the edges a and b (Fig. 12.7) r_{ab} does not depend on the presence or absence of a loop. In the presence of a strong magnetic field, current flowing along the portion creates a considerable electromotive force in cd loop due to the Hall effect. Current generated due to this EMF is proportional to magnetic field H and creates, in turn, additional Hall voltage proportional to H^2 in ab channel.

Note in brief that the above considered methods of studying the effective conductivity in a magnetic field can be used when studying the quantum Hall effect (QHE) [24, 26, 33]. It is particularly simple to show the "presence" of the quantum Hall effect (QHE) in a dual medium, writing down components of the effective conductivity tensor in a magnetic field in the form

$$\sigma^e_{xx} = \frac{\sigma_e}{1+\beta_e^2}, \quad \sigma^e_{xy} = -\sigma^e_{yx} = \frac{\sigma_e \beta_e}{1+\beta_e^2} \tag{12.5.16}$$

where σ_e and β_e were taken from (12.3.10). Letting $\sigma_1 \to \infty$, $\beta_1 \to \infty$, at $\sigma_1/\beta_1 =$ const we obtain

$$\sigma^e_{xx} = 0, \quad \sigma^e_{xy} = \sigma_1/\beta_1, \tag{12.5.17}$$

i.e., the diagonal dissipative part of conductivity tensor is equal to zero and the nondiagonal part is different from zero.

References

1. Balagurov BY (1978) Galvanomagnetic properties of thin inhomogeneous films Fizika of solid state, vol 20, pp 3332–3335 (in Russian)
2. Balagurov BY (1981) Reciprocity relations in two-dimensional percolation theory. Sov Phys JETP 54:355–358
3. Balagurov BY (1982) Galvanomagnetic properties of two-dimensional two-component systems. Sov Phys JETP 55:774–782
4. Balagurov BY (1983) Isomorphism of certain problems of percolation theory. Sov Phys JETP 58:331–340
5. Barabash SV, Bergman DJ, Stroud D (2001) Magnetoresistance of three-constituent composites: percolation near a critical line. Phys Rev B 64:174419-1–174419-7
6. Bergman DJ, Stroud D (1985) Scaling theory of the low-field Hall effect near the percolation threshold. Phys Rev B 32:6097–6099
7. Bergman DJ, Strelniker YM (1999) Strong-field magnetotransport of conducting composites with a columnar microstructure. Phys Rev B 59:2180–2198
8. Bergman DJ, Strelniker YM (1999) Magnetotransport in conducting composite films with a disordered columnar microstructure and an in-plane magnetic field. Phys Rev B 60:13016–13027
9. Bergman DJ, Strelniker YM (2000) Magneto-transport and magneto-optics in composite media with a two-dimensional microstructure. Phys B 279:1–4
10. Bergman DJ, Stroud DG (2000) High-field magnetotransport in composite conductors: effective-medium approximation. Phys Rev B 62:6603–6613
11. Bergman DJ, Li X, Strelniker YM (2005) Macroscopic conductivity tensor of a three-dimensional composite with a one- or two-dimensional microstructure. Phys Rev B 71:05120-1–035120-10
12. Dai U, Palevski A, Deutscher G (1987) Hall effect in a three-dimensional percolation system. Phys Rev B 36:790–792
13. Dykhne AM (1970) Contluctivity of a two-dimensional two-phase system. Phys JETP 32:63–64
14. Dykhne AM (1970) Anomalous plasma resistance in a strong magnetic field. Sov Phys JETP 32:348–350
15. Dykhne AM, Snarskiĭ AA (2006) Conductivity of 2D polycrystalline media in a magnetic field. Sov Phys JETP 102:475–479
16. Emets YP (1986) Electric characteristics of composites with regular structure Naukova Dumka, Kiev, p 191
17. Guttal V, Stroud D (2005) Model for a macroscopically disordered conductor with an exactly linear high-field magnetoresistance. Phys Rev B 71:201304-1–201304-4
18. Kvyatkovskii OE (1983) Effective conductivity of an inhomogeneous medium in a strong magnetic field. Sov Phys JETP 58:120–129
19. Sarychev AK (1993) Theory of high-field magnetotransport in a percolating medium. Phys Rev B 48:3145–3155
20. Shklovskii BI (1977) Critical behavior of the Hall coefficient near the percolation threshold. Sov Phys JETP 45:152–156
21. Strelniker YM, Bergman DJ (2000) Exact relations between magnetoresistivity tensor components of conducting composites with a columnar microstructure. Phys Rev B 61:6288–6297
22. Strelniker YM, Bergman DJ (2003) Exact relations between macroscopic moduli of composite media in three dimensions: application to magnetoconductivity and magneto-optics of three-dimensional composites with related columnar microstructures. Phys Rev B 67:184416-1–184416-9
23. Strelniker YM, Bergman DJ (2011) Strong-field macroscopic magneto-transport in a periodic composite medium: some new results. J Phys: Conf Ser 319:1–8

24. Arkhincheev VE, Batiyev EG (1989) On the theory of the Quantum Hall Effect in inhomogeneous media. Sol St Comm 71:1059–1060
25. Balagurov BYa (1987) Galvanomagnetic properties of inhomogeneous media in a weak magnetic field. Sov Phys JETP 66:1079–1088
26. Baskin ÉM, Éntin MV (2000) Quantum hall effect in an antidot lattice: Macroscopic limit. Sov Phys JETP 90:646–654
27. Bergman DJ (1989) Electrical transport properties near a classical conductivity of percolation threshold. Phys A 157:72–88
28. Bergman DJ (1987) Scaling theory of the low-field Hall effect and magnetoresistance near a percolation threshold. Phys Rev B 56:983–990
29. Bergman DJ, Duering E, Murat M (1990) Discrete network models for the low-field hall effect near the percolation threshold: theory and simulation. J Stat Phys 58:1–43
30. Bergman DJ, Kantor Y, Stroud D, Webman I (1983) Critical behaviour of the low-field hall conductivity of a percolation threshold. Phys Rev Lett 50:1512–1515
31. Bergman DJ, Strelniker YM, Sarychev AK (1997) Recent advances in strong magneto-transport in a composite medium. Physica A 241:278–283
32. Duering E, Bergman DJ (1989) Critical behavior of the hall effect near the percolation threshold using a new network model. Phys A 157:125–129
33. Dykhne AM, Ruzin IM (1994) Theory of the fractional quantum Hall effect: The two-phase model. Phys Rev B 50:2369–2379
34. Einziger R (1987) Metal oxide varisters. Annu Rev Mater Sci 17:299–321
35. Landau LD, Lifshitz EM (1984) Electrodynamics of continuous media. 2nd ed. Vol 8. Butterworth-Heinemann, Oxford 460 p
36. Levinshtein ME, Shur MS, Efros AL (1975) Galvanomagnetic phenomena in disordered systems. Theory and simulation. Sov Phys JETP 42:1120–1124
37. Morozovsky AE, Snarskii AA (1989) Galvanomagnetic effects in macroscopically inhomogeneous films near the percolation threshold in an inclined magnetic field. Sov Phys Semicond 23:762–765
38. Rohde M, Mickltz H (1987) Critical behavior of the Hall conductivity near the percolation threshold in granular Sn: Ar mixtures. Phys Rev B pp 7289–7291
39. Sampsell JB, Garland JC (1976) Current distortion effects and linear magnetoresistance of inclusions in free-electron metals. Phys Rev B 13:583–589
40. Sarychev AK, Bergman DJ, Strelniker YM (1993) High-field magnetotransport in a percolation medium. Europhys Lett 21:851–857
41. Skal AS, Shklovskii BI (1974) Topology of infinite cluster in the theory of percolation and hopping conduction. Sov Phys Semicond 8:1586–1592 (in Russian)
42. Skal AS (1981) Calculation of Hall effect in models of theory of percolation. J DAN USSR 260:602–604
43. Skal AS (1982) Topology of a two-component disordered system below and above the percolation threshold. Phyl Mag B 45:335–346
44. Skal AS, Andreev AA, Tschirner HU (1982) Percolation theory and transport coefficient in disordered systems. Phyl Mag B 45:323–333
45. Skal AS (1985) Metal-isolator transition in models of percolation theory: Hall effect. Fizika solid state 27:1407–1413
46. Skal AS (1986) Critical behavior of the kinetic coefficients of anisotropic composites. Sov Phys JETP 63:1205–1209
47. Skal AS (1987) Percolation an anisotropic conductivity, the Hall effect and thermopower in disordered systems. J Phys C 20:245–259
48. Snarskii AA (1986) Effective conductivity of strongly inhomogeneous media near the percolation threshold. Sov Phys JETP 64:828–831
49. Stachoviak H (1970) Effective electric conductivity tensor of polycrystalline metals in high magnetic fields. Physica 45:481–499
50. Straley JP (1980) Exponent theory of the Hall effect and conductivity near the percolation threshold J Phys C 13:L773–L776

51. Straley JP (1980) Conductivity anisotropy and the Hall effect in inhomogeneous conductors near the percolation threshold. J Phys C 13:4335–4345
52. Straley JP (1988) Hall effect in percolating systems. Phys Rev B 38:11639–11642
53. Stroud D (1975) Generalized effective-medium approach to the conductivity of an inhomogeneous material. Phys Rev B 12:3368–3373
54. Stroud D, Pan FP (1976) Effect of isolated inhomogeneities on the galvanomagnetic properties of solids. Phys Rev B 13:1434–1439
55. Abrikosov AA (1988) Fundamentals of the theory of metals North-Holland, Amsterdam 630 p
56. Balagurov BYa (1986) Conductivity of inhomogeneous media in strong magnetic fields. Sov Phys Solid State 28:1694–1698
57. Dreizin YuA, Dykhne AM (1973) Anomalous conductivity of inhomogeneous media in a strong magnetic field. Sov Phys JETP 36:127–136

Chapter 13
Flicker-Noise (1/*f*-Noise)

13.1 Flicker-Noise in Inhomogeneous Media

When a direct electrical current flows through a conducting sample, voltage fluctuations can be observed. One of the main characteristics of such fluctuations is their spectral density. The basic definitions and noise measurement techniques are given in [26, 9]. Noise spectral density is a name for Fourier transform (spectrum) from the time-domain correlator of fluctuation

$$S_U = \{\delta U \delta U\}, \tag{13.1.1}$$

where $\{\delta U \delta U\}$ is taken to mean the Fourier image of the time-domain correlator

$$\begin{aligned} \{\delta U \delta U\} &= 4 \int_0^\infty \mathrm{d}(t_1 - t_2) \cos \omega(t_1 - t_2) \{U(t_1) - \langle U \rangle, U(t_2) - \langle U \rangle\}, \\ \{\delta U \delta U\} &= 4 \int_0^\infty \mathrm{d}(t_1 - t_2) \cos \omega(t_1 - t_2) \{\delta U(t_1) \delta U(t_2)\}, \end{aligned} \tag{13.1.2}$$

$$\delta U(t) = U(t) - \overline{U(t)}, \tag{13.1.3}$$

$\{\delta U(t_1), \delta U(t_2)\}$ is the double correlation function, dash above $\overline{U(t)}$ means averaging over time.

In the state of thermodynamic equilibrium, i.e., in the absence of current, noise spectral density is proportional to temperature and does not depend on frequency—it is the so-called Nyquist noise. Current flow causes additional (sometimes called surplus) noise, the noise spectral density of which is inversely proportional to frequency. Such a noise is called 1/*f*-noise (*f* is frequency designation in radio

A.A. Snarskii et al., *Transport Processes in Macroscopically Disordered Media*, DOI 10.1007/978-1-4419-8291-9_13

engineering), although often, apart from the above-mentioned term "surplus," it is referred to as flickering noise or current noise. At low frequencies, the amplitude of noise spectral density exceeds other kinds of noise, due to its inverse proportionality to frequency.

Voltage fluctuations $\delta U(t)$ at direct current or current fluctuations $\delta I(t)$ at direct voltage owe their origin to resistance fluctuations $\delta R(t)$ of the sample. The physical reason for such resistance fluctuations (noise spectral density is inversely proportional to frequency) has not been established. Here, we will use a phenomenological approach, rather than discuss these possible mechanisms for 1/*f*-noise origination. 1/*f*-noise was discovered in a large number of different effects: in biology, such as sugar fluctuations in blood, in road traffic, in stock exchange quotation fluctuations, and many other phenomena.

Instead of noise spectral density it is convenient to use the relative spectral density of fluctuations (of noise)—the RSD S:

$$\frac{\{\delta X \delta X\}}{X^2}, \quad X = J, U, R, \tag{13.1.4}$$

specifically the RSD of resistance takes the form

$$S = \frac{\{\delta R \delta R\}}{R^2}, \tag{13.1.5}$$

in doing so, the linear conduction region the RSD of current and voltage coincide with a good precision [see 26]

$$\frac{\{\delta R \delta R\}}{R^2} = \frac{\{\delta I \delta I\}}{I^2} = \frac{\{\delta U \delta U\}}{U^2}. \tag{13.1.6}$$

Instead of the RSD S, use is often made of the specific RSD C:

$$C = VS, \tag{13.1.7}$$

where V is sample volume.

The value C is also called local current density at point $\mathbf{r}$ to which volume V is constricted. Exactly this value characterizes 1/*f*-noise of given macroscopically inhomogeneous sample at given point, in particular, 1/*f*-noise of given phase.

Note that in going from the RSD value to specific RSD, one should multiply by the volume, rather than divide, as in the case of standard specific values. It is due to the fact that the larger is the volume where noise is measured, the smaller is the RSD.

Then, for each phase we will introduce its constant C characterizing this homogeneous material, thus, a sample of volume V will be characterized by the value $S = C/V$. In papers [14, 39, 40], an analogue of Kirchhoff's rules is given for

the calculation of S, parallel $S_{\|}$ and series S_n connections of resistances $r_1, r_2, \ldots$ with the RSD S_1 and $S_2 \ldots$ in the form

$$S_n = \sum_i \left(\frac{r_i}{r_n}\right)^2 S_i, \quad S_{\|} = \sum \left(\frac{r_{\|}}{r_i}\right)^2 S_i, \tag{13.1.8}$$

where $r_{\|}$ and r_n is a total resistance of series and parallel-connected resistances $r_1, r_2, \ldots$.

As long as in the measurement of the RSD of current (voltage) its value is proportional to square of current (voltage), full (effective) RSD S_e of a sample with arbitrarily connected resistances will be expressed through current moment (voltage moment) [38, 39]:

$$S_e = \frac{\sum S_i I_i^4 r_i^2}{\left(\sum I_i^2 r_i\right)^2} = \frac{\sum S_i U_i^4 / r_i^2}{\left(\sum U_i^2 / r_i\right)^2}, \tag{13.1.9}$$

where $I_i(U_i)$ is current (voltage drop) on the ith bond. The expression (13.1.9) can be written in terms of specific RSD C, current density, and field intensity [53, 11]:

$$C_e = \frac{\left\langle C(\mathbf{r})(\mathbf{E}(\mathbf{r})\mathbf{j}(\mathbf{r}))^2 \right\rangle}{\langle \mathbf{E}(\mathbf{r})\mathbf{j}(\mathbf{r})\rangle^2} = \frac{\langle C(\mathbf{r})\sigma^2(\mathbf{r})\mathbf{E}^4(\mathbf{r})\rangle}{\left(\sigma_e \langle \mathbf{E}(\mathbf{r})\rangle^2\right)^2} = \frac{\langle C(\mathbf{r})\rho^2(\mathbf{r})j^4(\mathbf{r})\rangle}{\left(\rho_e \langle j(\mathbf{r})\rangle^2\right)^2}, \tag{13.1.10}$$

where $\langle \ldots \rangle$ is average in the volume.

The expression (13.1.10) for the effective specific RSD C_e can be obtained as follows. From the determination of the effective conductivity in the form

$$\sigma_e = \frac{\langle \sigma E^2 \rangle}{\langle E \rangle^2}$$

follows the expression for fluctuation σ_e:

$$\delta\sigma_e(t_1) = \frac{\langle \delta\sigma E^2 \rangle}{\langle E \rangle^2} \equiv \frac{\frac{1}{V}\int d\mathbf{r}_1 \delta\sigma(\mathbf{r}_1, t_1) E^2(\mathbf{r}_1)}{\langle E \rangle^2}. \tag{13.1.11}$$

Whence

$$\frac{\{\delta\sigma_e(t_1)\delta\sigma_e(t_e)\}}{\sigma_e^2} = \frac{\left\{\frac{1}{V}\int d\mathbf{r}_1 \delta\sigma(\mathbf{r}_1, t_1) E^2(\mathbf{r}_1) \cdot \frac{1}{V}\int d\mathbf{r}_2 \delta\sigma(\mathbf{r}_2, t_2) E^2(\mathbf{r}_2)\right\}}{\left(\sigma_e \langle E \rangle^2\right)^2}. \tag{13.1.12}$$

Interchanging spatial and temporal $\{\ldots\}$ averaging and taking into account that conductivity fluctuations are δ-correlated in space, we obtain

$$\{\delta\sigma(\mathbf{r}_1, t_1)\delta\sigma(\mathbf{r}_1, t_2)\} \sim \delta(\mathbf{r}_1 - \mathbf{r}_2), \tag{13.1.13}$$

where $\delta(\ldots)$ is Dirac delta-function, from (13.1.12) we obtain (13.1.10).

Thus, the effective value of the RSD of 1/*f*-noise in the inhomogeneous medium is weighted with weight $C(\mathbf{r})$ and orthonornmalized square of the Joule heat release $Q = \mathbf{E} \cdot \mathbf{j}$. Therefore, the more inhomogeneous is the medium, the more inhomogeneous is Q distribution in it and according to the Cauchy inequality $\left(\langle E^2 j^2\rangle \geq \langle \mathbf{E} \cdot \mathbf{j}\rangle^2\right)$, the larger is C_e value at approaching the percolation threshold for p both larger and smaller than the value p_c.

Different models of 1/*f* noise considered in papers [4, 7, 33]. In the paper [36], a new model of 1/*f* noise in non-equilibrium stationary state was described as a product as effective noise of composite network consisting of two types of resistors (that associated with thermally activated processes of breaking and recovery). Monte Carlo approach was applied for explanation of concentration dependence of 1/*f* noise for nanotube films [7].

It is shown that 1/*f* noise in 3D electron glass connected with percolating phenomena [44].

Another recent area of study of non-equilibrium noise in percolation media is an area of shot noise experiments and models—see, for example [12, 20]. Application of anomalous diffusion on fractal media for explanation of shot noise considered in paper [20]. Experimental of 1/*f* noise in percolation structures considered in the following papers [15, 16, 37, 41, 49].

13.2 Flicker-Noise in Inhomogeneous Media—EMT-Approximation

For the RSD S_e, just as for the effective conductivity, the EMT-approximation can be constructed [38]:

$$\frac{S_e}{d} = p\frac{S_1 g_1^2 + (d-1)S_e g_e^2}{[g_1 + (d-1)g_e]^2} + (1-p)\frac{S_2 g_2^2 + (d-1)S_e g_e^2}{[g_2 + (d-1)g_e]^2}, \tag{13.2.1}$$

where $g_i = 1/r_i$ is conductance of the ith bond, g_e is conductance of the entire network of resistances, $d = 2, 3\ldots$ is problem dimensionality, and the effective conductance g_e is determined in the EMT-approximation.

Equation (13.1.11), linear in the desired value S_e, in terms of C_e (13.2.1) is of the form

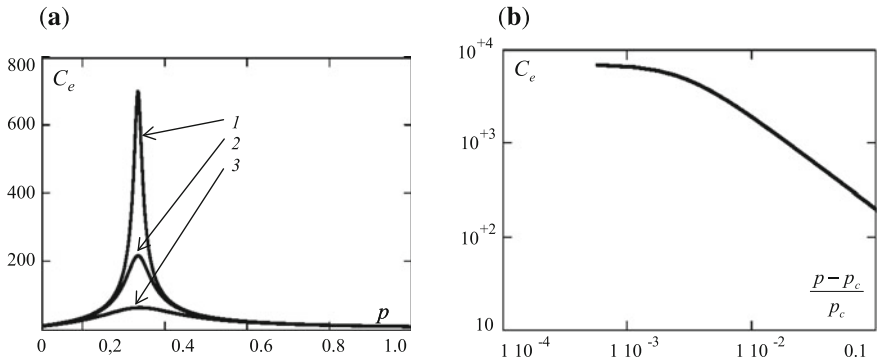

Fig. 13.1 Concentration dependence of specific RSD of 1/*f*-noise C_e for three-dimensional case within EMT-approximation: **a** view of C_e close to percolation threshold $p_c = 1/3$. Parameter values (in arbitrary units) $\sigma_2 = 1, C_1 = 1, C_2 = 10$, *1* $\sigma_1 = 10^2$, *2* $\sigma_1 = 10^3$, *3* $\sigma_1 = 10^4$; **b** view of C_e dependence on the proximity to percolation threshold above the percolation threshold

$$\frac{C_e}{d} = p\frac{C_1\sigma_1^2 + (d-1)C_e\sigma_e^2}{[\sigma_1 + (d-1)\sigma_e]^2} + (1-p)\frac{C_2\sigma_2^2 + (d-1)C_e\sigma_e^2}{[\sigma_2 + (d-1)\sigma_e]^2}, \tag{13.2.2}$$

Figure 13.1 shows concentration dependences C_e, obtained in the EMT-approximations. As is evident from Fig. 13.1, C_e increases on approaching the percolation threshold, and the maximum value $C_e(p_c)$ can exceed considerably the value C_1 and C_2 in the phases close to percolation threshold ($p_c = 1/3$ for the 3D case). The higher are the inhomogeneities, i.e., the larger is the σ_1/σ_2 value, the larger is $C_e(p = p_c)$. Representation of $C_e = C_e(p)$ dependence in a double logarithmic scale clearly shows the power dependence of $C_e = C_1|\tau|^{-k}$ on $\tau = (p - p_c)/p_c$, within the EMT-approximation $k = 1$. When p_c approaches smearing region, C_e saturation occurs. In [38] for the case of infinitely large inhomogeneity ($\sigma_2 = 0$) and for the region above the percolation threshold the critical index of 1/f noise within the EMT-approximation was obtained

$$C_e = C_1|\tau|^{-k}, \quad k_{EMT} = 1. \tag{13.2.3}$$

13.3 Flicker-Noise in Percolation Systems

In [54] based on the NLB-model authors considered cases above and below the percolation threshold. Above the percolation threshold at $\sigma_2 = 0$ for the critical index of noise k in [54] the following restrictions were obtained:

$$\mathrm{d}v + 1 - 2\zeta_R \le k' \le \mathrm{d}v - \zeta_R, \quad \zeta_R = t - (\mathrm{d}-2)v. \tag{13.3.1}$$

Below the percolation threshold at $1/\sigma_1 = 0$ we have

$$C_\mathrm{e} \sim |\tau|^{-k'}, \tag{13.3.2}$$

and according to [54] we get

$$\mathrm{d}v + 1 - 2\zeta_R \le k' \le \mathrm{d}v - \zeta_R, \quad \zeta_R = q + (\mathrm{d}-2)v. \tag{13.3.3}$$

Substitution of numerical values v, ζ_R, ζ_G from Table 5.1 into (13.3.1) and (13.3.3) yields the values

$$1.53 \le k_3 \le 1.6, \quad 0.38 \le k_3' \le 1.02. \tag{13.3.4}$$

Note that both (13.2.3) and (13.3.2) were obtained for the case of infinitely large inhomogeneity ($\sigma_1/\sigma_2 = \infty$). At the percolation threshold (in smearing region), the expressions for $C_\mathrm{e}(p > p_c)$ and $C_\mathrm{e}(p < p_c)$ must be equal to each other

$$C_\mathrm{e}(\tau = \Delta, p > p_c) \approx C_\mathrm{e}(|\tau| = \Delta, p < p_c), \tag{13.3.5}$$

and a contradiction immediately follows from (13.2.3) and (13.3.2), since according to (13.3.5) we have

$$C_1 \Delta^{-k} = C_2 \Delta^{-k'}, \tag{13.3.6}$$

and (13.3.6) suggests that the value of smearing region unlike the commonly accepted value $\Delta = (\sigma_2/\sigma_1)^{\frac{1}{t+q}}$ depends on the ratio C_2/C_1, rather than on σ_2/σ_1.

The second step of the HM will help to understand this contradiction and remove it [34]. As will be shown below, based on the HM, in the determination of critical behavior of C_e close to percolation threshold, of principal importance is account of finite conductivity of phases, and terms proportional to σ_2/σ_1 in C_e are not just small additions to the main expression, as in the case of σ_e.

Consider first the case above the percolation threshold and use the second HM step (see Fig. 5.13b). According to percolation structure model (see Fig. 5.13b) it can be written

$$C_\mathrm{e} = \frac{C_1 j_1^2 E_1^2 \frac{V_1}{V} + C_2 j_2^2 E_2^2 \frac{V_2}{V}}{\sigma_\mathrm{e}^2 \langle E \rangle^4}, \tag{13.3.7}$$

where index 1 refers to the bridge ($V_1 = a_0 N_1 a_0^2$ is bridge volume), and index 2 to the interlayer ($V_2 = a_0^2 N_2 a_0$ is interlayer volume), $V = \xi^3$.

Currents and fields are simply related to potential difference $\Delta\varphi$ at the ends of a sample with characteristic size ξ:

$$j_1 = \frac{\Delta\varphi}{R_1 a_0^2}, \quad E_1 = \frac{\Delta\varphi}{L_1}, \quad j_2 = \frac{\Delta\varphi}{R_2 N_2 a_0^2}, \quad E_2 = \frac{\Delta\varphi}{a_0}, \tag{13.3.8}$$

where $L_1 = a_0 N_1$ is bridge length, $N_2 a_0^2$ is interlayer area.

From the expressions (13.3.7) and (13.3.8) ($\sigma_e = \sigma_2 |\tau|^{-q}$) immediately follows [33, 34]:

$$C_e(p > p_c) = C_1 |\tau|^{-k} + C_2 h^2 |\tau|^{-w}, \quad h = \frac{\sigma_2}{\sigma_1} \ll 1, \quad p > p_c, \tag{13.3.9}$$

with the following critical index values:

$$k_3 = 4\nu_3 - t_3, \quad w_3 = q_3 + 2(\nu_3 + t_3). \tag{13.3.10}$$

Generalization for the d-dimensional case results in the expressions

$$k = 2\nu(d-1) - t, \quad w = q + 2(\nu + t). \tag{13.3.11}$$

The expression for 1/*f*-noise below the percolation threshold is found in a similar fashion [33, 34, 50]:

$$C_e(p < p_c) = C_2 |\tau|^{-k'} + C_1 h^2 |\tau|^{-w'}, \tag{13.3.12}$$

where

$$k' = 2\nu - q, \quad w' = 2q + t + 2\nu(d-1). \tag{13.3.13}$$

It is worthy to note that in the expressions for the effective conductivity the additional components are proportional to h and, for example, at $p > p_c$, $\sigma_e = \sigma_1 \tau^t + \sigma_1 h \cdot |\tau|^{-q} + \cdots$. are small additions, whereas similar components in (13.3.9) and (13.3.12), proportional to h^2, can be both much lower and much larger than the first component depending on the ratio C_1/C_2. Thus, if in the first inhomogeneity approximation the effective conductivity both above $\sigma_e \approx \sigma_1 \tau^t$ and below $\sigma_2 \approx \sigma_2 |\tau|^{-q}$ the percolation threshold is described by the first HM step, then the RSD of 1/*f*-noise C_e calls for account of the second HM step, and then the expressions (13.3.9) and (13.3.12) will serve as the first inhomogeneity approximation. Subsequent terms, now really always minor (beyond smearing region) as compared to the basic ones, could be obtained by the analysis of subsequent HM steps.

The expressions $C_e(p > p_c)$ (13.3.9) and $C_e(p < p_c)$ (13.3.12) allow consistent determination of the RSD of 1/*f*-noise in smearing region. Just like for σ_e, in smearing region the equality (13.3.5) should be met. Substituting (13.3.9) and (13.3.12) into (13.3.5) we get

$$C_1\Delta^{-k} + C_2h^2\Delta^{-w} = C_2\Delta^{-k'} + C_1h^2\Delta^{-w'}, \tag{13.3.14}$$

which yields two equations for the determination of Δ:

$$\Delta^{-k} = h^2\Delta^{-w'},\ h^2\Delta^{-w} = \Delta^{-k'}. \tag{13.3.15}$$

In turn, these two equations result, as they must, in identical values for smearing region Δ that coincide with the standard:

$$\Delta = h^{\frac{2}{w'-k}} = h^{\frac{2}{w-k'}} = h^{\frac{1}{t+q}}.$$

Note that compatibility of equation system (13.3.15) is only possible under quite certain relation between the four critical indices of 1/*f*-noise—k, k', w, w':

$$w - k' = w' - k. \tag{13.3.16}$$

Moreover, from the condition of compatibility of equation systems (13.3.15) and (13.3.16) follows a relation between certain combinations of critical indices of 1/*f*-noise and the so-called scaling factor $\varphi = t + q$

$$\frac{w - k'}{2} = \frac{w' - k}{2} = \varphi, \tag{13.3.17}$$

scaling relations similar to those mentioned above are given in [29].

Relations (13.3.16) and (13.3.17) do not depend on the model used and, thus, on the specific values k, k', w, w' that are different in different models and approximations.

Substitution of Δ into (13.3.9) or (13.3.12) results in the expression for the RSD of 1/*f*-noise in smearing region in the following form

$$C_e(\Delta) = C_1h^{-\omega} + C_2h^{-\omega'}, \tag{13.3.18}$$

where

$$\omega = 2\frac{k}{w - k'} = \frac{k}{t+q}, \quad \omega' = 2\frac{k'}{w - k'} = \frac{k'}{t+q}. \tag{13.3.19}$$

In the framework of the HM with regard to (13.3.117) and (13.3.13) we have

$$\omega = \frac{2\nu(d-1) - t}{t+q}, \quad \omega' = \frac{2\nu - q}{t+q}. \tag{13.3.20}$$

For the two-dimensional case ($t_2 = q_2 \approx \nu_2$), at the percolation threshold we write down

$$\omega_1 = \omega_2 = \frac{2v_2 - t_2}{2t_2} \approx \frac{1}{2}. \tag{13.3.21}$$

Relative contribution to the RSD of 1/*f*-noise depends only on the ratio between the RSD of 1/*f*-noise in phases and is independent of the value σ_2/σ_1:

$$C_e(\Delta) = (C_1 + C_2)h^{\frac{2v_2 - t_2}{2t_2}} \approx (C_1 + C_2)\sqrt{h}, \quad (2D) \tag{13.3.22}$$

From the analysis of expressions for C_e above (13.3.9) and below (13.3.12) the percolation threshold, it follows that there is a possible set of parameters, such that beyond smearing region the dominant contribution will be provided by the second term (Fig. 13.2) [29, 34]. For instance, above the percolation threshold for $C_2/C_1 \gg h^{(k-k')/(t+q)}$ and $\tau_c = \left(h^2 C_2/C_1\right)^{\frac{1}{w-k}}$ for the concentration range of good conducting phase $\Delta \ll \tau < \tau_c$ the critical index k is replaced by w (Fig. 13.2a), and below the percolation threshold for $C_2/C_1 \ll h^{(k-k')/(t+q)}$ and $\tau_c' = -(h^2 c_1/c_2)^{\frac{1}{w'-k'}}$ in the concentration range $|\tau| < |\tau_c'|$ the critical index k' is replaced by w'. The values τ_c and τ_c' can be calculated directly from (13.3.9) and (13.3.12).

Thus, in the measurement or numerical simulation, on approaching the percolation threshold, at $p > p_c$ critical index k' can be replaced by w' [33, 34] and k—by w [33, 34, 50]. Really, in some papers dedicated to experimental studies, one can come across critical indices: in the two-dimensional case $k_2/t_2 \approx 6.27 \pm 0.08$ [32], and in the three-dimensional case $k_3/t_3 \approx 5 \pm 1$ [13], that are close to w_2/t_2 and w_2'/t_2.

Table 13.1 lists the numerical values of critical indices obtained by numerical simulation and theoretical methods. A detailed discussion of the experimental data will take place after the description of critical behavior of 1/*f*-noise in the so-called Swiss Cheese media [21].

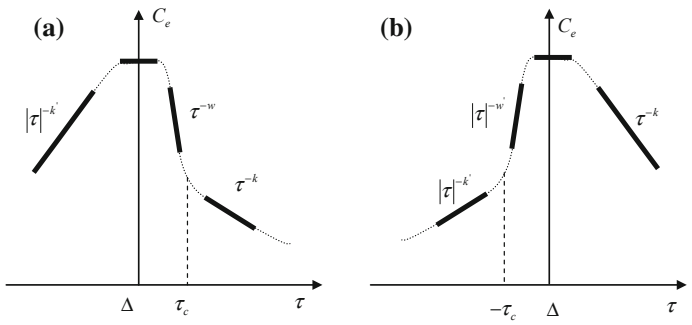

Fig. 13.2 Schematic representation of concentration dependence $C_e = C_e(\tau)$ in the double logarithmic range for two special cases: **a** above the percolation threshold; **b** below the percolation threshold

Table 13.1 The numerical values of critical indexes obtained by numerical simulation and theoretical methods

Critical index	Numerical value according to the HM [33, 34]	Exact boundary according to [54]	Numerical simulation
k_3	1.52	$1.4 \le k_3 \le 1.52$	1.47 [28], 1.57 ([3]) 1.58 [17], 1.49 [51] 1.58 [30]
k_3'	1.03	$0.42 \le k_3' \le 1.03$	0.55 [30], 0.58 [51] 0.68 [52]
$k_2 = k_2'$	1.37	$1.07 \le k_2 \le 1.37$	1.12 [39]
w_3	6.49		
w_3'	6.98		
$w_2 = w_2'$	6.57		
k_6	2	$2 \le k_6 \le 2$	2.06 ± 0.08 [2]
k_6'	1	$0 \le k_6' \le 1$	
w_6	7		
w_6'	7		
$\omega_2 = \omega_2'$	0.53		
ω_3	0.56		
ω_3'	0.38		

Note Exact boundaries [54]: $\mathrm{d}v + 1 - 2\zeta_R \le k \le \mathrm{d}v - 3\zeta_R, \mathrm{d}v - 1 - 2\zeta_R \le k' \le \mathrm{d}v - \zeta_R$

Note that the numerical values of indices k, k', w, w' and their exact boundaries in Table 13.1 were calculated in conformity with the use of "canonical" values of t, q and v, therefore, they are slightly different from those in [54].

13.4 Abnormally High Rate of Flicker-Noise in Self-dual Media

As it follows from the determination of the RSD of 1/*f*-noise (13.1.10), it is expressed through the fourth moment of electric current density or electric field intensity. For σ_e, which, in turn, is expressed through the second moment, there exists a universal expression for self-dual media (the Dykhne formula $\sigma_e = \sqrt{\sigma_1 \sigma_2}$). However, it can be easily shown than for the RSD of 1/*f*-noise as a more "intrinsic" characteristic depending on the fourth moment, there is no such relation. And, the expressions for C_e are different, for instance, for randomly inhomogeneous medium and self-dual medium with a checkerboard structure. The effect of "microgeometry" on the RSD of 1/*f*-noise was considered for some cases in [8]. Here we will consider a case of checkerboard type medium.

Paper [18] deals with 1/*f*-noise in the medium having a checkerboard structure, with D-point as its main element (Chap. 6)—Fig. 6.3. In [47] it was shown that the

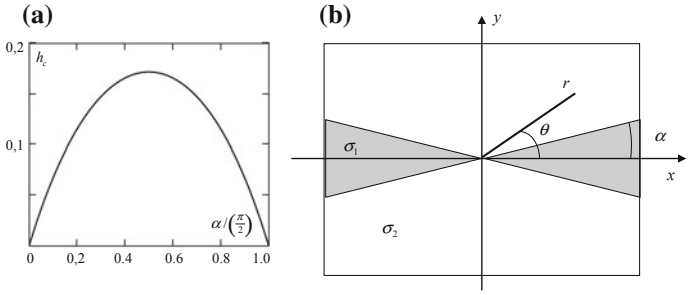

Fig. 13.3 Dependence $h_c = h_c(\alpha)$ (**a**) and location of phases close to D-point (**b**)

main Joule heat $\mathbf{E} \cdot \mathbf{j}$, the more so its square $(\mathbf{E} \cdot \mathbf{j})^2$, is released in the vicinity of D-point. The distribution of $\varphi(r, \theta)$ potential close to D-point (Fig. 13.3) is found similar to the way it was done for current trap in a two-dimensional polycrystalline medium:

$$\begin{aligned} \varphi_1(r, \theta) &= A_1 r^m \cos m\theta, \\ \varphi_2(r, \theta) &= A_2 r^m \sin\left[m\left(\frac{\pi}{2} - \theta\right)\right], \end{aligned} \tag{13.4.1}$$

where indices 1 and 2 are related to the first (σ_1) and second (σ_2) phases, while constant m and a relation between A_1 and A_2 are found from the boundary conditions.

At the phase boundaries, i.e., at $\theta = \pm\alpha$ there should be met the potential continuity

$$\varphi_1(r, \theta = \pm\alpha) = \varphi_2(r, \theta = \pm\alpha), \tag{13.4.2}$$

and the continuity of current components normal to phase boundary

$$j_{\theta 1}(r, \theta = \pm\alpha) = j_{\theta 2}(r, \theta = \pm\alpha), \tag{13.4.3}$$

where

$$j_{\theta k}(r, \theta) = \sigma_k E_\theta(r, \theta) = -\sigma_k \frac{1}{r} \frac{\partial \varphi_k}{\partial \theta}, \quad k = 1, 2. \tag{13.4.4}$$

Substitution of (13.4.1) into (13.4.3) and (13.4.4) leads to expressions

$$\mathrm{tg}(m\alpha)\mathrm{tg}\left[m\left(\frac{\pi}{2} - \alpha\right)\right] = \frac{\sigma_2}{\sigma_1}, \tag{13.4.5}$$

$$\sigma_1 A_1 r^m m \sin(m\alpha) = \sigma_2 A_2 m r^m \cos\left[m\left(\frac{\pi}{2}\right) - \alpha\right]. \tag{13.4.6}$$

Thus, according to (13.4.5) each value of σ_2/σ_1 ratio is matched by its own value of m parameter, and condition (13.4.6) allows expressing A_2 through A_1. With regard to (13.4.5) and (13.4.6), the square of electric field intensity in the first phase is equal to

$$E_1^2 = E_{r1}^2 + E_{\theta 1}^2 = \left(\frac{\partial \varphi_1}{\partial r}\right)^2 + \left(\frac{1}{r}\frac{\partial \varphi_1}{\partial \theta}\right) = A_1^2 m^2 r^{2(m-1)}. \tag{13.4.7}$$

E_2^2 is exactly of the same form, but with A_2 substituted for A_1. As long as the RSD of 1/*f*-noise C_e is proportional to $\int E^4 dV$ where $dV = 2\pi r\, dr$, from (13.4.5) it follows that

$$C_e \sim \int_0^a \frac{dr}{r^{3-4m}}. \tag{13.4.8}$$

Here, a is a size of the order of medium "box" size. As can be seen from (13.4.8), at

$$m \geq m_c = \frac{1}{2}, \tag{13.4.9}$$

the integral (13.4.8) becomes divergent which means an abnormal growth of 1/*f*-noise.

According to (13.4.5), for each angle α there exists such value $h_c = (\sigma_2/\sigma_1)_c$, whereby for $h < h_c$ the integral (13.4.8) becomes divergent and the amplitude of 1/*f*-noise C_e becomes abnormally large. Dependence $h_c = h_c(\alpha)$ is shown in Fig. 13.3, *a*, where $h_c = \mathrm{tg}(m_c\alpha)\mathrm{tg}[m_c(\pi/2 - \alpha)] = \sigma_2/\sigma_1$ and $m_c = 1/2$. In Fig. 13.3a, an area is separated where the amplitude of 1/*f*-noise is abnormally large. For a medium with checkerboard structure $(\alpha = \pi/2, h_c(\pi/2) = 0.172)$.

13.5 Flicker-Noise in the Systems with Exponentially Broad Spectrum of the Resistances

Consider now the RSD of 1/*f*-noise in the systems with exponentially wide resistance spectrum [35]. The results of such measurements are given in [10]. In this paper, the percolation effects in systems with such 1/*f*-noise have been called quantum percolation.

To determine the RSD of 1/*f*-noise, one should first formulate an assumption similar to the Houge hypothesis, i.e., assign the dependence of C on local conductivity σ. In Chap. 8, for the local resistance and conductivity it was assumed

$$r(x) = r_0 e^{-\lambda x}, \quad \sigma(x) = \sigma_0 e^{\lambda x}, \quad \lambda \gg 1, \tag{13.5.1}$$

where x is random variable uniformly distributed in the range [0,1].

According to the Houge hypothesis, $C \sim 1/n$, where $n(x)$ is current carrier concentration. As long as generally the specific conductivity $\sigma \sim n$, here the following hypothesis will be assumed:

$$C(x) = \frac{\alpha}{\sigma(x)}, \quad \alpha = \text{const}. \tag{13.5.2}$$

The RSD of 1/*f*-noise is calculated similar to σ_e in the systems with exponentially wide spectrum of properties (Chap. 8)—one should calculate the RSD of 1/*f*-noise of the bridge and interlayer in smearing region.

For the bridge according to (13.1.8) we have

$$S_1 = \sum \left(\frac{r(x)}{r_e}\right)^2 S(x), \tag{13.5.3}$$

where the sum is taken over all the bonds in the bridge, and according to (13.5.2) for the three-dimensional case, we will get

$$S(x) = \alpha \frac{r(x)}{a_0^2}. \tag{13.5.4}$$

Thus,

$$S_1 \sim \alpha \frac{\sum r^3(x)}{r_e^2} = \alpha \frac{N_1 \langle r^3 \rangle_1}{r_e^2}, \tag{13.5.5}$$

$\langle \ldots \rangle_1$ is calculated just as in Chap. 8 (8.2.3):

$$\langle r^3 \rangle_1 = \int_{x_1}^{1} r^3(x) P(x) \mathrm{d}x = \frac{r_0^3}{3(1-x_1)\lambda}\left(e^{-3\lambda x_1} - e^{3\lambda}\right) \approx \frac{r_1^3 e^{-3\lambda x_1}}{3(1-x_1)\lambda}, \tag{13.5.6}$$

$$x_1 = x_c + (1 - x_c)\Delta,$$

where Δ is the size of smearing region (8.2.14).

Substituting Δ into expressions (13.5.6) and (13.5.6) into (13.5.5), we find

$$S_1 \sim \alpha r(x_c) \lambda^{2 - \frac{3\alpha_1 + \alpha_2}{2}}, \tag{13.5.7}$$

or, passing from S_1 to specific characteristic, we have

$$C_1^e \sim \alpha r(x_c)\lambda^{2-\frac{3\alpha_1+\alpha_2}{2}+vd}. \tag{13.5.8}$$

The RSD of 1/*f*-noise of the interlayer is calculated in a similar fashion:

$$S_2 = \sum \left(\frac{r_e}{r(x)}\right)^2 S(x) \sim r_e^2 \sum \frac{1}{r(x)} = r_e^2 N \left\langle \frac{1}{r} \right\rangle_2. \tag{13.5.9}$$

Whence

$$S_2 \sim \alpha r(x_c)\lambda^{\frac{\alpha_1-\alpha_2}{2}}, \quad C_2^e \sim \alpha r(x_c)\lambda^{\frac{\alpha_1-\alpha_2}{2}+vd}. \tag{13.5.10}$$

Within both the NLB-model ($\alpha_1 = \alpha_2 = 1$) and in the HM ($\alpha_1 = \xi_R, \alpha_2 = \xi_G$) we write down

$$\frac{\alpha_1 - \alpha_2}{2} > 2 - \frac{3d_1 + d_2}{2}. \tag{13.5.11}$$

Thus, in the systems with exponentially wide resistance spectrum, 1/*f*-noise in smearing region is always larger in the interlayer than in the bridge, i.e., it determines the noise in the whole system

$$C_e \sim \frac{1}{\sigma} e^{-\lambda x_c}\lambda^m = \frac{\lambda^{2v}}{\sigma_e}, \tag{13.5.12}$$

$$m = \frac{\alpha_1 - \alpha_2}{2} + vd. \tag{13.5.13}$$

Within the NLB-model we have

$$m_{\text{NLB}} = vd, \quad d = 2, 3, \ldots. \tag{13.5.14}$$

Within the HM

$$m = \frac{t-q}{2} + 2v, \quad d = 2, 3, \ldots. \tag{13.5.15}$$

In [31], a numerical simulation on cubic network was conducted. The value of index $m - 2y$ was calculated, which proved to be equal to 0.78 ± 0.09, which is closer to (13.5.14) $m_{\text{NLB}} - 2y_{\text{NLB}} = 0.88$ than to (13.5.15) $m_{\text{иМ}} - 2y_{\text{иМ}} = 1.12$. It means that in the calculation of the second moments of current distribution the decisive contribution is made exactly by SDCB-"single disconnected bonds," the number of which in the interlayer $N_2 \sim \tau^{-1}$ [54]. Qualitatively, this conclusion can be explained as follows. As was previously described in Sect. 5.4 (see Figs. 5.11 and 5.12), the difference of the HM from the NLB-model lies in selecting N_1—the

number of bonds in the bridge and N_2—in the interlayer. In the NLB,N_1 and N_2 are SCB- and SDCB-bonds. If, as a result of this approach, when calculating the effective conductivity one takes into account only such bonds in the bridge and the interlayer, critical indices of conductivity t and q will be only approximately equal to their values established in numerical and field experiments.

In reality, in a bridge even the major element of percolation structure, one can come across twice and three times of paralleled bonds. Such bridge construction becomes too complicated for calculations. In the HM this complicated bridge is replaced (approximately) by a simple one, where all paralleled bonds are replaced by certain number of SCB, the total number of SCB being selected equal to $N_1 \sim \tau^{\xi_R}$, i.e., such that in the calculation of σ_e one could get the predetermined (canonical) value of critical index t.

A similar substitution takes place in the other element of percolation structure—the interlayer. Apart from SDCB (single disconnected bonds of small conducting phase), it comprises elements with two, three … bonds. In the HM these elements are taken into account and replaced by a certain number of "single" ones, such that full number of "single" elements be already not $N_2 \sim \tau^{-1}$, like in the NLB-model, and $N_2 \sim \tau^{\xi_G}$, such that critical index of the effective conductivity below the percolation threshold q be equal to canonical value.

For two-phase systems, when each conducting bond has resistance r_1, and bad conducting bond—r_2, such HM approach allows in many cases sufficiently precise calculation of critical indices. For systems with exponentially wide spectrum of resistances the situation is more difficult. While in the calculation of y—critical index of pre-exponential factor in the effective conductivity—the HM approach "works" (i.e., these predictions are more precise than in the NLB-model), in the calculation of higher current moments this is no longer the case. Even in smearing region the bridge and interlayer resistances are considerably different. And then two series couples of parallel-connected resistances in a bridge cannot be reduced to one resistance r_1, since in each couple the resistance values are considerably different and only one of them is essential for passing of the current. However, in the interlayer, one of the two series-connected resistances will be much larger than the other, and these couples have to be discarded from the interlayer, and only SDCB with $N_2 \sim \tau^{-1}$ remain, as accepted in the NLB-model.

Thus, the result of numerical simulation [31] allows one to assume that current-carrying cluster in systems with exponentially wide spectrum of resistance distribution on consideration of the fourth (and, probably, higher) current moment is different from that in two-phase systems.

Coming back to the expression for the RSD of 1/*f*-noise C_e (13.5.12), note that local Houge hypothesis assumed in (13.5.2) is not longer fulfilled for the entire sample:

$$C_e \sigma_e \sim \lambda^{2v} \gg 1. \tag{13.5.16}$$

In papers [27, 48] it was shown that in a number of cases local values of C in tunnel junctions may not depend on σ_1, i.e., instead of the Houge hypothesis (13.5.2) holds

$$C(x) \approx \frac{\alpha}{\sigma(x)^{\theta}}, \theta \to 0. \tag{13.5.17}$$

In paper [45], the RSD of 1/*f*-noise was calculated for systems with exponentially wide spectrum of resistance distribution, when (13.5.17) is met for the local noise. Calculations similar to those given above yield the expression

$$C_{\mathrm{e}} \sim \left(\sigma_0 \mathrm{e}^{\lambda x_c}\right)^{-\theta} \lambda^{m_\theta}. \tag{13.5.18}$$

It turned out that in the range $0<\theta<2$ critical index is universal, i.e., independent of parameter θ:

$$m_\theta = \nu d, \quad 0<\theta<2. \tag{13.5.19}$$

This theoretical conclusion is proved by numerical simulation (in more detail see in [45, 46]).

It is interesting to note that though $C_{\mathrm{e}}(\theta = 1)$ exponentially is considerably different from $C_{\mathrm{e}}(\theta = 0)$, for instance, at $\lambda \approx 30$ and $x_c = 0.75$, we have

$$\frac{C_{\mathrm{e}}(\theta = 0)}{C_{\mathrm{e}}(\theta = 1)} = \mathrm{e}^{\lambda x_c} \sim 10^9, \tag{13.5.20}$$

index m_θ both according to theory and the numerical calculation results remains the same.

The problem of calculation of current distribution in a system with exponentially wide spectrum of resistance distribution describes not only hopping conduction in doped semiconductors. To this problem, for example, is reduced the problem of properties of semiconductors with large-scale potential relief $V(\mathbf{r})$ modulating the bottom of conduction band [42, 43]. To solve the problem of determination of σ_{e} and RSD of 1/*f*-noise C_{e} in such semiconductors, one should first of all know the resistance of the bridge and the interlayer. Second, unlike the approach given above, it has specific features close to Swiss Cheese-media (Chap. 7), since in each of resistances that enter the bridge and the interlayer, current flows through passes in potential relief and its distribution in such passes is nonuniform. Account of this non-uniformity, similar to the way it happens, for instance, in the "necks" in Swiss-Cheese-problem, leads to renormalization of critical index y of effective conductivity [5] with addition of summand 1/2:

$$\sigma_{\mathrm{e}} = \sigma(x_c)\lambda^{-y}, \quad y = \frac{\alpha_1 - \alpha_2}{2} + \nu(d-2) + \frac{1}{2}, \tag{13.5.21}$$

where $\lambda = 2V_0/(KT) \gg 1, V_0$, is energy parameter determining large-scale potential $V(\mathbf{r})$ close to saddle value:

$$V(\mathbf{r}) = V_S + \frac{V_0}{b}\left(-x^2 + y^2 + z^2\right), \tag{13.5.22}$$

and V_S is pass height, b is spatial scale.

On meeting the Houge hypothesis $C(\mathbf{r}) = \alpha/n(\mathbf{r})$ with regard to current inhomogeneities on the passes, we get

$$C_e = \frac{\alpha}{n_c}\left(\frac{V_0}{KT}\right)^{\gamma}, \quad \gamma = \frac{3}{2} + m, \tag{13.5.23}$$

where m is the same as in (13.5.13), (13.5.14) is critical index of the RSD of 1/*f*-noise without account of current non-uniformity in each of the passes, constant 3/2 renormalizing critical index m is related exactly to this account; n_c is concentration of free carriers on the main (key) pass that determines $r(x_c)$.

In addition to the above, in [6] authors consider passes having two energy parameters instead of one.

13.6 Flicker-Noise for Fluctuation of Phase Concentration

Unexpected "percolation" mechanism of the RSD of 1/*f*-noise was discovered in high-quality thin superconducting films. In the works [22] (see also [19, 24, 25, 23]) when measuring 1/*f*-noise on the high-quality thin films in superconducting state there were obtained critical indices λ and λ' exceeding critical indices k and k' (Table 13.2).

In the superconducting state, the conductivity in high-quality thin films is described as the conductivity of a net of Josephson contacts interconnecting superconducting grains. Each of Josephson contacts has its own value of critical current I_c such that on passing current $I < I_c$ through the contact it is superconducting (no voltage drops on it), and at $I > I_c$ the contact is a conventional resistance. The value I_c is directly proportional to bond energy [1]. Temporal fluctuations of bond energy lead to fluctuations of the number of Josephson contacts

Table 13.2 Critical indices for bulk media k, k' and for thin superconducting films λ, λ'

Problem dimensionality	k	k'	$\frac{k}{t}$	$\frac{k'}{q}$	$\lambda = \frac{2}{t}$	$\lambda' = \frac{2}{q}$
2D	1.37	1.37	1.05	1.05	1.54	1.54
3D	1.52	1.03	0.76	1.41	1.0	2.74

in the sample, i.e., to fluctuation of superconducting phase concentration. For instance, below the percolation threshold $(p<p_c)$ we have

$$\rho_e \sim |p - p_e|^q. \tag{13.6.1}$$

Whence

$$\delta\rho_e = \frac{\partial\rho_e}{\partial p}\delta p \sim \rho_e^{1-\frac{1}{q}}\delta p(t), \tag{13.6.2}$$

And for the RSD of 1/*f*-noise we get

$$C_e = \frac{\{\delta\rho_e\delta\rho_e\}}{\rho_e^2} \sim \rho_e^{-\frac{2}{q}}\{\delta p\delta p\}, \quad p<p_c. \tag{13.6.3}$$

Thus, a new critical index λ' related to fluctuation of superconducting phase concentration is of the form

$$\lambda' = \frac{2}{q}. \tag{13.6.4}$$

The critical index above the percolation threshold is found similarly

$$\lambda = \frac{2}{t}. \tag{13.6.5}$$

As is evident from Table 13.2, for instance, in the three-dimensional case, below the percolation threshold $\lambda'_3 = 2.74$, which is twice as large a $k'_3/q_3 = 1.41$. The resulting critical indices λ' and λ are in good agreement with the experimental data, for instance, [23].

References

1. Abrikosov AA (1988) Fundamentals of the theory of metals. North-Holland, Amsterdam, 630 p
2. Balberg I, Wagner N, Hearn DW, Ventura JA (1988) Computer study of the electrical noise on high-dimensional percolating systems. Phys Rev B 37:3829–3831
3. Balberg I (1987) Recent developments in continuum percolation. Balberg I Phil Mag 56:991–1003
4. Bardhan KK, Mukherjee CD (2002) Finite coherence length of thermal noise in percolating systems. Phys Rev B 65:212302-1–212302-4 (2002)
5. Baskin EM, Morozovskii AE, Snarskii AA (1994) Anomalously high 1/f noise in a nonuniform semiconductor Sov. Phys JETP Lett 60:15–18
6. Baskin EM et al (1997) Effective properties for systems with distributed resistances in continuum space. Phys Rev B 56:11611–11618

7. Behnam A, Bosman G, Ural A (2008) Percolation scaling of 1/f noise in single-walled carbon nanotube films. Phys Rev B 78:085431-1–085431-9
8. Bergman DJ (1989) Nonlinear behaviour and 1/f noise near a conductivity threshold: effects of local microgeometry. Phys Rev B 39:4598–4609
9. Bochkov GN, Kuzovlev YuE (1983) New aspects in 1/f noise studies. Phys Usp 26:829–844
10. Breeze AJ, Carter SA, Alers GB, Heanney MB (2000) 1/f noise through the metal-nonmetal transition in percolating composites. Appl Phys Lett 76:592–594
11. Butterweck H (1975) An exact formula for the effects of resistor geometry on current noise. Philips Res Rep 30:316
12. Camino FE, Kuznetsov VV, Mendez EE (2003) Hopping conductivity beyond the percolation regime probed by shot-noise measurements. Phys Rev B 68:073313-1–073313-4
13. Chen CC, Chon YC (1985) Electrical conductivity fluctuation near the percolation threshold. Phys Rev Lett 54:2529–2532
14. Cohn RM (1950) The resistance of an electrical network. Proc Am Math Soc 1:316–324
15. Conrad BR, Cullen WG, Yan W et al (2007) Percolative effects on noise in pentacene transistors. Appl Phys Lett 91:242110-1–242110-13
16. Deville G, Leturcq R, L'Hote D et al (2006) 1/*f* noise in low density two-dimensional hole systems In GaAs. Physica E 34:252–255
17. Duering E, Bergman DJ (1990) Current distribution on a three-dimensional, bond-diluted, random-resistor network at the percolation threshold. J Stat Phys 60:363–381
18. Dykhne AM (1990) Theoretical Physics Institute, University Minnesota, Prep. TPI-MINN-90/59-T
19. Forgacs G, Schulman LM, Kiss LB, Svedlindh P, Lundgren L (1991) Methods for determining the distribution of Josephson coupling energies in high-Tc superconductors. Phys C 177:67–72
20. Groth CW, Tworzyd J, Beenakker CWJ (2008) Electronic shot noise in fractal conductors. Phys Rev Lett 100:176804-1–176804-6
21. Halperin BI, Feng S, Sen PN (1985) Differences between lattice and continuum percolation transport exponents. Phys Rev Lett 54:2391–2394
22. Kiss LB, Svedlindh P (1993) New noise exponents in random conductor-superconductor and conductor-insulator mixtures. Phys Rev Lett 71:2817–2820
23. Kiss LB, Svedlindh P (1994) Noise in high Tc superconductors. IEEE Trans Electron Devices 41:2112–2122
24. Kiss LB, Svedlindh P, Lundgren L, Hunder J, Ohlsen H, Stolt L, Gingl Z (1991) Scaling spontaneous fluctuations in high-Tc superconductor films. Physica B 172:441–444
25. Kiss LB, Larsson T, Svedlindh P, Lundgren L, Ohlsen H, Ottsson M, Hunder J, Stolt L (1993) Conductance noise and percolation in $YBa_2Cu_3O_7$ thin films. Physica C 207:318–332
26. Kogan SM (1985) Low-frequency current noise with a 1/f spectrum in solids. Phys Usp 28:170–195
27. Kogan SM, Nagaev KE (1984) Noise in tunnel junctions due to two-level system in dielectric layer. Sov Tech Phys Lett 19:132–134
28. Kolek A, Kusy A (1988) Critical exponents for conductance and 1/f noise in discrete-lattice percolation. J Phys C 21:L573–L578
29. Kolek A (1992) Multifractality and 1/f noise in the two-component random resistor network. Phys Rev B 45:205–208
30. Kolek A (1992) 1/*f* noise in binary random mixtures. Int J Electron 73:1095–1097
31. Kolek A, Snarskii AA, Morozovskii AE (1995) Structure of the percolation cluster and excess 1/f noise in systems with an exponentially broad spectrum of resistances. Sov Phys JETP 81:490–495
32. Mantese JV, Webb WW (1985) 1/f noise of granular metal-insulator composites. Phys Rev Lett 55:2212–2215
33. Morozovsky AE, Snarskii AA (1988) Critical behaviour of 1/f noise in percolation systems. Preprint IMF AN USSR, 31.88, p 15 (in Russian)
34. Morozovsky AE, Snarskii AA (1989) Critical behaviour of 1/f noise in percolation systems. Sov Phys JETP 68:1066–1069

35. Morozovsky AE, Snarskii AA (1993) Percolation description of the conductivity of random networks with a broad spectrum of the distribution of resistances. Sov Phys JETP 77:959–965
36. Pennetta C, Alfinito E, Reggiani L (2007) 1/f noise and long-term correlations in multi-species resistor networks. In: Tacano M, Yamamoto Y, Nakao M (eds) Proceedings of 19th international conference on noise and fluctuations (ICNF), Tokyo, 9–14 September 2007, AIP conference proceedings series 922, 431
37. Podzorov V, Uehara M, Gershenson ME et al (2000) Giant 1/f noise in perovskite manganites: evidence of the percolation threshold. Phys Rev B 61:R3784–R3788
38. Rammal R (1985) Flicker noise near the percolation threshold. J de Phys Lett 46:L129–L136
39. Rammal R, Tannous C, Brenton P, Tremblay A-MS (1985) Flicker (1/f) noise in percolation networks: a new hierarchy of exponents. Phys Rev Lett 54:1718–1721
40. Rammal R, Tannous C, Tremblay A-MS (1985) 1/f noise in random resistor networks: fractals and percolating systems. Phys Rev A 31:2662–2671
41. Sahoo A, Sieu D, Ramanathan S et al (2014) Conductivity noise study of the insulator-metal transition and phase co-existence in epitaxial samarium nickelate thin films. Phys Rev B 90:085116-1–085116-5
42. Shik AY (1975) Magnetoresistance of inhomogeneous semiconductors. Sov Phys Semicond 9:872–875 (in Russian)
43. Shklovskii BI, Efros AL (1984) Electronic properties of doped semiconductors. Springer, Berlin, 388 p
44. Shtengel K, Yu CC (2003) 1/f noise in electron glasses. Phys Rev B 67:165106-1–165106-8
45. Snarskii AA, Kolek A (1996) Excess 1/f noise in systems with an exponentially wide spectrum of resistances and dual universality of the percolation-like noise exponent. Sov Phys JETP 63:651–656
46. Snarskii AA, Kolek A (1997) Double university of 1/f noise percolation-like exponent in systems with exponentially wide spectrum of resistances. Physica A 241:355–359
47. Soderberg M, Grimvall G (1983) Current distributions for a two-phase material with chequer-board geometry. J Phys C 16:P1085–P1088
48. Speakman AM, Adkins CJ (1992) Noise in grown alumina tunnelling barriers. J Phys C 4:8053–8072
49. Topalian Z, Li S, Niklasson GA et al (2015) Resistance noise at the metal–insulator transition in thermochromic VO2 films. J Appl Phys 117:025303-1–025303-21
50. Tremblay A-MS, Fourcade B, Brenton P (1989) Multifractals and noise in metal-insulator mixtures. Physica A 157:89–100
51. Tremblay RR, Albinet G, Tremblay A-MS (1991) Noise and crossover exponent in the component random resistor network. Phys Rev B 43:11546–11549
52. Tremblay RR, Albinet G, Tremblay A-MS (1992) Noise and crossover exponent in conductor-insulator mixtures and superconductor-conductor mixtures. Phys Rev B 45:755–767
53. Wolf M, Muller K-H (1985) Noise in two-phase structures of Hashin-Shtrikman type: exact results. Phys Stat Sol A 92:K151–K153
55. Wright DC, Bergman DJ, Kantor Y (1986) Resistance fluctuations in random resistor networks above and below the percolation threshold. Phys Rev B 33:396–401

Chapter 14
Higher Current Moments

14.1 Definitions

The effective resistivity ρ_e is proportional to second current moment

$$\rho_e \sim \langle \rho j^2 \rangle, \tag{14.1.1}$$

and the relative spectral density of 1/*f*-noise, more "intimate" medium parameter,—to fourth current moment:

$$C_e \sim \langle C \rho^2 j^4 \rangle. \tag{14.1.2}$$

Both ρ_e, C_e, and σ_e can be expressed through moments of electric field intensity or moments of local Joule heat release $Q = \mathbf{E} \cdot \mathbf{j}$.

In case of conducting composites with a weak nonlinearity of one or both phases, when local conductivity can be represented as an expansion (see Chap. 17), it can be written

$$\sigma \approx \sigma_0(r) + \chi^{(3)} E^2 + \ldots, \tag{14.1.3}$$

and thus, in the calculation of the effective properties it is also necessary to consider higher current and field moments.

Therefore, one can formulate the problem of behavior of *n*-th field moment, current, Joule heat release. For two-phase media these moments can be "separated" into two phases

$$\langle Q^n \rangle = \frac{1}{V} \int_V Q^n \mathrm{d}V = p \langle Q^n \rangle_1 + (1 - p) \langle Q^n \rangle_2, \tag{14.1.4}$$

where $\langle \ldots \rangle_i = V_i^{-1} \int_{V_i} \ldots \mathrm{d}V$ is the average of *i*-th phase.

A.A. Snarskii et al., *Transport Processes in Macroscopically Disordered Media*, DOI 10.1007/978-1-4419-8291-9_14

Critical behavior of higher moments (with $n \geq 2$) was studied in many papers, in particular [3, 5, 8], current moments in percolation media were investigated and critical indices for the description of such moments were introduced. Numerical simulation for the determination of critical indices of higher moments in the two- and three-dimensional cases was performed in [2, 10] and in [7] based on the HM. There were obtained analytical expressions for critical indices and the problem of higher moment scaling was considered.

By analogy to relative spectral density of 1/*f*-noise we will introduce the following determination for the effective *n*-th moment of distribution of current (field, Joule heat release) in the form

$$C_{\mathrm{e}}(n) = \frac{\langle C(n,\mathbf{r})(\mathbf{E}(\mathbf{r})\cdot\mathbf{j}(\mathbf{r}))^n\rangle}{(\langle\mathbf{E}(\mathbf{r})\rangle\langle\mathbf{j}(\mathbf{r})\rangle)^n}, \quad n = 1, 2, \ldots \tag{14.1.5}$$

Moment $C_e(n)$ is normalized for $(\langle\mathbf{E}\rangle\langle\mathbf{j}\rangle)^n = \left(\sigma_{\mathrm{e}}\langle\mathbf{E}\rangle^2\right)^n = \sigma_{\mathrm{e}}^n\langle\mathbf{E}\rangle^{2n}$. In particular, such normalization (which includes σ_{e}) for $n = 1$ leads to identity

$$C_{\mathrm{e}}(n = 1) = 1, \tag{14.1.6}$$

and, thus, higher moments $C_{\mathrm{e}}(n > 1)$ provide information additional to the moment proportional to σ_{e}. For $n = 2$ with selection of $C(2,\mathbf{r}) = \{\delta\sigma\,\delta\sigma\}/\sigma^2$ the moment $C_{\mathrm{e}}(n = 2)$ is the relative spectral density of 1/*f*-noise. If $C(2,\mathbf{r}) = 1$ is selected, in this case $C_{\mathrm{e}}(n = 2)$ will be the moment of distribution of Joule heat release.

For the two-phase medium (14.1.5) it is logical to write as follows:

$$\begin{aligned} C_{\mathrm{e}}(n) &= \frac{1}{(\langle\mathbf{E}\rangle\langle\mathbf{j}\rangle)^n}\left[pC_1(n)\sigma_1^n\langle E^{2n}\rangle_1 + (1-p)C_2(n)\sigma_2^n\langle E^{2n}\rangle_2\right] \\ &= \frac{1}{(\langle\mathbf{E}\rangle\langle\mathbf{j}\rangle)^n}\left[pC_1(n)\rho_1^n\langle j^{2n}\rangle_1 + (1-p)C_2(n)\rho_2^n\langle j^{2n}\rangle_2\right]. \end{aligned} \tag{14.1.7}$$

Hence, $C_{\mathrm{e}}(n)$ is determined through partial (according to phases) moments of electric field intensity and current density. Note that with a selected normalization of $C_{\mathrm{e}}(n)$ (14.1.5), it is not the values of current density $\mathbf{j}(\mathbf{r})$ or field intensity $\mathbf{E}(\mathbf{r})$ that are essential, but only their directions $\mathbf{j}(\mathbf{r})/|\langle\mathbf{j}\rangle|$, $\mathbf{E}(\mathbf{r})/|\langle\mathbf{E}(\mathbf{r})\rangle|$.

14.2 Critical Exponents of the Higher Current Moments

Close to percolation threshold $C_{\mathrm{e}}(n)$ behaves universally, i.e., just as in the case of σ_{e} and the relative spectral density of 1/*f*-noise is characterized by critical indices. The HM allows (approximately, of course) expressing critical indices $C_{\mathrm{e}}(n)$ through the basic critical indices of percolation theory—critical index of correlation length and critical indices of the effective conductivity above and beyond the

percolation threshold. In so doing, use is made of the fact that correlation length is a universal parameter with critical index v that does not depend on the moment under consideration [11].

Similar to the way the relative spectral density of 1/*f*-noise was calculated in the HM, one can also find critical indices, describing the behavior of $C_e(n)$. For instance, above the percolation threshold (see paragraph 5.4):

$$C_e(n) = \frac{C_1(n) j_1^n E_1^n V_B/V + C_2(n) j_2^n E_2^n V_I/V}{\sigma_e^n \langle E \rangle^{2n}}, \tag{14.2.1}$$

where j_1 and E_1 is current and field in the bridge, j_2 and E_2 is current and field in the interlayer, $V_B = a_0^{d-1} l = a_0^d N_1$ is bridge volume, $V_I = a_0^d N_2$ is interlayer volume, $V = \xi^d$.

Introducing the average field $E = \Delta\varphi/\xi$, where $\Delta\varphi$ is potential difference on the size ξ and expressing E_1 and E_2 through $\Delta\varphi$, from (14.2.1) we immediately find [7]:

$$C_e(n) = C_1(n)\tau^{-k_n} + C_2(n)h^n\tau^{-w_n}, \tag{14.2.2}$$

and below the percolation threshold for the same reasons we have

$$C_e(n) = C_2(n)|\tau|^{-k'_n} + C_1(n)h^n|\tau|^{-w'_n}, \tag{14.2.3}$$

where

$$k_n = [2v(d-1) - t](n-1),\ k'_n = (2v - q)(n-1), \tag{14.2.4}$$

$$w_n = k'_n + n(t+q),\ w'_n = k_n + n(t+q), \tag{14.2.5}$$

There is a connection between the critical indices k_n, k'_n, w_n and w'_n [compare to (13.3.16)]:

$$k_n + w_n = k'_n + w'_n. \tag{14.2.6}$$

Substituting into (14.2.2) or (14.2.3) instead of τ the value of smearing region $\Delta = h^{\frac{1}{t+q}}$, we find the expression $C_e(n)$ in smearing region

$$C_e(n) = C_1(n)h^{s_n} + C_1(n)h^{-z_n}, \tag{14.2.7}$$

where

$$s_n = \frac{k_n}{t+q},\ z_n = \frac{k'_n}{t+q}. \tag{14.2.8}$$

Relationships (14.2.5), (14.2.6), and (14.2.8) are precise, independent of the employed model of percolation structure. They follow from the requirements to

Table 14.1 Indices values based on HM k_n and k'_n

n	$k_n(d=2)=k'_n(d=2)$	$k_n(d=3)$	$k'_n(d=3)$
2	1.37	1.52	1.03
3	2.73	3.04	2.06
4	4.1	4.56	3.09
5	5.47	6.08	4.12
6	6.83	7.6	5.12

have the same values of the effective coefficients below, above and on the percolation threshold itself (in smearing region). Concrete values of k_n and k'_n (14.2.4) (see Table 14.1) are of course approximate, since they are based on the HM.

The accuracy of critical indices describing the behavior of higher moments obtained on the basis of the HM can be estimated by considering the works [2, 10], where the numerical experiment (simulation by the Monte Carlo method) was performed on the random lattice of resistances. In these works n-th cummulant of fluctuations of resistances in the net $\sum_{\alpha} \left(i_\alpha^2\right)^n C_\alpha(n)$, was calculated, where $C_\alpha(n)$ is n-th cummulant of fluctuations of α-bond. This sum depending on the values of problem parameters can be written as the sum over all well-conducting bonds (in so doing, the resistances of poorly conducting bonds are selected as infinite $r_2 = \infty$) [2]:

$$\left\{\sum_{\alpha} \left(i_\alpha^2\right)^2\right\} \sim L^{-x_n}, \quad L < \xi, \tag{14.2.9}$$

or as a sum over poorly conducting bonds (in so doing, the resistance of well-conducting bonds $r_1 = 0$):

$$\left\{\sum_{\alpha} \left(i_\alpha^2\right)^n\right\} \sim L^{y_n}, \quad L < \xi. \tag{14.2.10}$$

The expressions (14.2.9) and (14.2.10) consider nets at the percolation threshold and with sizes $L \leq \xi$, braces mean averaging over random net realizations. In this case (see Chap. 9 and [3, 5, 8, 9]) the averaged over realizations values are proportional to sample size. When sample size exceeds the value ξ, this dependence must be replaced by concentration one, substituting consecutively into (14.2.9) and (14.2.10) instead of L the correlation length ξ, and instead of ξ its concentration dependence $|\tau|^{-\nu}$.

Critical indices x_n and y_n, obtained in [2, 10] by means of numerical simulation, can be also calculated within the HM. For instance, for the case of (14.2.9) the basic current flows through the bridge, therefore

$$\sum_{\alpha} i_{\alpha}^{2n} = i_{\alpha}^{2n} N_1 = a_0^{2(d-1)n} N_1 j_1^{2n}, \tag{14.2.11}$$

where it is taken into account that $i_\alpha = a_0^{d-1} j_1$, j_1 is current density in the bridge and, as long as in the correlation volume the entire current flows through the bridge, then $I = j_1 a_0^{d-1}$.

In [2, 10] it is assumed that $I = 1$, therefore, from (14.2.11) it follows

$$\sum_{\alpha} i_{\alpha}^{2n} = N_1 = \tau^{-\alpha_1}, \ \alpha_1 = t - \nu(d-2). \tag{14.2.12}$$

Comparing (14.2.12) and (14.2.9) $\left\{\sum_{\alpha} i^{2n}\right\} \sim L^{-x_n} \sim \tau^{\nu x_n}$, we find

$$-\nu x_n = t - \nu(d-2). \tag{14.2.13}$$

Similarly, for the case of $r_1 = 0$ (14.17) we obtain

$$-\nu y_n = (2n-1)[q + (d-2)\nu]. \tag{14.2.14}$$

Table 14.2 gives numerical values $-\nu x_n$ and $-\nu y_n$ obtained by numerical simulation [2, 10] and within the HM (14.2.13), (14.2.14).

In paper [4] numerical simulation on the flat disordered lattice was used to find critical indices describing the concentration dependence of partial moments of the electric field intensity

$$\psi_i^{(2n)} = \frac{1}{V} \int_{V_i} \left(\frac{\mathbf{E}(\mathbf{r})}{|\langle \mathbf{E}(\mathbf{r}) \rangle|} \right)^{2n} \mathrm{d}V, \quad i = 1, 2, \tag{14.2.15}$$

where i is phase number, integration is made over i-th phase.

Table 14.2 Numerical values $-\nu x_n$ and $-\nu y_n$

n	$-\nu x_n$		$-\nu y_n$	
	HM	Tremblay et al. [10], Albinet et al. [2]	**HM**	Tremblay et al. [10], Albinet et al. [2]
	$d = 2$			
1	1.3	1.3	1.3	1.3
2	1.3	1.1	3.9	4.0
3	1.3	1.02	6.5	6.6
$d = 3$				
1	1.12	1.12	1.61	1.9
2	1.12	1.1	4.83	5.7
3	1.12	1.03	8.05	9.5

According to [4] above the percolation threshold and beyond smearing region we have

$$\psi_1^{(n)} \sim \tau^{t(n)},\ \psi_2^{(n)} \sim \tau^{\mu(n)}, \tag{14.2.16}$$

$$\begin{array}{lll} t_{(2)} = 1.30 \pm 0.01, & t_{(4)} = 1.42 \pm 0.06, & t_{(6)} = 1.5 \pm 0.2, \\ \mu_{(2)} = 1.3 \pm 0.05, & \mu_{(4)} = 3.56 \pm 0.06, & \mu_{(6)} = 6.0 \pm 0.1. \end{array} \tag{14.2.17}$$

Within the IM, critical indices $t_{(n)}$ and $\mu_{(n)}$ (using the reasoning similar to given above in the calculation of x_n and y_n) are of the form

$$t_{(n)} = (n-1)t - (n-2)(d-1)\nu,\ \mu_{(n)} = q + (n-2)\nu \tag{14.2.18}$$

Substituting into these expressions $d = 2$ and the numerical values $t_2 = q_2 = 1.3,\ \nu_2 = 4/3$ into (14.2.18), we find

$$\begin{array}{lll} t_{(2)}(HM) = 1.3, & t_{(4)}(HM) = 1.23, & t_{(6)}(HM) = 1.17, \\ \mu_{(2)}(HM) = 1.30, & \mu_{(4)}(HM) = 3.97, & \mu_{(6)}(HM) = 6.63. \end{array} \tag{14.2.19}$$

As is obvious from Table 14.2 and comparison between (14.2.17) and (14.2.18), the HM, despite its simplicity, yields satisfactory agreement with numerical simulation.

Surely, the approach based on the HM of percolation structure, is approximate and restricted by not very high and not very low values of n. Thus, at high values of $n \to \infty$ on summation of currents the HM is "inferior" to SCB model. In the HM it is customary to choose N_1 as $N_1 \sim \tau^{\xi_R}$, at $n \to \infty$ it is necessary to come back to their precise value: $N_1 \sim \tau^{-1}$. Similarly, at $n \to 0$ it is necessary to sum over not only by the bonds in the bridge, but also by all the bonds where current flows, and their number is determined not through ξ_R, but through critical index describing the number of bonds in the blobs (backbone). A detailed analysis of situations beyond the HM was performed in [1, 6].

References

1. Aharony A, Blumenfeld R, Brenton P, Fourcade B, Harris AB, Meir Y, Tremblay A-MS (1998) Negative moments of currents in percolating resistor networks. Phys Rev B 40: 7318–7320
2. Albinet G, Tremblay RR, Tremblay A-MS (1993) Scaling behaviour of multifractal-moment distribution near the criticality. J Phys I 3:323–330 (France)
3. Arcangelis L, Redner S, Coniglio A (1985) Anomalous voltage distribution of random resistor networks and new model for the backbone at the percolation threshold. Phys Rev B 31: 4725–4727

4. Balagurov BY, Kashin VA (2004) Partial moments of electric field strength in the problem of conductivity of binary composites: numerical experiment on a plane disordered lattice. Sov Phys JETP 99:801–810. doi:10.1134/1.1826172
5. de Arcangelis L, Redner S, Coniglio A (1986) Multiscaling approach in random resistor and random superconducting networks. Phys Rev B 34:4656–4673
6. Kolek A (1996) Voltage distribution in a two-component random system. Phys Rev B 53:14185–14195
7. Morozovsky AE, Snarskii AA (1992) Multiscaling in randomly inhomogeneous media: effective conductivity, relative spectral density of 1/f noise, and higher-order moments. Sov Phys JETP 75:366–371
8. Rammal R, Tannous C, Brenton P, Tremblay A-MS (1985) Flicker (1/f) noise in percolation networks: a new hierarchy of exponents. Phys Rev Lett 54:1718–1721
9. Rammal R, Tannous C, Tremblay A-MS (1985) 1/f noise in random resistor networks: fractals and percolating systems. Phys Rev A 31:2662–2671
10. Tremblay RR, Albinet G, Tremblay A-MS (1991) Noise and crossover exponent in the component random resistor network. Phys Rev B 43:11546–11549
11. Tremblay A-MS, Tremblay RR, Albinet G, Fourcade B (1992) How many correlation lengths for multifractals? Phys A 183:398–410

Chapter 15
Thermoelectric Properties

15.1 EMT-Approximation

Thermoelectric effects provide an example of a medium where two thermodynamic fluxes simultaneously (**j** is an electric flux density, **q** is a heat flux density) are created by two thermodynamic forces: electric field intensity **E** and temperature gradient ∇T

$$\begin{cases} \mathbf{j} = \sigma\mathbf{E} + \sigma\alpha(-\nabla T), \\ \mathbf{q} = \sigma\alpha T\mathbf{E} + \kappa(1 + ZT)(-\nabla T), \quad ZT = \frac{\sigma\alpha^2}{\kappa}T, \end{cases} \tag{15.1.1}$$

where α is the Seebeck coefficient, κ is thermal conductivity, $Z = \sigma\alpha^2/\kappa$ is thermoelectric figure of merit (the Ioffe number, sign of merit).

Thermoelectric properties are "included" in (15.1.1) in off-diagonal components, the existence of which results in the fact that the electrical current is caused not only by the electrical field, but also by temperature gradient, hence, part of heat flux is related to the electrical filed (or, which is the same, to the electrical current, which, in fact, constitutes the Peltier effect).

There are many different strategies to improve thermoelectric properties. In composites, thermoelectric properties could be enhanced by inclusion of nanoparticles, by influence of nanowires, by influence of interface between different phases, and by special methods of preparation of different media. The influence of structure of composites on the thermoelectric characteristics considered in the following papers [2, 36]. Interesting application of theory of composites was considered in [2] paper, where it was applied for explanation of temperature dependence of electric conductivity and thermoelectric power. Influence of nanocontacts on thermoelectric properties of composites was developed in the paper [36].

The synthesis of composites consisting from nanoparticles is discussed in the paper [11, 27, 28]. Models of nanostructured materials are discussed in [13, 16, 23]. Model describing properties of thermoelectric nanocomposite materials consisting of granular regions is considered in paper [23].

A.A. Snarskii et al., *Transport Processes in Macroscopically Disordered Media*, DOI 10.1007/978-1-4419-8291-9_15

It is shown in [24] that composites material (particularly, material with metal/semiconductor interfaces) could lead to the increase of Seebeck coefficient (interface scattering of phonons could increase ZT). Another way to improve ZT by considering perfectly conducting channels considered in the papers is [20–22] (Influence of silicon nanowires), [19].

Weak tunneling between grains also could be a factor in improving ZT [17].

Optimization of structure for increasing efficiency of thermoelectric materials considered in the work [25]. Energy efficiency of composites is considered in the paper [39].

Just as the problem of calculation of the effective conductivity, the problem of calculation of the effective kinetic coefficients (including the coefficient of the effective thermoEMF) can be solved in different approximations. Consider first the EMT-approximation.

In order to construct the EMT-approximation for thermoelectric effects, it is necessary, like in the problem of σ_e, to have a solution of the problem of field and flux distribution for a secluded spherical inclusion. In this case it is a ball consisting of a medium with coefficients $\sigma_1,\ \kappa_1,\ \alpha_1$ (or $\sigma_2,\ \kappa_2,\ \alpha_2$) located in a medium with coefficients $\sigma_e,\ \kappa_e,\ \alpha_e$, with the values of field $\langle \mathbf{E} \rangle$ and temperature gradient $\langle \nabla T \rangle$ assigned on the infinity. Equations allowing to find potential distribution $\varphi(\mathbf{r})$ and temperature distribution $T(\mathbf{r})$, for the general case, are given, for instance, in [4]. In [38], in the approximation when corrections to σ_e and κ_e due to thermoelectric effects are small, the analytical solution of this problem is given for the three-dimensional case

$$\alpha_e = \frac{\langle \alpha\sigma/\Delta_0 \rangle}{\langle \sigma/\Delta_0 \rangle},\ \Delta_0 = (2\sigma_e + \sigma)(2\kappa_e + \kappa), \tag{15.1.2}$$

where σ_e and κ_e are found from the EMT-approximation (without regard to thermoelectric effects),

$$\left\langle \frac{\sigma_e - \sigma}{2\sigma_e + \sigma} \right\rangle = 0,\ \left\langle \frac{\kappa_e - \kappa}{2\kappa_e + \kappa} \right\rangle = 0,\ d = 3. \tag{15.1.3}$$

Similarly, one can write down (15.1.2) and (15.1.3) for the two-dimensional case.

For the three-dimensional case of the two-phase medium from expressions (15.1.2) and (15.1.3) it follows

$$\alpha_e = \frac{p\sigma_1\alpha_1(2\sigma_e + \sigma_2)(2\kappa_e + \kappa_2) + (1-p)\sigma_2\alpha_2(2\sigma_e + \sigma_1)(2\kappa_e + \kappa_1)}{p\sigma_1(2\sigma_e + \sigma_2)(2\kappa_e + \kappa_2) + (1-p)\sigma_2(2\sigma_e + \sigma_1)(2\kappa_e + \kappa_1)},\quad d = 3 \tag{15.1.4}$$

For the two-dimensional case instead of (15.1.3) one should use $\left\langle \frac{\sigma_e - \sigma}{\sigma_e + \sigma} \right\rangle = 0$, $\left\langle \frac{\kappa_e - \kappa}{\kappa_e + \kappa} \right\rangle = 0$ and $\Delta_0 = (\sigma_e + \sigma)(\kappa_e + \kappa)$, and therefore we have [4]:

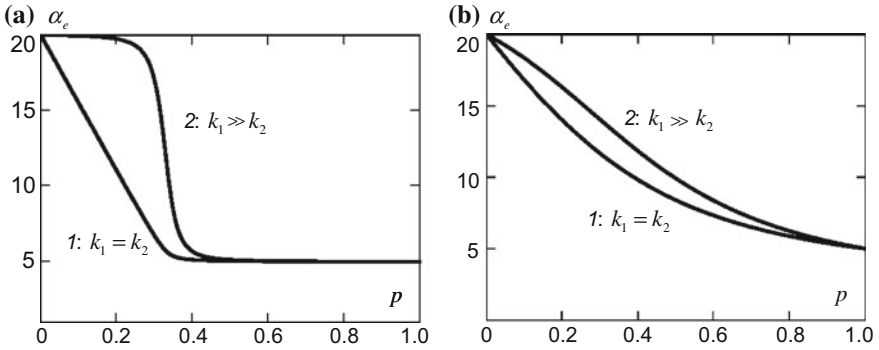

Fig. 15.1 Concentration dependence $\alpha_e = \alpha_e(p)$ for two limiting cases of phase thermal conductivity ratio: **a** at $\sigma_1 \gg \sigma_2 (\sigma_1/\sigma_2 = 10^3, \alpha_2/\alpha_1 = 4)$ $1 - \kappa_2/\kappa_1 = 5 \times 10^{-2} \ll 1 - 2 - \kappa_1 = \kappa_2$; **b** at $\sigma_1/\sigma_2 \approx 1 (\sigma_1/\sigma_2 = 6) 1 - \kappa_2/\kappa_1 \ll 1, 2 - \kappa_1 = \kappa_2$

$$\alpha_e = \frac{p\sigma_1\alpha_1(\sigma_e + \sigma_2)(\kappa_e + \kappa_2) + (1-p)\sigma_2\alpha_2(\sigma_e + \sigma_1)(\kappa_e + \kappa_1)}{p\sigma_1(\sigma_e + \sigma_2)(\kappa_e + \kappa_2) + (1-p)\sigma_2(\sigma_e + \sigma_1)(\kappa_e + \kappa_1)}, \quad d = 2. \tag{15.1.5}$$

As follows from the analysis of (15.1.4), the concentration dependence $\alpha_e = \alpha_e(p)$ behaves differently depending on the phase thermal conductivity ratio κ_2/κ_1 (Fig. 15.1). With a large inhomogeneity of electrical conductivity $\sigma_1/\sigma_2 \gg 1$ and thermal conductivity $\kappa_1/\kappa_2 \gg 1$ there is a step in the dependence of $\alpha_e(p)$ which disappears at $\kappa_1 \approx \kappa_2$. Smooth dependences are observed at weak inhomogeneity of conductivity.

In the case when current in one of the phases does not flow, i.e., if $\sigma_2 = 0$, $\alpha_e = \alpha_1$ is the value of pure phase over the entire range of σ_e existence, i.e., at $p > p_c$ (Fig. 15.2). In the case of $\kappa_1 \gg \kappa_2$ close to p_c there is easily observable drastic (percolation) transition of α_e from α_1 to α_2.

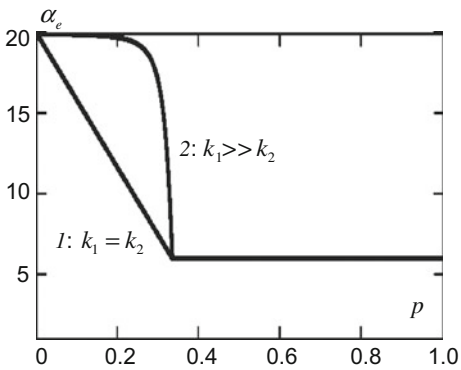

Fig. 15.2 Concentration dependence $\alpha_e = \alpha_e(p)$ at $\sigma_2 = 0$ for two limiting cases of phase thermal conductivity ratio: $1 - \kappa_2/\kappa_1 \ll 1$ and $2 - \kappa_1 = \kappa_2$

For the general case without requirement of $ZT \ll 1$ in [4] there was obtained (within the EMT) a system of equations to determine α_e, σ_e and κ_e, however, its investigation in the analytical form is difficult.

15.2 Thermoelectric Properties of the Self-dual Media

As in the "usual" (without thermoelectric effects) conductivity case, exact solution of α_e problem in the two-dimensional case for the self-dual media is possible. According to [3, 4]:

$$\alpha_e = \frac{\alpha_1\sqrt{\sigma_1\kappa_2} + \alpha_2\sqrt{\sigma_2\kappa_1}}{\sqrt{\sigma_1\kappa_2} + \sqrt{\sigma_2\kappa_1}} = \frac{\alpha_1\sqrt{\frac{\kappa_2}{\kappa_1}} + \alpha_2\sqrt{\frac{\sigma_2}{\sigma_1}}}{\sqrt{\frac{\sigma_2}{\sigma_1}} + \sqrt{\frac{\kappa_2}{\kappa_1}}}. \tag{15.2.1}$$

In particular, at $\sigma_2 = 0$ $\alpha_e(\sigma_2 = 0) = \alpha_1$ (Fig. 15.2).

For the self-dual media the effective σ_e and κ_e are of the form

$$\sigma_e = \sqrt{\sigma_1\sigma_2}\frac{\sqrt{\sigma_1\kappa_2} + \sqrt{\sigma_2\kappa_1}}{\sqrt{\left(\sqrt{\sigma_1\kappa_2} + \sqrt{\sigma_2\kappa_1}\right)^2 + T\sigma_1\sigma_2(\alpha_1 - \alpha_2)^2}}, \tag{15.2.2}$$

$$\kappa_e = \sqrt{\kappa_1\kappa_2}\frac{\sqrt{\sigma_1\sigma_2}}{\sigma_e}. \tag{15.2.3}$$

As long as percolation threshold in the self-dual media $p_c = 1/2$, α_e (15.2.1) leads to the value of α_e at the percolation threshold in the two-dimensional case. At $\kappa_1 \approx \kappa_2$ and strong conductivity inhomogeneity $\sigma_2/\sigma_1 = h \ll 1$ from (15.2.1) it follows

$$\alpha_e = \frac{\alpha_1 + \alpha_2 h^{\frac{1}{2}}}{1 + h^{\frac{1}{2}}} \approx \alpha_1 + \alpha_2 h^{\frac{1}{2}}. \tag{15.2.4}$$

As a rule, in the "metal" (σ_1) phase the thermo EMF is much lower than in the "semiconductor" phase $(\sigma_2 \ll \sigma_1)$ $\alpha_1 \ll \alpha_2$, then from (15.2.4) at the percolation threshold we obtain

$$\alpha_e \approx \alpha_2 h^{\frac{1}{2}},\ \alpha_2 h^{\frac{1}{2}} \gg \alpha_1, \tag{15.2.5}$$

i.e., α_e is limited by the low factor $h = \sigma_2/\sigma_1$.

At $\kappa_2 \ll \kappa_1$ and, as before, $\sigma_2/\sigma_1 \ll 1$ and $\alpha_1 \ll \alpha_2$ from (15.1.4) follows

$$\alpha_e \approx \alpha_2 \frac{\sqrt{\sigma_2/\sigma_1}}{\sqrt{\sigma_2/\sigma_1} + \sqrt{\kappa_2/\kappa_1}}, \tag{15.2.6}$$

and, if $\sqrt{\sigma_2/\sigma_1} \approx \sqrt{\kappa_2/\kappa_1}$, then

$$\alpha_e \approx \alpha_2, \tag{15.2.7}$$

i.e., as compared to the case of $\kappa_1 \approx \kappa_2$ at $p = p_c$ the value α_e is drastically increased. This behavior is in good agreement with the results of EMT-approximation (Fig. 15.1a).

(15.1.1) could be written down in the abstract form, suitable for any two-flow system with cross effects

$$\begin{array}{l} \mathbf{j} = A_{11}\mathbf{e} + A_{12}\mathbf{g}, \\ \mathbf{q} = A_{21}\mathbf{e} + A_{22}\mathbf{g}, \end{array} \quad \hat{A} = \begin{pmatrix} A_{11} & A_{12} \\ A_{21} & A_{22} \end{pmatrix}, \tag{15.2.8}$$

where $\hat{A}$ is tensor of local kinetic coefficients. In this case the effective values A^{e}_{ij} of the self-dual media (to an accuracy of notation), coinciding with (15.2.1), (15.2.3) can be written for tensor $\hat{A}^{\mathrm{e}}$ [35]:

$$\hat{A}^{\mathrm{e}} = \left(\mathrm{Det}\widehat{A}_1\,\mathrm{Det}\widehat{A}_2\right)^{\frac{1}{4}} \frac{\widehat{\Omega}_1 + \widehat{\Omega}_2}{\sqrt{\mathrm{Det}\left(\widehat{\Omega}_1 + \widehat{\Omega}_2\right)}}, \quad \widehat{\Omega}_n = \frac{\widehat{A}_n}{\sqrt{\mathrm{Det}\left(\widehat{A}_n\right)}}, \; n = 1, 2, \tag{15.2.9}$$

where subscript n denotes phase number.

Just as for the effective conductivity problem (see Chap. 6), there exist the exact solution for the two-dimensional polycrystal [35]

$$\hat{A}^{e} = \left(\mathrm{Det}\widehat{A}_{\parallel}\mathrm{Det}\widehat{A}_{\perp}\right)^{\frac{1}{4}} \frac{\widehat{\Omega}_{\parallel} + \widehat{\Omega}_{\perp}}{\sqrt{\mathrm{Det}\left(\widehat{\Omega}_{\parallel} + \widehat{\Omega}_{\perp}\right)}}, \quad \widehat{\Omega}_{\parallel,\perp} = \frac{\widehat{A}_{\parallel,\perp}}{\sqrt{\mathrm{Det}\left(\widehat{A}_{\parallel,\perp}\right)}}, \tag{15.2.10}$$

where $\widehat{A}_{\parallel}$ and $\widehat{A}_{\perp}$ are main values of tensor of local coefficients A_{ik}.

In "thermoelectric" terminology for the two-dimensional polycrystal [6] instead of (15.2.10) we have

$$\alpha^{\mathrm{e}} = \frac{\alpha_{\parallel}\sqrt{\sigma_{\parallel}\kappa_{\perp}} + \alpha_{\perp}\sqrt{\sigma_{\perp}\kappa_{\parallel}}}{\sqrt{\sigma_{\parallel}\kappa_{\perp}} + \sqrt{\sigma_{\perp}\kappa_{\parallel}}}, \tag{15.2.11}$$

$$\sigma^{\mathrm{e}} = \sqrt{\sigma_{\parallel}\sigma_{\perp}}\frac{\sqrt{\sigma_{\parallel}\kappa_{\perp}} + \sqrt{\sigma_{\perp}\kappa_{\parallel}}}{\sqrt{\left(\sqrt{\sigma_{\parallel}\kappa_{\perp}} + \sqrt{\sigma_{\perp}\kappa_{\parallel}}\right)^2 + T\sigma_{\parallel}\sigma_{\perp}\left(\alpha_{\parallel} - \alpha_{\perp}\right)^2}}, \tag{15.2.12}$$

$$\kappa^{\mathrm{e}} = \sqrt{\kappa_{\parallel}\kappa_{\perp}}\frac{\sqrt{\sigma_{\parallel}\sigma_{\perp}}}{\sigma_{\mathrm{e}}}. \tag{15.2.13}$$

The expressions for σ_{e} and κ_{e} (15.2.2) can be written in order to explicitly single out a component with "thermoelectric figure of merit" (in [32, 33] such figure of merit was called the internal figure of merit, certainly, it does not coincide with the effective figure of merit $Z_{\mathrm{e}} = \sigma_{\mathrm{e}}\alpha_{\mathrm{e}}^2/\kappa_{\mathrm{e}}$):

$$\tilde{Z}T = \frac{\sqrt{\sigma_1\sigma_2}}{\sqrt{\kappa_1\kappa_2}}\frac{\left(\alpha_1 - \alpha_2\right)^2}{\left(\sqrt{\frac{\sigma_2}{\sigma_1}}\Big/\sqrt{\frac{\kappa_2}{\kappa_1}} + \sqrt{\frac{\kappa_2}{\kappa_1}}\Big/\sqrt{\frac{\sigma_2}{\sigma_1}}\right)^2}T, \tag{15.2.14}$$

$$\sigma_{\mathrm{e}} = \frac{\sqrt{\sigma_1\sigma_2}}{\sqrt{1+\tilde{Z}T}}, \tag{15.2.15}$$

$$\kappa_{\mathrm{e}} = \sqrt{\kappa_1\kappa_2}\sqrt{1+\tilde{Z}T}. \tag{15.2.16}$$

Thus, condition of small influence of thermoelectric effects on the effective electric and thermal conductivity: $ZT \ll 1$ (15.2.14) is immediately obvious. The concept of thermoelectric figure of merit of phases (Ioffe number) $Z_i = \sigma_i\alpha_i^2/\kappa_i$ is essential in the calculation of the efficiency of thermoelectric devices (thermal generators, Peltier coolers, etc.) [12, 26]. Note that in $\tilde{Z}T$ (15.2.15) parameters of thermoelectric materials σ_1, κ_1, α_1 and σ_2, κ_2, α_2 form a peculiar dimensionless combination which is not, however, the function of $Z_1 = \sigma_1\alpha_1^2/\kappa_1$ and $Z_2 = \sigma_2\alpha_2^2/\kappa_2$. It means that at least in this case the influence of thermoelectric effects on the effective properties of composite (including the efficiency of thermoelectric devices created of such composite) cannot be expressed only through Z_1 and Z_2 (or through $Z_{\mathrm{e}} = \sigma_{\mathrm{e}}\alpha_{\mathrm{e}}^2/\kappa_{\mathrm{e}}$), but calls for more complicated (nontrivial) combinations of parameters, such, for instance, as in (15.2.14). The effective figure of merit characterizing the figure of merit (ability to convert thermal into electric energy) of composite also depends in a complicated way on the parameters of thermoelectric material of phases. Double-side restrictions of Z_{e} were considered in works [9, 10, 34].

15.3 Critical Region of Concentration—Behavior of α_e in the Vicinity of Percolation

In a medium with strongly inhomogeneous conductivity $(h = \sigma_2/\sigma_1 \ll 1)$ the distribution of currents and fields in the medium close to percolation threshold is "controlled," as detailed above (Chap. 5), by percolation structure—bridges and interlayers. The presence of additional processes, in this case thermoelectric, certainly affects the distribution of currents in the medium, however, bridges and interlayers still remain as the governing elements of percolation structure. Therefore, it should be expected (and these expectations are justified) that behavior of the effective kinetic coefficients, including α_e, close to percolation threshold is universal, i.e., described by critical indices.

Behavior of σ_e, κ_e and α_e in the critical region was first studied in the works [18, 37]. In [29, 30] numerical experiments were performed for the determination of critical indices. Prior to discussing these and other papers, let us suggest explanation based on the HM on a simple qualitative level the critical behavior of α_e for two different cases: $\kappa_1 \gg \kappa_2$ and $\kappa_1 \approx \kappa_2$. In doing so, we assume that $\sigma_2/\sigma_1 \ll 1$ and $\alpha_2 \gg \alpha_1$. As we see, the HM allows not only showing the difference in α_e behavior for these cases, but also determining critical indices α_e.

Consider first a medium below the percolation threshold [31] (see paragraph 5.4 Fig. 5.8a). In the presence of temperature gradient, this schematic is of the form (see Fig. 15.3a). Its equivalent electrical circuit with regard to EMF arising due to temperature difference $\Delta T = T_2 - T_1$ is shown in Fig. 15.3b, where R_2 is interlayer resistance, ε_1 is EMF created on the interlayer, R_ξ is resistance of parallel to interlayer part of poorly conducting medium (with characteristic size ξ), ε_2' is EMF created on this part.

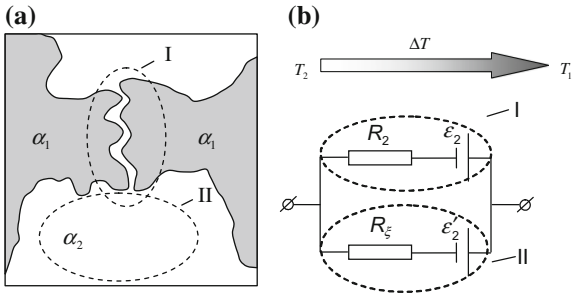

Fig. 15.3 Percolation structure below the percolation threshold (**a**) and the equivalent electrical circuit (**b**)

Temperature difference on size ξ: $\Delta T = T_2 - T_1$, total EMF ε_ξ on size ξ (circuit b in Fig. 15.3) is found as

$$\varepsilon_\xi = \left(\frac{\varepsilon_2}{R_2} + \frac{\varepsilon_2'}{R_\xi}\right) \Big/ \left(\frac{1}{R_2} + \frac{1}{R_\xi}\right), \tag{15.3.1}$$

whence

$$\alpha_e = \frac{\varepsilon_\xi}{\Delta T} = \frac{\varepsilon_2 + \varepsilon_2' \frac{R_2}{R_\xi}}{1 + \frac{R_2}{R_\xi}} \cdot \frac{1}{\Delta T} \approx \frac{\varepsilon_2 + \varepsilon_2' \frac{R_2}{R_\xi}}{\Delta T}, \tag{15.3.2}$$

where it is taken into account that the interlayer resistance R_2 is always much lower than R_ξ—the resistance of that part of poorly conducting phase that does not enter the interlayer, and

$$\varepsilon_2 = \Delta\alpha \Delta T_2, \quad \varepsilon_2' = \Delta\alpha \Delta T, \ \Delta\alpha = \alpha_2 - \alpha_1, \tag{15.3.3}$$

where ΔT_2 is temperature difference on the interlayer.

With a large difference in phase thermal conductivities $\kappa_1 \gg \kappa_2$, the temperature difference on the interlayer is practically the same as on the volume boundaries $\Delta T_2 \approx \Delta T$, then substituting (15.3.3) into (15.3.2), we get

$$\alpha_e \approx \Delta\alpha \tau^0, \quad \kappa_1 \gg \kappa_2, \tag{15.3.4}$$

i.e., in the case of $p < p_c$, $\kappa_1 \gg \kappa_2$, $\sigma_1 \gg \sigma_2$, $\alpha_2 \gg \alpha_1 \alpha_e$ is concentration independent.

In the case when phase thermal conductivities are approximately equal to $\kappa_1 \approx \kappa_2$, the temperature difference on the interlayer is much less than ΔT:

$$\Delta T_2 \approx \Delta T \frac{a_0}{\xi}, \quad \Delta T |\tau|^v \ll \Delta T. \tag{15.3.5}$$

Hence and from (15.3.3) it follows

$$\alpha_e = \frac{\Delta T a_0/\xi + \Delta T R_2/R_\xi}{\Delta T} \approx \Delta\alpha(|\tau|^v + |\tau|^q), \tag{15.3.6}$$

Where it is taken into account that $a_0/\xi \approx |\tau|^v$, a $R_2/R_\xi \approx |\tau|^q$.

As long as both in the two- and three-dimensional case $v > q$ (see Table 5.1), $|\tau|^q > |\tau|^v$, then from (15.3.6) we have

$$\alpha_e \approx \Delta\alpha |\tau|^q, \quad \kappa_1 \approx \kappa_2. \tag{15.3.7}$$

Weak dependence of α_e on τ at $\kappa_1 \approx \kappa_2$ and power drop of α_e at $\kappa_1 \gg \kappa_2$ is also predicted by the EMT-approximation.

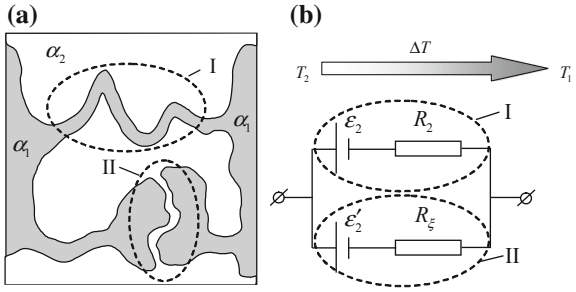

Fig. 15.4 Percolation structure: above the percolation threshold (**a**) and the equivalent electrical circuit (**b**)

Above the percolation threshold the percolation structure according to the HM (see paragraph 5.4 Fig. 5.7b) reduces to the following equivalent schematic (see Fig. 15.4a). Its equivalent electrical circuit with regard to EMF arising due to temperature difference $\Delta T = T_2 - T_1$ is shown in Fig. 15.4b, where R_1 and R_2 are bridge and interlayer resistances, ε_1 and ε_2 are EMF arising due to temperature difference on the bridge ΔT_1 and ΔT_2.

Similar to (15.4.23) for α_e, according to schematic in Fig. 5.7b we have

$$\alpha_e = \frac{\varepsilon_1/R_1 + \varepsilon_2/R_2}{1/R_1 + 1/R_2}\frac{1}{\Delta T} = \frac{\varepsilon_2 + \varepsilon_1 R_2/R_1}{1 + R_2/R_1}\frac{1}{\Delta T}. \tag{15.3.8}$$

In case of big difference in phase thermal conductivities $\kappa_1 \gg \kappa_2$, temperature differences on the bridge and interlayer are approximately equal

$$\Delta T_1 \approx \Delta T, \quad \Delta T_2 \approx \Delta T \tag{15.3.9}$$

For the bridge it is related to the fact that though bridge length $\sim a_0 N_1$, its length (the distance from one end to the other along the straight line) due to tortuosity is less and, as follows from simple geometrical considerations, is proportional to ξ.

According to (15.3.9)

$$\varepsilon_1 \approx \alpha_1 \Delta T, \quad \varepsilon_2 \approx \alpha_2 \Delta T, \tag{15.3.10}$$

on substitution to (15.3.8), with regard to $R_2/R_1 = G_1/G_2 = (\sigma_1/\sigma_2) \cdot |\tau|^{t+q}$ (see paragraph 5.4) we have

$$\alpha_e \approx \frac{\Delta\alpha + \alpha_1(\sigma_1/\sigma_2)|\tau|^{t+q}}{1 + (\sigma_1/\sigma_2)|\tau|^{t+q}}. \tag{15.3.11}$$

Taking into account that above smearing region $|\tau|^{t+q} \gg \sigma_1/\sigma_2$ let us convert (15.3.11) into

$$\alpha_e \approx \alpha_1 + \alpha_2 \frac{\sigma_2}{\sigma_1} |\tau|^{-(t+q)}. \tag{15.3.12}$$

Then it becomes readily apparent that two different types of behavior are possible depending on the ratio $(\alpha_2/\alpha_1)(\sigma_2/\sigma_1)$ and $|\tau|^{-(t+q)}$.

At

$$|\tau|^{t+q} \gg \frac{\alpha_2}{\alpha_1}\frac{\sigma_2}{\sigma_1}, \tag{15.3.13}$$

from (15.3.12) it follows that the effective Seebeck coefficient

$$\alpha_e \approx \alpha_1, \tag{15.3.14}$$

and does not depend on concentration.

On approaching the percolation threshold, i.e., with a reduction of τ, when the reciprocal (15.3.13) inequality is met, but provided that the system is still beyond the smearing region

$$\frac{\sigma_2}{\sigma_1} \ll |\tau|^{t+q} \ll \frac{\alpha_2}{\alpha_1}\frac{\sigma_2}{\sigma_1}, \tag{15.3.15}$$

from (15.3.12) we find

$$\alpha_e \approx \alpha_2 \frac{\sigma_2}{\sigma_1} |\tau|^{-(t+q)}. \tag{15.3.16}$$

These and some other regularities of α_e behavior were also obtained by rigid methods (see, for instance, [5, 7]), the results of which will be described below. Considered here the application of HM created on the basis of information on the behavior of σ_e close to percolation threshold allows vividly obtaining and explaining the nontrivial regularities in the behavior of the effective Seebeck coefficient α_e.

15.4 Isomorphism

In paper [37] a new method was proposed, subsequently generalized and developed in many works, for instance [5–7, 10, 18]. This method allows in a number of cases to reduce a two-flux problem with a cross component (with thermoelectric problem as their partial case) to single-flux problem, for instance, the problem of conductivity. In other words, this method allows establishing an exact correspondence

(isomorphism) between the problems of finding the effective kinetic coefficients for a system with thermoelectric effects and the effective electrical conductivity in a medium without thermoelectric effects.

Probably, the most vivid illustration of reducing one problem to the other belongs to Dykhne [15]. In particular, in [15] it is shown how expand the result [14] $\sigma_e = \sqrt{\sigma_1\sigma_2}$ to thermoelectric case. Let us write down the Eqs. (15.1.1) in the form

$$\left.\begin{aligned}\mathbf{j} &= s\mathbf{e} + a\mathbf{h}\\ \mathbf{q} &= b\mathbf{e} + k\mathbf{h}\end{aligned}\right\}, \tag{15.4.1}$$

where in the case of thermoelectric problem: $\mathbf{e} = -\nabla\varphi$, $\mathbf{h} = -\nabla T$ and $\mathrm{div}\mathbf{j} = 0$, $\mathrm{div}\mathbf{q} = 0$, $s = \sigma$, $a = \sigma\alpha, \ldots$

Local coefficients s, a, b, k are constants in each of the phases and equal to s_1, $a_1 \ldots$ and s_2, $a_2 \ldots$ in the first and second phases.

We introduce a new flux:

$$\mathbf{i} = \mathbf{j} + c\mathbf{q} = (s + cb)\mathbf{e} + (a + ck)\mathbf{h}, \tag{15.4.2}$$

where c is a certain coordinate-independent constant which will be chosen such that

$$\frac{a_1 + ck_1}{s_1 + cb_1} = \frac{a_2 + ck_2}{s_2 + cb_2} = \omega,\ \omega = \mathrm{const}. \tag{15.4.3}$$

Then (15.4.2) with regard to (15.4.3) can be rewritten as $\mathbf{i} = (s + cb)\left(\mathbf{e} + \frac{a+ck}{a+cb}\mathbf{h}\right)$, i.e.,

$$\mathbf{i} = (s + cb)\boldsymbol{\varepsilon}, \tag{15.4.4}$$

where $\boldsymbol{\varepsilon}$ is a new field,

$$\boldsymbol{\varepsilon} = \mathbf{e} + \omega\mathbf{h}. \tag{15.4.5}$$

Field ε and flux $\mathbf{i}$ satisfy the same equations $\mathrm{div}\varepsilon = 0$, $\mathrm{curl}\mathbf{i} = 0$, as the initial $\mathbf{j}$, $\mathbf{q}$ and $\mathbf{e}$, $\mathbf{h}$. That is why medium "current" $\langle\mathbf{i}\rangle = \mathbf{I}$ and medium "field" $\langle\varepsilon\rangle = \langle\mathbf{e}\rangle + \omega\langle\mathbf{h}\rangle$ are related in the same way as the medium field with the medium current in the one-flux problem. If, for instance, in the latter we select a case of self-dual medium $\langle\mathbf{j}\rangle = \sqrt{\sigma_1\sigma_2}\langle\mathbf{e}\rangle$, then

$$\mathbf{I} = \sqrt{(s_1 + cb_1)(s_2 + cb_2)}(\langle\mathbf{e}\rangle + \omega\langle\mathbf{h}\rangle). \tag{15.4.6}$$

Equation (15.4.3) for the determination of c is square, its solution gives two values of c_I and c_{II}. Thus, there are two equations:

$$\begin{aligned}\langle \mathbf{j}\rangle + c_I\langle \mathbf{q}\rangle &= \sqrt{(s_1 + c_I b_1)(s_2 + c_I b_2)}(\langle \mathbf{e}\rangle + \omega_I\langle \mathbf{h}\rangle),\\ \langle \mathbf{j}\rangle + c_{II}\langle \mathbf{q}\rangle &= \sqrt{(s_1 + c_{II} b_1)(s_2 + c_{II} b_2)}(\langle \mathbf{e}\rangle + \omega_{II}\langle \mathbf{h}\rangle).\end{aligned} \tag{15.4.7}$$

Solving these equations for $\langle \mathbf{j}\rangle$ and $\langle \mathbf{q}\rangle$, we obtain all the four effective kinetic coefficients.

In the most general form the isomorphism method was developed in [5], where it is realized not only for thermoelectric phenomena, but also for two- and three-dimensional galvanomagnetic effects and the problem of anisotropic medium conductivity. Afterwards, this method was expanded to thermogalvanomagnetic effects [8]. In [5] material Eqs. (15.1.1) are written as

$$\mathbf{j}_a = \sum_b \sigma_{ab}\mathbf{E}_b,\ a, b = 1, 2, \tag{15.4.8}$$

where $\mathbf{j}_1 \equiv \mathbf{j},\ \mathbf{j}_2 \equiv \mathbf{q}/T$, and it is shown that by means of linear transformation one can get

$$\mathbf{E}_a = \sum_b M_{ab}\mathbf{E}'_b,\ \mathbf{j}_a = \sum_b N_{ab}\mathbf{j}'_b. \tag{15.4.9}$$

The matrix of local kinetic coefficients σ_{ab} can be diagonalized simultaneously for two phases, which in the primed system is written as follows:

$$\mathbf{j}'_b = \sigma'_b(\mathbf{r})\mathbf{E}'_b. \tag{15.4.10}$$

Without going into details of rather tedious calculations, we cite only the final result. Given the known solution of problem of the calculation the effective electric conductivity σ_e in the medium without thermoelectric effects, which will be shown as

$$\sigma_\mathrm{e} = \sigma_1 f(p, h), \tag{15.4.11}$$

where $h = \sigma_2/\sigma_1$ and p, as a rule, is concentration of the first (good conducting phase), the matrix of kinetic coefficients $\hat{\sigma}$ in thermoelectric case is of the form

$$\hat{\sigma}_i = \begin{pmatrix} \sigma_i & \gamma_i \\ \gamma_i & \chi_i \end{pmatrix},\ \gamma_i = \sigma_i\alpha_i,\ \chi_i = \kappa_i/T + \sigma_i\alpha_i^2, \tag{15.4.12}$$

where $i = 1, 2$ denote phase number.

Then the effective kinetic coefficient according to [5] can be written as

$$\sigma_\mathrm{e} = \frac{(\mu\sigma_1 - \sigma_2)f(p, \lambda) - (\lambda\sigma_1 - \sigma_2)f(p, \mu)}{\mu - \lambda}, \tag{15.4.13}$$

$$\alpha_e = \frac{(\mu\gamma_1 - \gamma_2)f(p,\lambda) - (\lambda\gamma_1 - \gamma_2)f(p,\mu)}{(\mu\sigma_1 - \sigma_2)f(p,\lambda) - (\lambda\sigma_1 - \sigma_2)f(p,\mu)}, \tag{15.4.14}$$

$$\kappa_e = \frac{\sigma_1\kappa_1(\mu - \lambda)f(p,\lambda)f(p,\mu)}{(\mu\sigma_1 - \sigma_2)f(p,\lambda) - (\lambda\sigma_1 - \sigma_2)f(p,\mu)}, \tag{15.4.15}$$

Where functions $f(p,\lambda)$ and $f(p,\mu)$ are the same as in (15.4.11) (with substitution of h by λ and μ, respectively), and μ and λ are of the form

$$\begin{Bmatrix} \mu \\ \lambda \end{Bmatrix} = \frac{1}{4\sigma_1\kappa_1}\left\{\sqrt{\left(\sqrt{\sigma_1\kappa_2} + \sqrt{\sigma_2\kappa_1}\right)^2 + \sigma_1\sigma_2T(\alpha_1 - \alpha_2)^2}\right. \\ \left. \pm \sqrt{\left(\sqrt{\sigma_1\kappa_2} - \sqrt{\sigma_2\kappa_1}\right)^2 + \sigma_1\sigma_2T(\alpha_1 - \alpha_2)^2}\right\}^2. \tag{15.4.16}$$

According to method of derivation of these relations, the expressions (15.4.13)–(15.4.15) are valid for problems of any dimension, two-phase media with any structure (arrangement of phases whereby σ_e in problem (15.4.11) is isotropic).

Note that elimination of functions $f(p,\lambda)$ and $f(p,\mu)$ from (15.4.13)–(15.4.15) results in the ratio relating σ_e, κ_e, α_e and independent of concrete medium structure [5]

$$\frac{\kappa_e}{\sigma_e} = T\frac{\gamma_1\chi_2 - \gamma_2\chi_1 - (\sigma_1\chi_2 - \sigma_2\chi_1)\alpha_e - (\sigma_2\gamma_1 - \sigma_1\gamma_2)\alpha_e^2}{\sigma_2\gamma_1 - \sigma_1\gamma_2}. \tag{15.4.17}$$

In the case when the influence of thermoelectric effects on the electric and thermal conductivity is bad, i.e., at low figure of merit $Z_iT \ll 1$, the ratio (15.4.17) goes over to a simpler one [5, 18]:

$$\alpha_e = \frac{\alpha_1\sigma_1\kappa_2 - \alpha_2\sigma_2\kappa_1 - \sigma_1\sigma_2(\alpha_1 - \alpha_2)\kappa_e/\sigma_e}{\sigma_1\kappa_2 - \sigma_2\kappa_1} \\ = \alpha_1 + \frac{\sigma_1\sigma_2(\alpha_1 - \alpha_2)}{\sigma_1\kappa_2 - \sigma_2\kappa_1}\left(\frac{\kappa_1}{\sigma_1} - \frac{\kappa_e}{\sigma_e}\right), \tag{15.4.18}$$

where now $\sigma_e = \sigma_1 f(p, \sigma_2/\sigma_1)$, $\kappa_e = \kappa_1 f(p, \kappa_2/\kappa_1)$.

Thus, the behavior of the effective coefficient α_e in critical area is determined by the behavior of the effective conductivity (calculated without regard to thermoelectric effects), for which purpose it is sufficient to substitute function $f(p,h)$ from (15.4.12) into (15.4.13)–(15.4.15). In particular, it means that critical indices describing the behavior of α_e close to percolation threshold, can be combinations of only t, q, and ν—critical indices describing the behavior of σ_e.

The ratio (15.4.18) to a high accuracy was verified by means of numerical simulation [29] and experimentally [1].

As was considered above, within the EMT-approximation and by means of the HM percolation structure the behavior of α_e at $\kappa_1 \approx \kappa_2$ and $\kappa_1 \gg \kappa$ is qualitatively different.

Consider first, the case $\kappa_1 \approx \kappa_2$. If the inequality below is met

$$\left(\frac{\sigma_2}{\sigma_1}\right)^{\frac{t}{t+q}} \ll \frac{\alpha_2\sigma_2}{\alpha_1\sigma_1} \ll 1, \tag{15.4.19}$$

Then, as follows from (15.4.18), the effective coefficient α_e is changed considerably in the critical region

$$\alpha_e \approx \alpha_1,\ p > p_c,\ \tau^t \gg \alpha_2\sigma_2/\alpha_1\sigma_1,\ \tau \gg \Delta,\ \text{I}, \tag{15.4.20}$$

$$\alpha_e = \alpha_2 \frac{\sigma_2}{\sigma_1}\tau^{-t},\ p > p_c,\ \Delta \ll \tau \ll \left(\frac{\alpha_2}{\alpha_1}\frac{\sigma_2}{\sigma_1}\right)^{\frac{1}{t}},\ \text{II}, \tag{15.4.21}$$

$$\alpha_e = \alpha_2\left(\frac{\sigma_2}{\sigma_1}\right)^{\frac{q}{t+q}} = \alpha_2\Delta^q,\ |\tau| < \Delta,\ \text{III}, \tag{15.4.22}$$

$$\alpha_e = \alpha_2|\tau|^q,\ p < p_e,\ |\tau| \gg \Delta,\ \text{IV}, \tag{15.4.23}$$

where $(\sigma_2/\sigma_1)^{\frac{t}{t+q}} = \Delta$, as before, denotes smearing region.

For illustration, the regularities (15.4.20)–(15.4.23) are given in Fig. 15.5.

It is interesting to note that above the percolation threshold, beyond smearing region, where by all appearances "the leading part" should be played by the first phase $(\sigma_1,\ \kappa_1,\ \alpha_1)$, α_e is determined by α_2 in the II region.

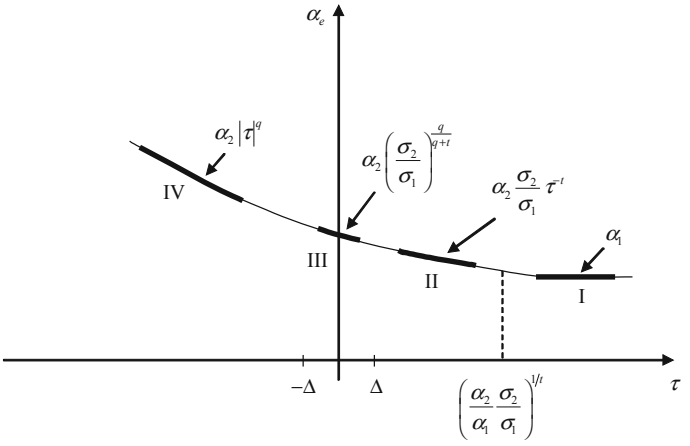

Fig. 15.5 Concentration dependence of the effective Seebeck coefficient in the critical region under close values of phase thermal conductivity $\kappa_1 \approx \kappa_2$ (see also Fig. 15.1a)

In the opposite case, when phase thermal conductivities are essentially different $(\kappa_1 \gg \kappa_2)$, a change in α_e from α_1 to α_2 occurs in the critical region unlike the case when they are close $(\kappa_1 \approx \kappa_2)$, when α_e is changed over the entire region of concentration change (see EMT-approximation yielding good precision beyond the critical region). At $\kappa_1 \gg \kappa_2$ several different cases are possible. At $\sigma_2/\sigma_1 \ll \alpha_2\sigma_2/\alpha_1\sigma_1 \ll 1$ or, which is the same, $\alpha_2 \gg \alpha_1$ and $\alpha_2\sigma_2 \ll \alpha_1\sigma_1$ and at $\sigma_2/\sigma_1 = \kappa_2/\kappa_1$ in (15.4.18) mathematical uncertainty appears. Analysis of general expressions (15.4.13)–(15.4.15) shows that in this case in the linear in α_i approximation the effective coefficient α_e is expressed not only through function $f(p,h)$ (15.4.11), but also through its derivative [7]:

$$\alpha_e = \alpha_1 + (\alpha_2 - \alpha_1)\frac{\partial \ln f(p,h)}{\partial h},\ h = \frac{\sigma_2}{\sigma_1} = \frac{\kappa_2}{\kappa_1}. \tag{15.4.24}$$

Then

$$\alpha_e \approx \alpha_1, \tau \gg \left(\frac{\alpha_2}{\alpha_1}\right)^{\frac{1}{t+q}}\Delta,\ p > p_c,\ \text{I}, \tag{15.4.25}$$

$$\alpha_e \approx \alpha_2\left(\frac{\sigma_2}{\sigma_1}\right)\tau^{-(t+q)},\ \Delta \ll \tau \ll \left(\frac{\alpha_2}{\alpha_1}\right)^{\frac{1}{t+q}}\Delta,\ p > p_c,\ \text{II}, \tag{15.4.26}$$

$$\alpha_e = \frac{t}{t+q}\alpha_2,\ |\tau| < \Delta,\ \text{III}, \tag{15.4.27}$$

$$\alpha_e = \alpha_2,\ |\tau| \gg \Delta,\ p < p_c,\ \text{IV}, \tag{15.4.28}$$

For illustration, the regularities (15.4.24)–(15.4.28) are depicted in Fig. 15.6.

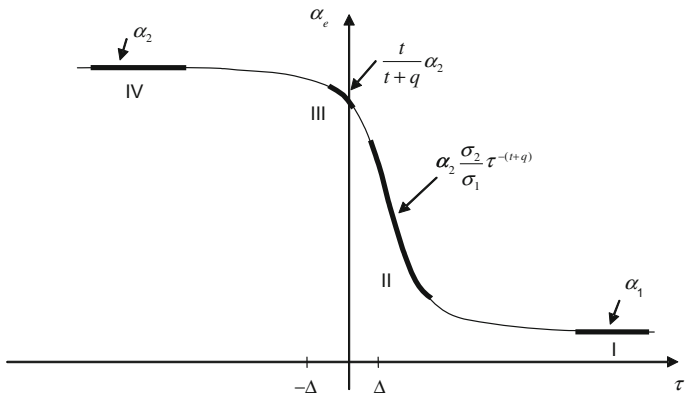

Fig. 15.6 Concentration dependence of the effective Seebeck coefficient in the critical region at $\alpha_2 \gg \alpha_1$ and $\alpha_2\sigma_2 \ll \alpha_1\sigma_1$ and at $\sigma_2/\sigma_1 = \kappa_2/\kappa_1$ (see also Fig. 15.1a)

References

1. Abroyan IA, Velichko VY, Chudnovsky FA (1985) Electric conductivity and thermoEMF in the area of two-dimensional flow with metal-semiconductor phase transition. Fizika of Solid State 27:1667–1669 (in Russian)
2. Ausloos M, Pekala M, Latuch J et al (2004) Unusual thermoelectric behavior of packed crystalline granular metals. J Appl Phys 96:7338–7345
3. Balagurov BY (1981) Reciprocity relations in two-dimensional percolation theory. Sov Phys JETP 54:355–358
4. Balagurov BY (1982) Thermoelectric properties of inhomogeneous thin films. Sov Phys Semicond 16:259–265 (in Russian)
5. Balagurov BY (1983) Isomorphism of certain problems of percolation theory. Sov Phys JETP T.58:331–340
6. Balagurov BY (1985) Thermoelectric properties of polycristals. Sov Phys Semicond 19:968–970 (in Russian)
7. Balagurov BY (1986) On thermoelectric properties of two-component media. Sov Phys Semicond 20:1276–1280 (in Russian)
8. Balagurov BY (1986) Thermogalvanomagnetic properties of two-dimensional two-component systems. Sov Phys Solid State 28:1156–1162
9. Bergman DJ, Fel L (1999) Enhancement of thermoelectric power factor in composite thermoelectric. J Appl Phys 85:8205–8216
10. Bergman DJ, Levy O (1991) Thermoelectric properties of a composite medium. J Appl Phys 70:6821–6833
11. Bulat LP, Drabkin IA, Karatayev VV et al (2013) Structure and transport properties of bulk nanothermoelectrics based on Bi_x Sb_{2-x} Te_3 fabricated by SPS method. J Electron Mater 42:2110–2113
12. Burshtein A (1962) Physical basis of calculation of thermoelectric semiconductor devices. Fiz-Mat Liter 135 [Moscow (in Russian)]
13. Drabkin IA, Karataev VV, Osvenski VB et al (2013) Structure and thermoelectric properties of nanostructured $(Bi, Sb)_2$ Te_3 (review). Adv Mater Phys Chem 119–132
14. Dykhne AM (1970) Contluctivity of a two-dimensional two-phase system. Sov Phys JETP 32:63–64
15. Dykhne AM (1980) Private communication
16. Faleev SV, Léonard F (2008) Theory of enhancement of thermoelectric properties of materials with nanoinclusions. Phys Rev B 77:214304-1–214304-9
17. Glatz A, Beloborodov IS (2009) Thermoelectric performance of granular semiconductors. Phys Rev B 80:245440-1–245440-4
18. Halpern V (1983) The thermopower of binary mixtures. J Phys C 16:L217–L220
19. Han G, Chen Z, Yang L et al (2015) Rational design of Bi_2Te_3 polycrystalline whiskers for thermoelectric applications. ACS Appl Mater Interfaces 7:989–995
20. Markussen T, Jauho A, Brandbyge M (2009) Surface-decorated silicon nanowires: a route to high-ZT thermoelectrics. Phys Rev Lett 103:055502-1–055502-5
21. Murakami S, Takahashi R, Tretiakov OA et al (2011) Thermoelectric transport of perfectly conducting channels in two- and three-dimensional topological insulators. J Phys Conf Ser 334:012013-1–012013-10
22. Neophytou N, Kosina H (2011) Effects of confinement and orientation on the thermoelectric power factor of silicon nanowires. Phys Rev B 83:245305-1–245305-49
23. Popescu A, Woods LM, Martin J et al (2009) Model of transport properties of thermoelectric nanocomposite materials. Phys Rev B 79:205302-1- 05302-7
24. Popescu A, Haney PM (2014) Interface scattering in polycrystalline thermoelectric. J Appl Phys 115:123701

25. Sakai A, Kanno T, Takahashi K et al (2014) Breaking the trade-off between thermal and electrical conductivities in the thermoelectric material of an artificially tilted multilayer. Scientific reports, 4
26. Samojlovich AG (1980) Eddy thermoelectric currents and energetic of anisotropic thermoelements (in problems of modern physics) Nauka, Leningrad, pp 304–318 (in Russian)
27. Scheele M, Oeschler N, Meier K et al (2009) Synthesis and thermoelectric characterization of Bi_2Te_3 nanoparticles. Adv Func Mater 19:3476–3483
28. Scheele M, Oeschler N, Veremchuk I et al (2010) ZT enhancement in solution-grown $Sb_{(2-x)}Bi_xTe_3$ nanoplatelets. ACS Nano 4:4283–4291
29. Skal AS (1985) Critical behavior of the thermoelectric power of binary composite materials. Sov Phys JETP T.61:301–305
30. Skal AS, Andreev AA, Tschirner HU (1982) Percolation theory and transport coefficient in disordered systems. Phyl Mag B 45:323–333
31. Snarskii A (1986) Effective conductivity of strongly inhomogeneous media near the percolation threshold. Sov Phys JETP 64:828–831
32. Snarskii AA, Adzhigai GV, Bezsudnov IV (2006) On the inherent figure of merit of thermoelectric composites Arxiv cond-mat 0609447.pdf, 1–7
33. Snarskii AA, Adzhigai GV, Bezsudnov IV (2005) On the inherent figure of merit of themoelectric composites. Thermoelectricity 4:76–83
34. Snarskii AA, Morozovskii AE (1985) Variational estimates for thermoelectric media. Sov Phys Techn Semicond 19:187–188
35. Snarskii AA, Tomchuk PM (1987) Kinetic phenomena in macroscopic inhomogeneous media (review). Ukrain Fiz Jur 32:66–92 (in Russian)
36. Snarskii AA, Sarychev AK, Bezsudnov IV et al (2012) Thermoelectric figure of merit for bulk nanostructured composites with distributed parameters. Microcrystalline Nanocrystalline, Porous, and Compos Semicond 46:659–665
37. Straley JP (1981) Thermoelectric properties of inhomogeneous materials. J Phys D 14:2101–2106
38. Webman I, Jortner J, Cohen MH (1977) Thermoelectric power in inhomogeneous materials. Phys Rev B 16:2959–2964
39. Yamashita O, Odaharab H, Ochic T et al (2007) Dependence of Seebeck coefficient on a load resistance and energy conversion efficiency in a thermoelectric composite. Mater Res Bull 42:1785–1803

Chapter 16
Effective Elastic Properties

16.1 Basic Concepts of Elasticity Theory

Due to the fact that the elastic macroscopically inhomogeneous media have a huge applied significance, a large number of monographs are dedicated to calculation of the effective elastic moduli of composites, such as [3, 10, 27, 34, 35]. There is no possibility and need to repeat the content of all the works. Some of them are strongly formalized and mainly include theorems and proofs of the existence of the effective kinetic coefficients in different cases. Some of the works are dedicated to concrete applications of empirical regularities discovered in practice. In [35] different numerous approximate methods for calculation of the effective elastic moduli have been described, except for the region close to percolation threshold. We will focus on the description of the effective elastic moduli of the two-phase strongly inhomogeneous components close to percolation threshold, as well as show that the main regularities of the effective kinetic coefficients can be explained within the HM-percolation structure. A review of original papers that consider critical behavior of the effective elasticity modules is given in [32, 33].

There are many different applications of network models/ percolation models in the theory of elasticity. Elasticity of networks could be studied in many different situations: static (study of effective modules), dynamic (study of vibrational properties, for example [22], non-equilibrium, for example [8]. Because elasticity equations are more complex (have more components) than linear equation, there are many different simplified elastic networks could be considered.

For example, in the paper [39] random network of rigid rods is considered. In the work [17] it is shown for bond-bending network with freely rotating cross-links, that the elastic exponent is different than in central force percolation network. In [9] mechanic stability of networks that have fiber-bending and fiber-stretching properties, see also [11, 18]. Critical elastic behavior observed in percolation network in [14]. Vibrational properties of networks considered in [1] (model of phonons in random elastic networks).

A.A. Snarskii et al., *Transport Processes in Macroscopically Disordered Media*, DOI 10.1007/978-1-4419-8291-9_16

There are many different non-equilibrium phenomena studied by the paradigm of spring networks: self-organization of networks, application of elastic for the description of fracture considered in [26, 31, 37] (see also [16, 25]). Self-organization of networks studied in the paper [8]. Appearance of rigidity in self-organized networks is described in [21]. Review of this area provided in the article [12]. Critical behavior of rheology of spring networks considered in [40], see also [7]. There are also unusual applications of percolation theory for study of composites [13]. This unexpected application of percolation theory was used for analysis of unusual elastic solids/leaks composites. Application of theory of elastic networks for explaining red blood cell membranes provided in [42].

There also an application of percolation theory for explaining of fracking phenomena. Different models of percolation (particularly invasion percolation) used for description of fracking phenomena [23, 24, 38].

Early in the investigation of the elastic properties of components close to percolation threshold, an opinion existed that in order to determine the effective kinetic coefficients it is sufficient to employ the analogy between the elasticity and conductivity problems—to replace the good conducting phase by the "soft" elastic phase, and bad conducting phase—by the "rigid" one. In fact, it is not the case, the conductivity problem is not directly reduced to the other problem—of elasticity, at least because the equations that determine the distribution of currents and fields in the conductivity problem, and deformations and stresses in the elasticity problem [20], belong to different classes. This in equivalence is also apparent from the fact that in the isotropic case conductivity is a scalar, and to determine the elastic properties of even a homogeneous isotropic body[1] two material constants will be needed—Young's modulus E and shear modulus μ which are tensor components. Hooke's law—the analog of Ohm's law—can be written down as [20]:

$$u_{ik} = \frac{1}{9k}\delta_{ik}\sigma_{ll} + \frac{1}{2\mu}(\sigma_{ik} - \frac{1}{3}\delta_{ik}\sigma_{ll}), \quad i,k,l = 1,2,3, \tag{16.1.1}$$

where u_{ik} is component of deformation tensor, σ_{ik} is stress tensor, $k = E\mu/3(3\mu - E)$ is uniform compression modulus.

The ratio (16.1.1) can be rewritten as

$$u_{ik} = \Omega_{iklm}\sigma_{lm}, \tag{16.1.2}$$

where Ω_{iklm} is fourth rank tensor, components of which according to (16.1.1) are expressed for the isotropic body through E and μ. A similar notation for the isotropic conducting medium has the form $j_i = \sigma\delta_{ik}E_k$, emphasizing again the difference between the elasticity and conductivity problems.

Percolation elasticity problems were actively studied by means of numerical simulation of different elastic lattices. Substitution of lattice elastic problem is

[1]In elasticity theory such a medium is called linearly elastic Hooke medium.

possible in several variants. If, for instance, we assign for the square net the coefficient of elasticity (Young's modulus) for each bond in the lattice, i.e. consider each bond as an elastic rod, such net on application of forces in certain direction will not resist the shear. In such a model the rods resist only tension and can easily, without efforts, change an angle between themselves. Such a model is called central —force Born model. It is matched by the following expression for the elastic deformation energy [19, 32]:

$$U_0 = \frac{\alpha_1}{2} \sum_{ij} [(\mathbf{u}_i - \mathbf{u}_j)\mathbf{r_{ij}}]^2 \ell_{ij}, \tag{16.1.3}$$

where α_1 is a constant related to rod elasticity, $\mathbf{u}_i$ is displacement of node i, $\mathbf{r_{ij}}$ is unity vector directed from node i to node j, ℓ_{ij} is elastic constant of the rod connecting nodes i and j.

Below we will consider a more realistic case, when the elastic energy exists in the model, related both to tension of rods (16.1.3) and to change of angle between them, which removes the "impossibility" of zero effective shear modulus

$$U = U_0 + \frac{\alpha_2}{2} \sum_{ijk} (\delta\theta_{ijk})^2 \ell_{ij} \ell_{ik}, \tag{16.1.4}$$

where α_2 is a constant related to a bend (change of angle between the rods), summation is done over all triplets of rods $j - i$ and $i - k$, a change in angle $\delta\theta_{ijk}$ can be represented as

$$\delta\theta_{ijk} = \begin{cases} \frac{(\mathbf{U_{ij}} \times \mathbf{r_{ij}} - \mathbf{U_{ik}} \times \mathbf{r_{ik}})(\mathbf{r_{ij}} \times \mathbf{r_{ik}})}{|\mathbf{r_{ij}} \times \mathbf{r_{ik}}|}, & \mathbf{r_{ij}} \nparallel \mathbf{r_{ik}}, \\ |(\mathbf{U_{ij}} + \mathbf{U_{ik}}) \times \mathbf{r_{ij}}|, & \mathbf{r_{ij}} \parallel \mathbf{r_{ik}}, \end{cases} \tag{16.1.5}$$

where $\mathbf{U_{ij}} = \mathbf{u_i} - \mathbf{u_j}$.

Such a model is called bond-bending. Thus, hereafter we will suppose that the medium has nonzero local moduli related both to tension (E) and to shear (μ).

16.2 Effective Module in the Vicinity of Percolation Threshold

Let us consider, within the HM, a strongly inhomogeneous in elastic constants medium below the percolation threshold, and the inhomogeneity will be considered so large that deformation of the first phase will be ignored. As can be seen from Fig. 16.1, describing the percolation structure at $p < p_c$, when there are portions of any direction in the interlayer. For simplicity, we will consider the two-dimensional case, divide the entire interlayer into portions extended along x direction (denote them A) and along y (B) (Fig. 16.1).

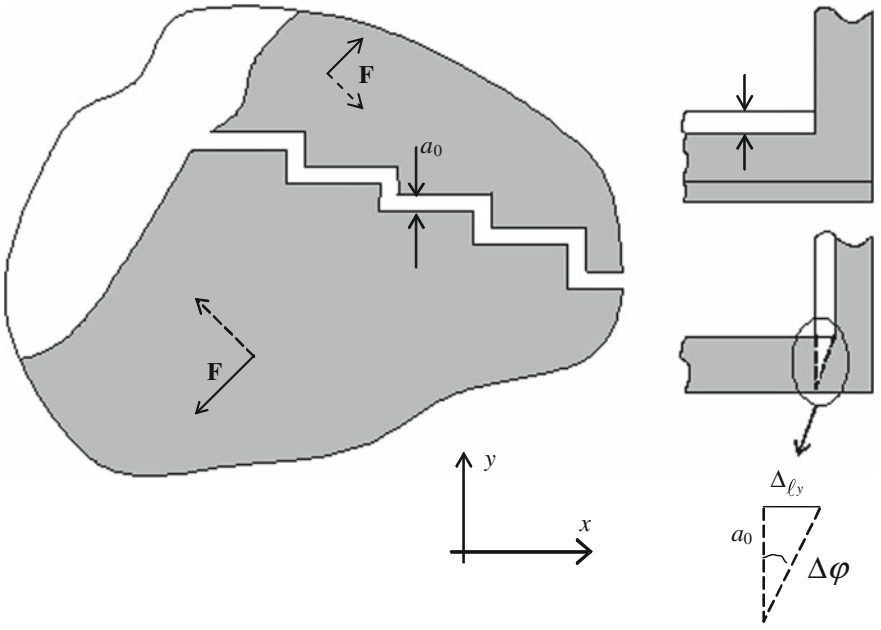

Fig. 16.1 Schematic of interlayer subject to tension. *Solid arrows*—tensile force **F**, *dashed arrows*—forces leading to shear deformation

For each type (A and B) of interlayer portions one can write down the Hooke's law for A portions

$$\frac{F_{yA}}{\ell_A H} = E_2 \frac{\Delta\ell_y}{a_0}, \quad \frac{F_{xA}}{\ell_A H} = \mu_2 \frac{\Delta\ell_x}{a_0}, \tag{16.2.1}$$

and for B portions

$$\frac{F_{yB}}{\ell_B H} = \mu_2 \frac{\Delta\ell_y}{a_0}, \quad \frac{F_{xB}}{\ell_B H} = E_2 \frac{\Delta\ell_x}{a_0}, \tag{16.2.2}$$

where F_{xA}, F_{yA}, F_{xB}, F_{yB}—x and y—are components of force **F** acting on the portion A and B, E_2, μ_2 are local moduli of elasticity of the "soft" (second, in terms of conductivity) phase, and $\Delta\ell_x$ and $\Delta\ell_y$ is displacement along the axes OX and OY(insert in Fig. 16.1), ℓ_A and ℓ_B is total length of portions A and B, H is thickness of the two-dimensional medium. Here we take into account that at small deformations the shear angle $\Delta\varphi$ (insert in Fig. 16.1) which enters the determination of

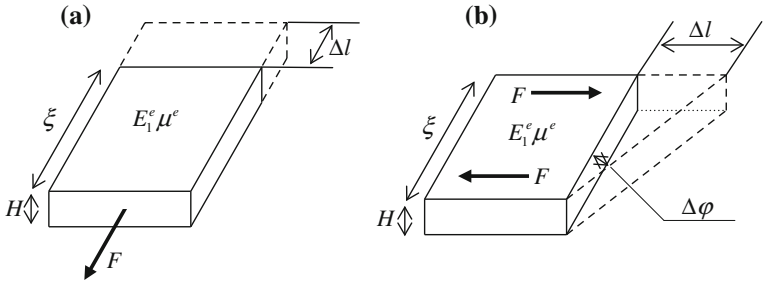

Fig. 16.2 Determination of the effective Young's modulus E^{e} and shear modulus μ^e (two-dimensional case): **a** $F/\xi H = E^{\mathrm{e}}\Delta l/\xi$; **b** $F/\xi H = \mu^e\Delta\varphi$, $\Delta\varphi \approx \Delta\mathbf{l}/\xi$

shear modulus μ is equal to displacement divided by the interlayer thickness —$\Delta\ell_x/a_0$ (for the portion B $\Delta\ell_y/a_0$). Expressing the tensile force $\mathbf{F}$ applied to the interlayer as

$$\mathbf{F} = (F_{xA} + F_{xB})\mathbf{i} + \big(F_{yA} + F_{yB}\big)\mathbf{j}, \tag{16.2.3}$$

through the displacement $\Delta\mathbf{l}$

$$\Delta\mathbf{l} = \Delta\ell_x\mathbf{i} + \Delta\ell_y\mathbf{j}, \tag{16.2.4}$$

and taking into account (16.2.1) and (16.2.2), we find $\mathbf{F} = (E_2 + \mu_2)(\ell H/a_0)\Delta\mathbf{l}$, where we assume that $\ell_A \approx \ell_B = \ell$. By determination of the Young's modulus (Fig. 16.2) $\mathbf{F}/\xi H = E^{\mathrm{e}}\Delta\mathbf{l}/\xi$. Then from (16.2.4) we have

$$E^{\mathrm{e}} = (E_2 + \mu_2)\frac{\ell}{a_0}. \tag{16.2.5}$$

taking into account that interlayer area according to the HM in the two-dimensional case is of the form

$$S = \ell a_0 = a_0^2 N_2, \quad N_2 = |\tau|^{-q_2}, \tag{16.2.6}$$

we find the expression for the description of critical behavior for the effective Young's modulus below the percolation threshold and critical index S_2

$$E_{\mathrm{e}} \approx (E_2 + \mu_2)|\tau|^{-S_2}, \quad S_2 = q_2, \quad d = 2. \tag{16.2.7}$$

Quite similarly are found the expressions describing the critical behavior of the effective Young's modulus in the three-dimensional case. The only difference is that interlayer portions in one of the directions are subject to tension, and in the other two directions—to shear, which causes a change in multiplier at τ in (16.2.6) in the form

$$E^{\mathrm{e}} \approx \frac{E_2 + 2\mu_2}{3} |\tau|^{-S_3}, \quad S_3 = q_3, \quad d = 3. \tag{16.2.8}$$

Thus, below the percolation threshold both in the two- and three-dimensional cases the critical index of Young's modulus coincides with the critical index of the effective conductivity

$$S = q, \quad p < p_c, \quad d = 2, 3. \tag{16.2.9}$$

Let's assume now that the external force to be applied to characteristic size ξ in such a way that the interlayer on the whole is subject to shear (see dashed arrows in Fig. 16.1). Repeating calculation similar to the above, for the effective shear modulus μ^{e} (see Fig. 16.2b) we obtain

$$\mu^{\mathrm{e}} \sim |\tau|^{-S}, \quad S = q. \tag{16.2.10}$$

A simplified conclusion (16.2.8)–(16.2.10), without regard to "crumpled" interlayer, is given in [36].

Numerical simulation represented in [4] for the two-dimensional case leads to (16.2.7) with a good precision. At the same time, $S < q$ was obtained in [2, 15]. For the three-dimensional case, arguments in favor of $S_3 = q_3$ are given in [5, 6]. In [5] arguments are provided that $S_2 = q_2$ is a precise equality.

Now we consider within the IM of percolation structure the behavior of the effective Young's modulus above the percolation threshold. For this purpose within the HM we equate the potential energies of the two-dimensional inhomogeneous medium and the comparison medium with the effective modules. In the two-dimensional case the main deformation of tortuous bridge under compression (tension) is bending. The energy of the unit length of bent rod according to [20] is the integral along the rod length—the bridge (Fig. 16.3):

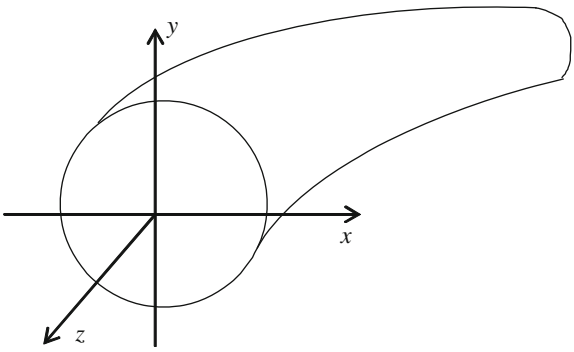

Fig. 16.3 Bridge portion in the three-dimensional case with cross-section at $z = \text{const}$.

$$U = \int \frac{M^2 d\ell}{2JE}, \tag{16.2.11}$$

where M is the moment of applied forces, J is the so-called moment inertia of section, equal to $J = \int x^2 \mathrm{d}s$, $\mathrm{d}s$ is section element. Axis oz is directed along the bridge (elastic rod); for certainty we assume that the bend occurs in plane (z, x).

The deformation energies of comparison medium in the two-dimensional (U_2) (see Fig. 16.2a) and three-dimensional cases (U_3) are of the form

$$U_2 = \left(\frac{F}{\xi H}\right)^2 \frac{\xi^2 H}{2E^{\mathrm{e}}}, \quad U_3 = \frac{F^2 \xi}{E^{\mathrm{e}} \xi^2}. \tag{16.2.12}$$

Equating (16.2.11) with U_2 from (16.2.12) at $M = F\xi$, and $\Delta\ell = a_0 N_1$, we find

$$E^{\mathrm{e}} \approx E_1 \frac{J}{H} \frac{1}{\xi^2 a_0 N_1}, \tag{16.2.13}$$

where as before, it is taken into account that the characteristic size (not the length!) of the bridge is of the order ξ. According to the HM of percolation structure, $N_1(d = 2) \approx \tau^{-t}$, whence follows the critical index of the effective Young's modulus in the two-dimensional case

$$E^{\mathrm{e}} \approx E_1 \tau^{f_2}, \quad f_2 = t_2 + 2v_2, \quad p > p_c. \tag{16.2.14}$$

In the three-dimensional case $\int \mathrm{d}\ell = a_0 N_1 \sim \tau^{-t+v}$ and for E^{e} we obtain the same relation between the critical indices of elasticity f, conductivity t and correlation length

$$E^{\mathrm{e}} \approx E_1 \tau^f, \quad f = t + 2v, \quad d = 2, 3. \tag{16.2.15}$$

With regard to numerical values of t and v (Table 5.1) (16.2.15) we have

$$f_2 = 3.97, \quad f_3 = 3.76. \tag{16.2.16}$$

In [19, 30] there was obtained a precise restriction of the kind

$$f \geq 1 + vd. \tag{16.2.17}$$

In [28] for reasons close to those considered above there was obtained a restriction of the kind

$$f \leq t + 2v, \tag{16.2.18}$$

and was shown that the value $f_2 = 3.97 = t + 2v$ is in good agreement with that found from the numerical simulation $f_2 = 3.96 \pm 0.04$ [41].

It should be noted that the numerical values of critical index f essentially differ in different papers. For instance, for the two-dimensional case in [29] $f_2 \approx 3$, however, in [5] it is asserted that the ratio (16.2.15) in the two-dimensional case is accurate.

Let us come back to reasoning within the HM. From the reasons stated for the determination of critical behavior of the effective Young's modulus E^{e} above (16.2.15) and below (16.2.7), (16.2.8) the percolation threshold it follows that critical behavior of the effective shear modulus μ^{e} is the same. Therefore, to determine the smearing region and the kind of E^{e} and μ^{e} in this region, one can act similarly to the way it was done for the case of the effective conductivity, namely, to equate E^{e} $(p < p_c)$ and E^{e} $(p > p_c)$ at $|\tau| \approx \Delta$. Then for the two-dimensional case we get

$$\frac{E_2 + \mu_2}{2} (\Delta_{\mathrm{E}})^{-q} \approx E_1 \Delta_E^f, \tag{16.2.19}$$

whence

$$\Delta_E = \left(\frac{E_2 + \mu_2}{2E_1} \right)^{\frac{1}{f+q}}. \tag{16.2.20}$$

Thus, on the percolation threshold (in smearing region) the effective modulus of elasticity will be of the form

$$E^{\mathrm{e}} \approx E_1 \left(\frac{E_2 + \mu_2}{2E_1} \right)^{S_2'}, \quad S_2' = \frac{t_2 + 2\nu_2}{2(t_2 + \nu_2)}, \tag{16.2.21}$$

where it is taken into account that $q_2 = t_2$.

Because in the two-dimensional case the percolation threshold $p = 1/2$, the expression for E^{e} should be invariant with a mutual replacement of phases, which calls for correction (16.2.21). The expression (16.2.21) for E^{e} can be artificially "symmetrised" by writing down

$$E^{\mathrm{e}} \simeq (E_1 + E_2)^{1-S'} \left(\frac{2}{E_1 + \mu_1} + \frac{2}{E_2 + \mu_2} \right)^{-S'}, \tag{16.2.22}$$

and since the medium is supposed to be strongly inhomogeneous—$E_1/E_2 \gg 1$, $\mu_1/\mu_2 \gg 1$, dependence (16.2.22), obeying symmetry requirements, practically does not differ from (16.2.21). The general universal expression for $E^{\mathrm{e}} = E^{\mathrm{e}}(E_1, E_2, \mu_1, \mu_2)$ in the two-dimensional case on the percolation threshold, similar to the Dykhne expression $\sigma_{\mathrm{e}} = \sqrt{\sigma_1 \sigma_2}$ and suitable for any values of the ratios E_1/E_2 and μ_1/μ_2, is hardly possible. Conditions of mutual duality of media are not unambiguously determined by E^{e} [3]—additional information is needed on the

medium structure. Therefore, universality of E^e close to percolation threshold apparently exists only for randomly inhomogeneous medium and only in the case of strong inhomogeneity ($E_1/E_2 \gg 1, \mu_1/\mu_2 \gg 1$). In so doing, the problem of the value of ratio, for instance, E_1/μ_1, remains beyond the scope of the HM.

In the three-dimensional case instead of (16.2.17) we write down

$$E^e \approx E_1 \left(\frac{E_2 + 2\mu_2}{3E_1} \right)^{S_3'}, \quad S_3' = \frac{t_3 + 2v_3}{t_3 + q_3 + 2v_3}, \tag{16.2.23}$$

and smearing region is of the form

$$\Delta_E = \left(\frac{E_2 + 2\mu_2}{3E_1} \right)^{\frac{1}{t_3 + q_3 + 2v_3}}. \tag{16.2.24}$$

The numerical values S_2' (16.2.21) and S_3' from (16.2.23) according to Table 1 in Sect. 5.3 are

$$S_2' = 0.75, \quad S_3' = 0.82. \tag{16.2.25}$$

Similar to the fact it was done for σ^e, in the determination of the elastic properties one can take into account corrections to E^e, including to consideration the second, third, etc. steps of the HM. Then above the percolation threshold ($p > p_c$) we obtain

$$E^e = E_1 \tau^f [A_0 + A_1 K_d \tau^{-(q+t)} + A_2 \left(K_d \tau^{-(q+t)} \right)^2 + \cdots], \tag{16.2.26}$$

where according to (16.2.21) and (16.2.23) we find

$$K_d = \frac{E_2 + (d-1)\mu_2}{E_1 d}, \quad d = 2, 3 \tag{16.2.27}$$

Below the percolation threshold (at $p < p_c$)

$$E^e \approx E_1 K_d |\tau|^{-q} [B_0 + B_1 K_d |\tau|^{-(q+t)} + B_2 \left(K_d |\tau|^{-(q+t)} \right)^2 + \cdots], \tag{16.2.28}$$

The expressions (16.2.7), (16.2.8), (16.2.13), (16.2.21), and (16.2.23) can be written down in a unified way, introducing, by analogy to σ^e, scaling function $F(z)$ of the form

$$E^e \approx E_1 K_d^{S'} F \left(\tau / K_d^{\frac{s}{t+q}} \right) \tau^f, \tag{16.2.29}$$

where $F(z)$ has the following asymptotics:

$$F(z) \sim \begin{cases} z^f, & z \to 0, \quad p > p_c, \quad \tau \gg \Delta_E, \\ 1, \ |z| \approx 1, & \qquad\qquad\quad \tau \approx \Delta_E\,, \\ |z|^{-q}, & z \to -\infty, \quad p < p_c, \quad |\tau| \gg \Delta_E. \end{cases} \tag{16.2.30}$$

References

1. Amir A, Krich JJ, Vitelli V et al (2013) Emergent percolation length and localization in random elastic networks. Phys Rev X 3, 021017-1–021017-1 1 (2013)
2. Arbabi S, Sahimi M (1990) Critical properties of viscoelasticity of gels and elastic percolation networks. Phys Rev Lett 65:725–728
3. Berdichevsky VL (1983) Variational principles of continuous mechanics, Nauka, M. 448 p (in Russian)
4. Bergman DJ (1986) Elastic moduli near percolation threshold in a two-dimensional random network of a rigid and nonrigid bonds. Phys Rev B 33:2013–2016
5. Bergman DJ (2002) Exact relations between critical exponents for elastic stiffness and electrical conductivity of two-dimensional percolating networks. Phys Rev E 0261124-1–026124-7
6. Bergman DJ (2003) Exact relation between elastic and electric response of d-dimensional percolating networks with angle bending forces. J Stat Phys 111:171–199
7. Bishop AR, Lookman T, Saxena A et al (2003) Elasticity-driven nanoscale texturing in complex electronic materials. Europhys Lett 63:289–295
8. Boolchand P, Lucovsky G, Phillips JC et al (2005) Self-organization and the physics of glassy networks. Philos Mag 85:3823–3838
9. Broedersz CP, Mao X, Lubensky TC et al (2011) Criticality and isostaticity in fiber networks. Nat Phys 7:983–988
10. Christensen R (2005) Mechanics of composite materials dover. New York 355 p (2005)
11. Chubynsky MV, Thorpe MF (2007) Algorithms for 3D rigidity analysis and a first order percolation transition. Phys Rev E 76:041135–1–041135–28
12. Chubinsky M (2009) Characterizing the intermediate phases through topological analysis. In: Micoulaut M, Popescu M (eds) Rigidity transitions and Boolchand intermediate phases in nanomaterials. INOE, Bucharest, Romania, pp 213–260
13. Dapp WB, Lucke A, Persson BNJ et al (2012) Self-affine elastic contacts: percolation and leakage. Phys Rev Lett 108:2443011–2443014
14. Farrago O, Kantor Y (2000) Entropic elasticity of phantom percolation networks. Europhys Lett 52:413–419
15. Feng S (1985) Percolation properties of granular elastic networks in two dimensions. Phys Rev B 32:R510–R513
16. Gabrielli A, Cafiero R, Caldarelli G (1999) Statistical properties of fractures in damaged materials. Europhys Lett 45:13–19
17. Head DA, MacKintosh FC, Levine AJ (2003) Non-universality of elastic exponents in random bond–bending networks. Phys Rev E 68:025101-1–025101-4
18. Head DA, Levine AJ, MacKintosh FC (2003) Distinct regimes of elastic response and deformation modes of cross-linked cytoskeletal and semiflexible polymer networks. Phys Rev E 68:061907-1–061907-16
19. Kantor Y, Webman I (1984) Elastic properties of random percolating systems. Phys Rev Lett 52:1891–1894

20. Landau LD, Lifshitz EM (1987) Theory of elasticity, 3rd edn, vol 7. Butterworth-Heinemann, Oxford 187 p
21. Micoulaut M, Phillips JC (2007) Onset of rigidity in glasses: from random to self-organized networks. J Non-Cryst Solids 353:1732–1740
22. Nakanishi H (1993) Effect of loops on the vibrational spectrum of percolation network. Physica A 196:33–41
23. Norris JQ, Turcotte DL, Rundle JB et al (2014) Loopless nontrapping invasion-percolation model for fracking. Phys Rev E 89:022119-1–022119-24
24. Norris JQ, Turcotte DL, Rundle JB et al (2015) Anisotropy in fracking: a percolation model for observed microseismicity. Pure Appl Geophys 172:7–21
25. Nukala PK, Simunovi S, Zapperi S (2004) Percolation and localization in the random fuse model. J Stat Mech Theory Exp 2004:P08001-1–P08001-21
26. Ostoja-Starzewski M, Sheng PY, Alzebdeh K (1996) Spring network models in elasticity and fracture of composites and polycrystals. Comput Mater Sci 7:82–93
27. Pobedrja BE (1984) Mechanics of composite materials. Moscow University 336 p (in Russian)
28. Roux S (1986) Relation between elastic and scalar transport exponent in percolation. J Phys A 19:L351–L356
29. Roux S, Guyon E (1985) Mechanical percolation: a small beam lattice study. J Phys Lett 46: L999–L1004
30. Roux S, Guyon E (1985) Mechanical percolation a small beam lattice study. C. R. Acad Sc Paris 301:367–370
31. Sadhukhan S, Dutta T, Tarafdar S et al (2011) Crack formation in composites through a spring model. Phys A 390:731–740
32. Sahimi M (1994) Applications of percolation theory. Taylor & Francis 258 p
33. Sahimi M (1998) Non-linear and non-local transport processes in heterogeneous media: from long-range correlated percolation to fracture and materials breakdown. Phys Rep 306:213–395
34. Sendeckyj GP (ed) (1974) Mechanics of composite materials, vol 2. Academic Press, New York 503 p
35. Shermergor TD (1977) Theory of elasticity for microinhomogeneous media. Nauka, Moscow 400 p (in Russian)
36. Snarskii AA (1988) Critical behaviour of elasticity modules for macroscopically inhomogeneous media near threshold percolation. Ukrain Fiz Jur T 33:1063–1065
37. Toussaint R (2005) Interating damage models mapped onto Ising and perolation models. Phys Rev E71:046127-1–046127-16
38. Wettstein J, Wittel FK, Araujo NAM et al (2012) From invasion percolation to flow in rock fracture networks. Physica A 391:264–277
39. Wilhelm J, Frey E (2003) Elasticity of stiff polymer networks. Phys Rev Lett 91:108103-1–108103-4
40. Yucht MG, Sheinman M, Broedersz CP (2013) Dynamical behavior of disordered spring networks. Soft Matter 9:7000–7006
41. Zabolitzky JG, Bergman DJ, Stauffer D (1986) Precision calculation of elasticity for percolation. J Stat Phys 44:211–223
42. Zhang R, Brown FLH (2008) Cytoskeleton mediated effective elastic properties of model red blood cell membranes. J Chem Phys 129:065101-1–065101-38

Chapter 17
Nonlinear Properties of Composites

17.1 Types of Nonlinearity

Up to now, in the calculation of the effective properties of composites it has been always assumed that local volt-ampere characteristics are linear, i.e., Ohm's law is met for each of the phases. Of course, there are cases, and they are numerous, when it is not the case. First, with increasing electrical field (or current), above certain values, slight deviation from linearity will occur. Such case is commonly called weak nonlinearity:

$$\mathbf{j} = \sigma\mathbf{E} + \gamma|\mathbf{E}|^2\mathbf{E} + \ldots \tag{17.1.1}$$

Here, often we restrict our consideration to the second component, and the "weakness" of nonlinearity determines the inequality

$$\gamma E^2 \ll \sigma. \tag{17.1.2}$$

With small fields the second component is ignored and then (17.1.1) goes over to a linear dependence, i.e., to Ohm's law.

Second, there are media wherein even under arbitrarily small fields the volt-ampere characteristic does not become linear. One of the kinds of such nonlinearity [14, 31]

$$\mathbf{j} = \chi|E|^{\beta}\mathbf{E} \tag{17.1.3}$$

is commonly called strong nonlinearity. Note that in this case even for arbitrarily small field (at $\beta \neq 0$) the law (17.1.3) doesn't approach the linear one.

There are many cases with more complicated nonlinearities, for instance, with the electrical damage (breakdown of poorly conducting part) the volt-ampere characteristic will be not smooth (probably it will be even discontinuous function).

A.A. Snarskii et al., *Transport Processes in Macroscopically Disordered Media*, DOI 10.1007/978-1-4419-8291-9_17

In ferromagnetic materials, dependence of magnetic permeability $\mu = \mu(H)$ is a nonmonotonous function of magnetic field intensity H, and with account of hysteresis—an ambiguous function (see Chap. 18).

To determine the effective properties of inhomogeneous medium, as has been above for the linear cases and remains valid for the nonlinear ones, means to find a relation between the average in volume field $\langle \mathbf{E} \rangle$ and current $\langle \mathbf{j} \rangle$. With a nonlinear volt-ampere characteristic, for instance, in case of weak nonlinearity (17.1.1), phase isotropy and isotropy of their geometric arrangement does not mean yet the isotropy of the effective coefficients [3, 25]. In the simplest case from (17.1.1) follows

$$\langle \mathbf{j} \rangle = \sigma_e \langle \mathbf{E} \rangle + \gamma_e \left\langle |E|^2 \right\rangle \langle \mathbf{E} \rangle, \tag{17.1.4}$$

however, γ_e can be second-rank tensor. The possibility of anisotropy origination is particularly illustrative on a specially selected example in [3]. Here, we do not consider such cases and consider that $\gamma^e_{ijkl} = \gamma_e(\delta_{ik}\delta_{lm} + \delta_{il}\delta_{km} + \delta_{im}\delta_{kl})/3$, what allows us writing down (17.1.4).

A review of papers dedicated to calculation of the effective properties of nonlinear composites within the EMT approximation is given in [22]. An appropriate generalization of the EMT method proposed in [8] for the linear case in different versions of nonlinearlity and was employed in [11, 12, 13, 33, 35], and some others. Below we will show how this EMT generalization "works" for the case of weak and strong nonlinearity, and in Chap. 18—for the nonlinearity inherent in ferromagnetic materials.

The first part of this chapter deals with the case of weak nonlinearity (17.1.1), and the second part with strong nonlinearity (17.1.3).

17.2 The Case of Weak Nonlinearity

The effective coefficient γ_e (17.1.4) is closely related to the relative spectral density of 1/*f*—noise. In [1, 32] it is shown that γ_e, as well as the relative spectral density of 1/*f*—noise C_e, is expressed through the fourth moment of field $\mathbf{E}$ of the linear problem as

$$\gamma_e = \frac{\left\langle \gamma(\mathbf{r})\mathbf{E}^4(\mathbf{r}) \right\rangle}{\langle \mathbf{E} \rangle^4}, \tag{17.2.1}$$

where $\mathbf{E}$ is field in a linear problem calculated at $\gamma(\mathbf{r}) = 0$. The proof of this surprising fact, apart from [1, 32], is given in many later works, and most vividly it is represented in [2].

Let us now show the way of calculating the effective coefficients by means of a generalized EMT method [36]. Consider n-phase medium, where $i = 1, \ldots n$ is used to label the phases. According to (17.2.1) it can be written as

$$\gamma_e = \frac{1}{\langle E\rangle^4}\sum p_i\gamma_i\langle E^4\rangle_i, \tag{17.2.2}$$

where $\langle\ldots\rangle_i$ means averaging over ith phase.

The basic approximation lies in the replacement

$$\langle E^4\rangle_i \to \langle E^2\rangle_i^2, \tag{17.2.3}$$

then (17.2.2) takes on the form

$$\gamma_e \approx \frac{1}{\langle E\rangle^4}\sum p_i\gamma_i\langle E^2\rangle_i^2, \tag{17.2.4}$$

and the problem reduces to determination of the second moment of field $\langle E^2\rangle_i$.

Let us use the following checked ratio:

$$\frac{\partial\sigma_e}{\partial\sigma_i} = p\frac{\langle E^2\rangle_i}{\langle E\rangle^2}, \tag{17.2.5}$$

whence

$$\langle E^2\rangle_i = \frac{\langle E\rangle^2}{p}\frac{\partial\sigma_e}{\partial\sigma_i}, \tag{17.2.6}$$

and the factor $\partial\sigma_e/\partial\sigma_i$ (17.2.6) is found from the EMT equation which for the n-phase case is of the form

$$\sum p_i\frac{\sigma_e - \sigma_i}{(d-1)\sigma_e + \sigma_i} = 0, \tag{17.2.7}$$

where d is a dimension of the problem.

Despite the approximation (17.2.3), the above-considered approach gives a good agreement with the numerical experiment both in the two-dimensional [34] and three-dimensional [36] cases. Figure 17.1 shows concentration dependence $\gamma_e = \gamma_e(p)$ for several value sets of local coefficients in the three-dimensional case. Conspicuous is a fact that drastic increase of γ_e near the percolation threshold. This fact becomes understandable if we recollect that γ_e, just as the relative spectral density of 1/*f*—noise, is determined by the fourth moment of field, and that the relative spectral density of 1/*f*—noise, as is shown in Chap. 13, is drastically increased in the critical region.

Notwithstanding the fact that the above-considered EMT modification describes well the concentration dependence of γ_e over a wide range, in the critical region at $|\tau| \ll 1$, due to its "origin" (from the linear version of EMT) it cannot provide a correct description of critical index values.

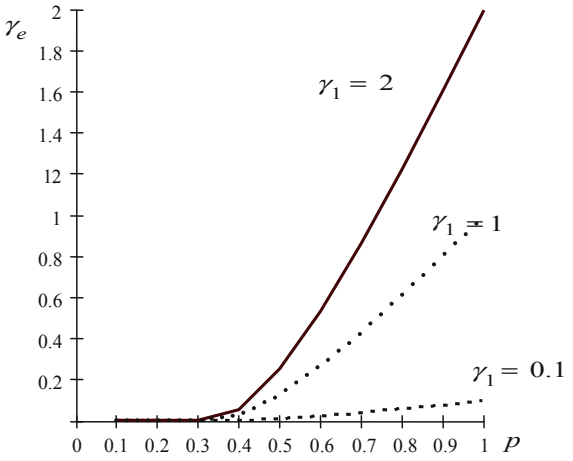

Fig. 17.1 Concentration dependence γ_e for three values of local coefficient of nonlinearity γ_1 at $\sigma_1 = 100,\ \sigma_2 = 1,\ \gamma_2 = 0$

For the first time, increase in nonlinearity on approaching the percolation threshold from below (from $p < p_c$) was indicated in [20], where for field calculation there was introduced such element of percolation structure as interlayer. There is no need to calculate critical indices of nonlinear conductivity γ_e ab initio. They, by the above-mentioned analogy are expressed through critical indexes of the relative spectral density of 1/*f*—noise. Indeed, comparing the expression (17.2.1) and C_e (see Chap. 13), we get

$$C_e = \frac{\langle C\sigma^2 E^4 \rangle}{\sigma_e^2 \langle E \rangle^4}, \tag{17.2.8}$$

whence we find the analogy

$$\gamma_e \to \sigma_e^2 C_e, \quad \sigma^2(\mathbf{r})C(\mathbf{r}) \to \gamma(\mathbf{r}), \tag{17.2.9}$$

i.e., γ_e is expressed through both C_e and σ_e, provided that for the latter the local $\sigma^2(\mathbf{r})C(\mathbf{r})$ are replaced by $\gamma(\mathbf{r})$. Thus, multiplying the expression for C_e above the percolation threshold

$$C_e = C_1 \tau^{-k} + (\sigma_2/\sigma_1)^2 C_2 \tau^{-w}, \quad p > p_c, \tag{17.2.10}$$

by σ_e^2 and taking into account that $\sigma_e = \sigma_1 \tau^t$, we find

$$\gamma_e = \gamma_1 \tau^{2t-k} + \gamma_2 \tau^{2t-w}, \quad p > p_c, \tag{17.2.11}$$

and similarly below the percolation threshold, we have

$$\gamma_e = \gamma_2 \tau^{-2q-k'} + (\sigma_2/\sigma_1)^4 \gamma_1 \tau^{-2q-w'}. \tag{17.2.12}$$

Thus, critical behavior of γ_e is described by four critical indices:

$$\gamma_e = \gamma_1 \tau^{-u} + \gamma_2 \tau^{-m}, \quad p > p_c, \tag{17.2.13}$$

$$\gamma_e = \gamma_2 \tau^{-u'} + (\sigma_2/\sigma_1)^4 \gamma_1 \tau^{-m'}, \quad p < p_c, \tag{17.2.14}$$

where

$$u = k - 2t, \quad m = w - 2t, \quad u' = k' + 2q, \quad m' = w' + 2q. \tag{17.2.15}$$

Like in the case of relative spectral density of 1/*f*—noise, the expressions of γ_e above and below the percolation threshold should be agreed, γ_e ($p > p_c$) must coincide with γ_e ($p < p_c$) in the smearing region, i.e., at $|\tau| = \Delta$. This agreement exists, if for critical indices of the relative spectral density of 1/*f*—noise k, k', w, and w' we use their values obtained by means of the HM (see Chap. 13). Substituting these values into (17.2.15), we obtain

$$u = 3t - 2\nu(d-1), \quad m = 2\nu + q, \quad u' = m, \quad m' = 2\nu(d-1) + t + 4q, \tag{17.2.16}$$

Table 17.1 gives their numerical values for two- and three-dimensional cases. Note that $u_{2,3} < 0$.

Smearing region, as it follows immediately from (17.2.13), (17.2.14), and (17.2.16), has, as it should be, the standard value $\Delta = (\sigma_2/\sigma_1)^{\frac{1}{t+q}}$. At $|\tau| \approx \Delta$ the first component in (17.2.13) becomes equal to the second one in (17.2.14) $\gamma_1 \Delta^{-u} = (\sigma_2/\sigma_1)^4 \gamma_1 \Delta^{-m'}$, and the second (17.2.13)—to the first one in (17.2.4)—is compared to (13.3.14).

It should be noted that the first component in (17.2.13) comprises factor τ in the positive degree and, therefore, in the critical region at $\tau \to 0$ it is much less than the second component (at nonzero γ_2). The same can be said about the second component in (17.2.14), it is small due to factor $(\sigma_2/\sigma_1)^4$. On the whole, both above and below the percolation threshold, the second "dielectric" phase is the main contributor to nonlinear conduction increase. This, of course, is related to the fact that in strongly inhomogeneous medium close to percolation threshold the local field is increased exactly in the "thin" interlayer (with thickness of order a_0), rather than in

Table 17.1 Indices values for two- and three-dimensional cases

Dimension	u	$m = u'$	m'
$d = 2$	−1.23	3.97	9.17
$d = 3$	−2.48	2.49	10.2

the "long" bridge (of length $\sim a_0\tau^{-\alpha_1}$). When value of γ_2 is not low in comparison to γ_1, we have

$$\gamma_e(p > p_c) \approx \gamma_2\tau^{-m}, \quad \gamma_e(p < p_c) \approx \gamma_2|\tau|^{-u'}, \tag{17.2.17}$$

and since $m = u'$, the increase in γ_e on approaching the percolation threshold occurs symmetrically.

On approaching the smearing region, both components in (17.2.14) increase. In the very smearing region from (17.2.13) and (17.2.14) ($|\tau| = \Delta$) it follows

$$\gamma_e = \gamma_1 h^{-\frac{u}{t+q}} + \gamma_2 h^{-\frac{m}{t+q}}, \quad h = \frac{\sigma_2}{\sigma_1}, \quad |\tau| \le \Delta, \tag{17.2.18}$$

and as long as $u < 0$ (see Table 17.1), with increasing inhomogeneity (i.e., when σ_1/σ_2 increases) the first component is reduced, and the second increased.

In the expressions for current (17.1.1) and (17.1.4) in the case of weak nonlinearity, it is assumed that each subsequent component—the second, third, etc.—is much less than the previous one. Critical field E_c is a such characteristic value of field that gives criterion of applicability of weak nonlinearity approximation. Specifically at $\langle E\rangle \ll E_c$ this approximation "works". If the expression for γ_e is known as (17.2.13) or (17.2.14), then E_c is easily determined. Thus, for the case of $p < p_c$:

$$\langle \mathbf{j}\rangle \approx \sigma_e|\tau|^{-q}\langle \mathbf{E}\rangle + \gamma_2|\tau|^{-u'}\langle \mathbf{E}\rangle^2\langle \mathbf{E}\rangle, \tag{17.2.19}$$

whence immediately follows the expression for E_c:

$$\sigma_e|\tau|^{-q}E_c = \gamma_2|\tau|^{-u'}E_c^3, \tag{17.2.20}$$

Thus, we could write down the following

$$E_c \sim |\tau|^M, \quad M = \frac{u' - q}{2}. \tag{17.2.21}$$

Within the HM, we have

$$M = \frac{u' - q}{2} = \frac{k' + q}{2}, \quad M_2 = 1.33, \quad M_3 = 0.88. \tag{17.2.22}$$

In [10] it was found that within the EMT $M_2 = M_3 = 1/2$, and double-sided boundaries for M are of the form

$$1.18 \le M_2 \le 1.33, \quad 0.66 \le M_3 \le 0.88, \tag{17.2.23}$$

which agrees with (17.2.22).

It should be noted that apart from condition $\langle E\rangle \ll E_c$, for the validity of weak nonlinearity approximation the local fields also should be such whereby, for instance, that the second components in (17.1.1) are little less than the first ones [28].

Just as the relative spectral density of 1/*f*—noise, the nonlinear conductivity γ_e "feels well" the medium structure. Its behavior, for instance, in self-dual media, differs from that in the two-dimensional randomly inhomogeneous media on percolation threshold. It is impossible to obtain a single expression for γ_e in *D*-media. Such an expression, unlike the effective conductivity, will depend on the kind of specific realization. Nevertheless, one can find general expression for the effective properties, independent of realization in one specific case [30]. The second component in this case should be much less than the first one. Then the Dykhne transformations $\mathbf{j} = \Lambda\mathbf{n} \times \tilde{\mathbf{E}}, \mathbf{E} = \Lambda^{-1}\mathbf{n} \times \tilde{\mathbf{j}}$ are converted (17.1.1) into

$$\tilde{\mathbf{j}} = \tilde{\sigma}\tilde{\mathbf{E}} + \tilde{\gamma}\tilde{\mathbf{E}}^2\tilde{\mathbf{E}}, \tag{17.2.24}$$

where

$$\tilde{\sigma} = \Lambda^2/\sigma, \quad \tilde{\gamma} = -\gamma(\Lambda/\sigma)^4, \quad \Lambda = \sqrt{\sigma_1\sigma_2}, \tag{17.2.25}$$

and the rest components in (17.2.24) are discarded due to their smallness.

Duality means that

$$\sigma_1^2\gamma_2 = -\sigma_2^2\gamma_1. \tag{17.2.26}$$

Repeating arguments similar to those given in Chap. 6, for medium fields $\langle\mathbf{E}\rangle$ and currents $\langle\mathbf{j}\rangle$, we arrive at reciprocity relations:

$$\tilde{\sigma}_e(p)\sigma_e(p) = \sigma_1\sigma_2, \quad \tilde{\gamma}_e(p) = -\tilde{\gamma}_e(p)(\sqrt{\sigma_1\sigma_2}/\sigma_e(p))^4. \tag{17.2.27}$$

Then in the case of mutually dual media $\tilde{\sigma}_e(p) = \sigma_e(1-p)$ and $\tilde{\gamma}_e(p) = \gamma_e(1-p)$, we can write down

$$\sigma_e(p)\sigma_e(1-p) = \sigma_1\sigma_2, \quad \tilde{\gamma}_e(1-p) = -\gamma_e(p)(\sqrt{\sigma_1\sigma_2}/\sigma_e(p))^4. \tag{17.2.28}$$

For the linear part of conductivity from (17.2.28) at p = 1/2 follows the Dykhne formula $\sigma_e = \sqrt{\sigma_1\sigma_2}$, and for the nonlinear one must assume

$$\gamma_e(p = 1/2) = 0. \tag{17.2.29}$$

Thus, the duality requirement from which follows the requirement of different signs of nonlinearity in phases (17.2.26): in one phase the nonlinearity increases medium conductivity, and in the other reduces it, leading to mutual compensation of these contributions for the entire medium in general. In this case, the effective medium conductivity will be linear.

The presence of *D*-points in the self-dual media leads, as in the case of 1/*f*—noise, to a divergence of the linear part of conductivity [23, 24, 26]:

$$\gamma_e \sim \frac{1}{h - h_e}, \quad h = \frac{\sigma_2}{\sigma_1}, \quad h_c = ctg\left(\frac{\alpha}{4}\right)\frac{1 + tg(\alpha/4)}{1 - tg(\alpha/4)}, \tag{17.2.30}$$

where the same notation is used as in Fig. 13.3 in Chap. 13.

Generally speaking, local electrical conductivity depends on temperature, and account of this fact can change the behavior of the nonlinear part of conductivity, especially for structures possessing peculiarities of *D*-points close to which the Joule heat release is concentrated. As it turned out [27], account of thermal conductivity in such structures (and, of course, temperature dependence of γ on local conductivity) can result in the elimination of peculiarities similar to (17.2.30).

17.3 The Case of Strong Nonlinearity

The kind of nonlinearity (17.1.3) that is commonly called strong nonlinearity is observed experimentally, for instance, in ZnO varistors [9, 19] and disordered alloys [21]. Theoretically, it was first studied in the critical region in [14, 31].

The most appropriate method for calculation of the effective conductivity of randomly inhomogeneous medium with nonlinearity of the type (17.1.3) over the entire concentration range was proposed in [13] (see also [11, 12]). This method is a generalization of EMT similar to that described above for the weak nonlinearity. Consider it by an example when only one of the phases is nonlinear [11]:

$$\mathbf{j} = \chi_1 |\mathbf{E}|^\beta \mathbf{E}, \quad \mathbf{j} = \sigma_2 \mathbf{E}, \tag{17.3.1}$$

and, thus, (17.3.1) can be rewritten as

$$\mathbf{j} = \sigma(\mathbf{E})\mathbf{E}, \quad \sigma(\mathbf{E}) = \begin{cases} \chi_1 |\mathbf{E}|^\beta, & \text{I phase}, \\ \sigma_2, & \text{II phase}, \end{cases} \tag{17.3.2}$$

where $\sigma(\mathbf{E})$ is coefficient of nonlinear conductivity relating the electrical field intensity to current density. In so doing, for the effective conductivity value we obtain

$$\langle \mathbf{j} \rangle = \sigma_e(\langle \mathbf{E} \rangle)\langle \mathbf{E} \rangle. \tag{17.3.3}$$

Calculation of σ_e with application of generalized EMT method consists in the fact that (the first approximation) the nonlinear conductivity in the first phase $\sigma(\mathbf{E}) = \chi_1 |\mathbf{E}(\mathbf{r})|^\beta$ is replaced by the constant:

$$\sigma(\mathbf{E}(\mathbf{r})) \to \sigma(\langle \mathbf{E} \rangle) = \chi_1 \left\langle |\mathbf{E}|^{\beta} \right\rangle_1, \tag{17.3.4}$$

and then the nonlinear law (17.3.1) is converted into linear, i.e., into Ohm's law, though with a so far unknown value $\langle |\mathbf{E}|^{\beta} \rangle_1$:

$$\mathbf{j} = \chi_1 \left\langle |\mathbf{E}|^{\beta} \right\rangle \mathbf{E} = \tilde{\sigma}_1 \mathbf{E}. \tag{17.3.5}$$

Now the medium consists of two phases with conductivities $\tilde{\sigma}_1$ and σ_2 and for such "linear" medium one can find within the linear EMT the effective conductivity, for instance, for the two-dimensional case:

$$\sigma_e = \frac{1}{2}\left[(1-2p)(\sigma_2 - \tilde{\sigma}_1) \pm \sqrt{(1-2p)^2(\sigma_2 - \tilde{\sigma}_1)^2 + 4\tilde{\sigma}_1\sigma_2}\right], \tag{17.3.6}$$

in so doing, the value $\langle |\mathbf{E}|^{\beta} \rangle_1$ remains so far unknown.

The second approximation lies in replacement (compare to (17.2.3))

$$\left\langle |\mathbf{E}|^{\beta} \right\rangle_1 \to \left\langle |\mathbf{E}|^2 \right\rangle_1^{\beta/2}, \tag{17.3.7}$$

where medium square of the field $\left\langle |\mathbf{E}|^2 \right\rangle_1$ is found from the ratio (17.2.6) which in this case is convenient to be written as

$$\left\langle |\mathbf{E}|^2 \right\rangle^{\beta/2} = \frac{1}{p^{\beta/2}} \left(\frac{\partial \sigma_e}{\partial \tilde{\sigma}_1}\right)^{\beta/2} \langle \mathbf{E} \rangle^{\beta}, \tag{17.3.8}$$

and under $\partial\sigma_e/\partial\tilde{\sigma}_1$ is meant derivative of σ_e from (17.3.6).

Thus, for the two unknown σ_e and $\left\langle |\mathbf{E}|^{\beta} \right\rangle_1 \to \left\langle |\mathbf{E}|^2 \right\rangle_1^{(\beta/2)}$ there are two nonlinear algebraic equations (17.3.6) and (17.3.8) solving which allows finding σ_e for the nonlinear inhomogeneous medium over the entire concentration range.

Despite the two essential approximations, the above schematic is in good agreement with the numerical experiments and allowed, in particular, explaining the dependences obtained during numerical calculation in [15]. One can say that to a large extent such appropriate EMT generalization is due to the fact that the linear EMT is based on field calculation in spherical (in the general case—ellipsoidal) inclusions, and, as is well known, the field inside such an inclusion does not depend on whether it is linear or not.

In the critical region close to percolation threshold in the case when one of the phases is strongly nonlinear, the problem of calculation of the effective coefficients was first considered in [14, 31]. For the case of $p > p_c$, there was obtained

$$\langle \mathbf{j} \rangle = \chi_1 \tau^{t(\beta)} |\langle \mathbf{E} \rangle|^{\beta} \langle \mathbf{E} \rangle, \quad p > p_c, \quad \sigma_2 = 0, \tag{17.3.9}$$

with critical index

$$t(\beta) = (d - 2 - \beta)v + (1 + \beta)\zeta(\beta), \tag{17.3.10}$$

where within the NLB model $\zeta(\beta) = 1$, and within the IM $\zeta(\beta) = \zeta_R$.

[20] deals with a case below the percolation threshold, when the second phase is nonlinear, and the first phase is a perfect conductor

$$\langle \mathbf{j} \rangle = \chi_2 |\tau|^{-q(\beta)} |\langle \mathbf{E} \rangle|^{\beta} \langle \mathbf{E} \rangle, \quad p < p_c, \quad \rho_1 = 1/\sigma_1 = 0, \tag{17.3.11}$$

where

$$q(\beta) = \zeta(\beta) - (d - 2 - \beta)v, \tag{17.3.12}$$

and within the NLB model $\zeta(\beta) = 1$, and within the HM $\zeta(\beta) = \zeta_G$.

Simultaneous account of nonlinearity of both phases with identical coefficient of nonlinearity $\beta_1 = \beta_2 = \beta$, but with $\chi_1 \gg \chi_2$ was provided in [19]. Account of final "conductivity" $\chi_1 \neq 0$ and $\chi_2 \neq 0$ of both phases yielded, in particular, the expression in the smearing region:

$$\langle \mathbf{j} \rangle = \left(\chi_1^{q(\beta)} \chi_2^{t(\beta)} \right)^{\frac{1}{t(\beta) + q(\beta)}} |\langle \mathbf{E} \rangle|^{\beta} \langle \mathbf{E} \rangle \tag{17.3.13}$$

where $t(\beta)$ is given in (17.3.10), and $q(\beta)$—in (17.3.12).

Below we consider a case [27] when phases have different volt-ampere characteristics ($\beta_1 \neq \beta_2$), in particular, they include the cases when both phases are linear ($\beta_1 = \beta_2 = 0$).

Consider, for instance, a problem when in the first and second phases the volt-ampere characteristics are equal, respectively, to

$$\mathbf{j} = \chi_1 |\mathbf{E}|^{-2/3} \mathbf{E}, \quad \mathbf{j} = \chi_2 |\mathbf{E}|^2 \mathbf{E}, \tag{17.3.14}$$

or

$$\mathbf{E} = \gamma_1 |\mathbf{j}|^2 \mathbf{j}, \quad \mathbf{E} = \gamma_2 |\mathbf{j}|^{-2/3} \mathbf{j}, \tag{17.3.15}$$

where

$$\chi_1 = \gamma_1^{-1/3}, \quad \gamma_2 = \chi_1^{-1/3}. \tag{17.3.16}$$

Figure 17.2 schematically represents these characteristics and shows E_c—the value of electric field intensity whereby current values in the first and second phases are compared. In region I of electrical fields the first phase conducts current better

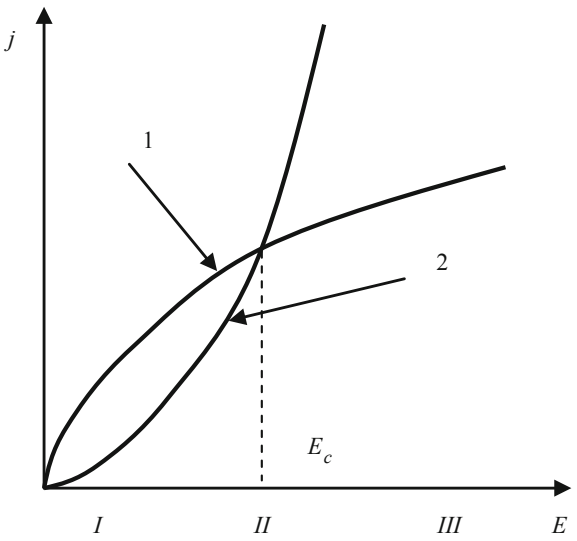

Fig. 17.2 Volt-ampere characteristics of the first "black"—1 and second "white"—2 phases

than the second one (it can be called "metal"), in region *II* the conducting properties of phases are approximately equal, in region *III* the phases "change places"—now the second phase conducts current better (plays the role of "metal").

To calculate the effective properties, let us use the second step of the HM. The bridge and interlayer resistances can be assigned based on the kind of volt-ampere characteristic. Consider a three-dimensional case:

$$U_1 = \frac{N_1}{a_0^5 \chi_1^3} J_1^3, \quad U_2 = \frac{a_0}{\chi_2 N_2} J_2^{1/3}, \tag{17.3.17}$$

where $U_{1,2}$ is voltage drop, $J_{1,2}$ are the bridge and interlayer currents.

In the derivation of (17.3.17), like in the linear case, it is taken into account that currents flowing through "single connected bonds"—SCB, of which a bridge is composed, are identical for each resistance and equal to full current through the bridge, and that voltage drop on each of "single disconnected bonds"—SDCB, of which the interlayer is composed, is identical and equal to voltage drop on the interlayer. Above the percolation threshold the bridge and the interlayer are connected in parallel, so full current J_ξ on sizes of the order of correlation length ξ is equal to the sum of currents $J_1 + J_2 = J_\xi$. Then

$$J_\xi = \left(\frac{a_0^5 \chi_1}{N_1}\right)^{1/3} U_\xi^{1/3} \left(1 + \frac{\chi_2}{\chi_1} \frac{N_2 N_1^{1/3}}{a_0^{8/3}} U_\xi^{8/3}\right), \tag{17.3.18}$$

where it is taken into account that $U_1 = U_2 = U_\xi$ is voltage drop on elements of order ξ.

Below the percolation threshold $U_\xi = U_1 + U_2$ and $J_1 = J_2 = J_\xi$, then we have

$$U_\xi = \left(\frac{a_0}{\chi_2 N_2}\right)^{1/3} J_\xi \left[1 + \left(\frac{\chi_2 N_2}{a_0}\right)^{1/3} \frac{N_1}{a_0^5 \chi_1^3} J_\xi^{8/3}\right], \quad p < p_c. \tag{17.3.19}$$

The use of both HM and NLB model assumes the presence of strong inhomogeneity—conductivity of the "black" phase should be much larger that that of the "white" phase, which is possible (see Fig. 17.2) in region *I*, when $E \ll E_c$ and $j \ll j_c$, where E_c and j_c for the considered case (17.3.14), (17.3.15) are of the form

$$E_c = \left(\frac{\chi_1}{\chi_2}\right)^{3/8}, \quad j_c = \left(\frac{\chi_1^9}{\chi_2^{1/8}}\right)^{3/8}. \tag{17.3.20}$$

As long as maximum current is a bridge current, and maximum field is an interlayer field, then

$$j_{\max} = |\langle \mathbf{j} \rangle||\tau|^{-2v}, \quad E_{\max} = |\langle \mathbf{E} \rangle||\tau|^{-v}, \tag{17.3.21}$$

and, thus, the medium is found in the region of fields *I*, if

$$|\langle \mathbf{E} \rangle| \ll E_c|\tau|^v = \left(\frac{\chi_1}{\chi_2}\right)^{3/8} |\tau|^v, \tag{17.3.22}$$

$$|\langle \mathbf{j} \rangle| \ll j_c|\tau|^{2v} = \left(\frac{\chi_1^9}{\chi_2^{1/8}}\right)^{3/8} |\tau|^{2v}. \tag{17.3.23}$$

The presence of factor τ in (17.3.22) and (17.3.23) means that the closer to percolation threshold is the first phase concentration, the more rigid are these conditions.

Apart from restrictions due to strong inhomogeneity, there are restrictions inherent in the model of percolation structure: above the percolation threshold its basic element should be a bridge, and below the percolation threshold—an interlayer. In other words, at $p > p_c$ the inequality $Q_1 \gg Q_2$ should be met, where Q_1 and Q_2 is heat release on the bridge and interlayer. Since at $p > p_c$ this inequality assumes the form $J_1 \gg J_2$, then with regard to (17.3.17) we have

$$U_2 \ll a_0 \left(\frac{\chi_1}{\chi_2}\right)^{3/8} |\tau|^{(3\xi_R + \xi_G)/8}, \quad p > p_c. \tag{17.3.24}$$

Below the percolation threshold the condition $Q_2 \gg Q_1$ is fullfilled, which with regard to $J_1 = J_2$, $U_2 \gg U_1$ brings about the following:

$$J_1 \ll a_0^2 \left(\frac{\chi_1^9}{\chi_2}\right)^{1/8} |\tau|^{(3\xi_R + \xi_G)/8}, \quad p < p_c. \tag{17.3.25}$$

If (17.3.22)–(17.3.25) are met, then (17.3.18) and (17.3.20) can be used to determine the effective properties of a nonlinear medium. Taking into account that in the three-dimensional case $J_\xi = |\langle \mathbf{j} \rangle| \xi^2$, $U_\xi = \langle \mathbf{E} \rangle \xi$ and $\xi = a_0 |\tau|^{-\nu}$, from (17.3.18) and (17.3.19) we obtain

$$\langle \mathbf{j} \rangle = \chi_1 |\tau|^{\tilde{t}} |\langle \mathbf{E} \rangle|^{1/3} \frac{\langle \mathbf{E} \rangle}{|\langle \mathbf{E} \rangle|} \left(1 + \frac{\chi_2}{\chi_1} |\tau|^{-\tilde{\varphi}} |\langle \mathbf{E} \rangle|^{8/3}\right), \quad p > p_c, \tag{17.3.26}$$

$$\langle \mathbf{j} \rangle = \chi_2 |\tau|^{-\tilde{q}} |\langle \mathbf{E} \rangle|^{3} \frac{\langle \mathbf{E} \rangle}{|\langle \mathbf{E} \rangle|} \left(1 - 3\frac{\chi_2}{\chi_1} |\tau|^{-\tilde{\varphi}} |\langle \mathbf{E} \rangle|^{8/3}\right), \quad p < p_c, \tag{17.3.27}$$

where

$$\tilde{t} = \frac{5\nu + \xi_R}{3}, \quad \tilde{q} = \nu + \xi_G, \quad \tilde{\varphi} = \tilde{t} + \tilde{q}, \tag{17.3.28}$$

and, within the HM we have

$$\tilde{t}_3 = \frac{4\nu_3 + t_3}{3}, \quad \tilde{q}_3 = 2\nu_3 + q_3, \quad \tilde{\varphi} = \frac{t_3 + 3q_3 + 10\nu}{3}, \tag{17.3.29}$$

Within the NLB model, ξ_R and ξ_G in (17.3.28) should be replaced by unity.

Substitution of ξ_R and ξ_G expressed through t, q, and ν in (17.3.24) and (17.3.25) shows that these two conditions coincide, i.e., it is the same thing written down in different ways:

$$|\langle \mathbf{E} \rangle| \ll \left(\frac{\chi_1}{\chi_2}\right)^{3/8} \tau^{(t + 3q + 10\nu)/8}, \tag{17.3.30}$$

or, which is the same,

$$\langle |\mathbf{j}| \rangle \ll \left(\frac{\chi_1^9}{\chi_2}\right)^{1/8} \tau^{(3t + q + 14\nu)/8}, \tag{17.3.31}$$

which denotes, as it should be, the smallness of second components as compared to the first one in (17.3.26) and (17.3.27).

Similarly to the linear case, using the expressions (17.3.26) and (17.3.27) one can find the size of the smearing region Δ and the effective properties of the nonlinear medium in this region. To determine Δ, having previously replaced $|\tau|$ by Δ, we equate the first components in (17.3.26) and (17.3.27) or the first and second components in (17.3.26) [or in (17.3.27)], and in all these cases we obtain

$$\Delta = \left(\frac{\chi_2}{\chi_1}\right)^{\frac{3}{t+3q+10v}} |\langle \mathbf{E} \rangle|^{\frac{8}{t+3q+10v}}. \tag{17.3.32}$$

As can be seen from (17.3.32), the size of the smearing region Δ depends on the average field value. As long as the critical region for which (17.3.26) and (17.3.27) are valid, is the concentration region $|\tau| \ll 1$, then for Δ from (17.3.32) the inequality $\Delta \ll 1$ must be also satisfied, or

$$|\langle \mathbf{E} \rangle| \ll \left(\frac{\chi_1}{\chi_2}\right)^{3/8}. \tag{17.3.33}$$

Note that if condition $|\langle \mathbf{E} \rangle| \ll E_c$ from (17.3.22) is satisfied, then, as long as $|\tau|^v \ll 1$, the condition (17.3.33) is known to be satisfied.

Substituting Δ from (17.3.32) to the first component (17.3.26) or (17.3.27), we find the effective properties of a nonlinear medium in the smearing region as

$$\langle \mathbf{j} \rangle = \left(\chi_1^{3(q+2v)} \cdot \chi_2^{t+4v}\right)^{\frac{1}{t+3q+10v}} |\langle \mathbf{E} \rangle|^{\frac{3t+q+14v}{t+3q+10v}} \frac{\langle \mathbf{E} \rangle}{|\langle \mathbf{E} \rangle|}, \quad |\tau| \le \Delta. \tag{17.3.34}$$

The numerical values of critical indices of conductivity (17.3.29) with a given selected kind of nonlinearity are of the form

$$\tilde{t}_3 = 1.84, \quad \tilde{q}_3 = 2.49, \quad \tilde{\varphi}_3 = 4.33. \tag{17.3.35}$$

Note that while above and below the percolation threshold, beyond the smearing region, the field dependence (17.3.26) and (17.3.27) for the medium current ($\sim |\langle \mathbf{E} \rangle|^{1/3}$ $p > p_c$ and $|\langle \mathbf{E} \rangle|^3$ $p < p_c$) coincides with that for pure phase. However, in the smearing region this value coincides with neither of them and is in the interval between them (17.3.35):

$$\frac{3t+q+14v}{t+3q+10v} = 1.47, \quad 0.33 < 1.47 < 3. \tag{17.3.36}$$

Let us consider calculation of the effective properties for the strong nonlinearity in the general case, when the dependences of j on E for the first and second phases are the following:

$$\mathbf{j} = \chi_1 |\mathbf{E}|^{\frac{1-\gamma}{\gamma}} \mathbf{E}, \quad \mathbf{j} = \chi_2 |\mathbf{E}|^{\beta-1} \mathbf{E}, \tag{17.3.37}$$

where β and γ are parameters assigning the kind of strong nonlinearity, in general case, is similar to that given above,

$$\langle \mathbf{j} \rangle = \chi_1 \tau^{\tilde{t}} |\langle \mathbf{E} \rangle|^{1/\gamma} \frac{\langle \mathbf{E} \rangle}{|\langle \mathbf{E} \rangle|} \left(1 + \frac{\chi_2}{\chi_1} \tau^{-\tilde{\varphi}} |\langle \mathbf{E} \rangle|^{\beta-1/\gamma}\right), \quad p > p_c, \tag{17.3.38}$$

$$\langle \mathbf{j} \rangle = \chi_2 \tau^{-\tilde{q}} |\langle \mathbf{E} \rangle|^{\beta} \frac{\langle \mathbf{E} \rangle}{|\langle \mathbf{E} \rangle|} \left(1 - \left(\frac{\chi_2}{\chi_1} \tau^{-\tilde{\varphi}} |\langle \mathbf{E} \rangle|^{\beta - 1/\gamma} \right)^{\gamma} \right), \quad p < p_c \tag{17.3.39}$$

$$\langle \mathbf{j} \rangle = \left(\chi_1^{\tilde{q}} \chi_2^{\tilde{t}} \right)^{1/\tilde{\varphi}} |\langle \mathbf{E} \rangle|^{\frac{\beta \tilde{t} + \tilde{q}/\gamma}{\tilde{\varphi}}} \frac{\langle \mathbf{E} \rangle}{|\langle \mathbf{E} \rangle|}, \quad |\tau| < \Delta. \tag{17.3.40}$$

Here the size of the smearing region, like in (17.3.32), depends on $\langle \mathbf{E} \rangle$:

$$\Delta = \left[\left(\frac{\chi_2}{\chi_1} \right) |\langle \mathbf{E} \rangle|^{\beta - 1/\gamma} \right]^{1/\varphi}, \tag{17.3.41}$$

and critical indices $\tilde{t}$, $\tilde{q}$, $\tilde{\varphi}$ (within the HM) are of the form

$$\tilde{t} = \frac{t + \nu(d-1)(\gamma - 1)}{\gamma}, \quad \tilde{q} = q + \nu(\beta - 1), \quad \tilde{\varphi} = \tilde{t} + \tilde{q}. \tag{17.3.42}$$

It is noteworthy that under certain values of nonlinearity parameters β and γ, namely, when $\beta \tilde{t} + \tilde{q}/\gamma = 0$, a medium which remains nonlinear above and below the percolation threshold, in the smearing region behaves linearly.

The above percolation description of the effective properties assumes considerable inhomogeneity, i.e., valid in region *I* (see Fig. 17.2), when $E \ll E_c$. Consider now the region which is close to E_c—region *II* in Fig. 17.2. Directly at point E_c, i.e., at $|\langle \mathbf{E} \rangle| = E_c$, the medium becomes homogeneous in conductivity, and close to E_c—though nonlinear, but weakly inhomogeneous. Therefore, for the analysis of its effective properties the percolation approach can be used no longer, but one can apply the EMT generalization of a linear case [11, 12, 13, 35]. This method, provided that the notation $\langle \mathbf{j} \rangle = \sigma_e(|\langle \mathbf{E} \rangle|) \langle \mathbf{E} \rangle$ is accepted, will lead to the first approximation in the small parameter $\frac{(|\langle \mathbf{E} \rangle| - E_c)}{E_c} \ll 1$. In so doing, for $\sigma_e(|\langle \mathbf{E} \rangle|)$ the following expression is obtained:

$$\sigma_e \approx \chi_2 \left(1 - 2 \frac{\gamma - 1}{(1-p)(\gamma - 1) - 2} p \frac{\langle \mathbf{E} \rangle - E_c}{E_c} \right). \tag{17.3.43}$$

In the third region of volt-ampere characteristic (see Fig. 17.2) at $E \gg E_c$ the elements of "black" and "white" phases change their places. It would seem that at replacement $\chi_1 \rightleftarrows \chi_2$, $p \rightleftarrows 1 - p$, one should observe the same percolation structure and the same properties. In so doing, however, one should be sure that at all medium points, not only in percolation elements (bridge and interlayer) at given average field $\langle \mathbf{E} \rangle \gg E_c$ the local field is larger than critical one. A detailed analysis of nonlinear medium in the region of fields *III* has not been addressed yet.

In the two-dimensional case in the self-dual media, at certain ratio of nonlinearity parameters β and γ, namely, at

$$\gamma = 1/\beta, \tag{17.3.44}$$

the exact solution of problem of the effective properties of inhomogeneous medium is possible.

Using the Dykhne transformation (see Chap. 6) one can find [29] that in the case (17.3.44) the volt-ampere characteristic is linear, and the effective conductivity is of the form

$$\sigma_e = \left(\chi_1^{\beta}\chi_2\right)^{\frac{1}{1+\beta}}. \tag{17.3.45}$$

In the case when $\beta = 1$, both phases are nonlinear, and σ_e (17.3.45) coincides with the effective conductivity obtained by A.M. Dykhne, $\sigma_e = \sqrt{\sigma_1\sigma_2}$. A discrete variant when a network of nonlinear resistances has a linear volt-ampere characteristic is considered in [4].

Numerical check of critical indices obtained for the case of strong nonlinearity was provided in many works. In [6, 7], critical index of conductivity above the percolation threshold was calculated by means of models of hierarchical fractal networks. In [16, 17] (see also the references cited) there were found numerical values of critical index of conductivity above the percolation threshold. It is noteworthy that in many papers where the numerical experiment was performed on the network models, strong nonlinearity can be written as

$$V = r|I|^{\alpha}\operatorname{sgn} I, \tag{17.3.46}$$

where V is voltage drop on the bond, r is its resistance, I is current through this bond, sgn is sign function.

In the numerical experiment where one seeks the average over realizations, resistance $\{R\}$ depending on L—sample size:

$$\{R\} \sim L^{\tilde{\zeta}(\alpha)}, \tag{17.3.47}$$

Such dependence at $L \gg \xi$ goes over (see Chap. 9) ($\xi \to \tau^{-\nu}$) to the following one:

$$R \sim \tau^{-\zeta(\alpha)}, \quad \zeta(\alpha) = \nu\tilde{\zeta}(\alpha). \tag{17.3.48}$$

For the effective "resistivity" γ_e in the d-dimensional case, we have

$$\gamma_e = R\xi^{d-1/\alpha}/\xi, \tag{17.3.49}$$

Passing to substituting field intensity $\langle E\rangle$ by V/ξ and current density $\langle \mathbf{j}\rangle$ by I/ξ^{d-1} into (17.3.46) we find

$$\langle E\rangle = \frac{V}{\xi} = R\frac{\left(\xi^{\alpha-1}\right)^{\alpha}}{\xi}\left(\frac{I}{\xi^{d-1}}\right)^{\alpha} \tag{17.3.50}$$

whence with regard to (17.3.48) we obtain

$$\gamma_{\mathrm{e}} \sim \tau^{-t_{\alpha}}, \quad t_{\alpha} = \alpha v(d-1) + \zeta(\alpha) - v. \tag{17.3.51}$$

As long as the effective coefficient γ_{e} in the case of strong nonlinearity is related to χ_{e} as follows:

$$\chi_{\mathrm{e}} = \gamma_{\mathrm{e}}^{-1/\alpha}, \tag{17.3.52}$$

we have from expression (17.3.51) the following

$$t(\alpha) = v(d-1) - \frac{\zeta(\alpha) - v}{\alpha}, \tag{17.3.53}$$

and in terms of parameter β ($\beta = (1-\alpha)/\alpha$) (17.3.53) changes, as it should be, to (17.3.10).

In [16, 17] the numerical values of $\zeta(\alpha)$ were found for different α and problem dimension d. It turned out that $\zeta(\alpha)$ does not differ much from unity and weakly depends on α, see Table 17.2, where the numerical values of index $\zeta(\alpha)$ are given for two-, three-, and six-dimensional problems and $\alpha = 5.0$ [16]. In the NLB model $\zeta(\alpha) = 1$, and within the HM $\zeta(\alpha) = \zeta_R$. Both models, at not very large values of β, yield satisfactory agreement with the numerical calculation. As in the case of problem of current moments, while moment degree is far from zero and not very large, the main elements of percolation structure are the bridge and the interlayer, which gives agreement between calculations within different models and the numerical calculations.

In [5, 6] a generalized problem is considered—the problem of determination of critical behavior of current moments in a strongly nonlinear medium, and it is shown that qth moment in a medium where $E \sim j^{\beta}$ is satisfied, is scaled as follows:

$$M_q(\beta) \sim L^{\tilde{\psi}(q,\beta)}, \tag{17.3.54}$$

Table 17.2 The numerical values of $\zeta(\alpha)$

Problem dimensionality	$\zeta(\alpha = 0.5)$
2	1.02 ± 0.08
3	1.02 ± 0.08
6	1.00 ± 0.01

where critical index $\tilde{\psi}(q,\beta)$ for different values of q and β yields for partial cases the well-known critical indices, for instance

$$\tilde{\psi}(1,1) = \xi_R, \quad \tilde{\psi}(\infty,\beta) = 1/v, \quad \tilde{\psi}(q,\infty) = 1/v, \quad \tilde{\psi}(q,-1) = D_B, \ldots. \tag{17.3.55}$$

References

1. Aharony A (1987) Crossover from linear to nonlinear resistance near percolation. Phys Rev Lett 58:2726
2. Balagurov B Ya (2001) Partial moments of electric field strength in the problem of conduction of binary composites. Sov Phys JETP 93:824–832
3. Bergman DJ (1999) Anisotropic nonlinear response of periodic square or cubic composites. Phys A 270:8–14
4. Bernasconi J, Shneider WR, Weismann HJ (1977) Some rigorous results for random planar conductance networks. Phys Rev B 16:5250–5255
5. Blumenfeld R (1989) Universality and superuniversality of multifractals in nonlinear resistor networks. J Stat Phys 1(2):223–241
6. Blumenfeld R, Meir Y, Harris AB, Aharony A (1986) Infinite set of exponents describing physics on fractal networks. J Phys A, 19:L791–L796
7. Blumenfeld R, Aharony A (1985) Nonlinear resistor fractal network, topological distances, singly connected bonds and fluctuations. J Phys A 18:443–448
8. Bruggeman DAG (1936) Berechnung verschiedener physikalischer Konstanten von heterogenen Substanzen, II. Ann Physik 25:645–672
9. Einziger R (1987) Metal oxide varisters. Annu Rev Mater Sci 17:299–321
10. Hiu PM (1994) Crossover electric field in percolating perfect-conductor–nonlinear-normal-metal composites. Phys Rev B 49:15334–15347
11. Hui PM, Cheung P, Kwong YR (1997) Effective response in nonlinear random composites. Phys A 241:301–309
12. Hui PM, Wan WMV (1996) Theory of effective response in dilute strongly nonlinear random composites. J Appl Phys Lett 69:1810–1812
13. Hiu PM, Woo YF, Wan WMV (1995) Effective response in random mixtures of linear and nonlinear conductors J Phys Cond Mat 7:593–597
14. Kenkel SW, Straley JP (1982) Percolation theory of nonlinear circuit elements. Phys Rev Lett 49:767–770
15. Levy O, Bergman DJ (1993) The bulk effective response of non-linear random resistor networks: numerical study and analytic approximations. J Phys C, 5:7095–7107
16. Meir Y, Blumenfeld R, Aharony A, Harris AB (1986) Series analysis of randomly diluted nonlinear resistor networks. Phys Rev B 34:3424–3428
17. Meir Y, Blumenfeld R, Harris AB, Aharony A (1987) Series analysis of randomly diluted nonlinear network with negative nonlinearity exponent. Phys Rev B 36:3950–3952
18. Morozovsky AE, Snarskii AA (1992) Effective properties of high anisotropic and non-linear metal/non-metal thin films. Int J Elec 5:925–927
19. Niklasson GA (1989) Applications of inhomogeneous materials: Optical and electrical properties. Phys A 157:482–488
20. Ohtsuki T, Keyes T (1984) Conduction in random networks on super-normal conductors: geometrical interpretation and enhancement of nonlinearity. J Phys A 11:L559–L563

21. Osofsky M, LaMadrid M, Bieri J-B, Contrata W, Gavilan J, Mochel J-M (1988) Nonlinear dc conductivity in disordered metals near the metal-insulator transition. Phys Rev B 38:8486–8489
22. Sahimi M (1998) Non-linear and non-local transport processes in heterogeneous media: from long-range correlated percolation to fracture and materials breakdown. Phys Rep 306:213–395
23. Satanin AM, Khor'kov SV, Ugol'nikov AYu (1995) Nonlinear conductivity of a disordered medium at the percolation threshold. Sov Phys JETP Lett T 62:322–325
24. Satanin AM, Khor'kov SV, Skuzovatkin VV (1997) Breakdown of the linear current regime in periodic structures. JETP 85:351–359
25. Satanin MA, Snarskii AA, Slichenko KV, Bezsudnov IV (1998) Harmonic generation in microinhomogeneous composites. Tech Phys 43:602–604
26. Satanin AM, Khor'kov SV, Skuzovatkin VV (1996) Breakdown of the linear current flow regime in periodic structures. Sov Phys JETP Lett 64:538–543
27. Satanin AM, Skuzovatkin VV (1999) Thermal stabilization of anomalies in inhomogeneous conducting structures. Sov Phys JETP 88:997–1004
28. Snarskii AA, Buda SI (1998) Reciprocity relations for the nonlinear conductivity of fractal resistors. Tech Phys 41:1381–1384
29. Snarskii AA, Slipchenko KV, Sevryukov VA (1999) Critical behavior of conductivity in two-phase, highly inhomogeneous composites. Sov Phys JETP 89:788–796
30. Snarskii AA, Tomchuk PM (1987) Kinetic phenomena in macroscopic inhomogeneous media (Review) Ukrain. Fiz Jur 32:66–92 (in Russian)
31. Straley JP, Kenkel SW (1984) Percolation theory for nonlinear conductors. Phys Rev B 29:6299–6305
32. Stroud D, Hui P-M (1988) Nonlinear susceptibilities of granular matter. Phys Rev B 37:8719–8724
33. Wan WMV, Lee HC, Hui PM, Yu KW (1996) Mean-field theory of strongly nonlinear random composites: strong power-law nonlinearity and scaling behavior. Phys Rev B 54:3946–3953
34. Yang CS, Hui PM (1991) Effective nonlinear response in random nonlinear resistor networks: numerical studies. Phys Rev B 44:12559–12561
35. Yu KW, Hui PM, Lee HC (1996) Decoupling approximation for strongly nonlinear composites. Phys Lett A 210:115–120
36. Zhang X, Stroud D (1994) Numerical studies of the nonlinear properties of composites. Phys Rev B 49:944–955

Chapter 18
Effective Properties of Ferromagnetic Composites

18.1 Nonlinearity and Hysteresis in Ferromagnets

In the present chapter we consider a randomly inhomogeneous medium, where one of the phases is ferromagnetic, and the other—nonmagnetic (dia- or paramagnetic, the susceptibility of which can be ignored).

The main characteristic of ferromagnetic composite is the effective magnetic permeability μ_e. By determination, μ_e interrelates the volume-averaged intensity $\mathbf{H}$ and magnetic field $\mathbf{B}$:

$$\langle \mathbf{B} \rangle = \mu_{\text{eff}}(\langle \mathbf{H} \rangle)\langle \mathbf{H} \rangle, \tag{18.1.1}$$

where $\langle \ldots \rangle = V^{-1} \int \ldots \mathrm{d}V$, V is averaging volume. Despite the formal similarity of problems of calculating the effective magnetic permeability and the effective conductivity, there are, at least, two principal moments that complicate the analysis considerably. First, local effective permeability $\mu(H)$ is characterized by a peculiar kind of nonlinearity (see Fig. 18.1) which reduces neither to weak nonlinearity, when at small fields the dependence $\mu(H)$ becomes linear (for instance, dependence of Ohm's law type), nor to strong nonlinearity, when power volt-ampere characteristic is assumed (in terms of the electrical fields and currents). At sufficiently large magnetic fields, the relative magnetic permeability is close to unity, i.e., a medium consisting of ferromagnetic and nonmagnetic phases is weakly inhomogeneous. At the same time, in the intermediate fields the relative magnetic permeability can reach large values and, thus, the medium becomes strongly inhomogeneous. Second, when in the ferromagnetic phase one cannot ignore the residual magnetization, the concept of magnetic permeability loses its unambiguity.

In paragraph 18.2 we consider a case when hysteresis loop can be ignored, i.e., when in the ferromagnetic phase the magnetic permeability is an unambiguous field function, and in 18.3 we consider a problem of determination of residual magnetization and coercive force.

A.A. Snarskii et al., *Transport Processes in Macroscopically Disordered Media*, DOI 10.1007/978-1-4419-8291-9_18

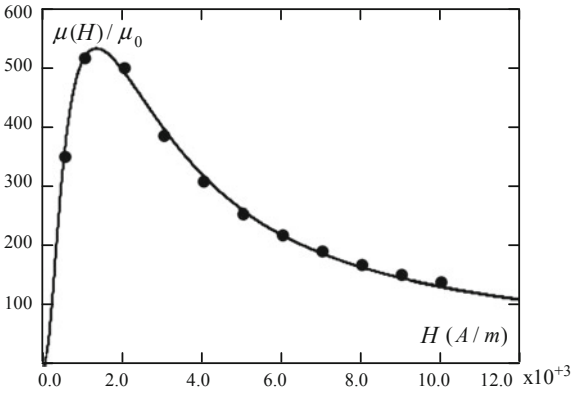

Fig. 18.1 The magnetic field dependence of relative magnetic permeability in ferromagnetic phase; points stand for the values of magnetic permeability for concrete material (steel); *solid curve* stands for analytical function approximating the experimental points

18.2 Hysteresis-Less Case

To determine the external field dependence of μ_e, let us use a modification of EMA-approximation [3, 6] proposed in [4, 5] for the case of power nonlinearity and described in the previous chapter. We will dwell in brief on the basic steps of this method for our case. A nonlinear phase with $\mu_1 = \mu_1(H)$ will be characterized by certain permanent magnetic permeability

$$\tilde{\mu}_1 = \langle \mu_1(H) \rangle_1, \tag{18.2.1}$$

where averaging is taken over the volume of inclusions.

Then for the determination of μ_{eff} one can use standard EMA-approximation for the three-dimensional case:

$$\mu_{\text{eff}} = \frac{1}{4}\left\{[(3p-1)\tilde{\mu}_1 + (2-3p)\mu_2] + \sqrt{[(3p-1)\tilde{\mu}_1 + (2-3p)\mu_2]^2 + 8\mu_2\tilde{\mu}_1}\right\}, \tag{18.2.2}$$

where p is ferromagnetic phase concentration. Further [see (17.2.6)] we have

$$\langle H^2 \rangle_1 = \frac{\langle H^2 \rangle}{p}\frac{\partial \mu_{\text{eff}}}{\partial \tilde{\mu}_1}. \tag{18.2.3}$$

The second approximation of this method for the determination of $\tilde{\mu}_1$ through $\langle H^2 \rangle_1$ yields

$$\tilde{\mu}_1 = \langle \mu(H) \rangle_1 \approx \mu_1\left(\sqrt{\langle H^2 \rangle_1}\right). \tag{18.2.4}$$

Substitution of (18.2.4) into (18.2.2) and (18.2.2) into (18.2.3) leads to a nonlinear equation for the determination of $\langle H^2 \rangle_1$

$$\langle H^2 \rangle_1 = \frac{\langle H^2 \rangle}{4p} \left\{ 3p - 1 + \frac{[(3p-1)\tilde{\mu}_1 + (2-3p)\mu_2](2-3p) + 4\mu_2}{\sqrt{[(3p-1)\tilde{\mu}_1 + (2-3p)\mu_2]^2 + 8\mu_2\tilde{\mu}_1}} \right\}. \quad (18.2.5)$$

Determining from (18.2.5) field $\langle H^2 \rangle_1$ and substituting it into (18.2.2), we find the effective magnetic permeability of ferromagnetic composite μ_{eff} as the function of concentration p of ferromagnetic medium, external magnetic field $\langle H \rangle$, and parameters of nonlinearity functions.

As an example, consider concrete dependence of local magnetic permeability shown in Fig. 18.1 as

$$\mu_1(H) = \mu_0 \left(1 + 1.57 \times 10^6 \times \frac{\tan h(5 \times 10^{-4} \times H)}{H} - 2.58 \times 10^5 \times \frac{\tan h(3 \times 10^{-3} \times H)}{H} \right), \quad (18.2.6)$$

where $\mu_0 = 4\pi \times 10^{-7}\,\text{N/A}^2$. Figure 18.2 shows calculated from (18.2.2) and (18.2.5) dependence of μ_{eff} on the concentration of ferromagnetic phase p and external field $\langle H \rangle$ [1, 2]. At $p = 1$, as expected, the field dependence of μ_{eff} coincides with dependence of magnetic permeability of pure ferromagnetic phase. For the magnetic fields whereby $\mu_1 = \mu_1(H) \gg 1$, the effective magnetic permeability μ_{eff} increases dramatically while crossing the percolation threshold.

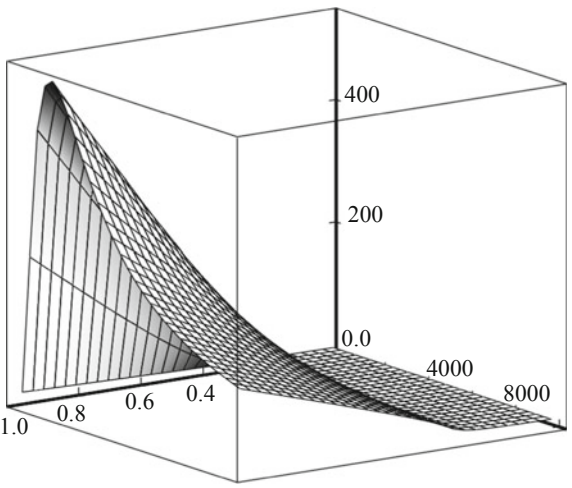

Fig. 18.2 Dependence of the effective magnetic permeability μ_{eff} on the concentration of ferromagnetic phase p and the intensity of volume-averaged magnetic field $\langle H \rangle$ from 0 to 10,000 A/m

18.3 Ferromagnetic Composites with a Nonzero Hysteresis Loop

In the case of a ferromagnetic phase with a nonzero hysteresis loop, an unambiguous determination of both local and effective magnetic permeability is impossible. The local value of magnetic permeability in this case loses its unambiguity, its value already depends on the history of sample magnetization. Therefore, complete solution of the problem of finding the effective magnetic permeability and dependence of $\langle \mathbf{B} \rangle$ on $\langle \mathbf{H} \rangle$ is only possible with knowledge of magnetization "history." However, even in this case, when we know magnetization history, for instance, a sample is first brought to technical saturation, following which demagnetization occurs along the so-called back of hysteresis loop (see the arrow in Fig. 18.3), a nonstandard situation is created for the determination of the effective characteristics. Namely, at $H = 0$ there is a nonzero Bvalue, wherein lies the presence of residual magnetization.

To calculate the effective coefficients of a composite, when one of the phases (or both) has hysteresis loop, we will apply local linearization method (*LL*-method) [8] (see also [2]). We will also find dependence of coercive force H_c and composite residual magnetization B_r on the concentration of ferromagnetic phase and the value of coercive force h_c and residual magnetization b_r in this phase. To determine the coercive force of composite, we pass over to terms of the effective magnetic resistance λ_{eff} found from equation:

$$\langle \mathbf{H} \rangle = \lambda_{\text{eff}}(\langle \mathbf{B} \rangle)\langle \mathbf{B} \rangle. \tag{18.3.1}$$

Let us consider in more detail the local linearization method for calculation of the effective magnetic resistance.

The first approximation in the LL-method lies in the local linearization of equation

$$\mathbf{H}(\mathbf{r}) = \lambda_i(\mathbf{B}) \cdot \mathbf{B}(\mathbf{r}) \tag{18.3.2}$$

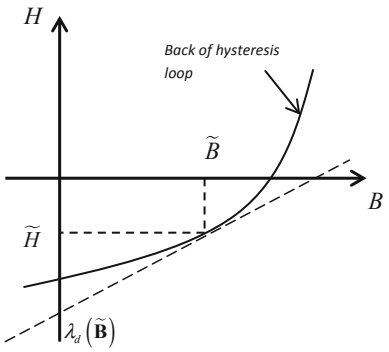

Fig. 18.3 Demagnetization curve

for certain induction value $\widetilde{\mathbf{B}}$, when local nonlinearity at $\mathbf{B} = \widetilde{\mathbf{B}}$ is replaced by linearized one (see Fig. 18.3) (index $i = 1$ for the first phase and $i = 2$ for the second phase). In this case we obtain

$$\mathbf{H} = \lambda_{di}\left(\widetilde{\mathbf{B}}\right) \cdot \mathbf{B} + \Omega, \tag{18.3.3}$$

where

$$\boldsymbol{\Omega}_i\left(\widetilde{\mathbf{B}}\right) = \mathbf{H}\left(\widetilde{\mathbf{B}}\right) - \lambda_{di}\left(\widetilde{\mathbf{B}}\right) \cdot \widetilde{\mathbf{B}} = \left(\lambda_i\left(\widetilde{\mathbf{B}}\right) - \lambda_{di}\left(\widetilde{\mathbf{B}}\right)\right) \cdot \widetilde{\mathbf{B}}, \tag{18.3.4}$$

$$\lambda_{di}\left(\widetilde{\mathbf{B}}\right) = \left.\frac{\mathrm{d}H_i(B)}{\mathrm{d}B}\right|_{B=\widetilde{B}}. \tag{18.3.5}$$

Let us next consider that field $< H >$ was brought to the values of technical saturation of ferromagnetic phase, following which it starts to be reduced. Thus, a medium is "situated" on the upper recurrent part of hysteresis loop, if hysteresis loop is considered in the axes with H along the abscissa and B along the ordinate. Our task is to determine the effective coefficients in the system using the law of (18.3.3) type relating local field and induction as

$$\langle \mathbf{H} \rangle = \lambda_{\mathrm{e}}(\langle \mathbf{B} \rangle) \cdot \langle \mathbf{B} \rangle + \boldsymbol{\Omega}_{\mathrm{e}}, \tag{18.3.6}$$

In order to do that, one should determine the value Ω_{e} (without selection of sample magnetization history it is equal to the effective coercive force of the entire sample H_c), and calculate λ_e like for linear laws (for instance, EMA). To determine Ω_{e}, let us draw an analogy between (18.3.3) and thermoelectric medium:

$$\mathbf{E} = \rho_i \cdot \mathbf{j} - \alpha_i \langle \nabla T \rangle, \tag{18.3.7}$$

where α_i is the Seebeck coefficient in ith phase, ρ_i is resistivity of ith phase, κ_i is thermal conductivity of ith phase. The law (18.3.7) is valid at low thermoelectric figure of merit $\left(T \cdot \alpha_i^2 \big/ (\rho_i \cdot \kappa_i) \ll 1\right.$, where T is temperature). Comparing (18.3.7) and (18.3.3) we see that the analogy exists, if $\alpha_i \langle \nabla T \rangle = \text{const}$ in each phase. When α_i in each of the phases is chosen as coordinate-independent, it is also necessary that

$$\langle \nabla T \rangle = \text{const} \tag{18.3.8}$$

for the entire sample. It is the second approximation of the *LL*-method. We will consider condition (18.3.8) to be met, then the relations describing a nonlinear medium after local linearization Eqs. (18.3.3–18.3.6) within the replacement of notation

$$\begin{array}{ll} -\alpha_i|\nabla T| \leftrightarrow \Omega_i, & -\alpha_{\mathrm{e}}|\nabla T| \leftrightarrow \Omega_{\mathrm{e}}, \\ \rho_i \leftrightarrow \lambda_{di}(\mathbf{B}), & \rho_{\mathrm{e}} \leftrightarrow \lambda_{\mathrm{e}}, \end{array} \tag{18.3.9}$$

coincide with thermoelectric system, where ρ_e is the effective resistance of thermoelectric linear system with local relations (18.3.7):

$$\langle \mathbf{E} \rangle = \rho_e \langle \mathbf{j} \rangle - \alpha_e \langle \nabla T \rangle, \tag{18.3.10}$$

The effective coefficient ρ_e in (18.3.10) can be found using, for instance, standard EMA-method (or any other linear approximation). By means of isomorphism between α_e and $\rho_e = 1/\sigma_e$ (see Chap. 15) we will determine α_e as

$$\alpha_e = \frac{(\alpha_1 \rho_{d2} - \alpha_2 \rho_{d1}) - \rho_e(\alpha_1 - \alpha_2)}{\rho_{d2} - \rho_{d1}}, \tag{18.3.11}$$

Taking into account replacement of notation (18.3.9) and that $H_c = \Omega_e(B = 0)$, $h_{c1} = \Omega_1(0)$ and $h_{c2} = \Omega_2(0)$, we obtain

$$H_c = \frac{(h_{c2}\lambda_{d1}(0) - h_{c1}\lambda_{d2}(0)) - \lambda_e(0)(h_{c2} - h_{c1})}{\lambda_{d2}(0) - \lambda_{d1}(0)}, \tag{18.3.12}$$

Figure 18.4 represents concentration dependence of the effective coercive force of the entire sample. To find λ_e, the three-dimensional EMA-approximation was used

$$\lambda_e = \frac{1}{2}\left\{(1-3p)\lambda_{d2} + (3p-2)\lambda_{d1} + \sqrt{[(1-3p)\lambda_{d2} + (3p-2)\lambda_{d1}]^2 + 8\lambda_{d1}\lambda_{d2}}\right\} \tag{18.3.13}$$

The residual magnetization B_r is calculated quite similarly (see Fig. 18.5) demonstrate a good agreement with numerical and experimental results mentioned in [7].

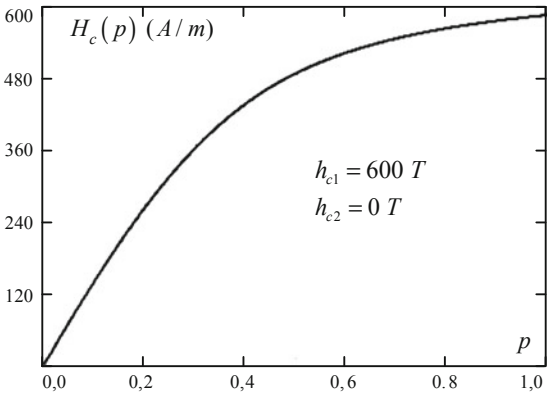

Fig. 18.4 Dependence of composite coercive force on the ferromagnetic phase concentration

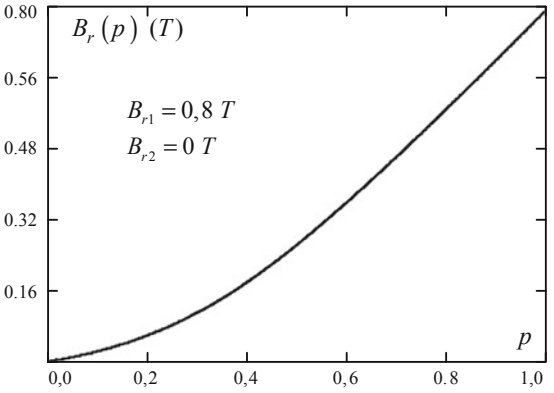

Fig. 18.5 Dependence of composite residual magnetization on the ferromagnetic phase concentration

References

1. Bakaev VV, Snarskii AA, Shamonin MV (2001) The effective magnetic permeability of a two-phase fibred ferromagnetic composite. Tech Phys T46:1571–1574-87
2. Bakaev VV, Snarskii AA, Shamonin MV (2002) The permeability and remanent magnetization of a randomly inhomogeneous two-phase medium. Tech Phys 47:125–128
3. Bruggeman DAG (1936) Berechnung verschiedener physikalischer Konstanten von heterogenen Substanzen, II Ann. Physik 25:645–672
4. Hiu PM, Woo YF, Wan WMV (1995) Effective response in random mixtures of linear and nonlinear conductors. J Phys C 7:593–597
5. Hui PM, Cheung P, Kwong YR (1997) Effective response in nonlinear random composites. Phys A 241:301–309
6. Landauer R (1952) The electrical resistence of binary metallic mixtures. J Appl Phys 23: 779–784
7. Shamonin M, Snarskii A, Zhenirovskyy M (2004) Effective magnetic permeability of ferromagnetic composites. Theoretical description and comparison with experiment. NDT&E Int 37:35–40
8. Snarskii AA, Shamonin MV, Zhenirovsky MI (2003) The effective properties of macroscopically nonuniform ferromagnetic composites: Theory and numerical experiment. Sov Phys JETP 96:66–77

Chapter 19
Temperature Coefficient of Resistance and Third Harmonic Generation Close to Percolation Threshold

19.1 Temperature Coefficient of Resistance

One of the important characteristics of composite materials is temperature dependence of resistance which can be expressed through temperature coefficient of resistance.

$$\mathrm{TCR} = \frac{1}{R}\frac{\mathrm{d}R}{\mathrm{d}T}. \tag{19.1.1}$$

The lower the temperature coefficient of resistance of a given material in a given temperature range, the less will be the temperature dependence of material resistance. With the use of composite materials as resistances in different electrical circuits, it is of critical importance to know temperature coefficient of resistance, since for the operating stability of electronic devices it should be as low as possible (see, for instance [5]), which is also concerned with temperature coefficients of resistance of thin-film composite resistors.

Temperature dependence of conductivity and thermoelectric properties in composites considered in the following papers [4] (application of percolation theory for the description of positive temperature coefficient effect of polymer composite) [1], (two-dimensional percolation models were used for explanation of temperature dependence of conductivity of copper- and nickel-doped Bi2Te3 crystals) [3].

Temperature coefficients of resistance of two-phase strongly inhomogeneous media close to percolation threshold p_c can be easily determined from the expressions for the effective resistivity [8]. For convenience, we pass on to specific temperature coefficient of resistance

$$\beta = \frac{1}{\rho_\mathrm{e}}\frac{\mathrm{d}\rho_\mathrm{e}}{\mathrm{d}T},\ \beta_i = \frac{1}{\rho_i}\frac{\mathrm{d}\rho_i}{\mathrm{d}T},\quad i = 1, 2, \ldots, \tag{19.1.2}$$

where i is phase number.

A.A. Snarskii et al., *Transport Processes in Macroscopically Disordered Media*, DOI 10.1007/978-1-4419-8291-9_19

Below the percolation threshold, where $\rho_e \approx \rho_2|\tau|^q(B_0 + B_1 h|\tau|^{-\varphi})$, $h = \sigma_2/\sigma_1 \equiv \rho_1/\rho_2$, $\varphi = t + q$, account of temperature dependence of ρ_1, and ρ_2 leads to the expression

$$\frac{d\rho_e}{dT} = B_0 \frac{d\rho_2}{dT}|\tau|^q + B_1 \frac{d\rho_1}{dT}|\tau|^{-\varphi}. \tag{19.1.3}$$

Dividing this expression by $\rho_2|\tau|^q$ and discarding higher components in the order of magnitude as compared to ρ_1/ρ_2, we obtain

$$\beta_e = B_0\beta_2 + B_1\beta_1 h|\tau|^{-\varphi},\ \varphi = t + q,\ p < p_c,\ \tau \gg \Delta, \tag{19.1.4}$$

In the same way, we find temperature coefficients of resistance above the percolation threshold and at the threshold—in the smearing region

$$\beta_e = A_0\beta_2 + A_1\beta_1 h|\tau|^{-\varphi},\ p > p_c,\ \tau \gg \Delta, \tag{19.1.5}$$

$$\beta_e = \frac{q}{\varphi}\beta_1 + \frac{t}{\varphi}\beta_2, \quad |\tau| \le \Delta. \tag{19.1.6}$$

As can be seen from (19.1.4) and (19.1.5), on approaching the percolation threshold, temperature coefficient of resistance can change its value. For instance, below the percolation threshold, in the case when temperature coefficient of resistance of poorly conducting phase β_2 is much larger than β_1, one can select such values of parameters and concentrations that

$$\beta_1 h|\tau|^{-\varphi} > \beta_2,\ \tau > \Delta. \tag{19.1.7}$$

It means that below the percolation threshold, the effective temperature coefficient of resistance will be characterized by temperature coefficient of resistance of well conducting phase and will depend on concentration.

A similar simple calculation can be also used to determine temperature coefficient of resistance of media with exponentially wide resistance distribution spectrum [8].

19.2 Third Harmonic Generation

The problem of temperature coefficient of resistance is closely related to a nonlinear temperature response—third harmonic and $1/f$-noise generation [2, 6, 7, 9–11]. On application of current with frequency ω, the presence of temperature dependence of resistance leads to third harmonic generation (with frequency 3ω).

To explain this effect, consider first a homogeneous case. From the determination of temperature coefficient of resistance (19.1.2), it follows that deviation of specific resistance $\delta\rho$ due to temperature deviation from the average value T_0 ($\delta T = T - T_0$) can be represented as

$$\delta\rho = \beta\rho(T_0)\delta T, \tag{19.2.1}$$

where δT is proportional to Joule heat release,

$$\delta T \approx \rho(T_0)j^2(\omega)F(\omega, T), \tag{19.2.2}$$

and $\rho(T_0)j^2(\omega)$ is Joule heat release and $F(\omega,\ T)$ is a function that characterizes heat outflow.

If alternating voltage is applied to a sample in such a way that

$$j(\omega) = j_0 \cos\omega t, \tag{19.2.3}$$

then from (19.2.1) and (19.2.2) we obtain

$$\delta\rho = \rho_0^2\beta F(\omega, T)j_0^2\cos^2(\omega t + \varphi_0), \tag{19.2.4}$$

where φ_0 is a phase, and it is also taken into account that at low overheats ($\beta\delta T \ll 1$) $\rho(T) \approx \rho_0(1 + \beta\delta T)$, and notation $\rho_0 = \rho(T_0)$ is introduced.

Thus, on passing current with frequency ω, the resistance changes by the law $\cos^2\omega t$, i.e., comprises the second harmonic ($\cos^2\ \omega t = 0.5 + 0.5\ \cos\ 2\omega t$), which results in the third harmonic generation. In fact, substituting $\delta\rho$ from (19.2.4) into $E(t) = (\rho + \delta\rho)j(\omega)$, after elementary transformation we obtain that $E(t)$ comprises odd harmonics ω and 3ω.

Making the same calculations for the effective resistivity $\langle\mathbf{E}\rangle = (\rho_e + \delta\rho_e)\langle\mathbf{j}\rangle$, where now

$$\delta\rho_e\langle j\rangle^2 = \langle j^2\delta\rho\rangle,\ \mathbf{j}(\mathbf{r}, \omega) = \mathbf{j}_0(\mathbf{r})\cos\omega t, \tag{19.2.5}$$

we find

$$\langle j_0\rangle^2\delta\rho = \langle\beta\rho_0^2 j_0^2\rangle F(\omega, T)\cos^2(\omega t + \varphi_0). \tag{19.2.6}$$

Here $\rho_0 = \rho_0(\mathbf{r})$ is permanent part of local resistivity.

Substituting $\delta\rho_e$ into $\langle\mathbf{E}\rangle = (\rho_e + \delta\rho_e)\langle\mathbf{j}\rangle$, for the amplitude of third harmonic of the field we find

$$\langle E\rangle = \rho_e(T_0)\langle j_0\rangle cos(\omega t) + \frac{1}{4}F(\omega, t)\frac{\langle\beta\rho_0^2 j_0^4\rangle}{\langle j_0\rangle}cos(3\omega t) + ..., \tag{19.2.7}$$

Therefore the amplitude of third harmonic $\langle E\rangle_{3f}$ and normalized for $\langle j_0\rangle^3$ amplitude B_{3f} can be expressed in the form

$$\begin{aligned}\langle E\rangle_{3f} &\sim \frac{\langle \beta\rho_0^2 j_0^4\rangle}{\langle j_0\rangle}\\ B_{3f} &= \frac{\langle E\rangle_{3f}}{\langle j_0\rangle^3} \sim \frac{\langle \beta\rho_0^2 j_0^4\rangle}{\langle j_0\rangle^4}.\end{aligned} \tag{19.2.8}$$

As can be seen from (19.2.8), B_{3f} is expressed through normalized fourth current moment and, to an accuracy of inessential factors, coincides with concentration behavior of $\rho_e^2 C_e$.

Just as the value of the relative spectral density of $1/f$-noise C_e, the value B_{3f} can "detect" the differences in the structure of inhomogeneous media, "inaccessible" to effective conductivity. Experiments illustrating this fact are given in [2, 10, 11] that studied media with different local structure, close to percolation threshold. For such media (two-phase, strongly inhomogeneous, $p \approx p_c$) for B_{3f} in [7] there were obtained concentration dependences above and below the percolation threshold with a finite ratio of phase conductivities, as well as in the smearing region

$$B_{3f} \approx \beta_1\left(\frac{\rho_e}{\rho_1}\right)^{\frac{k}{t}+2} + \beta_2 h^2\left(\frac{\rho_e}{\rho_1}\right)^{\frac{k'+2\varphi}{t}+2},\ p > p_c,\ \tau \gg \Delta, \tag{19.2.9}$$

$$B_{3f} \approx \beta_1\left(\frac{\rho_e}{\rho_2}\right)^{\frac{k}{t}+2} + \beta_2 h^2\left(\frac{\rho_e}{\rho_2}\right)^{\frac{k'+2\varphi}{t}+2},\ p < p_c,\ |\tau| \gg \Delta, \tag{19.2.10}$$

$$B_{3f} \approx \beta_1\left(\frac{\rho_e}{\rho_1}\right)^{\frac{k}{t}+2} + \beta_2 h^2\left(\frac{\rho_e}{\rho_2}\right)^{\frac{k'+2\varphi}{t}+2},\ |\tau| < \Delta, \tag{19.2.11}$$

where $h = \sigma_2/\sigma_1 = \rho_1/\rho_2$.

In (19.2.9)–(19.2.11) the concentration dependence of B_{3f} is written through function of concentration $\rho_e = \rho_e(\tau)$. In so doing, certainly, dependences $\rho_e(\tau)$ in (19.2.9)–(19.2.11) should correspond to indicated ranges of concentration change, for instance, in (19.2.9) $\rho_e(\tau) \approx \rho_1 \tau^{-t}$.

Snarskii [7] also deals with third harmonic generation in the systems with exponentially wide resistance spectrum. If pre-exponential factor is neglected, then

$$B_{3f} \sim \rho_e^3. \tag{19.2.12}$$

Similar to higher current moments (see Chap. 14) one can also consider generation of higher odd harmonics—$B_{5f}, B_{7f}, \ldots$. Certainly, their experimental studies due to fact of amplitude smallness are more complicated [10, 11].

References

1. Aleskerov FK, Kakhramanov KS, Kakhramanov SS (2012) Percolation effect in copper-and nickel-doped Bi_2Te_3 crystals. Inorg Mater 48:456–461
2. Dubson MA, Hui YC, Weissman MB, Garland JC (1989) Measurement of the fourth moment of the current distribution in two-dimensional random resistor networks. Phys Rev B 39:6807–6815
3. Kharlamov FV, Kharlamov F (2014) Dependency, the thermoelectric figure of merit of a material consisting of particles on the parameters of a material. J Appl Math Phys 2:953–959
4. Kono A, Shimizu K, Nakano H et al (2012) Positive-temperature-coefficient effect of electrical resistivity below melting point of poly(vinylidene fluoride) (PVDF) in Ni particle-dispersed PVDF composites. Polymer 53:1760–1764
5. Licznerski BW (1990) Thick-film cermets, their physical properties and application. Int J Elect 69:79–85
6. Satanin MA, Snarskii AA, Slichenko KV, Bezsudnov IV (1998) Harmonic generation in microinhomogeneous composites. Tech Phys 43:602–604
7. Snarskii AA (1995) Generation of third harmonic in strongly inhomogeneous composites near the percolation threshold. Tech Phys Lett 21:3–8 (in Russian)
8. Snarskii AA, Dziedzic A, Licznerski BW (1996) Temperature behaviour of percolation-like systems. Int J Elect 81:363–370
9. Weissman MB, Dollinger CD (1981) Noise from equilibrium enthalpy fluctuations in resistors. J Appl Phys 52:3095–3098
10. Yagil Y, Deutscher G, Bergman DJ (1993) The role of microgeometry in the electrical breakdown of metal-insulator mixtures. Int J Mod Phys B 7:3353–3374
11. Yagil Y, Deutscher G (1992) Third-harmonic generation in semicontinuons metal films. Phys Rev B 46:16115–16121

Chapter 20
Instability and Chaos in the Macroscopically Inhomogeneous Media with Weak Dissipation

20.1 Dual Media

Till now, we have considered cases when, at least in one of the phases, conductivity had a nonzero real part (see Chap. 11). In particular, for the two-dimensional medium at the percolation threshold A.M. Dykhne obtained a precise result (see Chap. 6):

$$\sigma_e = \sqrt{\sigma_1 \sigma_2} \tag{20.1.1}$$

However, cases are possible when the real part of local conductivity of phases is small (in the ideal case it is equal to zero), and the imaginary parts have different signs. It can be said that a medium consists of inductances and capacitances characterized by magnetic permeability and dielectric permittivity. One of the examples of such media is films consisting of metal islands divided by dielectric areas. The metal parts of the film possess inductance, and dielectric areas (often it is just air) are capacitive. In such media there are gigantic inhomogeneities of local fields (see, for instance [1–3]). In the derivation of formula (20.1.1) (see Chap. 6) no restrictions were imposed on the phase conductivity values. Thus, one of the phases can be a perfect conductor—conductivity σ in this case has only the imaginary negative part (inductance), and the second phase—a perfect dielectric, and conductivity σ in this case has only the imaginary positive part (capacitance). Thus, one can write

$$\sigma_1 = -\mathrm{i}y, \quad \sigma_2 = \mathrm{i}x, \quad x > 0, \quad y > 0, \tag{20.1.2}$$

where $x = \omega c$, $y = 1/\omega l$, and c and l are specific capacitance and inductance of material (F/m^3, H/m^3).

A.A. Snarskii et al., *Transport Processes in Macroscopically Disordered Media*, DOI 10.1007/978-1-4419-8291-9_20

Then from (20.1.1) it follows directly that

$$\sigma_e = \sqrt{xy} = \sqrt{c/l}. \tag{20.1.3}$$

According to (20.1.3), the effective conductivity of such a medium composed of imaginary phases with different signs is real, i.e., a medium "*composed of imaginary resistances, not leading to energy dissipation, possesses a real equivalent resistance, i.e. absorbs energy*" [4], wherein lies a paradox!

The paradox could be solved as follows. In work [14] it is shown that on the network with purely imaginary conductivities of bonds the problem of potential distribution coincides with Anderson localization problem. A small real addition to the imaginary part of conductivity of metal phase can be taken into account within the perturbation theory. Under this approach, in particular, the correlation length was calculated. It proved to be proportional to $1/\sqrt{\mathrm{Re}\,\sigma_{1,2}}$ (for the two-dimensional case). Thus, in the case of purely imaginary phases the correlation length diverges $\xi(\mathrm{Re}\,\sigma_{1,2} \to 0) \to \infty$. In other words, at the percolation threshold at $\mathrm{Re}\,\sigma_{1,2} = 0$ the concept of effective conductivity loses its physical meaning.

The above described paradox has well-illustrated the fact that one cannot just substitute the imaginary conductivities of phases of different signs into the expression for the effective conductivity obtained for the case of finite correlation radius. One should make it certain that correlation radius remains finite.

Let us illustrate [5] this by an example of *D*-medium obtained by mixing (see Chap. 6). In the "ordinary" case, at $\mathrm{Im}\,\sigma_1 = \mathrm{Im}\,\sigma_2 = 0$, as was shown [see (6.1.26)], the mixing procedure quickly converges to isotropic medium with the effective conductivity value

$$\sigma_e = \sqrt{\sigma_1\sigma_2}\sqrt{\frac{p\sigma_1 + (1-p)\sigma_2}{(1-p)\sigma_1 + p\sigma_2}}. \tag{20.1.4}$$

At $p = p_c = 1/2$ the expression (20.1.4) reduces to (20.1.1), and the iteration procedure [formula (6.1.25)] is a technique, well known from applied mathematics, for square root calculation by Newton method (see chapter 6, Fig. 6.7). In the case of conductivities with a zero real part and the imaginary parts with the identical signs (for instance, a medium consists of two media with different dielectric constants), to an accuracy of notation everything remains unchanged. While in the case of different signs of the imaginary parts, i.e., at $\mathrm{Re}\,(\sigma_1) = \mathrm{Re}\,(\sigma_2) = 0$ and $\mathrm{Im}\,(\sigma_1) \cdot \mathrm{Im}\,(\sigma_2) < 0$, the situation changes cardinally (Fig. 20.1) [6, 7, 11]. Taking into account that $\mathrm{Re}\left(\sigma_\perp^{(n)}\right) = \mathrm{Re}\left(\sigma_\parallel^{(n)}\right) = 0$ and introducing similar (20.1.2) notation for $\sigma_\perp^{(n)}$ и $\sigma_\parallel^{(n)}$, we obtain

$$\sigma_\perp^{(n)} = -\mathrm{i} \cdot Y_n, \quad \sigma_\parallel^{(n)} = \mathrm{i} \cdot X_n, \quad \mathrm{Im}X_n = \mathrm{Im}Y_n = 0. \tag{20.1.5}$$

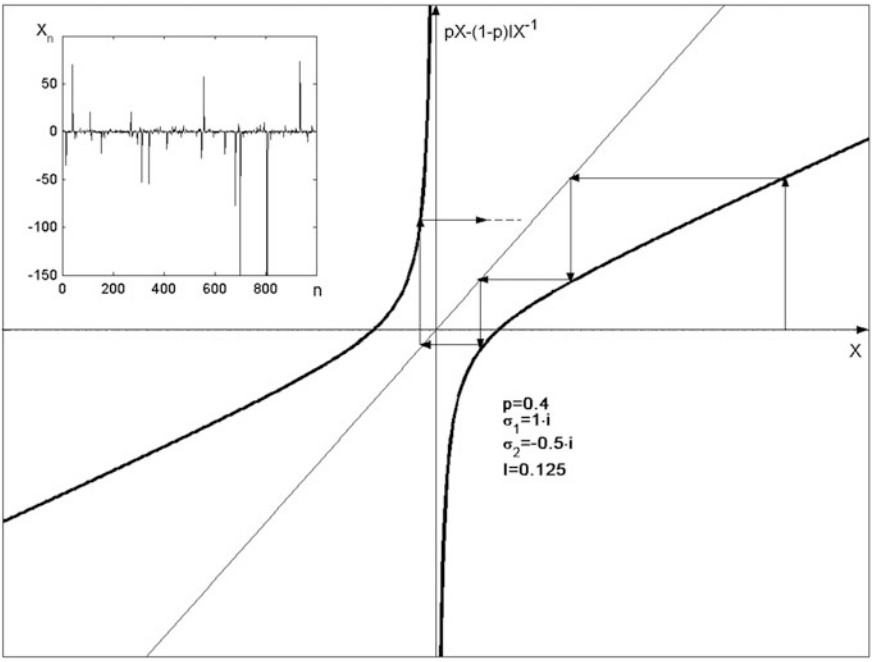

Fig. 20.1 Single-dimensional mapping $x \to px - (1-p)I/x$, $p = 0.4$, $\sigma_1 = 1\mathrm{i}$, $\sigma_2 = -0.5\mathrm{i}$, $I = 0.125$. The inset shows iteration process for these parameters (compare to Fig. 6.5)

On mixing, (Chap. 6) we have

$$\sigma_{||}^{(n+1)} = p\sigma_{||}^{n} + (1-p)\sigma_{\perp}^{n}, \quad \sigma_{\perp}^{(n+1)} = \frac{\sigma_{||}^{(n)}\sigma_{\perp}^{(n)}}{(1-p)\sigma_{\perp}^{(n)} + p\sigma_{||}^{(n)}}, \tag{20.1.6}$$

where $\sigma_{||}^{(1)} = p \cdot \sigma_1 + (1-p) \cdot \sigma_2$, $\sigma_{\perp}^{(1)} = \sigma_1 \cdot \sigma_2/((1-p) \cdot \sigma_1 + p \cdot \sigma_2)$, see (6.1.18).

Iteration process (20.1.6) possesses an invariant [see (6.1.19)] $\sigma_{||}^{(n)}\sigma_{\perp}^{(n)} = J$, which for the case (20.1.2) is of the form

$$I = xy\frac{py - (1-p)x}{(1-p)y - px}. \tag{20.1.7}$$

In terms of X_n (20.1.5) the iteration process (20.1.6) can be represented as follows (compare to (6.1.25))

$$X_{n+1} = pX_n - (1-p)\frac{J}{X_n}. \tag{20.1.8}$$

The fixed point of iteration process (20.1.8) X^* is formally equal to

$$X^* = \pm\sqrt{-J}. \tag{20.1.9}$$

By definition of X_n (20.1.5), $\mathrm{Im}\,(X_n) = 0$, hence the fixed point X^* exists only at $J < 0$. It is possible when any of the two inequality systems given below is satisfied

$$\begin{cases} py > (1-p)x, \\ (1-p)y < px, \end{cases} \quad I, \qquad \begin{cases} py < (1-p)x, \\ (1-p)y > px. \end{cases} \quad II. \tag{20.1.10}$$

To the shaded areas in Fig. 20.2 corresponds to an empty set of solutions of (20.1.10) system—there is no fixed point.

At $p = 1/2$ the resulting medium [11], on the one part, geometrically is a D-medium, and on the other, as can be seen from Fig. 20.2—there is no fixed point. Writing down in this case the mapping (20.1.8) as $N(z) = (z - J/z)/2, \mathrm{Im}\,J = 0, \mathrm{Re}\,J > 0$, it can be shown [13] that its Julia set—J_N, dividing attraction pools of stable fixed points $\pm\sqrt{J}$, coincides with the imaginary axis. Mapping on J_N induces one-dimensional mapping that reduces to (20.1.8) (at $p = 1/2$) and determines the dynamics on the Julia set. Mapping $N(Z)$ is conjugate to mapping $R(u) = u^2$ obtained by replacement of $u = (z + \sqrt{J})/(z - \sqrt{J})$. In so doing, the imaginary axis (Julia set) goes over to unit circumference, the dynamics on which is assigned by mapping $r(\theta) = 2\theta \bmod 2$. The latter, as is well known [13, 15], gives rise to a chaotic dynamics.

Thus, when medium parameters get to the shaded area, the iteration process does not converge, and at $p = 1/2$ there is a strictly deterministic chaos. In particular, it means that there is no self-averaging in such a medium, i.e., correlation radius tends to infinity.

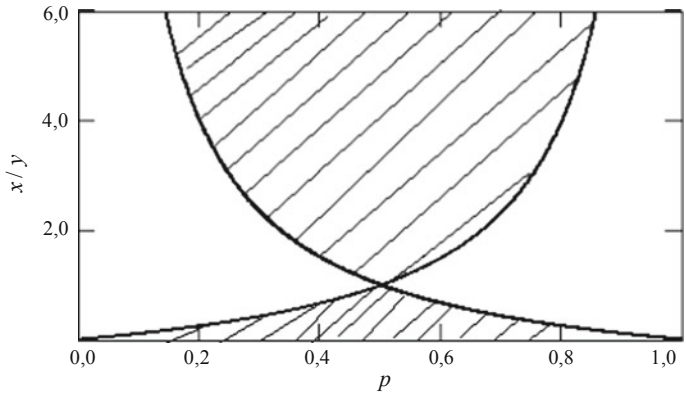

Fig. 20.2 Instability areas (*shaded*) of mixing procedure (20.1.8) depending on concentration p of the first phase and the ratio of phase conductivities x/y

For the network realization of D-media the absence of certain σ_e value in the finite network at $\mathrm{Im}\,(\sigma_1) \cdot \mathrm{Im}\,(\sigma_2) < 0$ was first noted in [9]. According to [9], at concentration values above p_c there is a continuous path from one contact to the other (from "$-\infty$" to "∞") both "from left to right" and "upwards" along the bonds that represent inductivity. However, the effective conductivity of a medium depending on the conductivity values of network elements can be both above and below zero, i.e., represent both capacitance and inductance. In the network media, at concentration other than threshold, the reciprocity relation means that the effective conductivity of the "basic" medium is of capacitive type ($\mathrm{Im}\,(\sigma_e) > 0$), whereas that of the "reciprocal" medium—of the inductive type ($\mathrm{Im}\,(\sigma_e) < 0$). Nothing is changed at concentration tending to threshold and, finally, the effective conductivities of the "basic" and dual media remain with different signs. At the same time, in the network media on the percolation threshold, if they are D-media, there is always at least one element (bond) with neither the first phase nor the second phase conductivity (Fig. 20.3). The conductivity of this D-bond is $\sqrt{\sigma_1 \sigma_2}$ (for more details see [9, 17]). In a continual two-phase case of D-media these bonds degenerate into points (Fig. 6.2). If such a D-bond is absent, then at $\mathrm{Re}\,\sigma_{1,2} = 0$ and $\mathrm{Im}\,\sigma_1 \mathrm{Im}\,\sigma_2 < 0$ the network will not be dual, in particular, conductances "from left to right" and "upwards" will have different signs—along one direction the medium will be a "capacitor", and along the other—a "capacitance", and if a D-bond is present, the medium is not, strictly speaking, a D-medium consisting of two phases. The effect of this bond should be the less, the larger is medium size. The latter proves true at $\mathrm{Im}\,\sigma_1 \mathrm{Im}\,\sigma_2 < 0$ only for the case of $\mathrm{Re}\,\sigma_{1,2} \neq 0$.

Figure 20.3 represents one of possible realizations of D-network of finite size [9]. Conductances z_1 are marked with black color and—z_2—with white. In the centre is a D-bond which, in order to satisfy the network variant of symmetry transformation (see Chap. 6) and condition $\tilde{\sigma}_e = \sigma_e$, should have resistance equal to $\sqrt{z_1 z_2}$. The D-bond (resistance) is a network analog of D-points in a continual case (see Fig. 6.2).

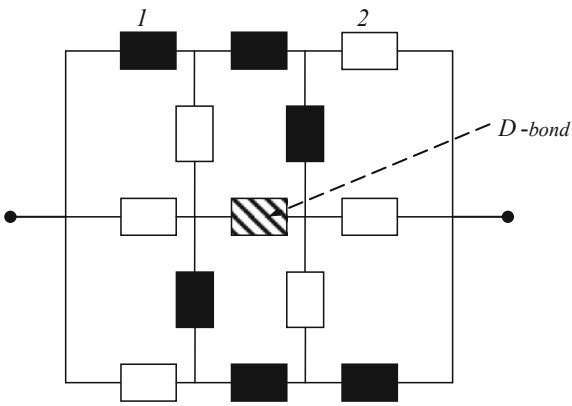

Fig. 20.3 Embodiment of a D-network of finite size

Let us now explain how in a D-medium at $\xi \to \infty$ and $\mathrm{Re}\,\sigma_{1,2} = 0$ there appears an absorption, i.e. the real value of the effective conductivity [5]. The answer lies in the limit $\xi \to \infty$ and the existence of fluctuations of conductivity with the nonzero real part. It is easy to verify that arbitrarily small real part added to σ_1 or σ_2 makes the above considered iteration process (20.1.8) stable. This process now converges to the real value $\sqrt{\sigma_1\sigma_2} = \sqrt{(\mathrm{Re}\,\sigma_1 + \mathrm{i}\,\mathrm{Im}\,\sigma_1)(\mathrm{Re}\,\sigma_2 + \mathrm{i}\,\mathrm{Im}\,\sigma_2)} \approx \sqrt{-\mathrm{Im}\,\sigma_1 \mathrm{Im}\,\sigma_2}$ (wherein small "initialization" real additions can be ignored). From Fig. 20.4 it is evident how small fluctuations take away phase point (in space $\{\mathrm{Re}\,\sigma - \mathrm{Im}\,\sigma\}$) from axis $\mathrm{Im}\,\sigma$ where it made chaotic jumps (Fig. 20.1) to the trajectory converging to the real axis. "Phase" trajectories quickly converge to the real axis. If small "initialization" additions are ignored, the trajectories "settle" on the axis $\mathrm{Re}\,\sigma_n$.

Thus, there simultaneously exist two limiting transitions $\xi \to \infty$ and $\mathrm{Re}\,\sigma_{1,2} \to 0$, and they cannot change places. Under medium finite size, competition will take place between the number of elements (bonds, medium size) and the value of the real conductivity part. If the number of elements "loses", then there is no self-averaging in the system and given random realization takes place. In such average inhomogeneous medium, naturally, exist large space fluctuations of Joule heat release, absorption, higher moments of current distribution, etc.

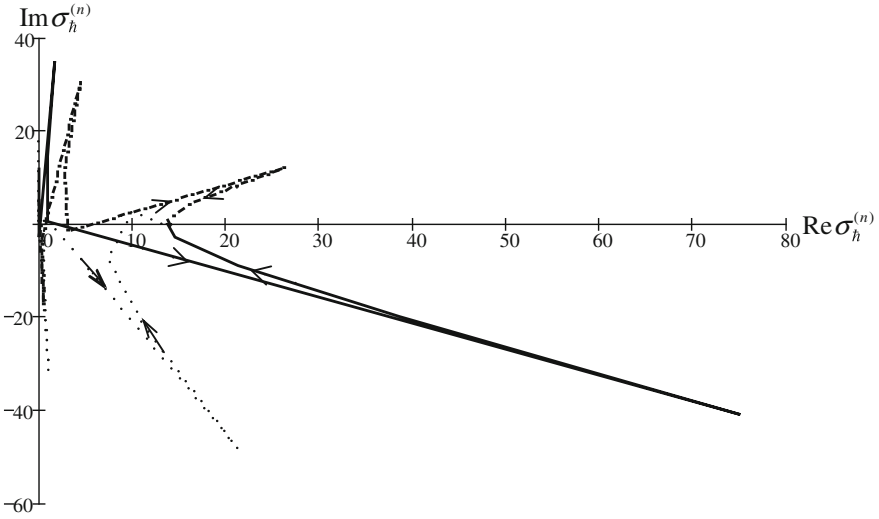

Fig. 20.4 "Phase" trajectories of iteration process (20.1.6) in space $\{\mathrm{Im}\,\sigma - \mathrm{Re}\,\sigma\}$ at small real "initialization" parts of phase conductivity: *dashed*—$\sigma_1 = 0.1 - 10 \cdot \mathrm{i}$, $\sigma_2 = 0.1 + 20 \cdot \mathrm{i}$; *continuous*—$\sigma_1 = 0.056 - 6.667 \cdot \mathrm{i}$, $\sigma_2 = 0.1 + 30 \cdot \mathrm{i}$; *points*—$\sigma_1 = 0.038 - 5 \cdot \mathrm{i}$, $\sigma_2 = 0.1 + 40 \cdot \mathrm{i}$

20.2 Ladder Filter

The above-mentioned paradox—the "appearance" of a real part of resistance in a medium consisting of elements with purely imaginary part of resistance—is present in the simplest theory of networks in the theory of ladder filter (LC-chain) and is still in the focus of attention [18]. Surprisingly, even in the "canonical" textbooks on the course of general physics, for instance, in [8, 16], one can come across the diametrically opposite opinions concerning the existence of a real part of resistance of ladder filter in a certain frequency range and, thus, the opposite explanations of this filter operation.

Consider LC-chain in more detail [5]. Impedance Z of infinite ladder chain (see Fig. 20.5) can be found by its consecutive construction, writing down the expression for Z_{n+1} in the form

$$Z_{n+1} = f(Z_n), \quad f(Z_n) = z_1 + \frac{Z_n z_2}{Z_n + z_2}, \quad n = 1, 2, \ldots, \infty, \tag{20.2.1}$$

where z_1, z_2 are complex resistances-conductances of chain elements.

At any z_1 and z_2 there always exists fixed point Z^* found from equation $Z^* = f(Z^*)$,

$$Z^* = \frac{z_1}{2} \pm \sqrt{\frac{z_1^2}{4} + z_1 z_2}. \tag{20.2.2}$$

If fixed point Z^* is stable, the impedance Z of infinite ladder chain exists and is the limit $\lim_{n\to\infty} Z_n = Z^*$. In the opposite case there is no limit for $\lim_{n\to\infty} Z_n$ (see Fig. 20.6) and there is no sense to speak of the impedance infinite chain.

Analysis (20.2.1) shows that in the ideal case of purely imaginary impedances (a chain consists of capacitances and inductances with zero active resistances). Under certain values of z_1 and z_2 there is no stable fixed point Z^*. Indeed, fixed point Z^* of the iteration process (20.2.1) is stable [15], if

$$|\mathrm{d}f(Z_n)/\mathrm{d}Z_n||_{Z_n = Z^*} < 1, \tag{20.2.3}$$

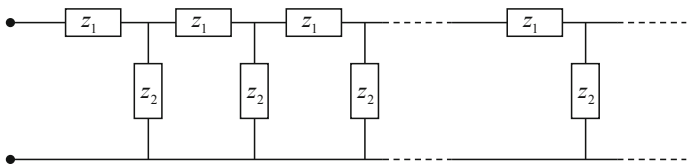

Fig. 20.5 Infinite ladder LC-chain (filter): $z_1 = \mathrm{i}\omega L$, $z_2 = 1/\mathrm{i}\omega C$

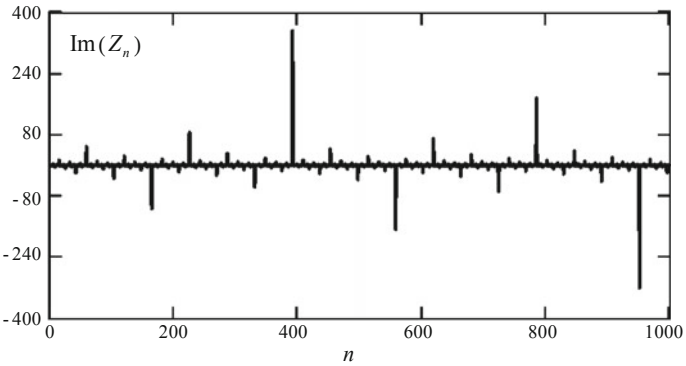

Fig. 20.6 Infinite ladder *LC*-chain (filter): $z_1 = \mathrm{i}\omega L$

In the case under consideration we have

$$\left|\frac{\mathrm{d}f(Z_n)}{\mathrm{d}Z_n}\right|\Bigg|_{Z_n=Z^*} = \left|\frac{1}{(1+Z^*/z_2)^2}\right| = \frac{4}{\left|\left(2+z_1/z_2 \pm \sqrt{(z_1/z_2)^2+4z_1/z_2}\right)^2\right|}, \tag{20.2.4}$$

Denoting $t = -z_1/z_2$, we rewrite condition (20.2.3) as

$$F(t) = \frac{4}{\left|\left(2-t \pm \sqrt{t^2-4t}\right)^2\right|} < 1. \tag{20.2.5}$$

Under a real t function,$F(t)$, as can be easily seen, behaves in the range

$$0 \le t \le 4 \tag{20.2.6}$$

somewhat unexpectedly—it does not depend on t and is precisely equal to unity. Thus, the inequality (20.2.5) is not met and the fixed point is unstable. Note that under arbitrary addition of a real part to z_1 or z_2, the instability condition is always met. It is attributable to the fact that system with $F(t) = 1$ is close to stability, and arbitrarily small shear would be sufficient.

At $t < 0$ the stable point exists and is of the form

$$Z^* = \frac{1}{2}\left(z_1 + \sqrt{z_1^2+4z_1z_2}\right), \quad t<0, \tag{20.2.7}$$

and at $t > 4$ the stable point is as follows

$$Z^* = \frac{1}{2}\left(z_1 - \sqrt{z_1^2 + 4z_1 z_2}\right), \quad t > 4. \tag{20.2.8}$$

Note different signs before the root in (20.2.7) and (20.2.8).

Consider in more detail the case of purely imaginary z_1 and z_2 of different signs, when $z_1 = \mathrm{i} \cdot \omega \cdot L$, $z_2 = 1/\mathrm{i} \cdot \omega \cdot C$, then from (20.2.5) and (20.2.7) it follows that at

$$\omega > \omega_0 = \frac{2}{\sqrt{LC}}, \tag{20.2.9}$$

the fixed point is stable and the impedance of infinite chain exists and, as expected, is purely imaginary

$$Z^* = \mathrm{i}\left(\frac{\omega L}{2} + \sqrt{\frac{\omega^2 L^2}{4} - \frac{L}{C}}\right), \tag{20.2.10}$$

and at

$$\omega < \omega_0 = \frac{2}{\sqrt{LC}} \tag{20.2.11}$$

there is no fixed stable point and, hence, one cannot speak of the impedance of infinite chain. Therefore, a statement in [8]: "*Looking at infinite network from terminal a′, we would see a characteristic impedance* $Z_0 = \sqrt{L/C - \omega^2 L^2/4}$" is invalid. And then, in [8]: *"For low frequencies, impedance is pure resistance, therefore it absorbs the energy"*. Thus, filter transmission for low frequencies according to [8] is related to its absorption caused by ($\mathrm{Re}\, Z_0 > 0$)—dissipation. Though, further in [8] one can read quite a valid statement: "*...it turns out that when a source is connected to a network, it must first supply energy to the first inductance and capacitance, then the second, third, etc. In networks of this kind the energy is permanently sucked from generator at a constant rate and flows to the network without stop. The energy is accumulated in the inductances and capacitances along the network"*. Thus, energy absorption by filter is present, while dissipation is not, i.e., one should clearly distinguish between energy absorption by a medium of *LC*-elements with and without dissipation. The point is that in [8] Z_0 is found from solving a quadratic equation on the assumption (incorrect) that impedance of chain of n links (at $\omega < \omega_0$) converges. In the work [18] behavior of Z_n at $n \to \infty$ is considered depending on the values of z_1 and z_2. As it should be, at $z_1 = \mathrm{i}\omega L$ and $z_2 = 1/\mathrm{i}\omega C$ in the range $\omega < \omega_0$ Z_n does not converge. The range $\omega < \omega_0$ is filter transmission range. In [18] filter transmission in this range is related (like in [8]), to the presence of dissipation in a system. To his question: "*How can relation for* Z_0

give a correct answer in practice, if we substantiated it to be incorrect?" the author [18] answers: "*...a real part of inductor always has the internal resistance* $r \neq 0$". In this case, the question of Z_n convergence at $n \to \infty$, certainly, stands no longer. With the existence of arbitrarily small real part in z_1 and/or z_2, the characteristic impedance $Z_0 = \sqrt{L/C - \omega^2 L^2/4}$ does exist. However, in real filters with a finite, sometimes very low, number of elements, a small real part in z_1 and/or z_2 apparently cannot change anything. Therefore, the "existence" of $Z_0 = \sqrt{L/C - \omega^2 L^2/4}$ cannot be used to explain filter transmission.

In reality, as is well known [12] (see also [10]), for a finite filter of n links with purely imaginary elements there are two solutions relating inlet voltage $U(t) = U_0 \cos \omega t$ and outlet voltage $U_n(t)$. The first one, valid for transmission range, is as follows

$$U_n(t) = U_0 \frac{\cos \beta/2}{\cos(n+1/2)\beta} \cos \omega t, \quad \cos \beta = 1 - LC\omega^2, \quad \omega < \omega_0 = 2/\sqrt{LC}. \tag{20.2.12}$$

At $\omega \ll \omega_0$ $U(t) \approx U_0 \cos \omega t$, i.e., a filter of purely imaginary elements with a finite, including very small, number of elements, transmits a signal without distortion. For other frequencies from the range $\omega < \omega_0$ the transmission is nonuniform, nevertheless, no "locking" occurs.

The second solution in the range $\omega > \omega_0$ is in the form

$$U_n(t) = U_0(-1)^n \frac{\exp\left(\frac{\xi}{2}\right) - \exp\left(-\frac{\xi}{2}\right)}{\exp\left(\left(n+\frac{1}{2}\right)\xi\right) - \exp\left(-\left(n+\frac{1}{2}\right)\xi\right)} \cos(\omega t), \tag{20.2.13}$$

where ξ is found from $\cosh \xi = \left|1 - LC\omega^2/2\right|$.

From (20.2.13) it is readily apparent that output signal amplitude is exponentially reduced with increasing the number of links n and with their sufficiently large number it can be written down that

$$U_n(t) = U_0(-1)^n \left(e^{\frac{\xi}{2}} - e^{-\frac{\xi}{2}}\right) e^{-\left(n+\frac{1}{2}\right)\xi} \cos(\omega t), \tag{20.2.14}$$

i.e., signal locking takes place, and filter does not pass frequencies above critical.

The filter operation can be qualitatively explained by the existence of resonances in transmission area. In the finite chain the transmission frequencies are close to resonances. In the infinite chain the resonances merge, and all transmission frequencies lie on the resonance frequencies.

References

1. Baskin EM, Entin MV, Sarychev AK, Snarskii AA (1997) Enhancement of high-frequency field in near-ideal metal mixture. Phys A 242:49–56
2. Brouers F, Blacher S, Sarychev AK (1995) Multifractality of giant field fluctuations in semicontinuous metal films. In: Novak MM (ed) Fractal reviews in the natural and applied sciences. London; Chapmen & Hall, pp 237–246
3. Ducourtieux S, Podolskiy VA, Gresillon S, Buil S, Berini B, Gadenne P, Boccara AC, Rivoal JC, Bragg WD, Banerjii K, Safonov VP, Drachev VP, Ying ZC, Sarychev AK, Shalaev VM (2001) Near-field optical studies of semicontinuous metal films. Phys Rev B 64:165403-1–165403-14
4. Dykhne AM (1970) Conductivity of a two-dimensional two-phase system. Sov Phys JETP 32:63–64
5. Dykhne AM, Snarskii AA, Zhenirovskii MI (2004) Stability and chaos in randomly inhomogeneous two-dimensional media and LC circuits. Phys Usp 47:821–828
6. Éntin MV (1997) High-frequency dielectric constant of a two-dimensionally disordered model medium. Sov Phys JETP 87:365–368
7. Éntin MV, Entin GM (1996) Scale invariance in percolation theory and fractals. Sov Phys Jetp Lett 64:467–472
8. Feynman R, Leighton P, Sands M (1977) Feynman lectures on physics. Mainly Electromagnetism and Matter, vol 2. Addison-Wesley, Reading, Massachusetts
9. Helsing J, Grimvall G (1990) Conductance in random inductance-capacitance networks. Phys Rev B 16:11364–11367
10. Landau LD, Lifshitz EM (1984) Electrodynamics of continuous media, vol 8, 2nd edn. Butterworth-Heinemann, Oxford, p 460
11. Luk'yanets SP, Morozovskii AE, Snarskii AA (1999) Transition to chaotization and loss of self-averagability in two-dimensional two-phase media at the percolation threshold. Tech Phys Lett 44:458–461
12. Mandelshtam LI (1972) Lectures on the theory of nonlinear oscillations. Nauka, Moscow, p 470 (in Russian)
13. Peitgen H, Richter PH (1986) The beauty of fractals: images of complex dynamical systems. Springer, Berlin, p 199
14. Saruchev AK, Shalaev VM (2000) Electromagnetic field fluctuations and optical nonlinearities in metal-dielectric composites. Phys Rep 335:275–371
15. Schuster H (1988) Deterministic chaos: an introduction. Physik-Verlag, Berlin, p 220
16. Sivuchin DV (1977) The general course of physics, vol III. Electricity. Nauka, Moscow, p 688 (in Russian)
17. Snarskii AA, Slipchenko KV, Bezsudnov IV (1998) Reciprocity relations for the effective electrical conductivity of randomly inhomogeneous media the fractal regime. Sov Phys JETP 86:811–814
18. Van Enk SJ (2000) Paradoxical behavior of an infinite ladder network of inductors and capacitors. Am J Phys 68:854–856

Chapter 21
Percolation-Similar Description of Abrikosov Vortex

There are many different applications of percolation theory in superconductivity. They could be divided into the following groups:

1. Microscopic case one—when the characteristic size of inhomogeneity small and used for an explanation of superconductivity.
2. Microscopic case two—when the characteristic size of inhomogeneity small and describe different phenomena, but not superconductivity itself.
3. Macroscopic case—when the size of inhomogeneity is macroscopic.

Percolation theory could be applied for explaining superconducting phenomena at different level of inhomogeneity. It could be applied for explanation of appearance of superconductivity, explanation of properties of inhomogeneous superconductors, or explanation of properties of mixtures of superconducting and normal components.

Models that used percolation theory for explanation of superconductivity considered in papers [5–7, 29, 34, 46, 47], where percolation used to describe appearance of superconducting order.

In [34] the theory of percolation and theory of networks are applied for explanation of lattice effects and superconductivity appearance. In [35] percolating networks of superconducting oxygen rich puddles were actually observed.

Percolation effects in granular superconductors are observed in works [18, 20, 44, 45]. Percolative Josephson media is considered in papers [13, 15–17].

In [45] two-dimensional random—resistor networks are modeled by resistances between two grains (it is governed either by Josephson junction coupling, Cooper pair's tunneling or by quasiparticle tunneling). Scaling coefficient of magnetic susceptibility for granular superconductors is determined in [20]. Percolation models are also used for description of mixture of superconducting and normal phases [21–26, 31].

A.A. Snarskii et al., *Transport Processes in Macroscopically Disordered Media*, DOI 10.1007/978-1-4419-8291-9_21

The influence of geometry and morphology of superconducting structure on critical currents and magnetic flux trapping in percolative type-II superconductors is considered in [23]. Vortex—glass model describes superconducting-normal transition as a percolating transition according to the paper [31]. In [10] a percolation transition was observed in $NbSe_2$ crystal where heterogeneous phase of vortices consists of ordered and disordered domains. Dependence of magnetoresistance from magnetic field is studied for thin amorphous superconducting thin films on the basis of percolation approach in [32].

Interesting application of percolation theory for enhancement of superconductivity (not connected with explanation of superconductivity itself) is considered in papers [4, 28]. Bianconi [4] work describes increase of T_c in network model.

Macroscopic inhomogeneities are observed in papers [14, 30].

Osofsky et al. [30] describe influence of oxygen inhomogeneities in $YBa_2Cu_3O_7$ crystals as macroscopic phenomena are based on percolation theory. For FeAs-based superconductors percolation effects are observed in the paper [11], where influence of neutron irradiation on the structure of crystal samples was described using percolation theory. Interesting applications of percolation theory were provided in [27, 39], where two different percolation thresholds are found in ferromagnet-superconductor composites.

One of the most interesting applications of percolation models in superconductivity is a description of pinning of Abrikosov vortices.

21.1 The Pinning of the Abrikosov Vortexes

One of the main applications of superconductors is using them as current conductors with a zero resistance. As a rule, conventional superconductors (type I superconductors) have small critical fields, owing to which they cannot pass high currents. Type-II superconductors [1] possess higher critical fields. It is due to the so-called mixed state existing in such superconductors. In this mixed state a superconductor is permeated by vortex threads—the Abrikosov vortices passing a magnetic field through the superconductor. The Abrikosov vortices are current tubes in the middle of which (the center or core of the vortex) a conductor is in a normal state. Exactly for this reason the external magnetic field can penetrate from one side of superconducting sample to the other. There is one quant of magnetic flux $\Phi_0 = \pi\hbar c/e$ passing through each Abrikosov vortex (Fig. 21.1). Beyond the region occupied with vortices the superconductor retains its superconducting properties, and it is exactly in this region that transport current (assigned from the outside) is passed. If the vortices are fixed, no energy dissipation occurs and superconductor in general is a perfect conductor with a zero resistance. However, vortices can move. The point is that on switching of transport current, there appears a force (it is customarily called the Lorentz force—F_L) that affects the vortex. The origin of F_L is due to the fact that, on the one side of vortex transport current is added to vortex current, and on the other side subtracted (Fig. 21.1), therefore,

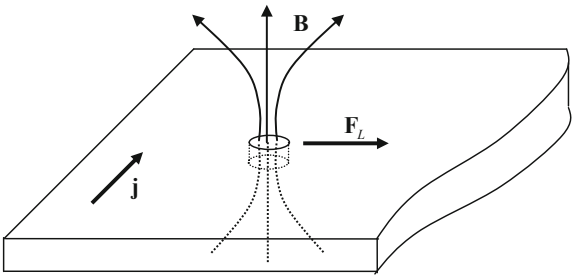

Fig. 21.1 Schematic of the Abrikosov vortex in a superconducting film: *j*—density of transport current assigned from outside, $\mathbf{F}_\mathrm{L}$ is Lorentz force affecting the vortex

forces affecting current in a magnetic field B (Ampere forces) are not compensated. The resulting of these forces is the Lorentz force—F_L, which [1] is expressed through a quant of magnetic flux Φ_0 in the form

$$\mathbf{F}_\mathrm{L} = \frac{1}{c}\Phi_0 \mathbf{j} \times \mathbf{b}, \tag{21.1.1}$$

where **b** is unity vector along the vortex axis.

With vortex motion at rate v it is exposed to viscous forces:

$$\mathbf{F}_\eta = -\eta \mathbf{v}, \tag{21.1.2}$$

where η is certain viscosity factor [1].

Moving vortices dissipate the energy, with dissipation power equal to $\mathbf{vF}_\eta$. The physical reason for dissipation lies in the fact that moving vortex converts conductor's superconducting portions into conventional, and vice versa.

To stop the motion of vortices and, thus, to get a perfect conductor wherein current is not dissipated, vortices should be fastened. The effect of fastening vortices to certain superconductor points is called pinning. In particular, in the high-temperature superconductors (HTSC) one of the kinds of pinning centers are charged defects creating the electrostatic potential. Random arrangement of such defects creates a random distribution of electrostatic pinning forces—$\mathbf{F}_p$.

If the distribution of pinning forces $D(F_p)$ is narrow, then with increasing transport current, the Lorentz force F_L will "conquer" pinning force almost for all vortices at once, and the entire lattice will start moving. Superconductor in this case will go over to a resistive state and the resistance will appear, though part of conductor outside the vortices will still be in the superconducting state.

21.2 The Case of the Wide Pinning Force Distribution

When the distribution of pinning forces is wide [40, 41], then, as transport current increases, so does the area of portions for which $F_\mathrm{L} > F_p$. However, their motion will occur only in a restricted space and within limited time till the areas with

$F_L > F_p$ coalesce and form an infinite cluster. It will happen at $F_L \geq F_{pc}$, where F_{pc} is such critical value of pinning force that the areas $F_L \leq F_{pc}$ form an infinite cluster —a connected array of channels (areas) passing through the entire sample. In this case, when the below equality is satisfied

$$F_p + F_\eta = F_L, \tag{21.2.1}$$

a stationary flow of vortices is possible at a rate

$$v = \frac{1}{\eta}\left(F_L - F_p\right) = \frac{1}{\eta}\left(\frac{j\Phi_0}{c} - F_p\right), \tag{21.2.2}$$

where it is assumed that viscosity force F_η is sufficiently large and can not be neglected as the influence of acceleration and inhibition portions of vortices at their interaction with pinning centers. Moreover, when considering the area of rather weak magnetic fields ($H \ll H_{c2}$), one can ignore the forces of interaction between the vortexes, since they are few ("one-particle" pinning mode).

The density of critical transport current j_c is governed by critical pinning force F_{pc} Eqs. (21.1.1) and (21.1.3) in the usual form

$$j_c = cF_{pc}/\Phi_0, \tag{21.2.3}$$

Consider motion of vortices at transport current close to critical:

$$\tau_j = \frac{j - j_c}{j_c} \ll 1, \tag{21.2.4}$$

Let us recall, as it is common practice in percolation theory, those film areas where $F_L > F_p$, i.e., where vortices can move, as a "black" phase. Then the "black" phase concentration is equal to

$$p = \int_0^{F_p} D\left(F_p\right) dF_p, \tag{21.2.5}$$

and for the homogeneous distribution of pinning forces, when $D\left(F_p\right) = 1/F_{pm} =$ const, $F_p \in \left[0, F_{pm}\right]$, where F_{pm} is maximum value of pinning force in the film. With any other smooth distribution $\tau = (p - p_c)/p_c$ and $\tau_j = (j - j_c)/j_c$ are proportional to each other, and in case of a homogeneous distribution they coincide.

To determine the volt-ampere characteristic of the resistive state of HTSC film, one should find the power of energy dissipation by vortices. We assume that the major energy is dissipated by vortices in the basic element of percolation structure above the percolation threshold—the bridge. Figure 21.2 schematically shows a portion of percolation structure above the percolation threshold. It should be taken into account that the Lorentz force is always unidirectional (along the *ox* axis in

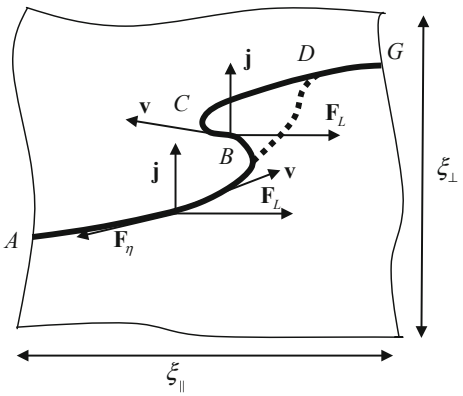

Fig. 21.2 Schematic of percolation structure portion wherein the Abrikosov vortex flows

Fig. 21.2) and, hence, it cannot "push" a vortex through *BC* portion. It means that transport current should be increased until the emerging portions of infinite cluster (one of them, *BD*, is shown in Fig. 21.2 as a dashed line) allow the vortex to pass through the infinite cluster from beginning to end (from *A* to *G*). Certainly, in the calculation of dissipation one should take into account only those portions of infinite cluster on which vortices move along the Lorentz force—*ABDG*. Thus, a conventional percolation model should be modified. The so-called model of diode percolation, or, more precisely, fully directed percolation (FDP) is the closest to the modification we need. The diode percolation modules are dealt with in a large number of papers (see, for instance, [2, 3, 8, 9, 12, 19, 36–38, 43]).

Consider a square lattice. With a diode percolation, "black" and "white" resistances and diodes are randomly scattered on the lattice, the latter passing an electric current is only in one direction. There are many versions of such models: (1) the lattice consists only of nonconducting bonds and diodes, (2) there are conducting bonds, (3) direction of scattered diodes is random, (4) not random, etc. We need the version shown in Fig. 21.3, when current is conducted only by diodes, on the average they have the same, local, direction, just as the Lorentz force, namely the diodes are diagonally directed upward or downward. In this *FDP* case the concentration of conducting diode does not include portions of *BC* type in Fig. 21.2, therefore, *FDP* problem (Fig. 21.3) and the problem of vortex flow, though close, are not identical to each other, and further calculation should be undertaken as the estimate of critical index.

Critical indices of *FDP*-model differ from such in a conventional percolation problem, moreover, now there are two indices of correlation length: $\nu_\parallel$—for the correlation length $\xi_\parallel$ along the average direction of diode conductivity—*ox*, and $\nu_\perp$—for the correlation length $\xi_\perp$ across the diode conductivity direction—*oy*:

$$\xi_\parallel = a_0 \tau^{-\nu_\parallel}, \quad \xi_\perp = a_0 \tau^{-\nu_\perp}, \tag{21.2.6}$$

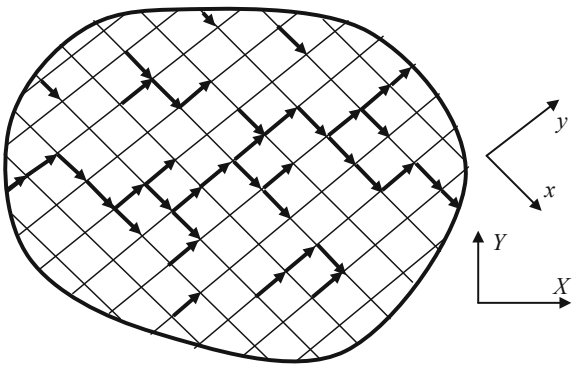

Fig. 21.3 Version of diode percolation—fully directed percolation (FDP): nonconducting bonds are marked by *thin lines*. *Arrows* are used to denote diodes and current flow direction in the diodes. All the diodes are directed either along *ox*, or *oy*, *OX*, and *OY* axes are the same as in Fig. 21.2

Dependence of the effective conductivity on τ in such a model is of conventional form, but with a different critical index:

$$\sigma_e = \sigma\tau^{t_+}, \tag{21.2.7}$$

where σ is diode conductivity in the direction of current passage.

For the two-dimensional case $\nu_\parallel \approx 1.73, \quad \nu_\perp \approx 1.097$ [12], $t_+ \approx 0.63$ [3].

The bridge length in *FDP*-model is found as follows. On the one hand, the resistance of media, corresponding to the correlation space with the unity thickness is of the form

$$R = \frac{1}{\sigma_e}\frac{\xi_\parallel}{\xi_\perp}, \tag{21.2.8}$$

on the other hand, this resistance is governed by the resistance of a bridge of length $l = a_0 N_1^+, \quad N_1^+ \approx \tau^{-\alpha_1^+}$.

$$R = \frac{1}{\sigma}N_1^+ = \frac{1}{\sigma}\tau^{-\alpha_1^+}, \tag{21.2.9}$$

Whence with regard to Eq. (21.2.7) we have

$$\alpha_1^+ = t_+ - \nu_\perp + \nu_\parallel, \tag{21.2.10}$$

Note that for d-dimensional case [37] $\alpha_1^+ = t_+ - (d-1)\nu_\perp + \nu_\parallel$. Thus, the bridge length becomes

$$l \approx a_0\tau^{-\alpha_1^+}, \tag{21.2.11}$$

The energy Q_1 dissipated by one vortex during time t_0 of passing the bridge, is as follows

$$Q_1 = \int_0^{t_0} F_\eta v \mathrm{d}t = l \int_0^{t_0} \left(F_\mathrm{L} - F_p\right) D\left(F_p\right) \mathrm{d}F_p, \tag{21.2.12}$$

where t_0 is passage time,

$$t_0 = \int_0^{t_0} \mathrm{d}t = \int_0^{l} \frac{\mathrm{d}v}{v} = \eta\, l \int_0^{F_{pc}} \frac{D\left(F_p\right)}{F_\mathrm{L} - F_p} \mathrm{d}F_p, \tag{21.2.13}$$

For the uniform distribution $D\left(F_p\right) = 1/F_{pm}$ and from Eqs. (21.2.12) and (21.2.13) we obtain

$$Q = \frac{lF_p^2}{2F_{pm}}, \quad t_0 = \frac{\eta\, l\, \ln(1/\tau)}{F_{pm}}, , \tag{21.2.14}$$

where it is taken into account that $j \approx j_c$.

The concentration of vortices is equal to B/Φ_0, and their number n in a bridge

$$n = \frac{a_0 lB}{\Phi_0} \sim \frac{a_0 B}{\Phi_0} \tau^{-\alpha_1^+}, \tag{21.2.15}$$

Hence, on the one hand, the power of energy dissipation of all vortices on the area $\xi_\parallel \times \xi_\perp$ is of order

$$Q = \frac{nQ_1}{t_0} = -\frac{a_0 BF_p^2 l}{2\Phi_0 \eta\, \ln \tau}, \tag{21.2.16}$$

on the other—motion of vortices results in the appearance of the electrical field [1], and Q can be written down as the Joule dissipation:

$$Q = jE\xi_\parallel \xi_\perp, \tag{21.2.17}$$

From the expressions (21.2.6), (21.2.11), and (21.2.17) we find

$$E = \frac{a_0 BF_{pc}^2}{2\Phi_0 \eta j_c \xi_\parallel \xi_\perp \ln(1/\tau)} = A\, \ln\left(\frac{j - j_c}{j_c}\right)\left(\frac{j - j_c}{j_c}\right)^\gamma, \tag{21.2.18}$$

where A is certain constant which is inessential for the determination of critical index, and critical index is of the form

$$\gamma = v_{\perp} - v_{\parallel} - \alpha_1^{+} = 2v_{\perp} - t_{+}, \tag{21.2.19}$$

and with regard to numerical values $v_{\perp}$ and t_{+} we obtain

$$\gamma \approx 1.6. \tag{21.2.22}$$

Experimental studies of a resistive state of HTSC really indicate to power dependence of voltage on current in the initial portions of volt-ampere characteristic. In doing so, factor γ varies over a wide range. In relatively weak fields ($H \leq 0.2\,\mathrm{T}$) the numerical values of γ lie in the range $\gamma = 1.3 - 1.5$ [42].

Percolation-like description of pinning was also used to describe the resistive state of HTSC film in variable (in sign) magnetic fields [33]. In case of a variable magnetic field, hence, the Lorentz force varies in time and direction. The superconductor transition to a resistive state does not require the presence of infinite cluster, the vortices dissipate the energy moving "hither and thither" along the finite portions of a cluster.

References

1. Abrikosov AA (1988) Fundamentals of the theory of metals. North-Holland, Amsterdam 630 p(1988)
2. Arora BM, Varma M, Dhar D, Phani MK (1983) Conductivity of a two-dimensional random diode-insulator network. J Phys. C 16:2913–2922
3. Balberg I, Binenbaum N (1986) Direct determination of the conductivity exponent in directed percolation. Phys Rev B V. 33, P. 2017–2019
4. Bianconi C (2013) Superconductor-insulator transition in a network of 2d percolation clusters. Lett J Exploring Front Phys 101:26003-1–26003-6
5. de Mello EVL, Caixeiro ES, Gonzalez JL (2002) A novel percolation theory for high temperature superconductors. Braz J Phys 32:705–709
6. de Mello EVL, Caixeiro ES, Gonzalez JL (2003) Is the superconducting state for the cuprates reached through a percolation transition? Act Phys Pol B 34:563–566
7. de Mello EVL, Dias DHN (2007) Phase separation and the phase diagram in cuprites superconductors. J Phys Condens Matter 19:086218-1–086218-9
8. De'Bell K, Essam JW (1983) Directed percolation: mean field theory and series expansions for some two-dimensional lattices. J Phys A 16:P.385–404
9. Dhar D, Barma M (1981) Monte Carlo simulation of directed percolation on a square lattice. J Phys C 14:L1–L6
10. Dogru O, Andrei EY, Higgins MJ et al (2005) Percolation transition in the heterogeneous vortex state of NbSe2. Phys Rev Lett 95:057004-1–057004-4
11. Eisterer M, Zehetmayer M, Weber HW et al (2010) Disorder effects and current percolation in FeAs based superconductors. Supercond Sci Technol 23:0540061–0540067
12. Essam JW, De'Bell K, Adler J, Bhatti FM (1986) Analysis of extended series for bond percolation on the directed square lattice. Phys Rev B 33:1982–1986
13. Forgacs G, Schulman LS, Kiss LB (1991) Method for determining the distribution of Josephson coupling energies in high- TC superconductors. Physica C 177:67–72
14. Gavrilkin SYu, Ivanenko OM, Martovitskii VP (2010) Percolative nature of the transition from 60 K to 90 K—phase in $YBa_2Cu_3O_6 + \delta$. J Exp Theor Phys 110:783–787

15. Glukhov AM, Pokhila AS, Dmitrenko IM et al (1997) Superconducting quantum interference in fractal percolation films. Probl 1/f Noise Phys B 240:242–253
16. Glukhov AM, Sivakov AG, Ustinov AV (2002) Observation of stochastic resonance in percolative Josephson media. Low Temp Phys 28:543–547
17. Granato E (1997) Current-voltage characteristics of diluted Josephson-junction arrays: scaling behavior at current and percolation threshold. Phys Rev B 56:14671–14676
18. Janssen H-K, Stenull O (2003) Percolating granular superconductors. Phys Rev E 67:046115-1–046115-8
19. Kinzel W, Yeomanis M (1991) Directed percolation: a finite-size renormalisation group approach. J Phys A 14:L163–L168
20. Knudsen HA, Hansen A (2000) Diamagnetic susceptibility and current distributions in granular superconductors at percolation. Phys Rev B 61:11336–11339
21. Kuzmin YI (2000) Fractal geometry of normal phase clusters and magnetic flux trapping in high-tc superconductors. Phys Lett A 267:66–70
22. Kuzmin YI (2001) Dynamics of the magnetic flux trapped in fractal clusters of a normal phase in superconductor. Phys Rev B 64:094519-1–094519-11
23. Kuzmin YI (2001) Resistive state of superconducting structures with fractal clusters of a normal phase. Phys Solid State 43:1199–1206
24. Kuzmin YI (2002) Giant dispersion of critical currents in superconductor with fractal clusters of a normal phase. Tech Phys Lett 28:568–571
25. Kuzmin YI (2003) Peculiarities of the resistive transition in fractal superconducting structures. Tech Phys Lett 29:414–417
26. Kuzmin YI (2005) Vortex dynamics in percolative superconductors containing fractal clusters of a normal phase. Trans Appl Supercond 15:3750–3753
27. Liu X, Panguluri RP, Huang Z et al (2010) Double percolation transition in superconductor-ferromagnet nanocomposites. Phys Rev Lett 104:035701-1–035701-4
28. Mayoh J, García-García AM (2014) Strong enhancement of bulk superconductivity by engineered nanogranularity. Phys Rev B 90:134513-1–134513-11
29. Mihailovic D, Kabanov VV (2005) Dynamic inhomogeneity, pairing and superconductivity in cuprates. In: Chapter superconductivity in complex systems vol 114 of the series structure and bonding, pp 331–364
30. Osofsky MS, Cohn JL, Skelton EF et al (1992) Percolation effects and oxygen inhomogeneities in YBa_2Cu_{307} crystals. Phys Rev B 45:4916–4922
31. Pfeiffer FO, Rieger H (2002) Superconductor-to-normal phase transition in a vortex glass model: numerical evidence for a new percolation universality class. J Phys Condens Matter 14:2361–2369
32. Porat E, Meir Y (2015) Magnetoresistance anisotropy in amorphous superconducting thin films: a site-bond percolation approach. Phys Rev B 92:024509-1–024509-5
33. Palti AM, Ruban AI, Snarskii AA (1998) Resistive state of HTSC film in a varying magnetic field. Low Temp Phys 24:336–339
34. Phillips JC (2007) Self-organized networks and lattice effects in high temperature superconductors. Phys Rev B 75:214503-1–214503-22
35. Poccia N, Chorro M, Ricci A et al (2014) Percolative superconductivity in $La_2CuO_{4.06}$ by lattice granularity patterns with scanning micro X-ray absorption near edge structure. Appl Phys Lett 104:221903-1–221903-9
36. Redner S (1982) Directed and diode percolation. Phys Rev B 25:3242–3250
37. Redner S (1982) Conductivity of random resistor-diode networks. Phys Rev B 25:5646–5655
38. Redner S, Mueller PR (1982) Conductivity of a random directed-diode network near the percolation threshold. Phys Rev B 26:5293–5295
39. Ruiz-Valdepenas L, Velez M, Valdes-Bango F et al (2013) Double percolation effects and fractal behavior in magnetic/superconducting hybrids. New J Phys 15(103025):1–13
40. Snarskii AA, Pashitskii EA, Pal'ti AM, Morozovskii AE (1995) Percolation mechanism for vortex depinning in the resistive state of thin films of type-II superconductors Sov. Phys JETP Lett 61:119–123

41. Snarskii AA, Pashitskii ÈA, Palti AM (1995) The diode percolation model of vortex flow in the resistive state of HTS films. Low Temp Phys 21:706–711
42. Solovjov VF, Pan VM, Freyhardt HC (1994) Anisotropic flux dynamics in single-crystalline and melt-textured YBa_2Cu_{3O7}. Phys Rev B 50:13724–13734
43. Sornette D (1988) Critical transport and failure in continuum crack percolation. J Phys France 49:1365–1377
44. Strelniker YM, Frydman A, Havlin S (2007) Percolation model for the superconductor-insulator transition in granular films. Phys Rev B 76:224528-1–224528-6
45. Strelniker YM, Havlin S, Frydman A (2007) Effective medium approximation for hopping conductivity and Josephson junctions. Phys B 394:368–371
46. Tahir-Kheli J, William AG III (2010) Universal properties of cuprate superconductors: T_c phase diagram. Room-temperature thermopower, neutron spin resonance, and STM incommensurability explained in terms of chiral plaquette pairing journal of physical chemistry letters, vol 1, pp 1290–1295
47. Tahir-Kheli J (2013) Resistance of high-temperature cuprate superconductors. New J Phys 15:073020

Chapter 22
Anderson Localization in the Percolation Structure

Theory of percolation was extensively used for explanation of quantum phenomena. For example, it was used for explanation of Anderson localization and quantum Hall effects.

Particularly, random network models used for explaining quantum phenomena in papers: [7] reviewed application of random network models, based on the percolation model, and used for explanation of integer quantum Hall effect [5], (model consisting of superconducting and quantum links used for explanation of integer quantum Hall transition) [8], (studied localization in quantum random networks) [4], (multifractal properties of RRN).

22.1 Anderson Localization

In metals, at low temperatures, the interference correction to conductivity—$\delta\sigma$ becomes significant. This correction is due to the presence of the nonzero probability of existence of electron trajectories with self-intersections. Correction $\delta\sigma$ at $T \to 0$ is increased and, when $\delta\sigma/\sigma \approx 1$, localization of electrons occurs, a sample ceases to conduct current and metal $\to$ dielectric transition takes place [1]. Such localization (in the limit $T = 0$) is commonly referred to as Anderson localization [2], and the metal that "turned" into dielectric—Anderson dielectric (*AD*).

Dependence of correction $\delta\sigma/\sigma$ on the sample size is different for three-, two-, and one-dimensional cases. In the following, we will need only the one-dimensional case. One-dimensionality here means that sample cross section b is much lesser than L_φ, where L_φ is characteristic length of coherence failure of electron wave function amplitude (we are dealing with macroscopic sizes [1]. For such one-dimensional case localization occurs when its length L exceeds critical length L_c,

A.A. Snarskii et al., *Transport Processes in Macroscopically Disordered Media*, DOI 10.1007/978-1-4419-8291-9_22

$$L_c = l\left(\frac{b}{\lambda}\right)^2, \tag{22.1.1}$$

where l is mean free path, λ is electron wavelength.

At $L > L_c$ with increasing L the sample conductance G drops off exponentially,

$$G \sim e^{-L/L_c}, \tag{22.1.2}$$

there is also a similar drop in dimensionless conductance $y = G/G_0$, where $G_0 = e^2/(\pi^2\hbar)$, e is electron charge.

Thus, as the length of such metal wire increases, it, eventually, ceases to be a conductor and is converted into *AD*.

22.2 Anderson Metal–Insulator Transition in Percolation Structure

In [6] authors considered the effect of Anderson localization on metal–dielectric junction in percolation structure, when a conducting bond (of length a_0) is metal and characterized by mean free path l or, which is the same, by dimensionless conductance y $(y \sim 1/l)$. The nonconducting bonds are a common (classical) dielectric. For the conducting bond there exists such a value of y_{c0} that in the case of $y > y_{c0}$ the bond would not conduct, passing from the metallic to *AD* state. In fact, increase in y means a drop in the mean free path, hence, a decrease in L_c—(22.1.1). When L_c becomes shorter than the bond length a_0, A. Thus, on the one hand, at $p = 1$ all bonds in the lattice are metallic, but they cease to conduct current with $y > y_{c0}$. On the other hand, at $p \leq p_c$ the lattice ceases to conduct current due to disappearance of a connected way in metal bonds. A general case of arbitrary concentration is given in Fig. 22.1, where a solid line $y_c = y_c(p)$ is a critical value of dimensionless conductance dividing metal phase *M* and Anderson dielectric *AD* at $T = 0$. *CD* is classical dielectric, p is concentration of metals bonds. Second phase conductivity is $\sigma_2 = 0$. Dashed line divides the conducting and nonconducting $p > p_c$ system states at finite temperatures when localization effects are marginal.

In the work [6] it was shown that $y_c = y_c(p)$ becomes zero (at $p \to p_c$) in power manner and is characterized by critical index. The physical reason for such behavior of $y_c(p)$ is related to the fact that close to percolation threshold the main element of percolation structure is a bridge—the one-dimensional way for current to be conducted when its length (to be more precise, the length of its continuous part) exceeds L_c and Anderson localization occurs.

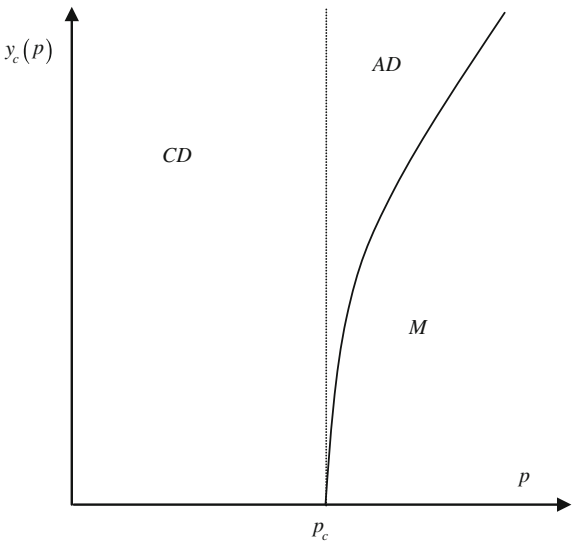

Fig. 22.1 Phase diagram in percolation lattice with regard to Anderson localization

For the calculation of critical index [9] we take into account that according to the first step of the HM, the bridge length is of the form

$$L \approx a_0 (p - p_c)^{-(t_3 - \nu_3)}. \tag{22.2.1}$$

Then from condition $L_c \approx L$ and (22.1.1) we obtain

$$a_0 (p - p_c)^{-(t_3 - \nu_3)} \approx l \left(\frac{b}{\lambda} \right)^2. \tag{22.2.2}$$

With regard to the fact that $y \sim 1/l$, we find

$$y_c(p) \sim (p - p_c)^A, \tag{22.2.3}$$

where

$$A = t_3 - \nu_3, \tag{22.2.4}$$

For the first time this critical index was obtained in [6] using other considerations.

Experimental discussion of Anderson localization in percolation systems can be found, for instance, in [3].

References

1. Abrikosov AA (1988) Fundamentals of the theory of metals North-Holland, Amsterdam 630 p
2. Anderson PW (1958) Absence of diffusion in certain random lattices. Phys Rev 109:1492–1505
3. Aronzon BA, Chumakov NK, Snarskii AA, Brotto J-M, Rokoto H, Leotin J (1998) Superlocalization in compensated InSb in the physics of semiconductors. In: Gershoni D (ed) 24th international conference, world scientific, pp 43–50
4. Barthélémy M, Buldyrev SV, Havlin S et al (2000) Multifractal properties of the random resistor network. Phys Rev E 61:R3283(R)
5. Dubi Y, Meir YY, Avishai Y (2005) Quantum hall criticality, superconductor-insulator transition and quantum percolation. Phys Rev B 71:125311-1–125311-4
6. Khmel'nitskii DE (1980) Anderson localization in a flow structure. Sov Phys Jetp Lett 32:229–232
7. Kramer B, Ohtsuki T, Kettemann S (2005) Random network models and quantum phase transitions in two dimensions. Phys Rep 417:211–342
8. Schubert G, Fehske H (2008) Diffusion and localization in quantum random resistor networks. Phys Rev B 78:155115-1–155115-6
9. Snarskii AA (1989) Kinetic phenomena in macro inhomogeneous and anisotropic media. Thesis, Kiev Polytechnic University

Chapter 23
Conclusion

The idea of the book could be formulated as follows: to find the basis of simple transport property which is represented by critical geometric elements that are responsible for this property and to use the knowledge of the geometry of these elements to explain many different transport properties. Schematically, it could be expressed as: [geometry] → [simple transport property] → [new geometry] → [complex transport properties]. The described idea could be extended for classification of existing models and for suggestions for new development. For example, new approaches to the problem of turbulence are self-organized critically, that include use of models of percolation structures [2–5] could be described as [non-stationary geometry] → [simple transport properties (advection, diffusion)] → [selection of a new geometry] → [combined diffusion].

Similar ideas could be applied for many different applications:

A. Extensions to the new percolation geometries and complex networks, see for example [1].
B. The proposed approach is considered for stable geometry when time of change of geometry ≫ characteristic time of transport process (time of measurement or time of change of transport properties). It will be interesting to extend it to the unstable geometry when [time of change of geometry] ∼ [characteristic time of transport process].
C. Application to finance: [all players] → [simple behavior] → [important players] → [result behavior of market] (similar to market microstructure).
D. Time series: [time series converted to network] → [some aggregated properties of time series] → [important sub-points] → [prediction for the future].
E. Algorithms: [all elements] → [simple algorithm] → [important elements] → [complex algorithms].

We hope that this approach could be applied for different additional area of percolation theory and beyond.

A.A. Snarskii et al., *Transport Processes in Macroscopically Disordered Media*, DOI 10.1007/978-1-4419-8291-9_23

References

1. Araujo NAM, Grassberger P, Kahng B et al (2014) Recent advances and open challenges in percolation. Eur Phys J Spec Top 223:2307–2321
2. Bakunin OG (2003) Correlation and percolation properties of turbulent diffusion. Phys-Uspechi (Adv Phys Sci) 46:733–744
3. Bakunin OG (2008) Turbulence and diffusion. Scaling versus equations. Springer, Berlin 278 p
4. Bakunin OG (2011) Chaotic flows. Correlation effects, transport and coherent structures. Springer, Berlin 364 p
5. Zelenyi LM, Milovanov AV (2003) Fractal topology and strange kinetics: from percolation theory to problems in cosmic electrodynamics. Phys-Uspechi (Adv Phys Sci) 49:749–788